

**BIOINSPIRED INORGANIC
NANOMATERIAL SYNTHESIS AND ITS
APPLICATIONS**

THESIS SUBMITTED TO THE UNIVERSITY OF PUNE

FOR THE DEGREE OF

DOCTOR OF PHILOSOPHY

IN

BIOTECHNOLOGY

BY

IMRAN UDDIN

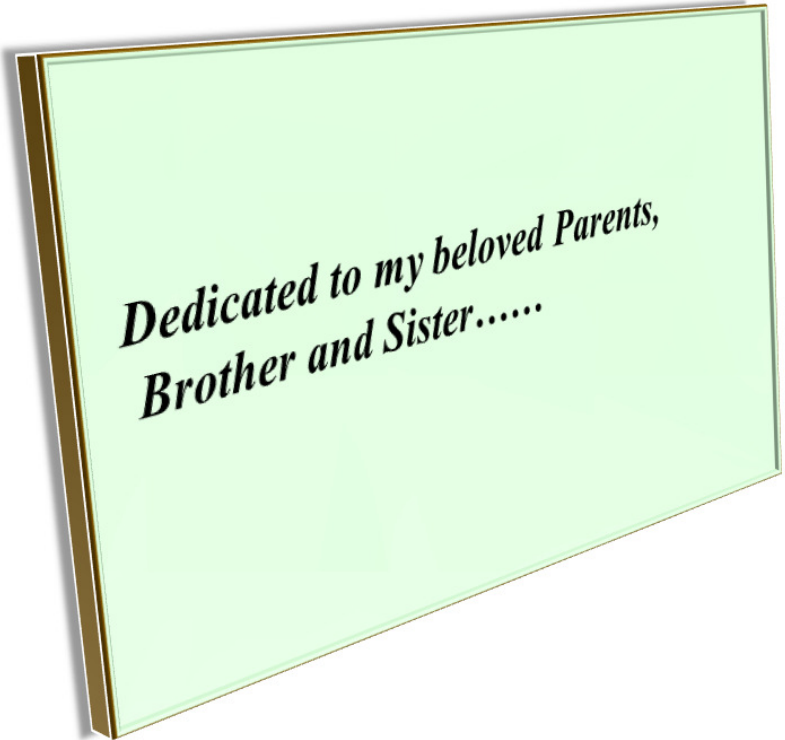
UNDER THE GUIDANCE OF

**Dr. ABSAR AHMAD
BIOCHEMICAL SCIENCES DIVISION
NATIONAL CHEMICAL LABORATORY
PUNE - 411008, INDIA**

AND CO-GUIDANCE OF

**Dr. PANKAJ PODDAR
PHYSICAL/MATERIALS CHEMISTRY DIVISION
NATIONAL CHEMICAL LABORATORY
PUNE - 411008, INDIA**

DECEMBER 2011



*Dedicated to my beloved Parents,
Brother and Sister.....*

CERTIFICATE

This is to certify that the work discussed in the thesis entitled “**BIOINSPIRED INORGANIC NANOMATERIAL SYNTHESIS AND ITS APPLICATIONS**” by **IMRAN UDDIN**, submitted for the degree of *Doctor of Philosophy in Biotechnology* was carried out under my supervision at the Biochemical Sciences and Physical/Materials Chemistry Divisions of the National Chemical Laboratory, Pune, India. Such materials as have been obtained by other sources have been duly acknowledged in this thesis. To the best of my knowledge, the present work or any part thereof has not been submitted to any other University for the award of any other degree or diploma.

Date:

Place: NCL, Pune

Dr. Absar Ahmad

(Research Guide)

CERTIFICATE

This is to certify that the work discussed in the thesis entitled “**BIOINSPIRED INORGANIC NANOMATERIAL SYNTHESIS AND ITS APPLICATIONS**” by **IMRAN UDDIN**, submitted for the degree of *Doctor of Philosophy in Biotechnology* was carried out under my joint supervision at the Biochemical Sciences and Physical & Materials Chemistry Divisions of the National Chemical Laboratory, Pune, India. Such materials as have been obtained by other sources have been duly acknowledged in this thesis. To the best of my knowledge, the present work or any part thereof has not been submitted to any other University for the award of any other degree or diploma.

Date:

Place: NCL, Pune

Dr. Pankaj Poddar

(Research Co-Guide)

DECLARATION

I hereby declare that the work described in this thesis entitled “**BIOINSPIRED INORGANIC NANOMATERIAL SYNTHESIS AND ITS APPLICATIONS**” submitted for the degree of *Doctor of Philosophy in Biotechnology* has been carried out by me at the Biochemical Sciences and the Physical/Materials Chemistry Divisions of the National Chemical Laboratory, Pune, India under the joint supervision of Dr. Absar Ahmad and Dr. Pankaj Poddar. Such materials as have been obtained by other sources have been duly acknowledged in this thesis. The work is original and has not been submitted in part or full by me for award of any other degree or diploma in any other University.

Date:

Place: NCL, Pune

Imran Uddin

(Research Student)

Acknowledgements

It gives me great pleasure to thank all those who were associated with me during my Ph.D. at National Chemical Laboratory, Pune (Maharashtra, India). The work described in this thesis would not have been possible without the direct or indirect involvement of all these people. Therefore, I would like to extend my sincere thanks and gratitude toward all these people who were there with me during my tenure here at N.C.L.

First and foremost, I express my deep sense of gratitude and indebtedness to my mentor and my research guide Dr. Absar Ahmad for his, guidance, fruitful discussions, constructive comments, suggestions, advice and continuous encouragement which have helped me breathe life into my dreams. I am most indebted to him for exposing me to such an exciting and interesting research area. I am greatly impressed by his tireless enthusiasm, passion, hard work, dedication and discipline in research. His constant support was invaluable and has helped me right from the very beginning to the completion of this thesis. I will always be thankful to him for teaching me valuable lessons of life directly or indirectly apart from research. It is my privilege to have been associated with a person like him.

I would also like to thank my research co-guide Dr. Pankaj Poddar for his support and guidance throughout my stay at National Chemical Laboratory and providing me initial lab-space for my research work.

I would also like to thank Dr. Sourav Pal, present Director and Dr. S. Sivaram, Ex-Director, N.C.L. for allowing me to carry out my research at the institute and providing the required facilities.

I am thankful to Dr. (Mrs.) Vidya Gupta, Chairman, Division of Biochemical Sciences for her support and help during the research work and allowing me to work in the Division of Biochemical Sciences, N.C.L.

I acknowledge the Council of Scientific and Industrial Research (CSIR), Government of India and Department of science and technology (DST), Government of India for providing me with the necessary funding and fellowship to pursue research at N.C.L.

I am also grateful to DST, INSA and N.C.L for providing me with the financial support for attending an international conference in Rome, Italy.

I would also like to thank my Ph.D committee members Dr. Archana Pundle and Dr. Debasish Mitra from the National Centre for Cell Science (N.C.C.S), Pune for their help, comments and suggestions.

My research work has involved significant contributions from a lot of collaborative work both within NCL and outside. Among them, my sincere thanks goes to Dr. Sanjay Gambhir for radiolabelling and biodistribution studies at Sanjay Gandhi Post-Graduate Institute of Medical Sciences (SGPGI). I would like to thank Dr. Arunava Gupta, Dept of Chemistry, University of Alabama for the magnetic measurement studies of CrO₂ nanoparticles. I would also like to thank Dr. P. V. Satyam and Mr. Umananda M. Bhatta of IOP, Bhubneshwar for their assistance with the HR-TEM analysis. I would like to present my sincere thanks to Dr. Ravi for providing me with BiOCl samples for bio-milling experiments and Dr. Selveraj for XRD analysis. I am grateful towards many people at the Center for Materials Characterization, NCL who have assisted me in the course of this work.

I would like to thank the Physical Chemistry Division office staff, Biochemical Sciences Division staff and administrative staff for helping me extensively with the routine official and administrative work.

This acknowledgement would be incomplete without the special mention of my Physical Chemistry Division and Biochemical Sciences Division lab-mates for their help in the experiments and encouragement for creating a cordial atmosphere during my doctoral work and bearing with me in good and bad times during my wonderful days of PhD.

During the course of my work I had pleasure of getting a helping hand with several project students. Their assistance during the presented work is gratefully acknowledged. I wish them all the best and a bright future.

Special thanks also goes to all my friends for their support and care in helping me overcome setbacks and stay focused on my study. I am thankful to them for giving me good company in Pune and for creating a perfect homely environment throughout my stay at N.C.L. I greatly value their friendship and deeply appreciate their belief in me.

This thesis has become possible due to the strong faith and constant encouragement from my family, without whose enduring support it would not have been possible to embark upon this journey of life. I thank my father Mr. Zahin Uddin Usmani and my mother Mrs. Mumtaz Usmani from the bottom of my heart for their blessings words of wisdom, trust, and unfailing love. I could not have made it through without them being there for me at all times. At this moment and always, I pay my most respectful regards to them, who are a constant source of inspiration in every walk of my life. I am thankful to my brother Ameen Uddin Usmani for his love, constant encouragement and moral support. Special thanks go to my beloved sister Mujahida Usmani and brother-in-law Amil Usmani who have always extended their help and love whenever I needed them the most.

This work would not have been possible without the grace of ALLAH the almighty for giving me strength and ability to complete my Ph.D thesis.

Imran Uddin.....

Table of Contents

Chapter 1	General Introduction	
	1.1 Historical Perspective	4
	1.2. Properties of nanomaterials	5
	1.2.1 Catalytic properties	7
	1.2.2 Lattice parameters	7
	1.2.3 Melting point	7
	1.2.4 Optical properties	8
	1.2.5 Mechanical properties	8
	1.2.6 Magnetic properties	8
	1.3 Synthesis of nanomaterials	9
	1.4 Bio-nanotechnology	12
	1.5 Lessons from nature for nanomaterial synthesis	12
	1.6 An overview on biomineralization	13
	1.7 Biological means for synthesizing nanomaterials	17
	1.8 Nano-biotechnology: current areas of biomedical applications	21
	1.8.1 Therapeutics	22
	1.8.2 Diagnostic	23
	1.8.3 Bio-imaging	23
	1.8.4 Cancer therapy	24
	1.9 Outline of the thesis	25
	References	28
Chapter 2	Bottom-up biosynthetic approach to synthesize Metal Oxides nanoparticles	43
Chapter 2A	Structure and microbial synthesis of sub-10 nm Bi₂O₃ nanocrystals	
	2.1.1 Introduction	48
	2.1.2 Experimental Details	50
	2.1.3 Morphological features of <i>Fusarium oxysporum</i>	50
	2.1.4 Results and Discussions	51
	2.1.4.1 TEM and SAED analysis	51
	2.1.4.2 HR-TEM analysis	52
	2.1.4.3 X-ray diffraction analysis	53
	2.1.4.4 FTIR analysis	55
	2.1.4.5 X-ray photoelectron spectroscopy (XPS) analysis	55
	2.1.4.6 Energy dispersive analysis of X-rays (EDAX) measurements	57
	2.1.4.7 TGA analysis	57
	2.1.5 Conclusions	58
	References	60

Chapter 2B	Fungus mediated synthesis of protein capped CrO₂ nanoparticles	
	2.2.1 Introduction	64
	2.2.2 Experimental Details	66
	2.2.3 Morphological features of <i>Trichothecium</i> sp.	67
	2.2.4 Results and Discussions	67
	2.2.4.1 TEM and SAED analysis	67
	2.2.4.2 HR-TEM analysis	69
	2.2.4.3 X-ray diffraction analysis	69
	2.2.4.4 X-ray photoelectron spectroscopy (XPS) analysis	70
	2.2.4.5 FTIR analysis	73
	2.2.4.6 UV-visible spectroscopic analysis	74
	2.2.4.7 TGA analysis	75
	2.2.4.8 Energy dispersive analysis of X-rays (EDAX) measurements	76
	2.2.4.9 Magnetic measurements	76
	2.2.5 Conclusions	78
	References	80
Chapter 2C	Fungus based synthesis of Mn₅O₈ nanoparticles	
	2.3.1 Introduction	85
	2.3.2 Experimental Details	87
	2.3.3 Results and Discussions	88
	2.3.3.1 TEM analysis	88
	2.3.3.2 HR-TEM and SAED analysis	89
	2.3.3.3 X-ray diffraction analysis	90
	2.3.3.4 FTIR analysis	91
	2.3.3.5 UV-visible spectroscopic analysis	92
	2.3.3.6 TGA analysis	94
	2.3.3.7 Energy dispersive analysis of X-rays (EDAX) measurements	94
	2.3.3.8 X-ray photoelectron spectroscopy (XPS) analysis	95
	2.3.3.9 Magnetic measurements	97
	2.3.4 Conclusions	99
	References	101
Chapter 3	Bottom-up biosynthetic approach to synthesize Bismuth sulphide nanoparticles	
	3.1 Introduction	106
	3.2 Experimental Details	109
	3.2.1 CT contrast study	109
	3.2.2 Radiolabelling of Bismuth sulphide (Bi ₂ S ₃) nanoparticles with Tc-99m	110

	3.2.3 Radiochemical purity (RCP)	110
	3.2.4 Biodistribution of radiolabelled nanoparticles	110
	3.3 Results and Discussions	110
	3.3.1 UV-visible spectroscopic analysis	110
	3.3.2 Photoluminescence (fluorescence) spectroscopic analysis	112
	3.3.3 TEM, HR-TEM and SAED analysis	113
	3.3.4 X-ray diffraction analysis	114
	3.3.5 TGA analysis	115
	3.3.6 FTIR analysis	116
	3.3.7 X-ray photoelectron spectroscopy (XPS) analysis	116
	3.3.8 Energy Dispersive Analysis of X-rays (EDAX) analysis	118
	3.3.9 CT Contrast analysis	119
	3.3.10 Radiolabelling and Biodistribution studies	120
	3.3.10.1 Complex formation study	120
	3.3.10.2 Biodistribution & Gamma Scintigraphic imaging of ^{99m}Tc - Bi_2S_3 nanoparticles in normal rat	120
	3.4 Conclusions	122
	References	123
Chapter 4	Top-down bio-milling technique for the size reduction of chemically synthesized BiOCl nanoplates	
	4.1 Introduction	127
	4.2 Experimental Details	130
	4.3 Results and Discussions	130
	4.3.1 Visible analysis	130
	4.3.2 TEM and SAED analysis	131
	4.3.3 HR-TEM analysis	134
	4.3.4 X-ray diffraction analysis	135
	4.3.5 FTIR and PAGE analysis	137
	4.4 Conclusions and future perspectives	138
	References	141
Chapter 5	General discussion and conclusions	
	5.1 Summary of the work	144
	5.2 Scope for future work	147
Appendix I	Instrumental details	149
Appendix II	List of publications	151
Appendix III	List of abbreviations	152

ABSTRACT

The surge in nanotechnology research has been attributed to the interesting properties of the nanoparticles that make them more versatile than their bulk forms for applications in diverse fields such as electronics, optics, catalysis, sensing, diagnostics, therapeutics and biomolecular imaging. Synthesis of stable nanoparticles has thus always been a challenge to material scientists over the years. For the synthesis of nanoparticles, many physical and chemical methods have been developed but the physical process required for synthesis of nanoparticles could be expensive and cumbersome while the chemical processes can be potentially toxic. An alternative to these processes could be biological synthesis protocols. Biological methods for synthesis of inorganic nanoparticles promise to be environmentally benign and cost effective with potential use in large-scale synthesis. These methods can overcome the problems of high pressure, temperature, extreme pH conditions, the requirement of hazardous chemicals, solvents and the expensive organometallic precursors that are usually associated with the chemical synthesis methods. The biologically synthesized inorganic nanomaterial surfaces are inherently capped by proteins and other biomolecules which not only facilitate further linking to other ligands but also provide the much needed surface passivation alongwith prevention from agglomeration and stable suspension in the aqueous medium; which often is difficult to attain by the wet-chemical approaches.

In the present thesis, we have explored a fungi mediated biological approach toward the synthesis of inorganic nanomaterial and an attempt has been made to design biological methods for the synthesis of complex transition metal oxide and metal sulphide nanoparticles. There are basically two different biosynthetic approaches for the synthesis of chemically difficult to synthesize nanoparticles: the “bottom-up” and the “top-down” approach.

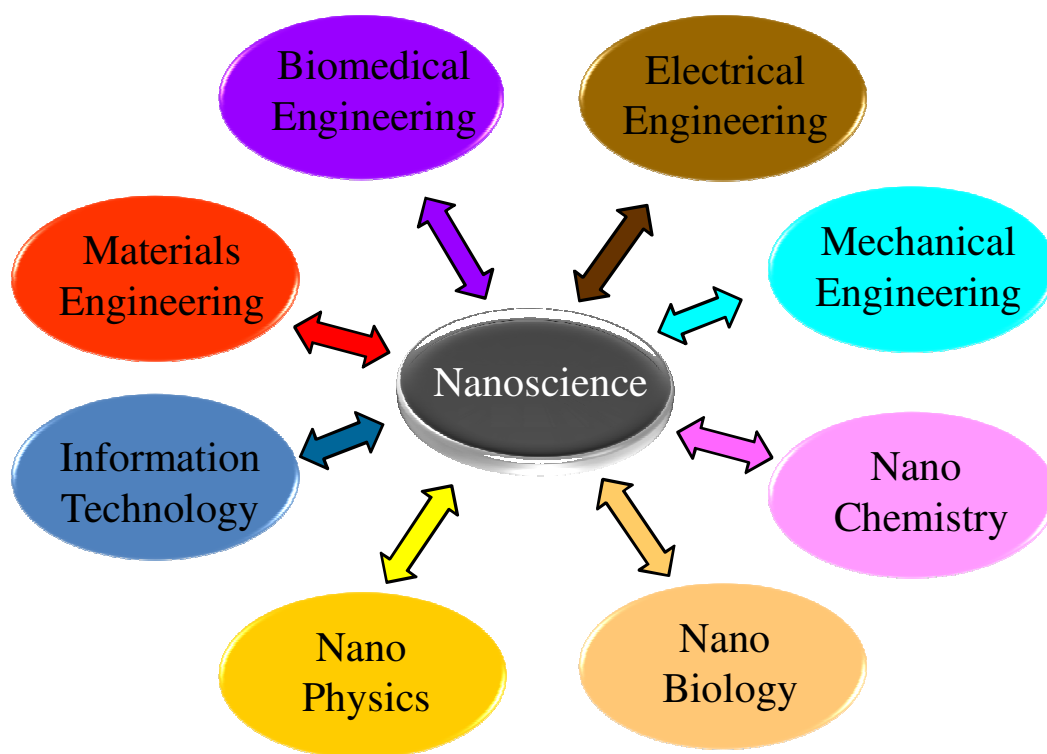
In the first approach (bottom-up), we demonstrate that the fungal biomass is capable of synthesizing some difficult phase of transition metal oxide and metal sulphide nanoparticles at room temperature by reacting the metal ion salts such as acetate, nitrate and chromate with the fungus *Fusarium oxysporum* and *Trichothecium* sp. We observed that the mesophilic fungus *Fusarium oxysporum*, on exposure to chemical precursors like bismuth nitrate is capable of synthesizing Bi_2O_3 nanoparticles having particle size 5-8 nm and similarly after reacting with manganese(II)acetate

tetrahydrate, synthesis of Mn_5O_8 nanoparticles of an average particle size of around 10-11 nm occurs. Magnetic measurements observed in the Mn_5O_8 particles show antiferromagnetic behavior. Furthermore, nanocrystalline chromium dioxide (CrO_2) was synthesized by using the fungus *Trichothecium* sp. and potassium dichromate ($\text{K}_2\text{Cr}_2\text{O}_7$) was used as precursor salt. These nanoparticles have particle size in the range of 21 to 25 nm and show ferromagnetic behavior.

Further, we have extended the same approach to synthesize bismuth sulphide (Bi_2S_3) nanoparticles using fungus *Fusarium oxysporum* alongwith bismuth nitrate ($\text{Bi}(\text{NO}_3)_3 \cdot 5\text{H}_2\text{O}$) and Na_2SO_3 as a precursors. The Bi_2S_3 nanoparticles thus formed show semiconductor behavior. These Bi_2S_3 nanoparticles were used in SPECT-CT probe for small-animal imaging. These were injected into rats and biodistribution image and clearance time from the blood was calculated.

In the second approach (top-down), we report the bio-milling of chemically synthesized BiOCl nanoplates using the alkalo-tolerant thermophilic fungus *Humicola* sp. In this, we show that the fungal biomass can be used to break-down the chemically synthesized larger particles (200-250 nm) into particles as small as 5-6 nm while maintaining their crystallinity and phase at the nanolevel. We have named this technique as “bio-milling”. We believe that this technique can be used to synthesize several oxides nanoparticles whose synthesis in the size less than 10 nm by conventional wet chemical methods is difficult.

Chapter 1



General Introduction

This chapter is an introduction to the thesis and gives a brief overview of the complexity involved in the understanding of nature and therefore, the importance of interdisciplinary research. It includes a brief introduction about nanotechnology and historical perspective of nanoscience. It also reveals the significant properties of nanoparticles, parameters that could alter nanoparticle properties, followed by the various synthesis methods and approaches to reach the nano level, and also its wide applications in different fields have been discussed. This chapter also gives emphasis on the biomineralization of inorganic materials, alongwith a brief overview of the biosynthesis of inorganic materials occurring naturally and rationale behind the biological method that we have used for the biosynthesis of inorganic nanomaterials. Finally, an outline of the chapter-wise work described in this thesis has been presented.

Nanotechnology is the ability to control, measure and manipulate matter on the atomic and molecular scale so as to exploit its properties and functions. In other words, nanotechnology is the creation of functional materials, devices and systems through control of matter on the nanometer length scale, exploiting novel phenomena and properties (physical, chemical and biological) present only at that length scale. The prefix "nano" comes from the Greek word *nanos* meaning "dwarf", which is a billionth of a meter (10^{-9}), which is equal to the length of ten hydrogen atoms or about one hundred thousandth of the width of a hair [1]. The nanoscale marks the nebulous boundary between the classical and quantum mechanical world. The term is given to those areas of science and engineering where phenomena taking place at the nanometre scale are utilized in the designing, characterization, production and application of materials, structures, devices and systems. It should be appreciated that nanotechnology is not in itself a single emerging scientific discipline but rather a meeting point of traditional sciences like chemistry, physics, biology and material sciences to bring together the required collective knowledge and expertise required for the development of these novel technologies [2]. Nanotechnology is expected to impact a large spectrum of existing technologies (examples include chemical, electronic, healthcare, polymer and defense industries) as well as initiate many new applications. The global market for nanotech products is expected to reach 1-2 trillion \$ by the year 2015 and is currently growing at a very robust rate. While high-tech applications and emerging markets (particularly biotech and IT sectors) are still the focus of many nanotech start-ups, the percentage of companies producing and selling made-to-order nanomaterials is steadily increasing.

Nature has been engaged in its own infinite and incredible miniaturization project since the dawn of life, billions of years ago. Nature has refined ingenious ways of creating the most efficient miniaturized functional materials. The field of nanoscience and nanotechnology has developed its own tools to observe nature and developed a motivation to create functional miniaturized structures and manipulation of materials at similar length scale, an art perfected by nature. In the process of miniaturization, several significant achievements have been accomplished and structures of micron and nanodimensions can now be routinely fabricated, even though control at complexity levels manifested by nature is still a distant goal. Figure 1.1 shows the

comparison between relative sizes of various naturally occurring objects and man-made materials at different length scales.

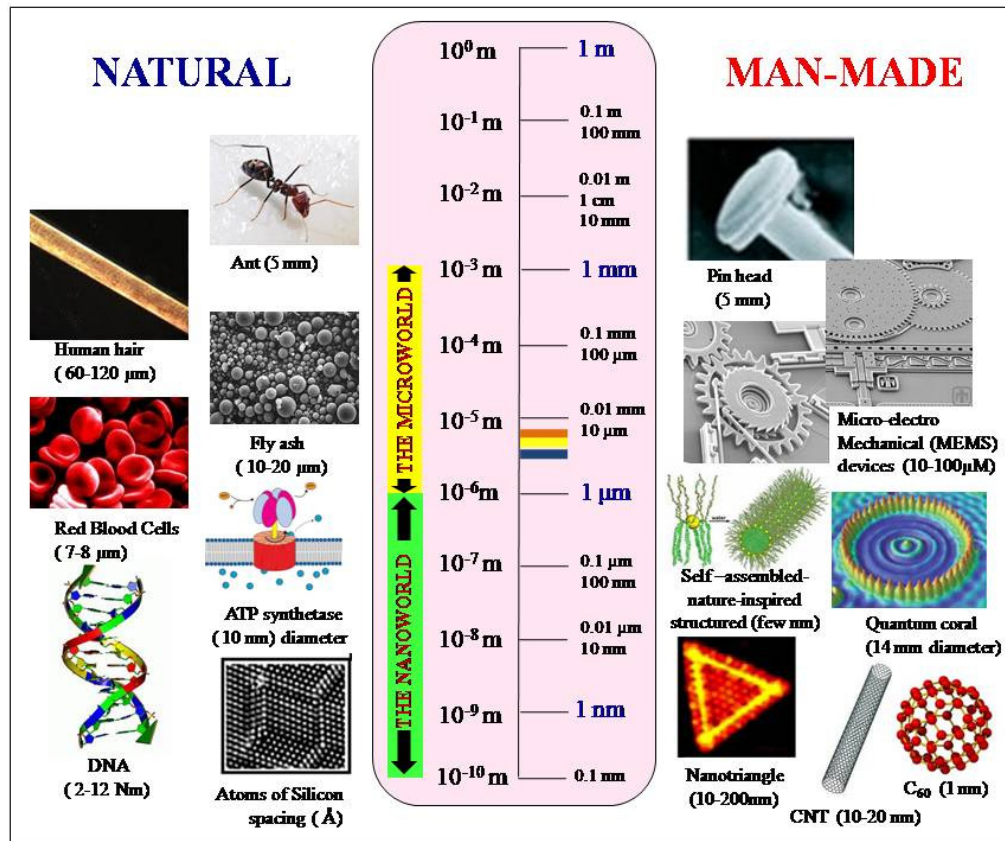


Figure 1.1: Picture representing the relative sizes of various naturally occurring objects/species and man-made materials. (Images courtesy: Josh Wolfe's report on Nanotechnology, www.forbeswolfe.com and various sources at <http://images.google.com>)

In order to reach this goal, researchers are trying to follow both “top-down” [3] and “bottom-up” [4] approaches. The top-down method begins with large homogenous objects and removes materials as needed, to create smaller-scale structures. Similar to the work of a sculptor in carving a face from a block of marble, this approach is epitomized by lithography techniques, the cornerstones of microelectronics fabrication. Laser induced chemical etching and ball-milling fall into this category. On the other hand, bottom-up approach involves putting together smaller components (such as individual atoms and molecules) to form a larger and more complex system by leveraging naturally occurring chemical, physical and biological processes.

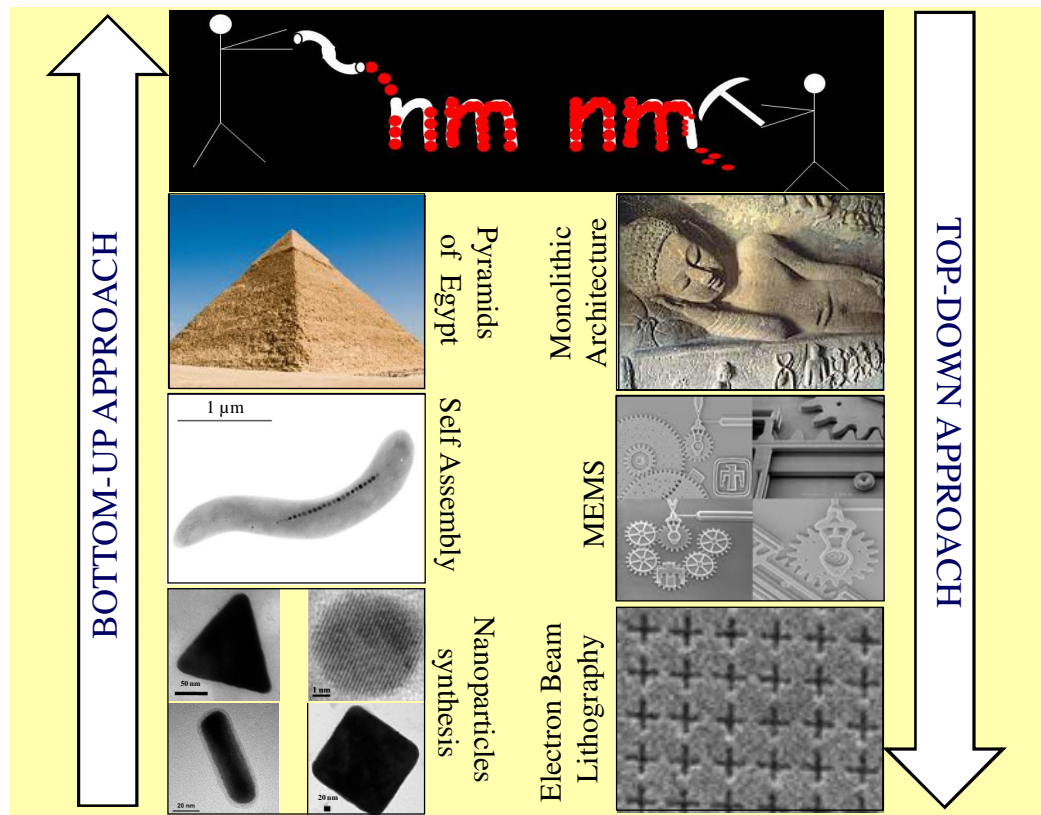


Figure 1.2: Cartoon showing the fabrication of materials by the top-down and bottom-up approaches. The monolithic architecture shown in the cartoon is a lord Buddha statue at Ajanta caves, India. (Images courtesy: idea to making cartoon for making bottom-up and top-down approach taken from the book “Nanochemistry” by G. A. Ozin and Arsenaul. Images for MEMS obtained from Sandia National Laboratories (SUMMITTM Technologies, www.mems.sandia.gov). The images of electron beam lithography, and magnetosomes self-assembly in magnetotactic bacteria *Magnetospirillum magnetotacticum* have been taken from various sources at <http://images.google.com>).

1.1 Historical Perspective

Mother Nature, for billions of years has been utilizing nanotechnology cleverly. Nanoparticles have been around for a long time and exposure of mankind to the nano-world is not new. In 1570, for the first time, nanoparticles were acknowledged with aurum potable (potable gold) and luna potable (potable silver) which were used as elixirs by the alchemists [5]. Research and applications of nanotechnology are not new at all. In earlier days, colloidal gold and silver had been used for staining glasses like “Purple of Cassius”, a colloid with heterocoagulation of gold nanoparticles and tin oxide [6-7]. Another famous and oldest example is that of the Lycurgus cup of 4th century AD which presently resides at the British Museum, London. The beauty of this

cup is that it looks red in transmitted light and green in reflected light, which is because the cup contains silver and gold nanoparticles [8]. There are various other applications of nanotechnology which were in use for many centuries, such as healing sols of gold and silver in traditional medicine [5]. Nanoparticles were also used in colouring the window panes of chapels and palaces [9- 10]. After a long course of time, in 1857, Michael Faraday for the first time synthesized deep red coloured solution of gold nanoparticles by reduction of an aqueous solution of chloroaurate ions using phosphorus in CS₂ [11]. Soon after that, in 1861, Thomas Graham coined the term “colloid” for suspended particles in liquid medium [12]. Significant contributions also came from research by R. A. Zsigmondy (1895-1925) in the field of colloidal chemistry, who for the first time used the “nanometer” scale clearly to measure the particle size [13]. The first seeds of nanotechnology were sown by the brilliant Nobel Laureate physicist Richard Feynman in his famous 1959 lecture entitled “**There's plenty of room at the bottom**” in which he first proposed that the properties of materials and devices at the nanometer range would present future opportunities and it is now considered to be the foundation for modern nanoscience research [14]. During recent developments in 1974, Norio Taniguchi coined the term “Nanotechnology” [15]. Further inventions like quantum dots [16], discovery of fullerene (C₆₀) [17], carbon nanotubes [18], graphene [19] and advent of scanning probe microscopy [20] gave milestones to nanoscience research. In 1980's, the basic idea of nanotechnology was explored in much more depth and reached greater public awareness due to the efforts of Dr. Eric Drexler who promoted the technological significance of nanoscale phenomena and devices through his speeches and his book entitled “Engines of Creation-The coming era of Nanotechnology and Nanosystems” and so the term acquired its current sense. Nanotechnology today is set to bring about a revolution in almost all fields of science. The progress has been made possible by the emergence of tools and technologies that have made visualization and manipulation of nanoparticles possible.

1.2 Properties of nanomaterials

Materials reduced to the nanoscale can suddenly show unique properties. These novel properties have thrown open avenues for new technologies and applications that were not achievable with bulk materials. There are numerous reasons why size reduction

can in principle, affect behaviour of materials. The important changes which occur when bulk objects are converted to nanosized particles are as follows: nanoparticles have a very large surface area to volume ratio, large surface energy, disturbed coordination number, random molecular motion, reduced imperfection and quantum effects.

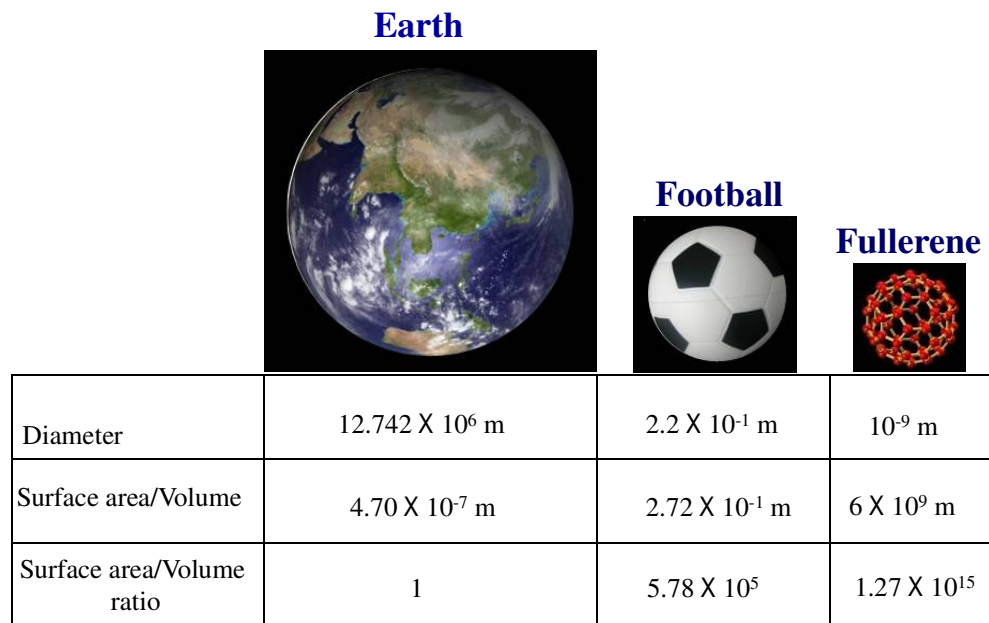


Figure 1.3: Picture representing the relative sizes and surface area/volume ratio of the earth, a football and a fullerene molecule (Images courtesy: Various sources at <http://images.google.com>).

The most apparent change resulting from the size reduction is the enormous increase in the surface-to-volume ratio of nanoparticles which increases the percentage of surface atoms and further surface energy will increase, which makes the surface of the nanoparticles highly active. A schematic representation is shown in Figure 1.3. So, as the size of the particle decreases, the surface effects become more prominent. For example, iron nanoparticles of sizes 3 nm, 10 nm and 30 nm will have 50 %, 10 % and 5 % of atoms on surface [21]. There are other factors that can strongly regulate nanoparticle properties including their shape [22], surface composition [23], dielectric environment of the particle [24] and their interparticle interactions [25]. In nano-regime, particles show unusual behavior in comparison to their bulk state because they are comparable to the de Broglie wavelength of the charge carrier, and their high

surface area to volume ratio [26]. The following section briefly discusses the changes in the properties of the nanoparticles of nanometer size.

1.2.1 Catalytic properties

Catalysis is a surface phenomenon, and for a given material the available surface area directly governs its catalytic efficiency. The increment of catalytic activity with size can be rationalized on the basis of the increasing surface to volume ratio, or number of atoms at the surface increase tremendously with decreasing particle size, since the surface atoms are more active due to the presence of unsaturated co-ordinations or dangling bonds [27, 28]. For example, bulk state gold is considered to be a noble metal but the nanoparticles of gold are observed to be excellent catalysts for the oxidation of carbon monoxide [29]. Thus, the reduction in the size of the particles renders them as excellent catalysts [30]. Besides this, the shape of the nanostructures plays an important role in catalytic properties. Their shape regulates the surface reactivity because reacting species show different adsorption affinity towards different faces of the catalyst [31].

1.2.2 Lattice parameters

Due to higher surface to volume ratio, considerable lattice contraction is observed in nanoparticles, which increases with the decrease of particle size [32]. The lattice contraction or lattice strain is generated due to the hydrostatic pressure on the surface induced by the intrinsic surface stress. We know very well that as particle size decreases, surface energy of nanoparticle increases, due to the large percentage of the atoms exposed to the surface. The increase in surface energy further induces the stress, which is responsible for elastic contraction of the lattice parameter.

1.2.3 Melting point

Nanoparticles have lower melting temperatures as compared with their bulk forms. As most of the atoms are situated on the surface of smaller particles and they have an access to free energy due to the large number of unsaturated bonds, the melting point also decreases with decreasing particle size. It is supposed that the surface atoms are more susceptible to thermal displacement and initiate the melting process due to their lower coordination. Since it decreases the co-ordination number of atoms and atoms on the surface can be easily rearranged than those atoms present inside the nanoparticles. Such a surface melting process is thought to be the major cause for the lowering of melting point [33].

1.2.4 Optical Properties

The reduction to nanomaterials dimensions has pronounced effects on their optical properties. Optical properties are most significant for noble metal nanoparticles (gold and silver) and semiconductors. These properties are dependent on composition, size, shape and surrounding medium of the nanoparticles [34]. In metal and semiconductor nanoparticles, size and shape dependent optical properties arise due to quantum confinement. As the particle size decreases, electronic structure is altered from continuous electronic bands to discrete or quantized electronic levels because of which discrete optical transitions between the electronic bands or increase in energy level spacing occurs [35]. Optical properties are more meaningful for the noble metal nanoparticles (gold, silver, etc.), as dispersion of the nanoparticles results into beautiful colours [36]. The optical properties of metal nanoparticles can be attributed to the phenomenon of surface plasmon resonance (SPR), which arises due to the coherent excitation of all the free electrons within the conduction band in response to the alternating electric field of incident electromagnetic radiation. In 1908 Mie *et al.* explained this phenomenon on the basis of Maxwell's equations on scattering [37]. In spite of that, noble metal nanoparticles possess plasmon resonances in the visible spectrum, which gives rise to such intense colours.

1.2.5 Mechanical properties

The mechanical properties of materials increase with a decrease in size. Mechanical strength of the material depends on several parameters such as impurities, dislocations, etc. Generally, imperfections such as dislocations, micro-twins, impurities, etc. lead to less mechanical strength. So nanomaterials like nanowires and nanorods exhibit more mechanical strength due to the smaller cross-section, due to which there is a lesser probability of any imperfection, as nanoscale dimension permits the elimination of such imperfections [38].

1.2.6 Magnetic properties

Nanomaterials show novel magnetic properties [39]. They show distinctly different magnetic behavior as compared to that of bulk materials. The bulk ferromagnetic materials usually form multiple magnetic domains; but at nanoscale, the ferromagnetic particles form single domains; with large single magnetic moments. When the particle size reduces below a certain limit, ferromagnetic particles become

unstable, since increase in surface energy provides sufficient energy for domains to spontaneously switch polarization directions as a result of which ferromagnetic particles turn to paramagnetic ones. However, nanometer sized ferromagnetic turned to paramagnetic particles behave differently from the conventional paramagnetic and are referred to as super paramagnetic [40]. In case of superparamagnetism, magnetizations of the particles (or magnetic spin) are randomly distributed and they are aligned only under an applied magnetic field, and the alignment disappears once the external field is withdrawn. These particles do not show hysteresis in magnetization, since there is only one domain per particle. In short, we can say that ferromagnetism of bulk material disappears and gets transferred to superparamagnetism in nanoscale due to high surface energy.

So, it is clear from the above discussion that nanoparticles have these unique and interesting properties which can lead to a large number of important applications in innumerable fields. Nanoscience and nanotechnologies incorporate exciting areas of research and development at the interface between biology, chemistry and physics. They are widely seen as having huge potential and are attracting substantial and increasing investments from governments and from industrial companies in many parts of the world. Today, nanotechnology has been used in not just developing new techniques and tools but has also played a crucial role in improving the existing technologies. In present day, the application of nanomaterials extends to wide ranging areas such as diagnostic tools [41], therapeutic agents [42], sensors [43], catalysts [44], solar cells [45], cosmetics [46], drug/gene delivery vehicles [47], surface enhanced Raman Spectroscopy [48], fuel cells [49], photonic band gap materials [50], single electron transistors [51], nonlinear-optical devices [52], plasmonics devices [53], coating materials [54], cell labeling and imaging [55], optoelectronics [56], information storage [57], chemical/optical computers [58], improved national security [59], refrigeration [60], self cleaning paints [61] and environmental clean up [62] to list a few.

1.3 Synthesis of Nanomaterials

The area of nanotechnology, which includes the synthesis of nanoscale matter, understanding/utilizing properties, and organization of nanoscale structures into predefined superstructures promises to play an increasingly important role in many

ultimate technologies. Since the nanoparticles possess remarkable attention-grabbing properties, to develop new procedures for the synthesis of nanoparticles is now an essential aspect of nanoscience. Nanoparticles can be synthesized in many ways. Important criteria for the synthesis of nanoparticles are control over size, shape, surface functionalities and various properties of nanoparticles. In recent times, formulation of inorganic nanoparticles have been demonstrated by various physical, chemical and biological means. Different methods that comprise these routes have been summarized in figure 1.4. Some of the physical routes leading to successful synthesis of nanoparticles were achieved through Spray pyrolysis [63], photoirradiation [64], radiolysis [65], ultrasonication [66], solvated metal atom dispersion (SMAD) [67], laser ablation [68], vapor deposition [69], thermal decomposition [70], electrochemical methods [71], chemical vaporization [72], physical vaporization [73], electrospinning [74], lithography [75], sputtering [76], etc. However, chemical routes are most commonly practiced, have an easy route and have received huge attraction for the synthesis of nanoparticles due to a better control over the size and shape of nanoparticles. Inorganic nanoparticles such as metals, metal oxides and semiconducting nanoparticles can be synthesized chemically by reduction or oxidation of metal ions, or by the precipitation of the necessary precursor ions in the solution phase.

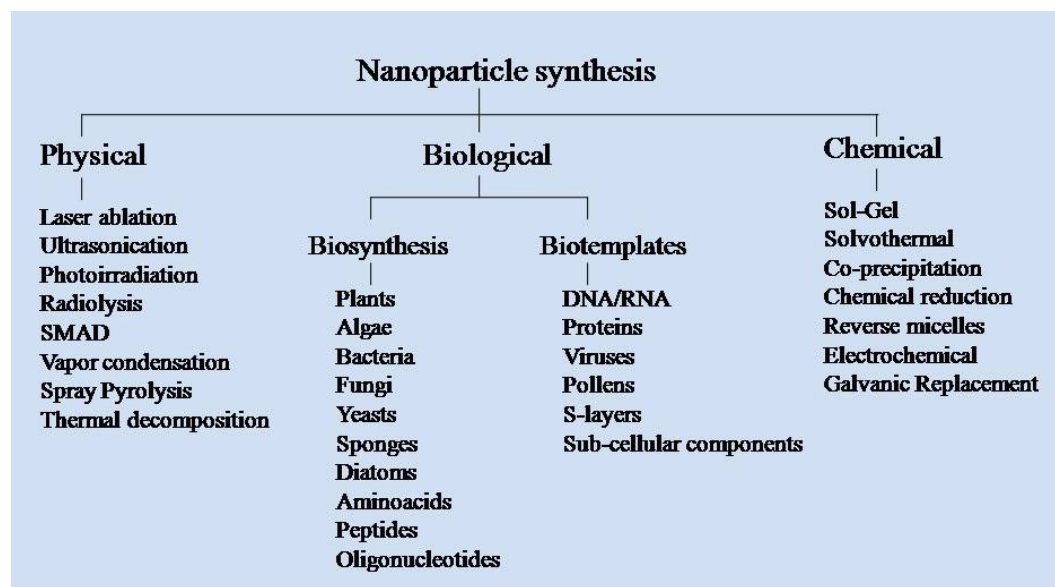


Figure 1.4: Schematic outline of the various approaches for the synthesis of nanoparticles

The control of size, shape, stability and the assembly of nanoparticles have been achieved by using different capping agents, solvents and templates. Various types of capping agents have been used ranging from ions [82] to polymeric molecules [83] and even biomolecules [84]. In chemical route as a solvent, either water or non-aqueous organic solvents [85] have been used for the synthesis of nanoparticles. Besides this, a few reports are also available on the synthesis of nanoparticles in ionic liquids [86] and supercritical fluids [87]. The choice of solvent for the synthesis of nanoparticles depend on the signified application of the nanoparticles. The control of size, shape and stability of nanoparticles can be attained by different capping agents and templates. Likewise, different templates such as micelles [88], polymers [89], mesoporous materials [90], carbon nanotubes (CNTs) [91], biomolecules [92], microorganisms [93] and many more have been used to ease control over the synthesis of desired size, shape and assembly of nanoparticles.

So, it is clear from the above mentioned synthesis procedures that inspite of the success in achieving excellent result in control over shape, size and crystallinity, these methods involve the use of hazardous reagents, volatile solvents and physico-chemical conditions along with the high cost factor involved in maintaining temperatures and pressures. There are efforts to reduce or eliminate hazards involved in this process to human health and the environment through the research on the alternative synthesis methods by learning from the nature. Therefore, it is necessary to develop environmental friendly green chemistry based methods for the synthesis of nanoparticles. Biological sources are a good choice as an environment friendly approach for the synthesis of nanoparticles under ambient conditions of temperature, pressure and pH. Biological synthesis of nanomaterial has been shown to have several advantages over chemical synthesis including high productivity and low cost and protein/biomolecules restrict the growth of particles over nanometer dimensions and thus act as capping/stabilizing agents. On the other hand, these biomimetic approaches employ biological means like microorganisms (fungus, bacteria), biomolecules (DNA, proteins, enzymes, etc.), where the microbes participate via reduction, oxidation or hydrolysis of the transition metal ion precursors and also by acting as templates. The as-synthesized nanomaterial surfaces are inherently functionalized by proteins and other biomolecules which not only facilitates further linking to other ligands but also provides the much needed surface passivation, prevention from agglomeration and

stable suspension in the aqueous medium which often is a nightmare in the wet-chemical approaches. In the next sections of this chapter, we will discuss the biosynthetic approach to synthesize nanomaterials with a brief introduction of bio-nanotechnology, overview of biomineralization with an example of biomineralization in natural environment, biomimetic approaches for mimicking natural biomineralization and finally how we can emulate and follow the nature's way of biomineralization in laboratory.

1.4 Bio-nanotechnology

Bio-nanotechnology, as the name suggests, is a marriage of nanotechnology and biotechnology. In other words, we can say that nano-biotechnology is the unification of biotechnology and nanotechnology. Nano-biotechnology is the branch incorporating biology along with nanotechnology in order to cater the needs of living beings. This hybrid discipline can also mean making atomic-scale machines by imitating or incorporating biological systems at the molecular level, or building tiny tools to study or change natural structure properties atom-by-atom. The potential opportunities offered by this interface are truly outstanding and great expectations are held in the areas of prevention, diagnostic, drug discovery and treatment. Bio-nanotechnology is concerned with molecular scale properties and applications of biological nanostructures and as such it sits at the interface between the chemical, biological and the physical sciences. Bio-nanotechnology seeks to modify and find technological uses of natural nanocomponents and often studies existing elements of nature in order to fabricate new devices. So, in short we can conclude [94] that nanotechnology provides the tools and technology platform for transformation and investigation of biological systems, and biology offers inspirational models and bio-assembled components to nanotechnology.

1.5 Lessons from nature for nanomaterial synthesis

There is a long history of gaining inspiration from nature's biological structures to design practical materials. Nature knows very well how to build extremely specialized materials, which are constructed, indeed engineered, to exert specific biological functions [95]. The morphological diversity and complexity of naturally occurring forms and patterns has been the motivation for mankind to simulate nature and to adapt the ideas from nature to attain functional values [96]. Scientists have long been

inspired by the beautiful structures and functional properties of the materials formed within living organisms. The wide variety of biological system encourages researchers to build up modified syntheses protocols derived from nature. Hence, their findings have been successfully organized into the area of biomimetics or bioinspired research, which provides alternative approaches towards synthesis of nanomaterials with technological applications [97]. In nature, there are ample of examples of multifunctional materials, devices and systems that researchers and engineers could investigate based upon their synthesis, function and their practical utility in everyday applications [98]. So, after learning from nature, in this thesis there is an effort to synthesize inorganic nanomaterials using fungi.

1.6 An Overview on Biomineralization

Biomineralization can be defined as the process by which living organisms produce minerals, often to harden or stiffen existing tissues. More simply we can say that biomineralization represents the formation of inorganic solids by living organisms. Evolution on earth has resulted in the appearance, diversification and proliferation of organisms capable of producing complex structures from hard inorganic materials *via* processes collectively known as biomineralization [99]. The process of biomineralization is very common in biological world and mediated mostly by plants and animals. Unicellular organisms such as bacteria and algae are also capable of synthesizing inorganic nanomaterials, both intracellularly and extracellularly. Till date around 60 biominerals have been identified, most of which comprise silicates, iron oxides, calcium carbonates, calcium phosphates, or sulfides [100]. For example Magnetite (Fe_3O_4), which is naturally found in the magnetosomes of magnetotactic bacteria or other iron - reducing bacteria, is a well accepted example of controlled biomineralization that nature is able to synthesize [101]. In magnetite (Fe_3O_4), nanocrystals are aligned with the Earth's geomagnetic field and help the aquatic animals as a biomagnetic compass during migration [102]. CaCO_3 is one of the most abundant biominerals formed by living organisms. CaCO_3 based biomaterials such as nacre of mollusc shell and coccoliths have complex structures of nano to submicron length scales. Remarkably, the molluscs produce shells that contain a distinct crystalline form of calcium carbonate such as aragonite, or may contain segregated layers of calcite and aragonite [103]. In another famous example of calcium

carbonate, fishes grow structures known as otoliths or “ear stones” within the inner ear that assist in inertial sensing. These otoliths are composed of the aragonite polymorph of calcium carbonate [104]. In addition to the crystalline forms of calcium carbonate, an amorphous phase of this mineral is synthesized by sea urchins to produce spines (spicules) [105]. In case of marine sponges, silica spicules are produced that have been demonstrated to possess light-guiding characteristics and may reach lengths up to 3 m. Similarly, diatoms are a type of unicellular eukaryotic algae which develop frustules which are intricately detailed silica cell walls that are organized over multiple length scales [106]. Beside this, mammals and birds are good examples for biominerals formed via the precipitation of calcium-based materials. Alike silica, magnetite and calcium carbonates, biomineralization of MnO_2 and gypsum has been shown to occur on the S-layer of photosynthetic bacteria [108] and the occurrence of zinc-iron sulphide within the body of hydrothermal vent worms *Alvinella pompejana* [108]. Figure 1.5 shows images of some of the above mentioned exquisite structures obtained by biologically controlled synthesis of nanomaterials in biomineralization process.

Biomineralized synthesis materials have been studied in great detail and in each of the examples listed above, specialized biomolecules have been found, or are thought to play a major role in directing the formation of these often complex inorganic structures and we also found that minerals, macromolecules and water are the major components of these biomaterials. During this process, inorganic phases and inorganic materials grow within or on the organic matrix or vesicles inside the cell and the organisms maintain a nice control over the composition, grain size, habit and intracellular or surface location of the produced minerals.

Biominerals play an important traditional role as critical structural components of organisms like teeth, the siliceous shell of diatoms and most of the important ion reservoirs for cellular function like Ca^{2+} and bone. These biominerals have highly evolved functional roles and magnetotactic sensing, buoyancy and balance regulation are a few examples which we have already discussed in the above section. Another interesting aspect of biominerals is that they play an important protective role and help in detoxification in certain organisms. Thus organisms starting from protozoa to eukaryotes apply principles of biomineralization (cellular processing, supramolecular organization, and interfacial recognition) to form materials such as Abalone nacre to

efficiently remove potentially toxic species from their immediate environment. Hence, nature translates us as to how biological systems maintain nanoscale control over structural biominerals, and has unveiled the biomimetic routes to novel materials synthesis.

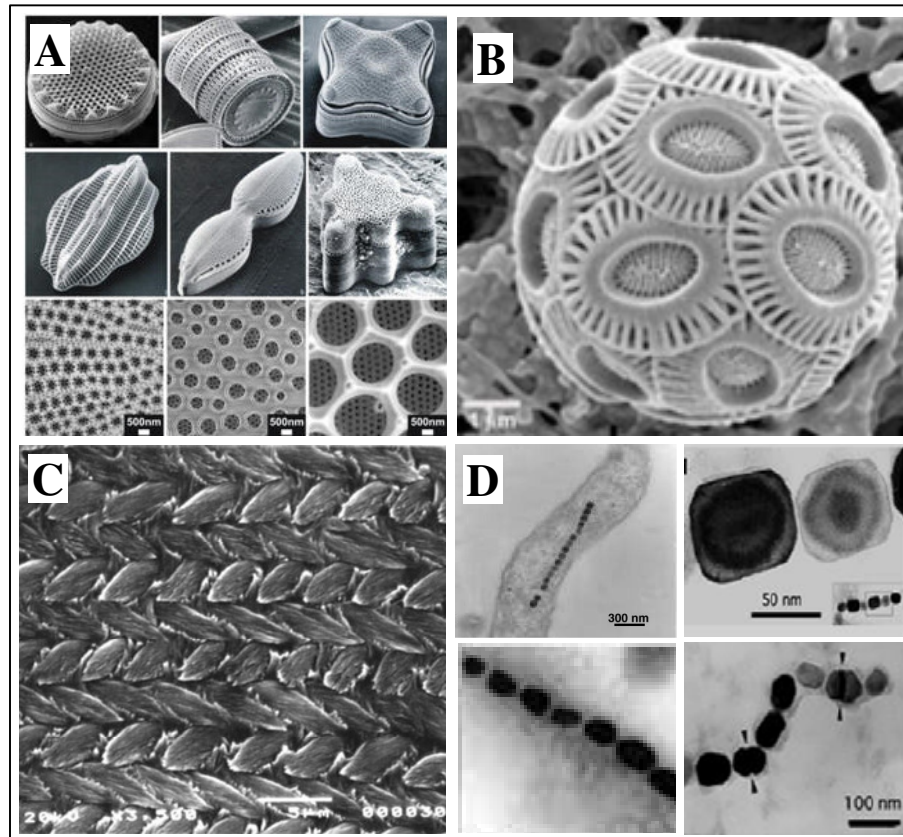


Figure 1.5: Images of various inorganic nanomaterials obtained by biologically controlled synthesis. (A) Diatomic silica (B) Calcareous structures in coccolith (C) Intricately architected mouse incisor tooth has enamel rods and (D) Magnetite nanocrystals from magnetotactic bacteria. (Image courtesy: Various sources at <http://images.google.com> and reference [109]).

Large variety of minerals are synthesized in nature and they can be traced to various groups of organisms including plants, animals and microorganisms listed in table 1.1. Since we know very well that these composite materials consist of an inorganic component and an organic matrix which comprises of biomacromolecules like proteins, lipids or polysaccharides which mainly control the morphology of the inorganic compound, it was found that most of these macromolecules have similar functional groups. They are rich in carboxylate groups and in addition to it have

phosphate and sulfate groups. The presence of all these charged groups makes these macromolecules excellent candidates for interacting with the mineral ions in solution or with the surfaces of the solid phase.

Table 1.1 Various biominerals and their roles in biological systems

Biogenic minerals	Biological System	Biological location	Biological function
Calcium carbonate (calcite, vaterite, aragonite)	Plants, aves, mammals, many marine organisms, coccoliths	Mollusc shell, eye lens, crab cuticle, egg shells, leaves, inner ear	Exoskeleton, optical, mechanical strength, protection, gravity receptor, buoyancy device, calcium storage
Calcium phosphate (hydroxyapatite, dahllite, octacalcium phosphate)	Mammals, fish, bivalves	Bone, teeth, scales, gills, gizzard plates, Mitochondria	Endoskeleton, ion store, cutting/grinding, protection
Calcium oxalates (whewellite, wheddellite)	Plants, fungi, mammals	Leaves, hyphae, renal stones	Protection/deterrent, calcium storage/removal, pathological
Iron oxides (magnetite, greigite, goethite, lepidocrocite, ferrihydrite)	Bacteria, algae, dinoflagellates, chitons, trouts, euglena, human brain, salmons	Intracellular, teeth, head, filaments, ferritin protein	Magnetotaxis, magnetic orientation, mechanical strength, iron storage
Sulfates (gypsum, celestite, barite)	Jellyfish, acantharia, loxodes, chara, photosynthetic bacteria	Statoconia, cellular, intracellular, tatoliths	Gravity receptor, skeleton, gravity device/receptor
Silicon oxides (amorphous silica)	Diatoms, radiolarians, sponges, plants, microbes, etc.	Cell wall, cellular, leaves	Exoskeleton, protection, mechanical support, plant nutrient, resistance against pests and predators

Bioinspired research is based on identifying and emulating the principles of biomineralization in natural systems. After knowing the natural mechanism, scientists have to develop clean, green nanomaterials through biomimetic and biosynthetic approaches. One of the important aspect of biology is the ability of biomolecules to self assemble into supramolecular structures. Biological self-assembly occurs at the molecular scale and the shape and size of self assembled structures are controlled on the nanoscale. This intrinsic ability has stimulated the interest of scientists to develop a “bottom-up” approach to nanomaterial synthesis. Nature, like a good architect produces nanoparticles of various defined shapes and sizes using genetic control. We can exploit similar mechanisms to create nanoparticles using biological molecules or organisms. Hence, biomineral systems offer ample opportunity for the development of biomimetic strategies for the synthesis and processing of nanomaterials. Biological methods for synthesis of nanoparticles employ use of living organisms, molecules of biological origin such as peptides and biological templates such as DNA. The interest in inorganic nanoparticles is growing tremendously as they provide superior material properties with functional versatility.

1.7 Biological means for synthesizing nanomaterials

Nature has devised various processes for the synthesis of nano and micro scaled inorganic materials which have contributed to the development of relatively new and largely unexplored area of research based on the biosynthesis of nanomaterials. The development of reliable, eco-friendly processes for the synthesis of nanoscale materials is an important aspect of nanotechnology. It is only recently that microorganisms have been explored as potential biofactories for the synthesis of nanoparticles. These methods employ biological means like microorganisms (fungus, bacteria), biomolecules (DNA, protein, enzymes etc.), to reduce metal ions to form nanoparticles. It is feasible to synthesize nanoparticles at room temperature, neutral or mild pH and close to ambient conditions without the requirement of hazardous chemicals, solvents and expensive organometallic precursors which is not possible by any physical or chemical methods. This approach has brought a turning point in method of synthesis of nanoparticles. Heavy metal ions are toxic to the biological systems; hence microorganisms like bacteria, yeast and fungi detoxify these metal ions by reducing them into metallic state, which are nontoxic to them. The as-synthesized nanomaterial surfaces are inherently functionalized by proteins and other

biomolecules which not only facilitates further linking to other ligands but also provides much needed surface passivation, prevention from agglomeration and stable suspension in the aqueous medium which often is a nightmare in the wet-chemical approaches. Fungi are very good candidates for the development of extracellular processes as they secrete a variety of enzymes and are easy to grow and simple to handle.

Various nanomaterials from simple metals to more complex systems such as metal sulphides and metal oxides can be synthesized by the deliberate synthesis of nanomaterials using micro-organisms. The first of such report is probably by Klaus *et al.*, where they isolated an organism *Pseudomonas stutzeri* AG259 from silver mine and exposed it to Ag^+ ions. Formation of silver nanoparticles of well defined size and distinct morphology within the periplasmic space of the bacteria was seen [111]. Later on many such synthesis were reported, a few of which are listed here such as the intracellular synthesis of octahedral gold nanoparticles by *Bacillus subtilis* which has been reported by Beveridge *et al.* [112]. Konishi *et al.* reported an intracellular synthesis route of Au nanoparticles by Fe(III)-reducing bacteria *Shewanella algae* under anaerobic environment and in the presence of hydrogen gas [113]. Similarly Nair and Pradeep have demonstrated the formation of Ag, Au and Ag-Au alloy by exposing gold and silver ions to *Lactobacillus* strains isolated from buttermilk [114]. Yong *et al.* have demonstrated the synthesis of palladium nanoparticles ~20 nm in size using a bacterium *Desulfovibrio desulfuricans* [115]. Lengke and co-workers have also demonstrated extracellular and intracellular biosynthesis of platinum nanoparticles using cyanobacteria *Plectonema boryanum* [116]. Ahmad *et al.* have extensively studied the biosynthesis of nanoparticles of various compositions using bacteria and fungi as living nanofactories. In this attempt, fairly monodispersed gold nanoparticles were synthesized using the extremophilic actinomycete, *Thermomonospora* sp. [117], *Verticillium* sp. [118] and *Fusarium oxysporum* [119]. In another report, gold-silver alloy nanoparticles of varying compositions have also been synthesized using *Fusarium oxysporum* [120].

In addition to metal nanoparticles, several reports have been published dealing with the synthesis of semiconductor nanoparticles such as CdS, ZnS, etc. Dameron and co-workers intracellularly synthesized nanocrystalline CdS quantum dots using two different yeast species *Candida glabrata* and *Schizosaccharomyces pombe* [121].

Sweeny *et al.* [122] have reported the intracellular synthesis of CdS nanoparticles by *E. coli*. Further, Labrenz *et al.* [123] have reported the synthesis of ZnS nanoparticles by sulphate reducing bacteria of the family *Desulfobacteriaceae*. Kowshik *et al.* [124] synthesized PbS nanocrystals by using *Torulopsis* sp. Furthermore, Ahmad *et al.* synthesized the CdS semiconductor nanoparticles by enzymatic reduction of sulphate ions to sulphide ions by using fungus *Fusarium oxysporum* [125]. Ahmad and co-workers also demonstrated the *in vitro* synthesis of CdS nanoparticles using proteins from fungi, along with external co-factors [126]. Fungi produce large number of proteins/enzymes and the biosynthetic nanoparticles using specific enzyme secreted by fungi has many attractive associated features. Extracellular biosynthesis of nanoparticles will always be advantageous over the intracellular synthesis for large scale, since nanoparticles can be readily isolated and purified from the extracellular reaction solution. This procedure has been employed for different metal oxide nanoparticles synthesis. Ahmad *et al.* have shown the extracellular synthesis of several binary oxides such as SiO₂, TiO₂, ZrO₂, Bi₂O₃, Fe₃O₄ and ternary metal oxide like BaTiO₃ nanoparticles by employing *Fusarium oxysporum* and the appropriate metal ion precursors [127]. Also, Kumar *et al.* [128] reported the extracellular synthesis of Cobalt oxide (Co₃O₄) nanoparticles from the marine bacterium *Brevibacterium casei*. In another example, Ahmad and co-workers extracellularly synthesized CaCO₃ and SrCO₃ crystals after reacting CaCl₂ and SrCl₂ respectively to fungus *Rhodococcus* sp. and *Fusarium oxysporum* [129]. In continuation to the biosynthetic approach, Ahmad *et al.* reported bioleaching of silica nanoparticles of diverse morphologies from naturally available materials such as white sand and zircon sand as well as from the agro-industrial by-product rice husk by using the fungus *Fusarium oxysporum* [130].

In addition to the microbial approach to synthesize the nanomaterials, plant extracts have also been used for gold and silver nanoparticle synthesis. It is very well known that a number of species of plants are capable of accumulating large percentage of gold within them. One of them is *Equisetum* sp. (horsetail) [131, 132]. Besides metal accumulation in plant cells, plants are also known for the biomineralization of many inorganic materials. For example, calcium oxalate, calcium carbonates and silicon dioxides are found in cactaceae family plants [133]. This allows an opening to explore plants as a means for synthesizing metal nanoparticles analogously. So, Yacaman and

co-workers have shown that gold and silver nanoparticles are formed inside different parts of the Alfalfa plant by uptaking corresponding metal ion precursors from the growth media [134]. The intracellular synthesis of metal nanoparticles using plants is not important from the commercial application point of view because of high cost and labor extensive processes for the extraction and purification of metal and therefore, the extracellular synthesis of metal nanoparticles is in high demand due to an easy and cheap source for the same purpose. Keeping this objective in mind, Ahmad *et al.* concentrated on extracellular synthesis of various metal nanoparticles using different plant extracts and they have shown that various plant extracts like that of *Geranium* sp. [135], neem (*Azadirachta indica*) [136], lemon grass (*Cymbopogon flexuosus*) [137] and amla (*Emblica officinalis*) [138] can be used for the size and shape-directed biosynthesis of gold, silver and gold-silver bimetallic core-shell nanoparticles. As discussed earlier, biomineralization processes are regulated by proteins or other biological macromolecules. After considering this aspect, researchers explore proteins identified from biomineralizing organisms and attempts have been made to synthesize various nanostructures. Most of the work in this direction has been facilitated by the systematic use of biological structures that act as templates for the synthesis of nanomaterials with complex morphologies. These templates include bacterial cell surfaces [139], viruses [140], DNA [141], proteins [142], small peptides [143] and even pollen grains [144] have been used for the synthesis of nanostructures with variety of compositions, sizes and shapes.

So, in conclusion we can say that several biomimetic synthesis approaches, where biomolecules or microbes participate either in the reduction, oxidation or hydrolysis of the precursors or act as templates, are gaining popularity as these novel synthesis methods do not require high temperature, pressure or extreme pH conditions. The extracellular synthesis of nanomaterials by using whole cell microorganisms like fungi is an exciting possibility and could lead to eco-friendly and economically viable methods towards the large-scale synthesis of nanomaterials of technological interests. Here in this thesis, we report two different biosynthetic approaches (top-down and bottom-up) for extracellular synthesis of different nanomaterials by using different fungal sources. In the first approach (bottom-up) we demonstrate that fungal biomass is capable of synthesizing some difficult phase of transition metal oxides nanoparticles (Bi_2O_3 , CrO_2 and Mn_5O_8) and Bi_2S_3 nanoparticle at room temperature

by reacting the metal ion salts with the fungal biomass. In the second approach (top-down) we show that the fungal biomass can be used to break-down the chemically synthesized larger particles (150-200 nm) into particles as small as 5-6 nm while maintaining the crystallinity and phase at the nano level. In both the approaches, the particles surfaces are passivated by a robust layer of proteins which provides stability in aqueous medium. A brief outline of the work presented in this thesis is given in the last section.

1.8 Nano-biotechnology: current areas of biomedical applications

Nano-biotechnology, an integration of physical sciences, molecular engineering, biology, chemistry and biotechnology holds considerable promise of advances in pharmaceutical and health care. It has originated to allow researchers to work at the cellular and molecular levels to produce major advances in life sciences and healthcare. Today, nanotechnology gives us the ability to work at molecular level, atom-by-atom to create materials and structures with new capabilities that will fundamentally change medicine, biotechnology and many other industries [145]. Nanoparticles provide a particularly useful platform, demonstrating unique properties with potentially wide-ranging therapeutic applications. The applications of nanotechnology, particularly in the biomedical arena, involve benefits for health care, public safety, environmental monitoring and forensics [146]. For example, nanoscale manipulations may enable tissue regeneration, *in vivo* medical monitoring by nanoscale robots, precise and convenient drug delivery, novel drug formulations, real-time molecular pathology, affordable testing and diagnosis and monitoring of a wide variety of diseases [147]. Nanomaterials have unique physico-chemical properties, such as ultra small size, large surface area to mass ratio, and high reactivity, which are different from bulk materials of the same composition. These properties can be used to overcome some of the limitations found in traditional therapeutic and diagnostic agents. Reducing the scale of devices adds a clear advantage to biological applications as molecular size scales are reached. This is because the typical size dimensions of biomolecular components which are comparable with the dimensions of man-made nanoparticles. Using nanoparticles as biomolecular probes allows us to probe biological processes without interfering with them. Inorganic nanoparticles, such as carbon nanotubes, quantum dots and gold nanoshells, have been adopted for

biomedical use, due to their unique optical and physical properties. Compared to conventional materials, inorganic nanomaterials have several advantages such as simple preparative processes and precise control over their shape, composition and size. In addition, inorganic porous nanomaterials are fundamentally advantageous for developing multifunctional nanomaterials, due to their distinctive inner and outer surfaces [148]. The range of biomedical applications of nanoparticles is numerous; some of the important applications are;

1.8.1 Therapeutics

Advances in nanotechnology have a significant impact in the field of therapeutics delivery. The development of nanoparticles for the delivery of therapeutic agents has introduced new opportunities for the improvement of medical treatment. There are several advantages to using nanoparticles for therapeutics delivery. The use of materials on the nanoscale level provides unprecedented freedom to modify some of the most fundamental properties of therapeutic carriers, such as solubility, diffusivity, biodistribution, release characteristics and immunogenicity [149]. Precise nanoparticle engineering has yielded longer circulation half-lives, superior bioavailability and lower toxicity. Encapsulation of therapeutic agents for targeting to specific site and for long term stability in the blood stream is a common application of bio-nanotechnology [150]. Functionalization of nanoparticles will allow localization of drugs to specific organs or cells, increasing efficacy and decreasing effects on healthy cells. Nanoparticle encapsulation for existing drug compounds may be the earliest dramatic impact of bio-nanotechnology in the medical industry [151]. In the last two decades, a number of nanoparticle-based therapeutic agents have been developed for the treatment of cancer, diabetes, pain, asthma, allergy, infections, etc. [152]. The most commonly investigated silicon-based materials for drug delivery are porous silicon and silica. Architectures include calcified nanopores, platinum-containing nanopores, porous nanoparticles, and nano-needles. Surface-functionalized carbon nanotubes (CNTs) can be internalized within mammalian cells, and when linked to peptides may be used as vaccine delivery structures. Fullerenes have also shown drug targeting capability. Tissue-selective targeting and intracellular targeting of mitochondria have been shown with use of fullerene structures. Typical metals include gold, platinum, palladium and metal-oxides like iron oxide and gadolinium oxide. When linked to or embedded within polymeric drug carriers, metal nanoparticles can be

used as thermal release triggers when irradiated with infrared light or excited by an alternating magnetic field [153]. Among the metallic nanoparticles, Au nanoparticles have immense potential for cancer diagnosis and therapy on account of their surface plasmon resonance (SPR) enhanced light scattering and absorption. Conjugation of Au nanoparticles to ligands specifically targeted to biomarkers on cancer cells allows molecular-specific imaging and detection of cancer. Additionally, Au nanoparticles efficiently convert the strongly absorbed light into localized heat, which can be exploited for the selective laser photothermal therapy of cancer [154].

1.8.2 Diagnostic

Nanoparticles, especially of inorganic materials such as silica, gold and silver, have been used for diagnostics applications. Gold nanoparticles tagged with short segments of DNA can be used for detection of genetic sequence in a sample. Magnetic nanoparticles bound to a suitable antibody are used to label specific molecules, structures or microorganisms. Superparamagnetic nanoparticles are useful for magnetic resonance imaging, cell-tracking cells and for calcium sensing. Diagnostically, paramagnetic iron oxide nanoparticles are used as contrast agents in magnetic resonance imaging. These have a greater magnetic susceptibility than conventional contrast agents. Targeting of these nanoparticles enables identification of specific organs and tissues [155]. Multicolour optical coding for biological assays has been achieved by embedding different-sized quantum dots into polymeric microbeads. Quantum dots are inorganic fluorophores that offer significant advantages over conventionally used fluorescent markers. They have high sensitivity, broad excitation spectra, stable fluorescence with simple excitation, and no need for lasers. The most important potential applications of quantum dots are for cancer diagnosis. Luminescent and stable quantum dots bioconjugates enable visualization of cancer cells in living animals [156]. Nanopore technology for analysis of nucleic acids converts strings of nucleotides directly into electronic signatures. ‘Nanotechnology-on-a-chip’ is one more dimension of ‘lab-on-a-chip’ technology [157].

1.8.3 Bio-imaging

Advances in imaging have occurred in conjunction with the development of nanoparticles, which are used to enhance existing imaging techniques by serving as

contrast agents or as markers in various optical techniques. A number of molecular imaging techniques, such as optical imaging (OI), magnetic resonance imaging (MRI), ultrasound imaging (USI), positron emission tomography (PET), computed tomographic imaging (CT) and others have been reported for imaging of *in vitro* and *in vivo* biological specimens [158].

Nanoparticles with strong optical and magnetic interactions may be functionalized for binding to specific cells, tissues, tumours, or sub-cellular components [159]. Nanoparticles are loaded with contrast agents like perfluorocarbon emulsion for ultrasound, gadolinium in the case of magnetic resonance imaging (MRI), or radionuclides for computed tomography (CT) imaging and are then coated in ligands molecules specifically designed to target and bind to the tissue to be imaged [160]. For cancer imaging, proteins related to angiogenesis, or rapid growth of vasculature can be used as targets for the ligands and direct the contrast agents to accumulate preferentially at tumour sites [161]. Quantum dots described above offer unique imaging possibilities as a result of their high brightness, ease of functionalization and excellent tuneability. By selecting quantum dot fluorescence wavelengths in the near infrared, it is possible to work at wavelengths where tissues are relatively transparent and making deeper imaging and tumour analysis by fluorescence spectroscopy possible [162]. Inorganic nanoparticles like gold and silver can also be used as imaging agents due to their strong interaction with electromagnetic fields. Bio-nanotechnological developments in this area are leading to more effective imaging agents that can more accurately target tumour sites and this alongwith increased brightness can lead to earlier detection of tumour.

1.8.4 Cancer therapy

Nanoparticulate technology is of particular use in developing a new generation of more effective cancer therapies capable of overcoming the many biological, biophysical and biomedical barriers that the body stages against a standard intervention. Nanoparticles show much promise in cancer therapy by selectively gaining access to tumour due to their small size and modifiability [163]. In cancer treatment and detection, the nanoparticles serve many targeted functions in chemotherapy, radiotherapy, immunotherapy, immunodetection, thermotherapy, imaging, photodynamic therapy and anti-angiogenesis [164]. Nanotechnological

advances are at the bottom of the next paradigm shift in cancer research, diagnostics and therapy by improving direct visualization of malignant cells, targeting at molecular level and safely delivering large amounts of chemotherapeutic agents to desired cells. Nanoparticles and their use in drug delivery is a far more effective antitumor method than conventional chemotherapy, which is typically limited by the toxicity of drugs to normal tissues, short circulation half-life in plasma, limited aqueous solubility, and non-selectivity restricting therapeutic efficacy [165].

Gold nanoparticles and quantum dots attach themselves onto the epidermal growth factors receptor (EGFR) present on the cell surface of cancer cells which is helpful in detecting the cancer cells. Iron oxide nanoparticles encased in a biocompatible material can make the detection of cancer cells easier, even if the cancer cells are small; these nanoparticles stick to the tumor cells turning them into little magnets which are then attracted to the tip of a biopsy needle. Due to their strong scattering, gold nanorods have excellent potential as optical contrast agents for molecular imaging. Furthermore, the strongly absorbed IR radiation can be converted into heat efficiently, making it a promising potential photothermal therapeutic agent. In photothermal therapy, optical radiation is absorbed and transformed into heat. The heat causes the proteins and DNA to denature, irreversibly damaging the cells and, consequently, causing their death [166].

1.9 Outline of the thesis

The work presented in this thesis describes novel biological protocols for the synthesis of complex transition metal oxide and metal sulphide nanoparticles using bottom-up and top-down approaches. This is an attempt to extend the biological synthesis protocols towards a possibility of scale-up. An important outcome of these approaches is that metal oxides (Bi_2O_3 , CrO_2 , Mn_5O_8 and BiOCl) and metal sulphide (Bi_2S_3) nanoparticles can be synthesized using these routes. Many exciting results were obtained during the course of experiments, which are described in detail. The thesis is composed of five chapters and the chapter wise description of these studies is described as follows:

Chapter 1 describes the brief and general introduction about nanotechnology and historical perspective of nanoscience. It also reveals the significant properties of nanoparticles, parameters that could alter nanoparticle properties, followed with the

various synthesis methods and approach to reach the nano level and also the wide applications in different fields have been discussed. Finally, in this chapter, we discussed a brief overview of biomineralization and biosynthesis of nanomaterials.

Chapter 2 describes the bottom-up biosynthetic approach to synthesize metal oxides nanoparticles. This chapter is further divided into three parts where synthesis of metal oxide nanoparticles Bi_2O_3 , Mn_5O_8 , and CrO_2 using fungus *Fusarium oxysporum* and *Trichothecium* sp. is described.

Part 2A describes the structural and microbial synthesis of sub-10 nm Bi_2O_3 nanocrystals using fungus *Fusarium oxysporum*. The Bi_2O_3 so formed is characterized by TEM, XRD, FTIR, XPS and TGA. As-synthesized as well as calcined particles showed excellent crystallinity. Structural investigation was done using selected area electron diffraction (SAED) and powder XRD shows that particles primarily crystallize in the α -phase with monoclinical structure.

Part 2B describes the extracellular synthesis of protein functionalized CrO_2 nanoparticles using the fungus *Trichothecium* sp. and potassium dichromate ($\text{K}_2\text{Cr}_2\text{O}_7$) is used as precursor salt in ambient conditions. This finding was confirmed by various techniques such as XRD, XPS, FTIR, HR-TEM etc. The TEM analysis of CrO_2 nanoparticles indicated that the overall particles are irregular in shape with quasi spherical morphology and with an average particle size of 21-25 nm in diameter. HR-TEM images and XPS confirm the presence of Cr_2O_3 layer over the CrO_2 nanoparticle. XRD and SAED analysis showed that particles are well crystalline having tetragonal symmetry. TGA studies showed that at temperatures higher than 340°C , CrO_2 starts decomposing into Cr_2O_3 . Magnetic studies show that CrO_2 is a ferromagnetic material. The presence of Cr_2O_3 layer over the CrO_2 nanoparticles is explained by magnetic measurements in M-H curve, which suggest that CrO_2 nanoparticles synthesized by *Trichothecium* sp. show ferromagnetic and antiferromagnetic exchange bias between core CrO_2 and Cr_2O_3 layer.

Part 2C describes extracellular synthesis of Mn_5O_8 nanoparticles in the size range of 5-8 nm at room-temperature using fungus *Fusarium oxysporum*. The Mn_5O_8 so formed is characterized by TEM, XRD, FTIR, XPS, and TGA. The compound Mn_5O_8 exists in mixed valencies of Mn^{2+} and Mn^{4+} , which was confirmed by XPS data.

Mn₅O₈ has a monoclinical structure and magnetic studies show that Mn₅O₈ has antiferromagnetic nature. These Mn₅O₈ nanoparticles are capped with protein which stabilizes the nanoparticles against aggregation.

Chapter 3 describes the fungus mediated synthesis of Bi₂S₃ nanoparticles by reacting the fungus *Fusarium oxysporum* with bismuth (III) nitrate pentahydrate (Bi(NO₃)₃·5H₂O) and Na₂SO₃ as precursor at room temperature. The protein capped Bi₂S₃ nanoparticles maintain a long-term stability and shows a band gap of 3.04 eV. TEM images showed that the particles are quasi spherical in shape with an average particle size of 15 nm. Selected area electron diffraction (SAED) and powder XRD shows that particles are perfectly crystalline with an orthorhombic structure. Further characterization of Bi₂S₃ nanoparticles was done using techniques such as UV, PL, XPS, FTIR and TGA. These Bi₂S₃ nanoparticles were used for SPECT-CT probe for small animal imaging. This was injected into rats and the biodistribution image and clearance time from blood was calculated.

Chapter 4 describes the synthesis of BiOCl nanoparticles by top-down (bio-milling) approach using the biological system i.e. in *Humicola* sp. This green technique has a potential for commercial application into large scale synthesis of nanomaterials with a simple route and is named as “biomilling”. Bio-milling is a “Green Top-Down Approach” used to synthesize complex oxide nanoparticles with particle sizes less than 10 nm with the proper crystalline phase by synergically utilizing both chemical and biological synthesis techniques. We present this novel technique developed at N.C.L, Pune (India) by which fungal biomass can be used to break-down the chemically synthesized larger particles (200-250 nm) into particles as small as 5-6 nm while maintaining the crystallinity and phase at the nanolevel. We believe that this technique can be used to synthesize several complex oxide nanoparticles whose synthesis in the size less than 10 nm by conventional wet-chemical methods is very difficult.

Chapter 5 summarizes the work presented in this thesis and emphasizes on the possible further research in this area.

References

- [1] Guozhong Cao., *Nanostructures and Nanomaterials: Synthesis, Properties and Applications*, Imperial College Press, UK, April **2004**, ISBN: 1-86094-415-9, pp. 448.
- [2] Maier, S. A., Brongersma, M. L., Kik, P. G., Meltzer, S., Recquicha, A. A. G., Atwater, H. H., *Adv. Mater.*, **2001**, 13, 1501.
- [3] (a) Garrigue, P., Delville, M. H., Labrugere, C., Cloutet, E., Kulesza, P. J., Morand, J. P., Kuhn, A., *Chem. Mater.*, **2004**, 16, 16, 2984. (b) Xia, D., Li, D., Ku, Z., Luo, Y., Brueck, S. R. J., *Langmuir.*, **2007**, 23, 10, 5377. (c) Jang, J., Oh, J. H., *Adv. Mater.*, **2004**, 16, 18, 1650. (d) Amendola, V., Meneghetti, M., Granozzi, G., Agnoli, S., Polizzi, S., Riello, P., Boscaini, A., Anselmi, C., Fracasso, G., Colombatti, M, Innocenti, C., Dante Gatteschi, D., Sangregorio, C., *J. Mater. Chem.*, **2011**, 21, 3803. (e) Mazumder, B., Uddin, I., Khan, S., Ravi, V., Selvraj, K., Poddar, P., Ahmad A., *J. Mater. Chem.*, **2007**, 17, 3910.
- [4] (a) Sajanlal, P. R., Sreepasad, T. S., Samal, A. K., Pradeep, T., *Nano. Rev.* **2011**, 2, 5883. (b) Wang, Y., Xia, Y., *Nano Lett.*, **2004**, 4, 10, 2047. (c) Schmid, G. *Chem. Rev.* **1992**, 92, 8, 1709.
- [5] (a) Antonii, F., *Panacea Aurea-Auro Potabile*, Bibliopolio Frobeniano, Hamburg, **1618**. (b) Kunckels, J., *Nuetliche Observationes oder Anmerkungen von Auro und Argento Potabili*, Schutzens, Hamburg **1676**. (c) Helcher, H. H., *Aurum Potabile oder Gold Tinstur*, J. Herbord Klossen, Breslau and Leipzig **1718**. (d) Lloyd, J. U., *Elixirs and Flavoring Extracts: Their History, Formulae, and Methods of Preparation*, **1892**, New York: William Wood and Company. (e) Ostwald, W., *Kolloid, Z.*, **1909**, 4, 5.
- [6] Fulhame, Mrs., *An Essay on Combustion with a View to a New Art of Dying and Painting.*, Cooper, J., London, **1794**.
- [7] <http://www.colloidalgold.com/history.htm>
- [8] Savage, G., *Glass and Glassware*; Octopus Book: London, **1975**. (b) Wagner, F. E., Haslbeck, S., Stievano, L., Calogero, S., Pankhurst, Q. A., Martinek, K. P., *Nature.*, **2000**, 407, 691. (c) Turkevich, J., *Gold Bull.*, **1985**, 18, 86. (d) Ayers, A., *Ceramics of the World: From 4000 BC to the Present*, New York, **1992**, 284. (e) Zhao, H., Ning, Y., *Gold. Bull.* **2000**, 33, 103.

-
- [9] Reibold, M., Paufler, P., Levin, A. A., Kochmann, W., Patzke, N., Meyer, D. C., *Nature.*, **2006**, 444, 226.
- [10] Fulhame, M., *An Essay on Combustion with a View to a New Art of Dying and Painting*; J. Cooper: London, **1794**.
- [11] Faraday, M., *Philos. Trans. R. Soc. London.*, **1857**, 147, 145.
- [12] Graham, T., *Philos. Trans. R. Soc.*, **1861**, 151, 183.
- [13] Zsigmondy, R., Alexander, J., *Colloids and the Ultramicroscope: A Manual of Colloid Chemistry and Ultramicroscopy.*, John Wiley & Sons, New York, **1914**.
- [14] Feynman, R. P., *Eng. Sci.*, **1960**, 23, 22.
- [15] Taniguchi, N., *Proceedings of the international conference on production engineering. Tokyo, Part II*, Japan Society of Precision Engineering, **1974**: 18, Tokyo, JSPE.
- [16] Alivisatos, A. P., *ACS. Nano.*, **2008**, 2, 1514.
- [17] Kroto, H. W., Heath, J. R., O'Brien, S. C., Curl, R. F., Smalley, R. E., *Nature.*, **1985**, 318, 162.
- [18] Iijima, S., *Nature.*, **1991**, 354, 56.
- [19] (a) Geim, A. K., Novoselov, K. S., *Nat. Mater.* **2007**, 6, 183. (b) Geim, A. K., *Science.*, **2009**, 324, 1530.
- [20] (a) Binnig, G., Rohrer, H., Gerber, Ch., Weibel, E., *Surface Studies by Scanning Tunneling Microscopy*, **1982**, 49, 57. (b) Binnig, G., Rohrer, H., *Rev. Mod. Phys.*, **1987**, 59, 615. (c) Binnig, G., Quate, C. F., Gerber, C., *Phys. Rev. Lett.*, **1986**, 56.
- [21] Klabunde, K. J., *Nanoscale Materials in Chemistry* (Ed.), **2000**, John Wiley, New York, pp. 18.
- [22] (a) El-Sayed, M. A., *Acc. Chem. Res.*, **2001**, 34, 257. (b) Link, S., El-Sayed, M. A., *J. Phys. Chem. B.*, **1999**, 103, 8410. (c) Burda, C., Chen, X., Narayanan, R., El-Sayed, M. A., *Chem. Rev.*, **2005**, 105, 1025.
- [23] (a) Chen, S., Ingram, R. S., Hostetler, M. J., Pietron, J. J., Murray, R. W., Schaaff, T. G., Khoury, J. T., Alvarez, M. M., Whetten, R. L., *Science.*, **1998**, 280, 2098. (b) Miles, D. T., Murray, R. W., *Anal. Chem.*, **2003**, 75, 1251. (c) Chen, S., Pei, R., *J. Am. Chem. Soc.*, **2001**, 123, 10607. (d) Quinn, B. M., Liljeroth, P., Ruiz, V., Laaksonen, T., Kontturi, K., *J. Am. Chem. Soc.*, **2003**, 125, 6644.
-

-
- [24] (a) Itoh, T., Asahi, T., Masuhara, H., *Appl. Phys. Lett.*, **2001**, 79, 1667. (b) Rechberger, W., Hohenau, A., Leitner, A., Krenn, J. R., Lamprecht, B., Aussenegg, F. R., *Opt. Commun.*, **2003**, 220, 137. (c) Yan, B., Yang, Y., Wang, Y. *J. Phys. Chem. B.*, **2003**, 107, 9159.
- [25] (a) Xu, H., Bjerneld, E. J., Kall, M., Borjesson, L., *Phys. Rev. Lett.*, **1999**, 83, 4357. (b) Kelly, K. L., Coronado, E., Zhao, L. L., Schatz, G. C., *J. Phys. Chem. B.*, **2003**, 107, 668. (c) Jensen, T., Kelly, L., Lazarides, A., Schatz, G., *Cluster Sci.*, **1999**, 10, 295. (d) Al-Rawashdeh, N., Foss, C. A., *Jr. Nanostruct. Mater.* **1997**, 9, 383.
- [26] (a) Raimondi, F., Scherer, G. G., Kötz, R., Wokaun, A., *Angew. Chem. Int. Ed.*, **2005**, 44, 2190. (b) Henry, C. R., *Surf. Sci. Rep.*, **1998**, 31, 231. (c) Zhang, J. H., *Acc. Chem. Res.*, **1997**, 30, 423.
- [27] Schmid, G., *Nanoparticles: From Theory to Application.*, **2004**, Eds., Wiley-VCH: Weinheim.
- [28] Aiken III, J. D., Finke, R. G., *J. Mol. Cata. A:Chem.*, **1999**, 145, 1.
- [29] (a) Haruta, M., Date M., *Appl. Catal. A.*, **2001**, 222, 427. (b) Zhong, C. J., Maye, M. M., *Adv. Mater.* **2001**, 13, 1507.
- [30] (a) Lewis. L. N., *Chem. Rev.*, **1993**, 93, 2693. (b) Astruc, D., Lu, F., Aranzaes, J. R., *Angew. Chem. Int. Ed.*, **2005**, 44, 7852.
- [31] (a) Wang, Z. L., Ahmad, T. S., El-Sayed, M. A., *Surf. Sci.*, **1997**, 380, 302. (b) Narayanan, R., El-Sayed, M. A., *Nano Lett.*, **2004**, 4, 1343. (c) Narayanan, R., El-Sayed, M. A. *J. Phys. Chem. B.*, **2004**, 108, 5726.
- [32] Aiken III, J. D., Finke, R. G., *J. Mol. Cata. A:Chem.*, **1999**, 145, 1.
- [33] (a) Buffat, P., Borel, J. P., *Phys. Rev. A.*, **1976**, 13, 2287. (b) Castro, T., Reifenberger, R., Choi, E., Andres, R. P., *Phys. Rev. B.*, **1990**, 42, 8548. (c) Beck, R. D., St. John, P., Homer, M. L., Whetten, R. L., *Science.*, **1991**, 253, 879. (d) Martin, T. P., Naher, U., Schaber, H., Zimmermann, U., *J. Chem. Phys.*, **1994**, 100, 2322.
- [34] Burda, C., Chen, X., Narayanan, R., El-Sayed, M. A., *Chem. Rev.*, **2005**, 105, 1025.
- [35] (a) Alivisatos, A. P., *Science.*, **1996**, 271, 933. (b) Gaponenko., *Optical Properties of Semiconductor Nanocrystals.*, **1998**, Cambridge University Press: Cambridge, U.K. (c) Brus, L. E., *Appl. Phys. A.*, **1991**, 53, 465.
-

-
- [36] Moores, A., Goettmann, F., *New. J. Chem.*, **2006**, 30, 1121.
- [37] (a) Link, S., El-Sayed, M. A. *Int. Rev. Phys. Chem.*, **2000**, 19, 409. (b) Link, S., El-Sayed, M. A., *Annu. Rev. Phys. Chem.*, **2003**, 54, 331. (c) Kreibig, U., Vollmer, M., *Optical Properties of Metal Clusters.*, **1995**, Springer: Berlin, Germany. (d) Kerker, M., *The Scattering of Light and Other Electromagnetic Radiation*, **1969**, Academic: New York. (e) Bohren, C. F., Huffman, D. R., *Absorption and Scattering of Light by Small Particles.*, **1983**, Wiley: New York.
- [38] Weertman, J. R., Averbach, R. S., “*Nanomaterials: synthesis, properties, and applications*” eds. Edelstein, A. S. Cammarata, R. C. London institute of Phys. Publ. **1996**, chp. 13, 323.
- [39] (a) Darling, S. B., Bader, S. D., *J. Mater. Chem.*, **2005**, 15, 4189. (b) Jun, Y. W., Seo, J. W., Cheon, A., *Acc. Chem. Res.*, **2008**, 41, 179. (c) Krishnan, K. M., Pakhomov, A. B., Bao, Y., Blomqvist, P., Chun, Y., Gonzales, M., Griffin, K., Ji, X., Roberts, B. K., *J. Mater. Sci.*, **2006**, 41, 793.
- [40] (a) Frankel, J., Dorfman, J., *Nature.*, **1930**, 126, 274. (b) Bucher, J. P., Douglass, D. C., Bloomfield, L. A. *Phys. Rev. Lett.*, 1991, 70, 2283.
- [41] (a) Rosi, N. L., Mirkin, C. A., *Chem. Rev.*, **2005**, 105, 1547. (b) Lawrie, G. Grondahl, L., Battersby, B., Keen, I., Lorentzen, M., Surawski, P., Trau, M., *Langmuir.*, **2006**, 22, 497.
- [42] (a) Liu, G., Men, P., Kudo, W., Perry, G., Smith, M. A., *Biochim. Biophysic. Acta.*, **2005**, 1741, 246. (b) Loo, C., Lin, A., Hirsch, L., Lee, M. H., Barton, J., Halas, N., West, J., Drezek, R., *Tech. Cancer. Res. Treat.*, **2004**, 3, 33. (c) Liu, G., Men, P., Harris, P. L. R., Rolston, R. K., Perry, G., Smith, M. A., *Neuroscience. Lett.*, **2006**, 406, 189. (d) Chan, W. C. W., *Biol. Blood Marrow. Trans.*, **2006**, 12, 87.
- [43] (a) Haes, A. J., Van Duyne, R. P., *Anal. Bioanal. Chem.*, **2004**, 379, 920. (b) Niemeyer, C. M., *Angew. Chem. Int. Ed.*, **2001**, 40, 4128. (c) Niemeyer, C. M., *Angew. Chem. Int. Ed.*, **2003**, 42, 5974. (d) Parak, W. J., Gerion, D., Pellegrino, T., Zanchet, D., Micheel, C., Williams, S. C., Bodreau, R., Gros, M. A. L., Larabell, C. A., Alivisatos, A. P., *Nanotechnology.*, **2003**, 14, R15. (e) Caski, A., Maubach, G., Born, D., Reichert, J., Fritzsche, W., *Single Mol.*, **2002**, 3, 275.
-

-
- [44] (a) Roucoux, A., Schulz, J., Patin, H., *Chem. Rev.*, **2002**, 102, 3757. (b) Lewis, L. N., *Chem. Rev.*, **1993**, 93, 2693.
- [45] (a) Andersen, N. A., Lian, T., *Ann. Rev. Phys. Chem.*, **2005**, 56, 491. (b) Yae, S., Kobayashi, T., Abe, M., Nasu, N., Fukumuro, N., Ogawa, S., Yoshida, N., Nonomura, S., Nakato, Y., Matsuda, H., *Solar Energy Mater. Solar. Cells.*, **2007**, 91, 224. (c) Hagfeldt, A., Graetzel, M., *Acc. Chem. Res.*, **2000**, 33, 269. (d) Bueno, J. T., Shchukina, N., Ramos, A. A., *Nature.*, **2004**, 430, 326.
- [46] (a) Cengiz, E., Wissing, S. A., Muoller, R. H., Yazan, Y., *Intl. J. Cosmetic Sci.* **2006**, 28, 371. (b) Villalobos-Hernández, J. R., Muoller-Goymann, C. C., *Int. J. Pharmaceutics.*, **2006**, 322, 161.
- [47] (a) Langer, R., *Sci. Am.*, **2003**, 288, 50. (b) Otsuka, H., Nagasaki, Y., Kataoka, K., *Adv. Drug. Delivery. Rev.*, **2003**, 55, 403. (c) McAllister, D. V., *Proc. Natl. Acad. Sci. USA.*, **2003**, 100, 13775.
- [48] Li, X., Xu, W., Zhang, J., Jia, H., Yang, B., Zhao, B., Li, B., Ozaki, Y., *Langmuir.*, **2004**, 20, 1298.
- [49] Fichtner, M., *Adv. Engg. Mater.*, **2005**, 7, 443.
- [50] Moran, C. E., Steele, J. M., Halas, N. J., *Nano. Lett.*, **2004**, 4, 1497.
- [51] (a) Simon, U., In *Nanoparticles: From Theory to Application*, Schmid, G., Ed. Wiley-VCH, Weinheim, Germany, **2004**. (b) *Nanomaterials: Synthesis, Properties, and Applications*, edited by A. S. Edelstein and R. C. Cammarata (Institute of Physics Publishing, Bristol, U.K., **1996**).
- [52] (a) Maier, S. A., Brongersma, M. L., Kik, P. G., Meltzer, S., Requicha, A. A. G., Atwater, H. A., *Adv. Mater.*, **2001**, 13, 1501. (b) Maier, S. A., Brongersma, M. L., Kik, P. G., Atwater, H. A., *Phys. Rev. B.*, **2002**, 65, 193408. (c) Wang, Y., *Acc. Chem. Res.*, **1991**, 24, 133. (d) Yoffe, A. D., *Adv. Phys.*, **1993**, 42, 173.
- [53] (a) Zou, S., Schatz, G. C., *Phy. Rev. B.*, **2006**, 74, 125111. (b) Maier, S. A., Friedman, M. D., Barclay, P. E., Painter, O., *Appl. Phys. Lett.*, **2005**, 86, 1. (c) Maier, S. A., Brongersma, M. L., Kik, P. G., Meltzer, S., Requicha, A. A. G., Atwater, H. A., *Adv. Mater.*, **2001**, 13, 19, 1501.
- [54] (a) Pradell, T., Molera, J., Bayés, C., Roura, P., *Appl. Phys. A.*, **2006**, 83, 203. (b) Jose-Yacaman, M., Rendon, L., Arenas, J., Serra Puche, M. C., *Science.*, **2006**, 273, 223. (c) Baglioni, P., Giorgi, R., *Soft. Matter.*, **2006**, 2, 293.
-

-
- [55] (a) Yelin, D., Oron, D., Thiberge, S., Moses, E., Silberberg, Y., *Optics Express.*, **2003**, 11, 1385. (b) Wang, Y., Xie, X., Wang, X., Ku, G., Gill, K. L., Oneal, D. P., Stoica, G., Wnag, L. V., *Nano Lett.*, **2005**, 4, 1689. (c) Sokolov, K. Follen, M., Aaron, J., Pavlova, I., Malpica, A., Lotan, R., Richards-Kortum, R., *Cancer Res.*, **2003**, 63, 9, 1999. (d) El-Sayed, I. H., Huang, X., El-Sayed, M. A., *Nano Lett.*, **2005**, 5, 829. (e) Grainger, R. G., *Brit. J. Rad.*, **1882**, 55, 1. (f) Parak, W. J., Pellegrino, T., Plank, C., *Nanotechnology.*, **2005**, 16, R9. (g) Chan, W. C. W., Nie, S. M., *Science.*, **1998**, 281, 2016. (h) Bruchez, M., Moronne, Jr. M., Gin, P., Weiss, S., Alivisatos, A. P., *Science.*, **1998**, 281, 2013.
- [56] Jackson, J. B., Westcott, S. L., Hirsch, L. R., West, J. L., Halas, N., *J. Appl. Phys. Lett.*, **2003**, 82, 257.
- [57] Matejivic, E., *Annu. Rev. Mater. Sci.*, **1985**, 15, 483.
- [58] Heath, J. R., Kuekes, P. J., Snider, G. S., Williams, R. S., *Science.*, **1998**, 280, 1716.
- [59] (a) Koper, O. B., Lucas, E., Klabunde, K. J., *J. Appl. Toxicol.*, **1999**, 19, 559. (b) Wagner, G. W., Koper, O. B., Lucas, E., Decker, S., Klabunde, K. J., *J. Phys. Chem. B.*, **2000**, 104, 5118.
- [60] Shull, R. D., McMichael, R. D., Swartzendruber, L. J., Benett, L. H., *Studies of Magnetic Properties of Fine Particles and Their Relevance to Materials Science.*, Pormann, J. J., Fiorani, D., (eds.) Elsevier Publishers, Amsterdam, **1992**, pp. 16.
- [61] Roco, M. C., Williams, R. S., Alivisatos, P., (eds.) *Interagency Working Group in Nanoscience Engineering and Technology (IWGN) Workshop Report: Nanotechnology Research Directions; Vision for Nanotechnology R and D in the Next Decade*, Int. Tech. Research Institutes, WTEC Division, Loyola College **1999**.
- [62] (a) Kiwi, J., Gratzel, M., *Angew. Chemie. Int. Ed.*, **1979**, 18, 624. (b) Riegel, G., Bolton, R. J., *J. Phys. Chem.*, **1995**, 280, 1716. (c) Boronina, T., Klabunde, K. J., Sergeev, G. B., *Environ. Sci. Technol.*, **1995**, 29, 1511. (d) Li, Y. X., Klabunde, K. J., *Langmuir.*, **1991**, 7, 1388. (e) Lucas, E., Klabunde, K. J., *Nanostruct. Mater.*, **1999**, 12, 179. (f) Khaleel, A., Kapoor, P., Klabunde, K. J., *Nanostruct. Mater.*, **1999**, 11, 459. (g) Koper, O., Lagadic, I., Volodin, A., Klabunde, K. J., *Chem. Mater.*, **1997**, 9, 2468.
-

-
- [63] (a) Validzic, I. Lj., Jokanovic, V., Uskokovic, D. P., Nedeljkovic, J. M., *J. Euro. Ceram. Soc.*, **2007**, 27, 927 (b) Kim, J. H., Germer, T.A., Mulholland, G.W., Ehrman, S.H., *Adv. Mater.*, **2002**, 14, 518 (c) Suh, W. H., Suslick, K.S., *J. Am. Chem. Soc.*, **2005**, 127, 12007. (d) Okuyama, K., Lenggoro, I. W., *Chem. Eng. Sci.*, **2003**, 58, 537. (e) Osakada, K., Yamamoto, T. J., *Chem. Soc. Chem. Commun.*, **1987**, 1117.
- [64] (a) Chen, T., Chen, S., Sheu, S., Yeh, C., *J. Phys. Chem. B.*, **2002**, 106, 9717. (b) Marignier, J. L., Belloni, J., Delcourt, M. O., Chevalier, J. P., *Nature.*, **1985**, 317, 344. (c) Jin, R., Cao, Y. C., Hao, E., Metraux, G. S., Schatz, G. C., Mirkin, C. A., *Nature.*, **2003**, 425, 487.
- [65] (a) Kurihara, K., Kizing, J., Stenius, P., Fender, J. H., *J. Am. Chem. Soc.*, **1983**, 105, 2574. (b) Joshi, S. S., Patil, S. F., Iyer, V., Mahumuni, S., *Nanostruct. Mater.*, **1998**, 7, 1135. (c) Dimitrijevic, N. M., Bartels, D. M., Jonah, C. D., Takahashi, K., Rajh, T., *J. Phys. Chem. B.*, **2001**, 105, 954.
- [66] (a) Li, C., Cai, W., Li, Y., Hu, J., Liu, P., *J. Phys. Chem. B.*, **2006**, 110, 1546. (b) Dhas, N. A., Raj, C. P., Gedanken, A., *Chem. Mater.*, **1998**, 10, 1446. (c) Nemamcha, A., Rehspringer, J., Khatmi, D., *J. Phys. Chem., B.*, **2006**, 110, 383. (d) Pol, V. G., Grisaru, H., Gedanken, A., *Langmuir.*, **2005**, 21, 3635. (e) Suslick, K. S., Fang, M., Hyeon, T., *J. Am. Chem. Soc.*, **1996**, 118, 11960.
- [67] (a) Stoeva, S. I., Prasad, B. L. V., Uma, S., Stoimenov, P. K., Zaikovski, V., Sorensen, C. M., Klabunde, K. J., *J. Phys. Chem. B.*, **2003**, 107, 7441. (b) Ponce, A. A., Klabunde, K. J., *J. Mol. Catal.*, **2005**, 225, 1. (c) Klabunde, K. J., Timms, P. S., Skell, P. S., Ittel, S., *Inorg. Synth.*, **1979**, 19, 59. (d) Davis, S. C., Klabunde, K. J., *Chem. Rev.*, **1982**, 82, 153.
- [68] (a) Amendola, V., Polizzi, S., Meneghetti, M., *J. Phys. Chem. B.*, **2006**, 110, 7232. (b) Balchev, I., Minkovski, N., Marinova, Ts., Shipochka, M., Sabotinov, N., *Mater. Sci. Eng. B.*, **2006**, 135, 108. (d) Mafune, F., Kohno, J., Takeda, Y., Kondow, T., *J. Phys. Chem. B.*, **2000**, 104, 8333. (e) Zhu, X. P., Suzuki, T., Nakayama, T., Suematsu, H., Jiang, W., Niihara, K., *Chem. Phys. Lett.*, **2006**, 427, 127. (d) Becker, M. F., Brock, J. R., Cai, H., Henneke, D. E., Keto, J. W., Lee, J., Nichols, W. T., Clicksman, H. D., *Nanostruct. Mater.*, **1998**, 10, 853.
- [69] (a) Wegner, K., Walker, B., Tsantilis, S., Pratsinis, S. E., *Chem. Eng. Sci.*, **2002**, 57, 1753. (b) Oha, S., Choi, C., Kwon, S., Jin, S., Kim, B., Park, J., *J. Magn.*
-

-
- Magn. Mater.*, **2004**, 280, 147. (c) Chevallier, J., *Thin Solid Films.*, **1977**, 40, 223.
- [70] (a) Wang, Y., Zhang, L., Meng, G., Liang, C., Wang, G., Sun, S., *Chem. Commun.*, **2001**, 2632. (b) Teng, X., Black, D., Watkins, N. J., Gao, Y. H., *Nano Lett.*, **2003**, 3, 261. (c) Wang, Y., Herricks, T., Xia, Y., *Nano Lett.*, **2003**, 3, 1163. (d) Hou, Y., Kondoh, H., Kogure, T., Ohta, T., *Chem. Mater.*, **2004**, 16, 5149.
- [71] (a) Reetz, M. T., Helbig, W., *J. Am. Chem. Soc.*, **1994**, 116, 7401. (b) Reetz, M. T., Winter, M., Breinbauer, R., Thurn-Albrecht, T., Vogel, W., *Chem. Eur. J.*, **2001**, 7, 1084. (c) Reetz, M. T., Helbig, W., Quaiser, S. A., Stimming, U., Breuer, N., Vogel, R. *Science.*, **1995**, 267, 367. (d) Natter, H., Hempelmann, R., *Electrochim. Acta.*, **2003**, 49, 51.
- [72] (a) Maisels, A., Kruis F. E., Fissan, H., Rellinghaus, B., Zahres, H., *Appl. Phys. Lett.*, **2000**, 77, 4431. (b) Swihart, M. T., *Curr. Opin., Colloid Interface Sci.*, **2003**, 8, 127.
- [73] (a) El-Shall, M. S., *Appl. Surf. Sci.*, **1996**, 106, 347. (b) Wegner, K., Walker, B., Tsantilis, S., Pratsinis, S. E., *Chem. Eng. Sci.*, 2002, 57, 1753. (c) Vitulli, G., Bernini, M., Bertozzi, S., Pitzalis, E., Salvadori, P., Coluccia, S., Martra, G., *Chem. Mater.*, **2002**, 14, 1183.
- [74] (a) Frenot, A., Chronakis, H. S., *Current opin. Colloid interf. Sci.*, **2003**, 8, 64. (b) Reneker, D. H., Chun, I., *Nanotechnology.*, **1996**, 7, 216. (c) Fong, H., Liu, W., Wang, C. S., Vaia, R. A., *Polymer.*, **2002**, 43, 775.
- [75] (a) Liu, H. I., Beigelsen, D. K., Ponce, F. A., Johnson, N. M., Pease, R. F., *Appl. Phys. Lett.*, **1994**, 64, 1383. (b) Xia, Y., Rogers, J. A., Paul, K. E., Whitesides, G. M., *Chem. Rev.*, **1999**, 99, 1823. (c) Yin, Y., Gates, B., Xia, Y., *Adv. Mater.*, **2000**, 12, 1426. (d) Lee, S. W., Oh, B-H., Sanedrin, R. G., Salaita, K., Fujigaya, T., Mirkin, C. A., *Adv. Mater.*, **2006**, 18, 1133. (e) Wang, L., Uppuluri, S. M., Jin, E. X., Xu, X., *Nano Lett.*, **2006**, 6, 361. (f) Kuo, C. W., Shiu, J. Y., Chen, P., *Chem. Mater.*, **2003**, 15, 2917.
- [76] (a) Wagener, M., Gunther, B., *J. Magnet. Mag. Mater.*, **1999**, 201, 41. (b) Mwabora, J. M., Lindgren, T., Avendano, E., Jaramillo, T. F., Lu, J., Lindquist, S. E., Granqvist, C. G., *J. Phys. Chem. B.*, **2004**, 108, 20193.
-

-
- [77] (a) Cannas, C., Musinu, A., Peddis, D., Piccaluga, G., *Chem. Mater.*, **2006**, 18, 3835. (b) Ismail, A. A., *Appl. Cata B. Environ.*, **2005**, 58, 115. (c) Babapour, A., Akhavan, O., Moshfegh, A. Z., Hosseini, A. A., *Thin Solid Film.*, **2006**, 515, 771. (d) Lu, Y., Yin, Y., Mayers, B. T., Xia, Y., *Nano Lett.*, **2002**, 2, 183.
- [78] (a) Gao, F., Lu, Q., Komarneni, S., *Chem. Mater.*, **2005**, 17, 856. (b) Rosemary, M. J., Pradeep, T., *J. Colloid. Interface Sci.*, **2003**, 268, 81.
- [79] Bronstein, L. M., Chernyshov, D. M., Timofeeva, G. I., Dubrovina, L. V., Valetsky, P. M., Obolonkova, E. S., Khokhlov, A. R., *Langmuir.*, **2000**, 16, 3626.
- [80] (a) Sun, Y., Mayers, B. T., Xia, Y., *Adv. Mater.*, **2003**, 15, 641. (b) Jin, Y., Dong, S., *J. Phys. Chem. B.*, **2003**, 107, 12902. (c) Chen, J., Saeki, F., Wiley, B. J., Cang, H., Cobb, M. J., Li, Z. Y., Au, L., Zhang, H., Kimmey, M. B., Li, X. D., Xia, Y., *Nano Lett.*, **2005**, 5, 473.
- [81] (a) Jayakumar, O. D., Salunke, H. G., Kadam, R. M., Mohapatra, M., Yaswant, G., Kulshreshtha, S. K., *Nanotechnology.*, **2006**, 17, 1278. (b) Yang, H., Song, X., Zhang, X., Ao, W., Qiu, G., *Mater. Lett.*, **2003**, 57, 3124.
- [82] (a) Clifffel, D. E., Zamborini, F. P., Gross, S. M., Murray, R. W., *Langmuir.*, **2000**, 16, 9699. (b) Yonezawa, T., Onoue, S., Kimizuka, N., *Langmuir.*, **2000**, 16, 5218. (c) Thomas, K.G., Zajicek, J., Kamat, P. V., *Langmuir.*, **2002**, 18, 3722.
- [83] (a) Henhar, R. S., Norstern, T. B., Rotello, V. M., *Adv. Mater.* **2005**, 17, 657. (b) Xiong, Y., Washio, I., Chen, J., Cai, H., Li, Z. Y., Xia, Y., *Langmuir.*, **2006**, 22, 8563.
- [84] (a) Selvakannan, P. R., Mandal, S., Phadtare, S., Gole, A., Pasricha, R., Adyanthaya, S. D., Sastry, M., *J. Colloid. Interface. Sci.*, **2004**, 269, 97. (b) Zhong, Z., Patskovskyy, S., Bouvrette, P., Luong, J. H. T., Gedanken, A., *J. Phys. Chem. B.*, **2004**, 108, 4046. (c) Fujiki, Y., Tokunaga, N., Shinkai, S., Sada, K., *Angew. Chem. Int. Ed.*, **2006**, 45, 4764. (d) You, C. C., De, M., Han, G., Rotello, V. M., *J. Am. Chem. Soc.*, **2005**, 127, 12873. (e) Sanyal, A., Mandal, S., Sastry, M., *Adv. Funct. Mater.*, **2005**, 15, 273.
- [85] (a) Brust, M., Fink, J., Bethell, D., Schiffrin, D. J., Kiely, C. J., *J. Chem. Soc. Chem. Commun.*, **1995**, 1655. (b) Cardenas-Trivino, G., Klabunde, K. J., Dale,
-

-
- E. B., *Langmuir.*, **1987**, 3, 986. (d) Cozzoli, P. D., Comparelli, R., Fanizza, E., Curri, M. L., Agostiano, A., le Laub, D., *J. Am. Chem. Soc.* **2004**, 126, 3868.
- [86] (a) Kim, K. S., Demberelnyamba, D., Lee, H., *Langmuir.*, **2004**, 20, 556. (b) Wang, Y., Yang, H., *Chem. Commun.*, **2006**, 2545.
- [87] (a) Ohde, H., Hunt, F., Wai, C. M., *Chem. Mater.*, **2001**, 13, 4130. (b) Viswanathan, R., Lilly, G. D., Gale, W. F., Gupta, R. B., *Ind. Eng. Chem. Res.*, **2003**, 42, 5535.
- [88] (a) Bronstein, L., Kramer, E., Berton, B., Burger, C., Forster, S., Antonietti, M., *Chem. Mater.*, **1999**, 11, 1402. (b) Jana, N. R. *Small.*, **2005**, 1, 875.
- [89] (a) Zhao, M., Crooks, R. M., *Angew. Chem. Int. Ed.*, **1999**, 38, 364. (b) Zhao, M., Sun, L., Crooks, R. M., *J. Am. Chem. Soc.*, **1998**, 120, 4877. (c) Niu, Y., Crooks, R. M., *Chem. Mater.*, **2003**, 15, 3463. (d) Scott, R. W. J., Wilson, O. M., Crooks, R. M., *J. Phys. Chem. B.*, **2005**, 109, 692.
- [90] (a) Hou, S., Harrell, C. C., Trofin, L., Kohli, P., Martin, C. R., *J. Am. Chem. Soc.*, **2004**, 126, 5674. (b) Go1ring, P., Pippel, E., Hofmeister, H., Wehrspohn, R. B., Steinhart, M., Go1sele, U., *Nano Lett.*, **2004**, 4, 1121.
- [91] (a) Quinn, B. M., Dekker, C., Lemay, S. G., *J. Am. Chem. Soc.*, **2005**, 127, 6146. (b) Guo, D. J., Li, H. L., *J. Colloid. Interface. Sci.*, **2005**, 286, 274. (c) Govindaraj, A., Satishkumar, B. C., Nath, M., Rao, C. N. R., *Chem. Mater.*, **2000**, 12, 202.
- [92] (a) Wong, K. K. W., Douglas, T.; Gider, S., Awschalom, D. D., Mann, S., *Chem. Mater.*, **1998**, 10, 279. (b) Willner, I., Baron, R., Willner, B., *Adv. Mater.*, **2006**, 18, 1109. (c) Klem, M. T., Willits, D., Solis, D. J., Belcher, A. M., Young, M., Douglas, T., *Adv. Funct. Mater.*, **2005**, 15, 1489.
- [93] (a) Douglas, T., Young, M., *Nature.*, **1998**, 393, 152. (b) Nam, K. T., Kim, D. W., Yoo, P. J., Chiang, C. Y., Meethong, N., Hammond, P. T., Chiang, Y. M., Belcher, A. M., *Science.*, **2006**, 312, 885. (c) Reiss, B. D., Mao, C., Solis, D. J., Ryan, K. S., Thomson, T., Belcher, A. M., *Nano Lett.*, **2004**, 4, 1127.
- [94] Goodsell, D. S., *Bionanotechnology, lessons from nature.*, **2004**, Eds.; Wiley-Liss: Weinheim.
- [95] (a) Addadi, L., Weiner, S., *Angew. Chem. Int. Ed.*, **1992**, 31, 153. (b) Weiner, S., Addadi, L., *J. Mater. Chem.*, **1997**, 7, 689.
-

-
- [96] Dujardin, E., Peet, C., Stubbs, G., Culver, J. N., Mann, S., *Nano Lett.*, **2003**, 3, 413.
- [97] Fratzl, P., *J. Royal. Soc. Interface.*, **2007**, 4, 637.
- [98] Tamerler, C., Sarikaya, M., *Acta. Biomaterialia.*, **2007**, 3, 289.
- [99] (a) Lowenstam, H. A., Weiner, S., *On Biomineralization*; Oxford University Press: New York, **1989**. (b) Mann, S., *Angew. Chem., Int. Ed.*, **2000**, 39, 3392.
- [100] (a) Lowenstam, H. A., *Science.*, **1981**, 211, 1126. (b) Mann, S., Webb, J., William, R. J. P., *Biomineralization; Chemical and Biochemical Perspectives.*, VCH Publishers, Weinheim, **1989**. (c) Simkiss, K., Wilbur, K. M., *Biomineralization*, Academic, San Diego, **1989**.
- [101] Lang, C., Schuler, D., Faivre, D., *Macromolecular Biosci.*, **2007**, 7, 144 .
- [102] Jun, Y. W., Seo, J. W., Cheon, J., *Acc. Chem. Res.*, **2008**, 41, 170 .
- [103] Komeili, A., *Annu. Rev. Biochem.*, **2007**, 76, 351.
- [104] Bazyliński, D. A., Frankel, R. B., *Nat. Rev. Microbiol.*, **2004**, 2, 217.
- [105] Sollner, C., Burghammer, M., Busch-Nentwich, E., Berger, J., Schwarz, H., Riekel, C., Nicolson, T., *Science.*, **2003**, 302, 282.
- [106] (a) Muller, W. E. G., Wendt, K., Geppert, C., Wiens, M., Reiber, A., Schroder, H. C., *Biosens. Bioelectron.*, **2006**, 21, 1149. (b) Muller, W. E. G., Eckert, C., Kropf, K., Wang, X. H., Schlomacher, U., Seckert, C., Wolf, S. E., Tremel, W., Schroder, H. C., *Cell. Tissue. Res.*, **2007**, 329, 363. (c) Sundar, V. C., Yablon, A. D., Grazul, J. L., Ilan, M., Aizenberg, J., *Nature.*, **2003**, 424, 899.
- [107] Baeuerlein, E., *Angew. Chem. Int. Ed.*, **2003**, 42, 614.
- [108] Zbinden M., Martinez I., Guyot F., Cambon-Bonavita, M. A., Gaill F., *Eur. J. Mineral.*, **2001**, 13, 653.
- [109] (a) Mann, S., *Biomineralization: Principles and Concepts in Bioinorganic Mater. Chemi.*, **2001**, Oxford University Press, Oxford. (b) Sarikaya, M., *PNAS.*, **1999**, 96, 25, 14183. (c) Young, J. R., *Reviews in Mineralogy and Geochemistry.*, 2003, 54, 1, 189.
- [110] Weiner, S., Traub, W., Lowenstam, H. A., *Biomineralization and Biological Metal Accumulation* (Eds. Westbroek, P.; Jong, E. W.; Dordrecht, R.), **1983**, pp. 205.
-

-
- [111] (a) Klaus, T., Joerger, R., Olsson, E., Granqvist, C. G., *Proc. Natl. Acad. Sci., U.S.A.* **1999**, 96, 13611. (b) Klaus, T. J., Joerger, R., Olsson, E., Granqvist, C. G., *Trends Biotechnol.*, **2001**, 19, 15.
- [112] (a) Beveridge, T. J., Murray, R. G. E., *J. Bacteriol.*, **1980**, 141, 876. (b) Fortin, D., Beveridge, T. J., *From biology to biotechnology and medical applications*. In: Baeuerien E (ed) *Biomineralization*, Wiley-VCH, Weinheim, **2000**, pp. 7.
- [113] Konishi, Y., Nomura, T., Tsukiyama, T., Saitoh, N., *Trans. Mater. Res. Soc. Jpn.* **2004**, 29, 2341.
- [114] Nair, B., Pradeep, T. *Cryst. Growth Des.*, **2002**, 2, 293.
- [115] Yong, P., Rowson, N.A., Farr, J. P. G., Harris, I.R., Macaskie, L. E., *Biotechnol. Bioeng.*, **2002**, 80, 369.
- [116] Lengke, M., F., Fleet, M., E., Southam, G., *Langmuir.*, **2006**, 22, 7318.
- [117] Ahmad, A., Senapati, S., Khan, M. I., Kumar, R., Sastry, M., *Langmuir.*, **2003**, 19, 3550.
- [118] (a) Mukherjee, P., Ahmad, A., Mandal, D., Senapati, S., Sainkar, S. R., Khan, M. I., Ramani, R., Parischa, R., Ajayakumar, P. V., Alam, M., Sastry, M., Kumar, R., *Angew. Chem. Int. Ed.*, **2001**, 40, 3585. (b) Mukherjee, P., Ahmad, A., Mandal, D., Senapati, S., Sainkar, S. R., Khan, M. I., Parischa, R., Ajayakumar, P. V., Alam, M., Kumar, R., Sastry, M., *Nano Lett.*, **2001**, 1, 515.
- [119] (a) Mukherjee, P., Senapati, S., Mandal, D., Ahmad, A., Khan, M. I., Kumar, R., Sastry, M., *Chem. Bio. Chem.*, **2002**, 3, 461. (b) Ahmad, A., Mukherjee, P., Senapati, S., Mandal, D., Khan, M. I., Kumar, R., Sastry, M., *Colloids. Surf B.*, **2003**, 28, 313.
- [120] Senapati, S., Ahmad, A., Khan, M. I., Sastry, M., Kumar, R. *Small.*, **2005**, 1, 517.
- [121] Dameron, C., T. Reese, R. N., Mehra, R. K., Kortan, A. R., Carrol, P. J., Steigerwald, M. L., Brus, L. E., Winge, D. R., *Nature*, **1989**, 338, 596.
- [122] Sweeney, R. Y., Mao, C., Gao, X., Burt, J. L., Belcher, A. M., Georgiou, G., Iverson, B. L., *Chem. Biol.*, **2004**, 11, 1553.
- [123] Labrenz, M., Druschel, G. K., Thomsen-Ebert, T., Gilbert, B., Welch, S. A., Kemner, K. M., Logan, G. A., Summons, R. E., Stasio, G. D., Bond, P. L., Lai, B., Kelly, S. D., Banfield, J. F., *Science.*, **2000**, 290, 1744.
-

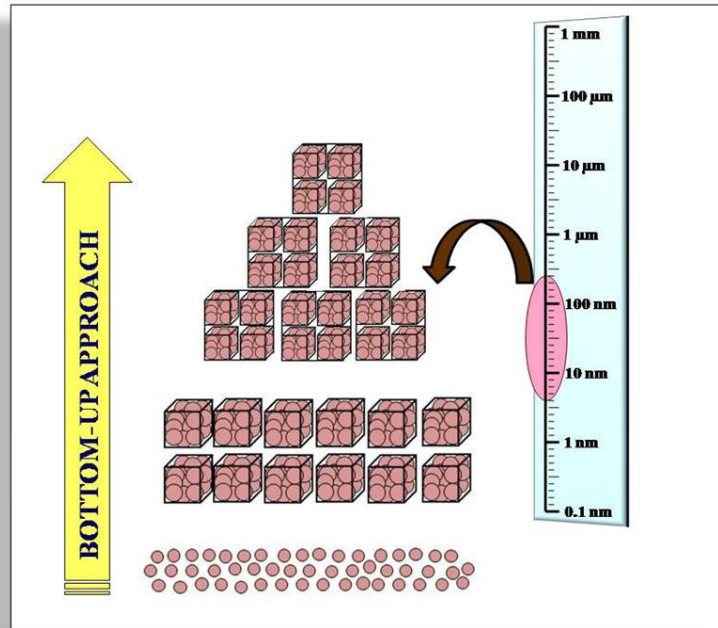
-
- [124] (a) Kowshik, M., Vogel, W., Urban, J., Kulkarni, S. K., Paknikar, K. M., *Adv. Mater.*, **2002**, 14, 815. (b) Kowshik, M., Deshmukh, N., Vogel, W., Urban, J., Kulkarni, S. K., Paknikar, K. M., *Biotechnol. Bioeng.*, **2002**, 78, 583.
- [125] Ahmad, A., Mukherjee, P., Mandal, D., Senapati, S., Khan, M. I., Kumar, R., Sastry, M., *J. Am. Chem. Soc.*, **2002**, 124, 12, 108.
- [126] Ahmad, A., Mukherjee, P., Senapati, S., Mandal, D., Khan, M. I., Kumar, R., Sastry, M., *Colloids and Surfaces B: Biointerfaces*, **2003**, 28, 313.
- [127] (a) Bansal, V., Rautaray, D., Bharde, A., Ahire, K., Sanyal, A., Ahmad, A., Sastry, M., *J. Mater. Chem.*, **2005**, 15, 2583. (b) Bansal, V., Sanyal, A., Rautaray, D., Ahmad, A., Sastry, M., *Adv Mater.*, **2005**, 17, 889. (c) Bansal, V., Rautaray, D., Ahmad, A., Sastry, S., *J. Mater. Chem.*, **2004**, 14, 3303. (d) Uddin, I., Adyanthaya, S., Syed, A., Selvaraj, K., Ahmad, A., Poddar, P., *J. Nanosci. Nanotechnol.*, **2008**, 8, 3909. (e) Bharde, A., Rautaray, D., Bansal, V., Ahmad, A., Sarka, I., Yusuf, S. M., Sanyal, M., Sastry, M., *Small.*, **2006**, 2, 1, 135. (f) Bansal, V., Poddar, P., Ahmad, A., Sastry, M., *J. Am. Chem. Soc.*, **2006**, 128, 36, 11958.
- [128] Kumar, U., Shete, A., Harle, A. H., Kasyutich, O., Schwarzacher, W., Pundle, Poddar, P., *Chem. Mater.*, **2008**, 20, 1484.
- [129] (a) Rautaray, D., Ahmad, A., Sastry, M., *J. Am. Chem. Soc.*, **2003**, 125, 14656. (b) Rautaray, D., Sanyal, A., Bharde, A., Ahmad, A., Sastry, S., *Cryst. Growth Des.*, **2005**, 5, 399.
- [130] (a) Bansal, V., Ahmad, A., Sastry, M., *J. Am. Chem. Soc.*, **2006**, 128, 14059. (b) Bansal, V., Syed, A., Bhargava, S. K., Ahmad, A., Sastry, M., *Langmuir.*, **2007**, 23, 4993.
- [131] Cannon, H. L., Shacklette, H. T., Bastron, H., *Metal Absorption by Equisetum (horsetail).*, United States Geological Survey Bulletin 1278-A, **1968**, A1.
- [132] Shacklette, H. T., Lakin, H. W., Hubert, A. E., Curtin, G. C., *Absorption of Gold by Plants.*, United States Geological Survey Bulletin 1314-B, **1970**, 1.
- [133] (a) Arnott, H. J., **1982.**, *Three systems of biomineralization in plants with comments on the associated organic matrix.* In (Ed: Nancollas, G. H.), *Biological Mineralization and Demineralization.* Springer Verlag, Berlin, pp. 199. (b) Monje, P. V., Baran, E. J., **2004.**, *Plant biomineralization.* In (Ed:
-

-
- Hemantaranjan, H.), *Advances in Plant Physiology*, vol. 7. Scientific Publishers, Jodhpur, pp. 403.
- [134] (a) Lakin, H. W., Curtin, G. C., Hubert, A. E., Shacklette, H. T., Doxtader, K. G., *Geochemistry of Gold in the Weathering Cycle*, United States Geological Survey Bulletin, **1974**, 1330, 1. (b) Torresdey, J. L. G., Parson, J. G., Gomez, E., Videa, J. P., Troiani, H. E., Santiago, P. Yacaman, M. J., *Nano Lett.* **2002**, 2, 397. (b) Torresdey, J. L.G., Gomez, E., Peralta, J. P., Parsons, J. G., Troiani, H., Yacaman, M. J., *Langmuir.*, **2003**, 19, 1357.
- [135] (a) Shankar, S. S., Ahmad, A., Sastry, M., *Biotech. Progress.*, **2003**, 19, 1627. (b) Shankar, S. S., Ahmad, A., Parischa, R., Sastry, M., *J. Mater. Chem.*, **2003**, 13, 1822.
- [136] Shankar, S. S., Rai, A., Ahmad, A., Sastry, M., *J. Colloid. Interf. Sci.*, **2004**, 275, 496.
- [137] (a) Shankar, S. S., Rai, A., Ankamwar, B., Singh, A., Ahmad, A., Sastry, M., *Nat. Mater.*, **2004**, 3, 482. (b) Shankar, S. S., Rai, A., Ahmad, A., Sastry, M., *Chem. Mater.*, **2005**, 17, 566.
- [138] Ankamwar, B., Damle, C., Ahmad, A., Sastry, M., *J. Nanosci. Nanotechnol.*, **2005**, 5, 1665.
- [139] Ball, P., *Made To Measure: New Materials for the 21st Century*, **1997**, Princeton University Press, New Jersey.
- [140] (a) Shenton, W., Douglas, T., Young, M., Stubbs, G., Mann, S., *Adv. Mater.*, **1999**, 11, 253. (b) Dujardin, E., Peet, C., Stubbs, G., Culver, J. N., Mann, S., *Nano Lett.*, **2003**, 3, 413. (c) Ongaro, A., Griffin, F., Beecher, P., Nagle, L., Iacopino, D., Quinn, A., Redmond, G., Fitzmaurice, D., *Chem. Mater.*, **2005**, 17, 1959.
- [141] Braun, E., Eichen, Y., Sivan, U., Ben-Yoseph, G., *Nature.*, **1998**, 391, 775.
- [142] Hall, S. R., Shenton, W., Engelhardt, H., Mann, S., *Chem Phys Chem.*, **2003**, 3, 184.
- [143] (a) Bhattachargee, R. R., Das, A. K., Haldar, D., Si, S., Banerjee, A., Mandal, T. K., *J. Nanosci. Nanotechnol.*, **2005**, 5, 7, 1141. (b) Naik, R. R., Jones, S. E., Murray, C. J., McAuliffe, J. C., Vaia, R. A., Stone, M. O., *Adv. Funct. Mater.*, **2004**, 14, 25.
- [144] Hall, S. R., Bolger, H., Mann, S., *Chem. Commun.* **2003**, 2784.
-

-
- [145] Defrancesco. L., *Nat. Biotechnol.*, **2003**, 21, 1127.
- [146] Gao, X., Cui, Y., Levenson, R. M., Chung, L. W. K., Nie, S., *Nat. Biotechnol.*, **2004**, 22, 969.
- [147] Pilarski, L. M., Mehta, M. D., Caulfield, T., Kaler, K. V. I. S., Backhouse, C. J., *Bull. Sci. Technol. Soc.*, **2004**, 24, 1, 40.
- [148] Son, S. J., Bai, X., Lee, S. B., *Drug. Discovery. Today.*, **2007**, 12, 15/16, 657.
- [149] Wang, A. Z., Gu, F., Zhang, L., Juliana M Chan , Moreno, A. R., Shaikh, M. R., Farokhzad, O. C., *Expert. Opin. Biol. Ther.*, 2008, 8, 8, 1063.
- [150] Mohanraj, V. J., Chen, Y., *Trop. J. Pharmacol. Res.*, **2006**, 5 1, 561.
- [151] Zhang, L., Gu, F. X., Chan, J. M., Wang, A. Z., Langer, R. S., Farokhzad O. C., *Clin. Pharmacol. Ther.*, **2008**, 83, 5, 761.
- [152] Hughes, G. A., *Nanomed. Nanotechnol. Bio. Med.*, **2005**, 1, 22.
- [153] Andujar, C. B., Tung, L. D., Thanh, N. T. K., *Annu. Rep. Prog. Chem., Sect. A.*, **2010**, 106, 553.
- [154] Cai, W., Gao, T., Hong, H., Sun, J., *Nanotechnol. Sci. Appl.*, **2008**, 1, 17.
- [155] Rosi, N. L., Mirkin, C. A., *Chem. Rev.* **2005**, 105, 1547.
- [156] Riehemann, K., Schneider, S. W., Luger, T. A., Godin, B., Ferrari, M., Fuchs, H., *Angew. Chem. Int. Ed.*, **2009**, 48, 872.
- [157] Venkatesan, B. M., Bashir, R., *Nat. Nanotechnol.*, **2011**, 6, 615.
- [158] Cai. W., Chen. X., *Small.*, **2007.**, 3, 11, 1840.
- [159] Erathodiyil, N., Ying, J. Y., *Acc. Chem. Res.*, **2011**, 44, 10, 925.
- [160] De, M., Ghosh, P. S., Rotello, V. M., *Adv. Mater.*, **2008**, 20, 1.
- [161] Huang, X., El-Sayed, I. H., Qian, W., El-Sayed, M. A., *J. Am. Chem. Soc.*, **2006**, 128, 6, 2115.
- [162] Michalet, X., Pinaud, F. F., Bentolila, L. A., Tsay, J. M., Doose, S., Li, J. J., Sundaresan, G., Wu, A. M., Gambhir, S. S., Weiss, S., *Science.*, **2005**, 307, 538.
- [163] Praetorius, N. P., Mandal, T. K., *Recent Patents on Drug Delivery & Formulation* **2007**, 1, 37.
- [164] Cho, K., Wang, X., Nie, S., Chen, Shin, D. M., *Clin. Cancer. Res.*, **2008**, 14, 5, 1311.
- [165] Peppas, L. B., Blanchette, J. O., *Adv. Drug. Delivery. Rev.*, **2004**, 56, 1649.
- [166] Huang, X., Jain, P. K., El-Sayed, I., El-Sayed, M. A., *Nanomedicine.*, **2007**, 2, 5, 681.
-

Chapter 2

Bottom-up biosynthetic approach to synthesize Metal Oxides nanoparticles



*This chapter describes the introductory remark of bottom-up approach to synthesize metal oxides nanoparticles and how the bottom-up biosynthetic approach is much better in comparison with top-down and other wet-chemical techniques which often employ toxic chemicals, physico-chemical conditions, high temperature and pressure. This chapter is divided into three parts where the synthesis of metal oxide nanoparticles: Bi_2O_3 , Mn_5O_8 and CrO_2 , using fungus *Fusarium oxysporum* and *Trichothecium* sp. is described.*

Bottom-up approach involves putting together smaller components (such as individual atoms and molecules) to form a larger and more complex system by leveraging naturally occurring chemical, physical and biological processes. Bottom-up approach refers to building-up of the material atom-by-atom, molecule-by-molecule or cluster-by-cluster. It is the atom-by-atom assembly and begins by designing and synthesizing custom made molecules that have the ability to self organize themselves into higher order mesoscale and macroscale structures. Below certain size range, synthesis of nanoparticles by the top-down approach becomes costly and laborious. Top-down approach can also produce surface defects, internal stresses and contamination due to harsh conditions at the time of synthesis of nanoparticles, which may affect surface and physical properties of the nanomaterials. Therefore, top-down approach reaches its practical and theoretical limits, where as bottom-up approach promises a better chance to obtain nanostructures with less defects, more homogenous chemical composition, and better short and long range ordering. This is because the bottom-up approach is driven mainly by the reduction of Gibbs free energy, so that the nanostructures and nanomaterials produced are in a state closer to thermodynamic equilibrium.

Broadly speaking, bottom-up approach should be able to produce devices in parallel and much cheaper rates than top-down methods. Generally, the bottom-up approach offers greater control over the structural properties rather than the top-down approach. Moreover, large scale synthesis of nanomaterials remains a challenge because when a structure falls into the nanometer scale, it narrows down the choice for a top-down approach as all the tools we possess are too big to deal with such tiny objects.

Bottom-up strategies by which the nanomaterial is built up from its constituent elements generally involve two phases namely nucleation phase and growth phase. In nucleation phase, metal ions contained in the precursors are reduced by a suitable reducing agent in the presence of a capping ligand to produce tiny seed particles. When the solution becomes supersaturated, these seed particles precipitate spontaneously. Nucleation phase is followed by the growth phase where the precipitated seeds capture dissolved atoms or molecules and grow in size. Usually the restriction of the condensation or the growth at a particular point leads to the formation of particles of desired size and shape.

Metal oxide nanoparticles are of great interest due to their improved optical and electronic properties with applications such as piezoelectric, electro-optic and

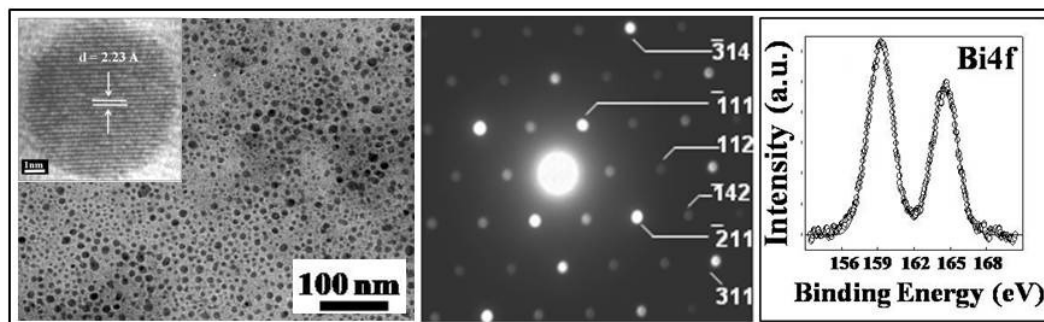
dielectric materials and are less toxic or more biocompatible than metal nanoparticles. Metaloxides such as titania (TiO_2), zirconia (ZrO_2), silica (SiO_2), iron oxide (Fe_3O_4), alumina (Al_2O_3), zinc oxide (ZnO), etc. play an important role in many key technologies and globally constitute an exceptionally large volume industry. In going to attain nanoscale dimensions, the properties of these nanooxides change dramatically and have important potential applications. Nanooxides in large quantities are currently produced by chemical methods. Although chemical synthesis procedures result in a good control over shape, size and crystallinity, they often employ toxic chemicals, volatile solvents and intense physico-chemical conditions. Another major disadvantage with chemical methods is that they are energy intensive and thus increase the production costs. Therefore, researchers are currently more interested toward the development of environmentally benign procedures for nanoparticle synthesis that do not use toxic chemicals. As a result, researchers have been focusing their attention toward the biological processes for nanomaterial synthesis as they operate at environmentally benign conditions. Many biological organisms synthesize highly functional inorganic materials of complex composition and structure like bones and teeth for example. Classical examples of microorganisms that synthesize nanooxides are diatoms (amorphous silica) and magnetotactic bacteria (magnetic iron oxide nanoparticles). The synthesis of these oxide nanoparticles is achieved at room temperature and under benign solvent conditions. Recognizing that production of nanomaterials by biological methods would address the shortcomings of the chemical method and lead to potentially large cost reduction. Ahmad *et al.* have developed methods for the synthesis of gold and silver nanoparticles, metal sulphides and nanooxides such as titania, zirconia, silica, iron oxide, etc. in an aqueous solution. The quality of the nanooxides produced by this process is comparable to the commercially available products. It uses microbes or other biological materials to synthesize nanoparticles. The biomimetic approaches of the controlled synthesis of nanomaterials based on the use of microbes are fast gaining popularity where the microbes participate via reduction, oxidation or hydrolysis of the transition metal ion precursors and also by acting as templates. The as-synthesized nanomaterial surfaces are inherently functionalized by proteins and other biomolecules which not only facilitate further linking to other ligands but also provide the much needed surface passivation, prevention from agglomeration and stable suspension in the aqueous medium which often is difficult to attain by the wet-chemical approaches.

The development of reliable, eco-friendly processes for the synthesis of nanoscale materials is an important aspect of nanotechnology. The mechanism for synthesis of nanoparticles by biological systems has better control over shape, size and kinetics together with characterization and applications. It is feasible to synthesize nanoparticles at room temperature, neutral or mild pH and close to ambient conditions, which is not possible by any physical or chemical methods. This approach has brought a turning point in method of synthesis of nanoparticles. Heavy metal ions as we know are toxic to biological systems. Hence microorganisms like bacteria, yeast and fungi detoxify these metal ions by reducing them into metallic state, which are nontoxic to them. These metal atoms then come together and grow to the nanometer sizes leading to the formation of nanoparticles, which are stabilized by biological system. In chemical synthesis, one needs a capping agent such that nanoparticles should not sinter with each other. On the contrary, in biological synthesis one does not need a capping agent because proteins secreted by the fungus are used here as capping agent.

In bottom-up approach, we demonstrate that fungal biomass is capable of synthesizing some difficult phase of transition metal oxide nanoparticles at ambient condition. Here we used the room temperature bottom-up biosynthetic approach for the synthesis of Bi_2O_3 , Mn_5O_8 and CrO_2 nanoparticles by extra-cellularly challenging the mesophilic fungus *Fusarium oxysporum* and alkalotolerant mesophilic fungus *Trichothecium* sp. respectively. In this approach, the surface of the particles is capped by protein which provides stability in aqueous medium. This chapter is divided into three parts.

- 2A. Structure and microbial synthesis of sub-10 nm Bi_2O_3 nanocrystals.
- 2B. Fungus mediated synthesis of protein capped CrO_2 nanoparticles.
- 2C. Fungus based synthesis of Mn_5O_8 nanoparticles.

Chapter 2A



Structure and Microbial Synthesis of Sub-10 nm Bi_2O_3 Nanocrystals

*This chapter describes a biological route for the synthesis of bismuth oxide nanoparticles mediated by fungus *Fusarium oxysporum*. The fungus, on exposure to the aqueous solutions of bismuth nitrate as a precursor, results in extracellular biosynthesis of bismuth oxide nanoparticles in the size range of 5-8 nm under ambient conditions. The particle surfaces are passivated by a robust layer of proteins which provides stability in aqueous medium. Structural investigation done using selected area electron diffraction (SAED) and powder XRD shows that particles primarily crystallize in the α -phase with a monoclinic structure. The particle size analysis was performed using TEM. Further material characterization was done using techniques such as XPS, FTIR and TGA.*

The work described in this chapter has been published as: *Structure and Microbial Synthesis of Sub-10 nm Bi_2O_3 Nanocrystals*” Imran Uddin, Suguna Adyanthaya, Asad Syed, K. Selvaraj, Absar Ahmad*, Pankaj Poddar*, *J. Nanosci. Nanotechnol.*, 2008. 8, 3909 – 3913.

2.1.1 Introduction

Bismuth oxide (Bi_2O_3) has a relevant importance in modern solid state technology. In its nanoparticulate form, it is an interesting optoelectronic material, with a large band-gap, high value of refractive-index, dielectric-permittivity, as well as remarkable photoconductivity and photoluminescence [1, 2] which makes it a favorite material where tunability of both optical and electronic properties are required. In small size, Bi_2O_3 shows an increase in the band gap like other semiconductor materials and shows a clear blue shift in the absorbance [3]. Bi_2O_3 nanoparticles also have potential application as an additive into the optical glass/polymer formulations to increase their refractive index and specific gravity. Bismuth oxide as a component finds use in wide applications in gas sensors [4], optical coatings [5], photovoltaic cells, optical communication devices, optoelectronics, oxide electrolytes and fuel cell [6, 7]. Bismuth oxide nanoparticles exhibit enhanced thermoelectric properties at room temperature. So it is particularly interesting as potential thermoelectric and “green” lubricant materials. Bismuth oxide is incorporated into specialty polymers and materials for bone implants, dental prosthetic devices, catheters, sutures and surgical instruments to make them detectable by X-rays without the toxicity or carcinogenicity associated with other heavy metals. Bismuth oxide has been used extensively for years in the medical appliance industry to impart X-ray opacity. Other applications for bismuth oxide include ceramic additives for varistors that are used for electrical surge protectors, additives to reduce processing temperatures for high-temperature ceramics that are used in gas and in fluid detectors to improve automotive fuel efficiency and reduce smog, additives into optical glass formulations to increase refractive index and specific gravity, and as an additive in a variety of medical creams and ointments. All these special properties explain the interest and great efforts devoted to the synthesis and characterization of bismuth oxide nanoparticles.

The crystalline structure of this material is quite rich with different polymorphs [8, 9]. Bismuth oxide has five main polymorphic forms that are known as: $\alpha\text{-Bi}_2\text{O}_3$ (monoclinic), $\beta\text{-Bi}_2\text{O}_3$ (tetragonal), $\gamma\text{-Bi}_2\text{O}_3$ (face-centered-cubic), $\delta\text{-Bi}_2\text{O}_3$ (face-centered cubic) and $\omega\text{-Bi}_2\text{O}_3$ (triclinic). Each polymorph possesses distinct crystalline structure and physical (electrical, optical, etc.) properties [10]. Among these phases, the low-temperature α -phase and high-temperature δ -phase are stable, and the others are high temperature metastable phases [11]. The stability of these polymorphic forms

of Bi_2O_3 is known to depend upon various conditions such as temperature, thermal treatment, chemical doping, etc [12, 13]. The room temperature phase is monoclinic which transforms to a cubic phase at high temperature (known as $\delta\text{-Bi}_2\text{O}_3$). This phase of Bi_2O_3 is also reported to have extremely high ionic conductivity which makes it a potential candidate for the fuel cell electrolytes as well as for sensor applications [14, 15]. Thus, minor doping of Bi_2O_3 with various oxides results in the formation of a body-centered-cubic solid solution (b.c.c), referred to as $\gamma\text{-Bi}_2\text{O}_3$ [16].

In an effort to get monodispersed nanoparticles of Bi_2O_3 , several synthesis methods have been attempted. Typically Bi_2O_3 is prepared via the oxidation of bismuth metal at 800°C , via thermal decomposition of carbonates or hydroxides produced by the addition of alkali metal hydroxides to bismuth salt solution [17]. These powders on calcinations yields fine particles of Bi_2O_3 . Flame spray pyrolysis [18] is also used to produce nano-sized Bi_2O_3 particles. Recently, few methods on “gel to crystalline” conversion route and citrate-gel techniques have been used to make Bi_2O_3 which resulted in particles as small as 50 nm in size [19, 20]. A microemulsion based technique was also used that reported particles with further smaller size (5 to 10 nm); however, this method reported poor crystallinity of the particles. Several of these conventional wet-chemical methods are known to often use high temperatures, high pressure and multi-step techniques. Often, the as-synthesized particles are agglomerated due to their delicate surface coatings which do not often provide enough surface passivation and stability over a period of time. Ahmad *et al.* have recently developed a novel technique based on fungi which is capable of synthesizing a variety of materials (often size less than 10 nm) such as metals, alloys, binary oxides as well as ternary oxides [21]. This eco-friendly, room temperature method is capable of selectively performing reduction and oxidation reactions at different pH values which gives it additional advantages often enjoyed by chemical methods alone.

In this chapter, we present the fungus based room temperature synthesis of sub-10 nm Bi_2O_3 nanoparticles, where protein is acting both as a capping as well as a reducing agent. The structure and crystallinity of these particles was characterized by powder XRD, selected area electron diffraction (SAED) and high resolution transmission electron microscopy (HR-TEM). XRD analysis showed that particles are well crystalline with a mixture of monoclinic and tetragonal phases. Further material characterization was done using techniques such as XPS, FTIR and TGA. Mesophilic

fungus *Fusarium oxysporum* was used for this purpose which is discussed in the sections below.

2.1.2 Experimental Details

Bismuth (III) nitrate pentahydrate [$\text{Bi}(\text{NO}_3)_3 \cdot 5\text{H}_2\text{O}$] of guaranteed reagent (GR) grade was obtained from Merck Chemicals. Malt extract powder, yeast extract powder, glucose, and peptone were obtained from Himedia and used as-received. The mesophilic fungus *Fusarium oxysporum* was cultured and fungal mycelia was inoculated in 500 ml Erlenmeyer flask containing 100 ml of MGYB broth composed of malt extract (0.3%), glucose (1%), yeast extract (0.3%) and peptone (0.5%) at 28°C, under shaking conditions (200 rpm) for 72 hours. After incubation, we washed the fungal mycelia thoroughly under sterile conditions and harvested. 20 gram of fungal mycelia which was then resuspended in 100 ml aqueous solution of 10^{-3}M Bismuth(III) nitrate 5-hydrate ($\text{Bi}(\text{NO}_3)_3 \cdot 5\text{H}_2\text{O}$) in 500 ml Erlenmeyer flasks and kept on shaker at 28°C and 200 rpm. The reaction was carried out for a period of 96 hours and fungal biomass was separated by filter paper to collect biomass in sterile conditions.

The biogenic products of the reactions were collected under sterile conditions at various time intervals during the reaction by separating the fungal mycelia from the aqueous extract through filtration. The filtrate was then used to check the formation of nanoparticles. To remove the unbound protein and unreacted precursor, we centrifuged the filtrate three times at 15,000 rpm for 30 minutes and each time the precipitate was resuspended in the de-ionized water. Further characterization of the purified products as well as of the calcined products (400°C for three hours) were carried out by Transmission electron microscopy (TEM), Selected area electron diffraction (SAED) analysis, X-ray diffraction (XRD) analysis, Fourier transform infrared (FTIR) spectroscopy, Thermogravimetric analysis (TGA), Electron dispersive X-rays (EDAX) analysis and X-ray photoemission spectroscopy (XPS).

2.1.3 Morphological features of *Fusarium oxysporum*

Mesophilic fungus *Fusarium oxysporum* was used for synthesis of Bi_2O_3 nanoparticles. Figure 2.1.1 shows that the fungus *Fusarium oxysporum* grown on potato dextrose agar (PDA) produced slow growing colonies. Colonies on PDA showed the following characters: snow white, circular, hyphae profusely branched

and septate. The fungus produced three types of spores called macroconidia, microconidia and chlamydo spores. Macroconidia, fusoid with prominent foot cell, three septate, fewer in number than microconidia. Microconidia are produced from short lateral phialide. Microconidia are oval to cylindrical, straight to curved, variable in shape and size, produced abundantly and single celled. Chlamydo spores formed after 10-15 days produce from lateral hyphae.

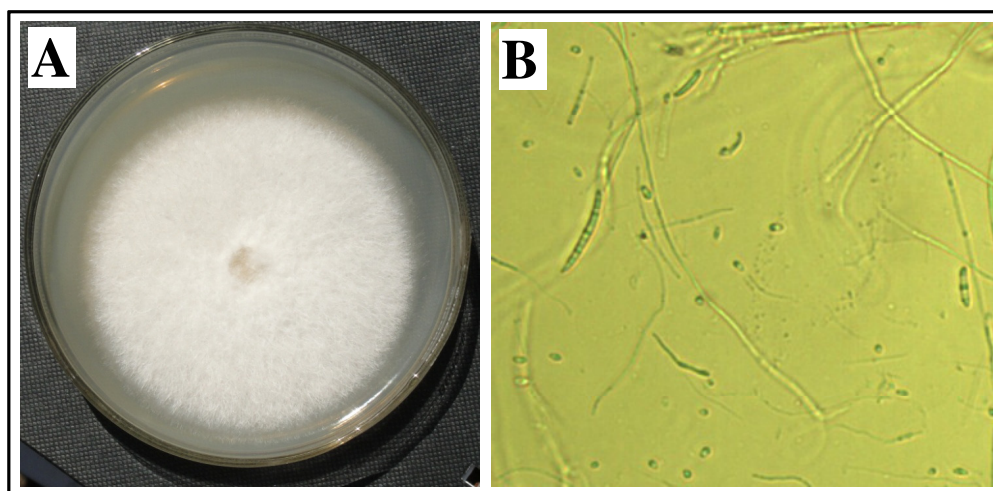


Figure: 2.1.1: Morphological features of *Fusarium oxysporum*. The *Fusarium oxysporum* was grown on PDA for microscopic observation (A) Macroconidia, microconidia and chlamydo spores produced on agar medium (B)

2.1.4 Results and Discussions

2.1.4.1 TEM and SAED analysis

In Figure 2.1.2 (A, B) we have shown representative transmission electron micrograph images of as-synthesized nanoparticles, which shows an overall quasi-spherical morphology. The inset figure 2.1.2A shows the particle size distribution curve; it was calculated that average particle size is between 5-8 nm. In the figure 2.1.2 (C), we have shown the selected area electron diffraction (SAED) pattern, which shows a nice spot pattern confirming the single crystallinity of the as-synthesized protein coated nanoparticles. We indexed the SAED spot {311}, {020}, {252}, {023}, {113}, and {653} for monoclinic crystal lattice ($a=5.849\text{\AA}$, $b=8.169\text{\AA}$, $c=7.512\text{\AA}$, $\alpha=\gamma$, $\beta=112.98^\circ$) with space group $P2_1/c(14)$. We know that proteins cap the as-synthesized nanoparticles and calcination at 400°C for three hours burns capped proteins/biomolecules.

Thus, to further investigate the effect of calcination on the particle morphology as well as crystallinity, we calcined these particles at 400°C for 3 hours in air, which resulted into degradation of protein layer. In Figure 2.1.2 D and E, we have shown the TEM images of the calcined particles, which shows significant increase in the average particle size up to 12 nm (Inset figure 2.1.2 D).

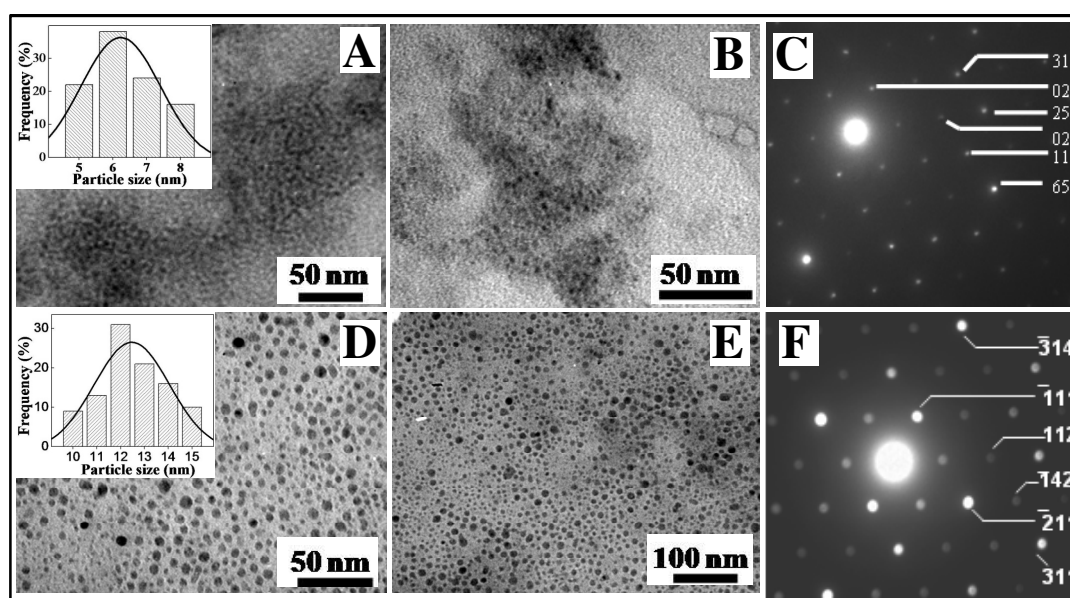


Figure 2.1.2: TEM images of as-synthesized (A and B) Bi_2O_3 nanoparticles obtained after 72 hours of reaction between *Fusarium oxysporum* and $\text{Bi}(\text{NO}_3)_3 \cdot 5\text{H}_2\text{O}$. SAED pattern (C) shows the crystalline nature of particles. Calcination of as synthesized nanoparticles leads to an increase in particle (D and E) size. The inset figures A, D shows particle size distribution of as-synthesized and calcined nanoparticles respectively. Image F shows SAED pattern obtained from calcined nanoparticles.

The SAED pattern for the calcined samples presented in the figure 2.1.2 (F) again reveals a well-defined spot pattern, which shows the increased crystallinity, indexed again based on monoclinic phase of Bi_2O_3 . These spot pattern were referred for $\{\bar{3}14\}$, $\{\bar{1}11\}$, $\{112\}$, $\{\bar{1}42\}$, $\{\bar{2}11\}$ and $\{311\}$ crystal planes, which matches well with the reported values [22].

2.1.4.2 HR-TEM analysis

To further investigate, crystallinity at the single particle level, we performed HR-TEM. In Figure 2.1.3, we have shown the HR-TEM images of Bi_2O_3 nanoparticles after 72 hours of reaction for as-synthesized (figure 2.1.3A) and calcined (figure 2.1.3B) particles. Both the figures show clearly resolved lattice fringes of Bi_2O_3

nanoparticles which indicate very good crystallinity with very few defects. In fact, our HR-TEM images are in-consistent with the SAED patterns shown above where primarily dot patterns are observed. The extent of single-crystallinity and defect free structure observed here in biologically synthesized particles is quite remarkable. The lattice planes show a spacing of $\sim 3.04 \text{ \AA}$ for the as-prepared sample (fig. 2.1.3A) and $\sim 2.23 \text{ \AA}$ for the sample calcined at 400°C (Fig. (2.1.3B)) having the lattice planes $\{012\}$ and $\{222\}$ respectively.

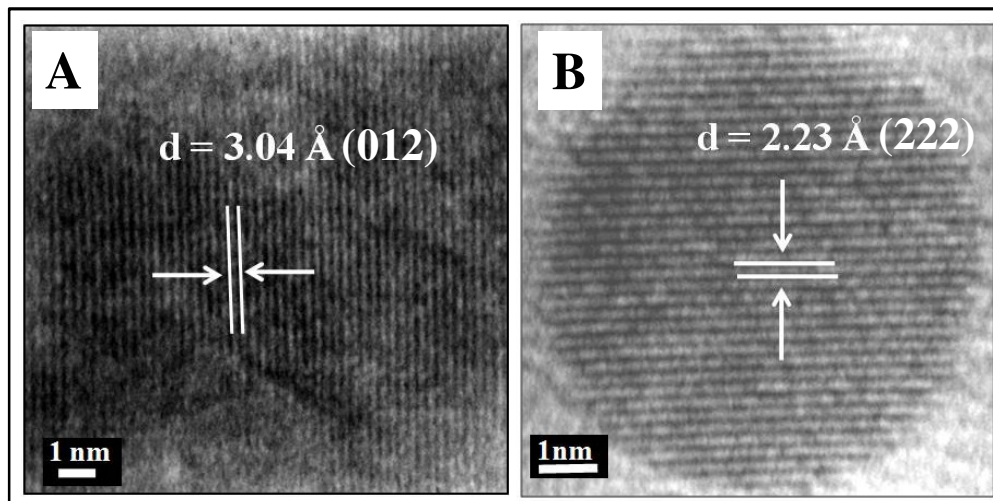


Figure 2.1.3: HR-TEM micrograph of Bi_2O_3 nanoparticles synthesized using *Fusarium oxysporum* before (A) and after calcination at 400°C for 3 hours (B).

2.1.4.3 X-ray diffraction analysis

To confirm the crystalline phase of as-synthesized material in detail, we prepared samples for powder X-ray diffraction. In the bulk form, bismuth oxide is known to show five main structural modifications, which possess distinct crystalline structures and physical (electrical, optical, etc.) properties [8, 9]. Two stable polymorphic forms include the first one which is stable at relatively lower temperature monoclinic $\alpha\text{-Bi}_2\text{O}_3$ and the other one which is stable at high temperature cubic $\delta\text{-Bi}_2\text{O}_3$. Other polymorphs are high temperature metastable phases known as tetragonal $\beta\text{-Bi}_2\text{O}_3$ and b.c.c. $\gamma\text{-Bi}_2\text{O}_3$. The α -form, stable at room temperature, is usually described as being monoclinic, although this structure may be better described as orthorhombic. The bismuth ions have a pseudo-octahedral coordination with one vacant site, and the vacancies are ordered so as to create a layered structure. Above 717°C , the δ -form has the cubic fluorite structure with randomly distributed oxide vacancies.

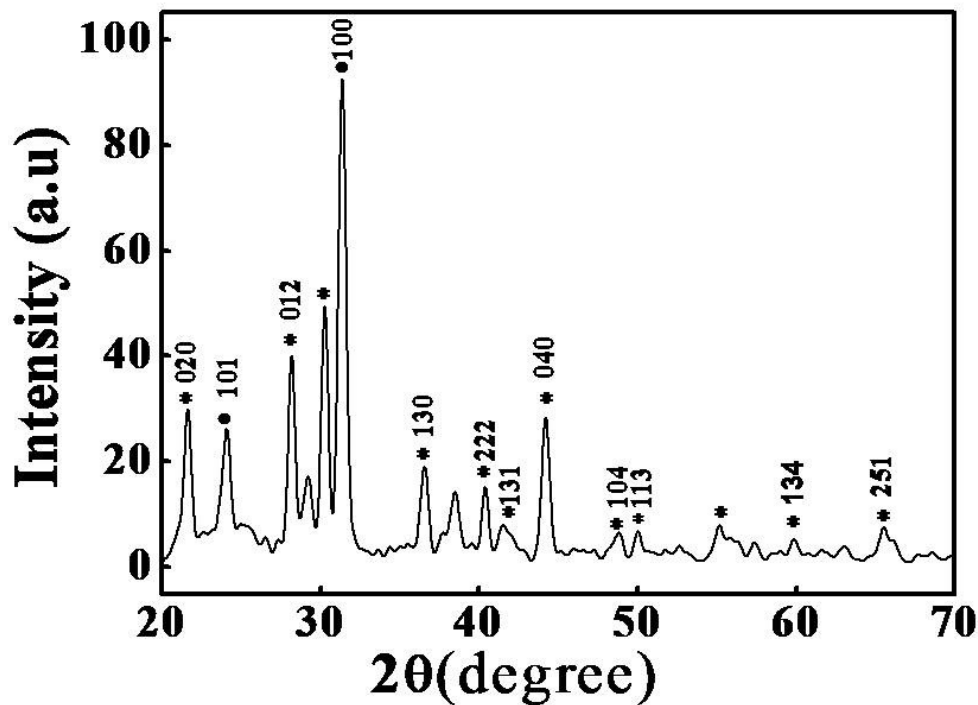


Figure 2.1.4: Powder XRD-pattern of as-synthesized Bi_2O_3 nanoparticles. Peaks assigned by * and • represent monoclinic and tetragonal phases respectively.

In Figure 2.1.4, we have presented the room temperature XRD pattern obtained from as-synthesized particles which shows predominantly monoclinic $\alpha\text{-Bi}_2\text{O}_3$ phase [22]. However, two of the peaks from the XRD pattern, out of which {100} one is most intense, indicates the presence of tetragonal phase as well. The co-existence of both monoclinic and tetragonal phase at the room temperature is quite remarkable in bio-synthesized Bi_2O_3 as we have already mentioned earlier that the presence of the metastable tetragonal phase is more dominant at high temperatures. In contrast to this, Bi_2O_3 synthesized by most of the wet-chemical techniques shows presence of monoclinic phase only at the room temperature. The mechanism involved in the synthesis based on microorganisms is quite complex in comparison to the traditional wet-chemical techniques and is still not understood in detail. However, it is not uncommon for fungus to synthesize the phases which are more energy intensive and otherwise possible to be synthesized only at extreme conditions by using the chemical techniques.

2.1.4.4 FTIR analysis

In Figure 2.1.5, we have shown Fourier transform infrared (FTIR) spectra for the precursor $\text{Bi}(\text{NO}_3)_3 \cdot 5\text{H}_2\text{O}$, uncalcined and calcined Bi_2O_3 nanoparticles synthesized after 72 hours of reaction between *Fusarium oxysporum* and bismuth nitrate. The figure 2.1.5 (A) on the left shows the presence of a prominent absorption in the range from 400 to 800 cm^{-1} for the uncalcined and calcined nanoparticles due to each type of Bi-O stretching modes [23–24].

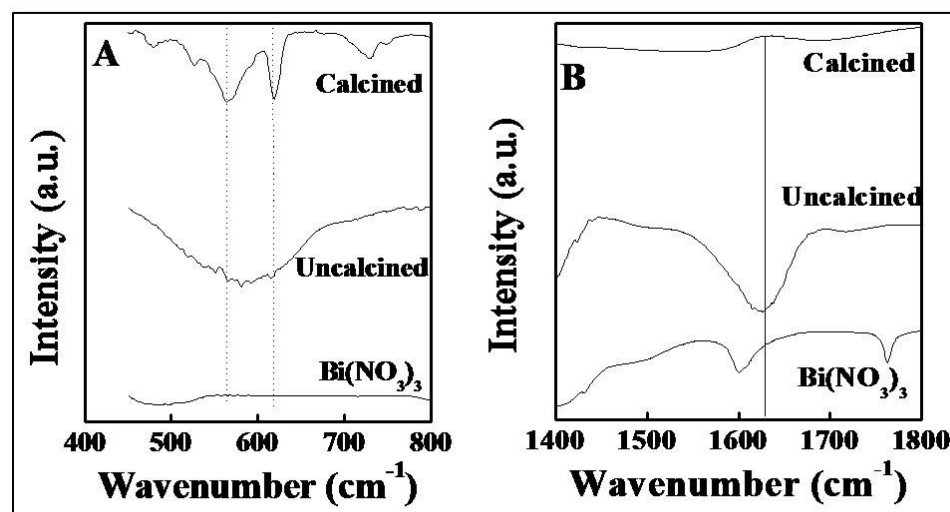


Figure 2.1.5: (A) FTIR spectra of precursor used: $\text{Bi}(\text{NO}_3)_3 \cdot 5\text{H}_2\text{O}$, uncalcined and calcined Bi_2O_3 nanoparticles synthesized by the reaction between $\text{Bi}(\text{NO}_3)_3 \cdot 5\text{H}_2\text{O}$ and fungus *Fusarium oxysporum* respectively. (B) Presence of amide bands suggests that proteins are associated with the nanoparticles.

It can be noticed that after calcination, the absorption peaks are more prominent and separated. In the Figure 2.1.5 (B), the disappearance of bands around 1650 and 1540 cm^{-1} for the calcined nanoparticles (present in the uncalcined sample as a broad absorption band) is due to the loss of amide I and II bands which arise due to the carbonyl stretch and -N-H stretch vibrations respectively in the amide linkages of the proteins [25]. This shows the degradation of protein from the surface of bismuth oxide nanoparticles after calcination.

2.1.4.5 X-ray photoemission spectroscopy (XPS) analysis

The chemical analysis of Bi_2O_3 nanoparticles was carried out by X-ray photoemission spectroscopy (XPS) from the as-synthesized Bi_2O_3 nanoparticles after 72 hours of reaction between the fungus *Fusarium oxysporum* and bismuth (III) nitrate

pentahydrate [$\text{Bi}(\text{NO}_3)_3 \cdot 5\text{H}_2\text{O}$]. The sample was prepared on silicon wafer. The core level spectra were background corrected using the Shirley algorithm and the chemically distinct species were resolved using a nonlinear least squares curve fitting procedure.

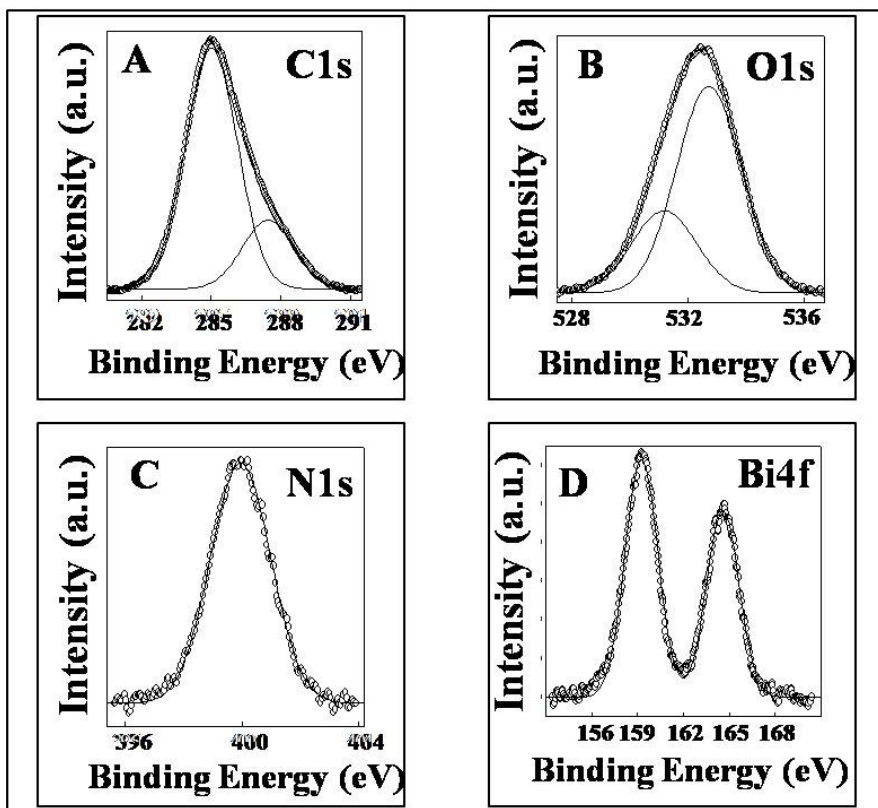


Figure 2.1.6: XPS spectra of biosynthesized Bi_2O_3 nanoparticles synthesized by reaction between *Fusarium oxysporum* and $\text{Bi}(\text{NO}_3)_3 \cdot 5\text{H}_2\text{O}$ for 72 hours. The core level spectra was recorded from C 1s (A), O 1s (B), N 1s (C) and Bi 4f (D). The raw data is shown in the form of symbols, while the chemically resolved components are shown as solid lines.

The core level binding energies (BEs) were aligned with respect to the C 1s binding energy (BE) of 285 eV. In Figure 2.1.6, we have presented background corrected X-Ray photoemission spectroscopy (XPS) of the biogenic bismuth oxide nanoparticles. In figure 2.1.6A, two deconvoluted peaks correspond to the chemically distinct C 1s core levels originating from the hydrocarbon chains, α - carbon and -COOH groups present in the proteins bound to the surface of Bi_2O_3 nanoparticles with binding energies 285 and 288 eV respectively [26-27]. The peak in figure 2.1.6B corresponds to the chemically distinct O 1s core level with binding energy 532 eV.

This could be assigned to mixed contributions from surface hydroxide [28] and C=O group present in capping proteins. In figure 2.1.6C, the peak corresponds to the 400 eV binding energy of N 1s. This could be assigned as amino group present in the capping proteins [29]. Thus, from XPS data of O 1s and N 1s, it can be concluded that proteins are definitely associated with Bi₂O₃ nanoparticles. The figure 2.1.6D shows Bi 4f spectrum which could be resolved into two peaks (4f_{5/2} and 4f_{7/2}) due to spin-orbit coupling with binding energies 159 eV and 165 eV respectively [30-32].

2.1.4.6 Energy dispersive analysis of X-rays (EDAX) measurements

The formation of bismuth oxide nanoparticles is also supported from Energy Dispersive Analysis of X-rays (EDAX). Figure 2.1.7 shows the EDAX spectrum of Bi₂O₃ nanoparticles. This technique helps in determining the chemical composition of the sample. A typical spectrum is presented in figure 2.1.7 where the signal of bismuth atoms

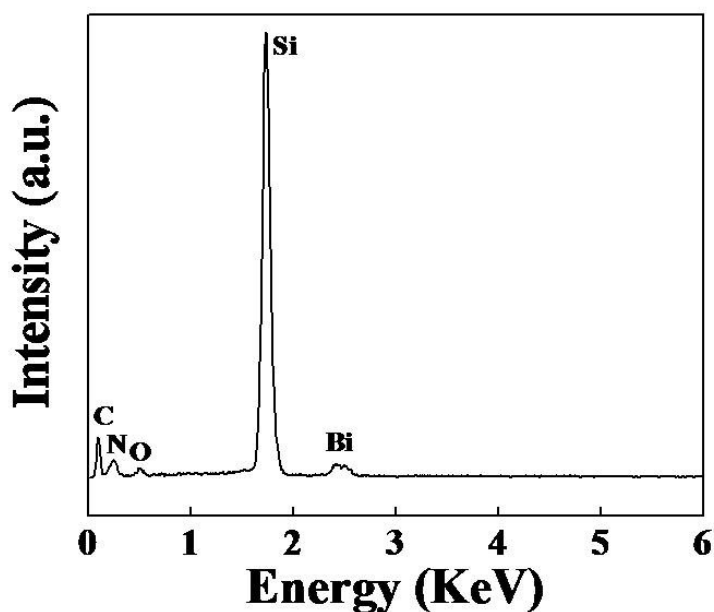


Figure 2.1.7: EDAX spectrum recorded from the Bi₂O₃ nanoparticles formed in the filtrate after 72 hours reaction of (Bi(NO₃)₃ · 5H₂O) with *Fusarium oxysporum*.

can be identified along with the signals of carbon, nitrogen and oxygen, which are originated from the proteins present in the sample. These signals are likely to be due to the proteins bound/intercalated within the Bi₂O₃ oxide nanostructure secreted by the fungus. The large peak is of Si signal, which is due to substrate.

2.1.4.7 TGA analysis

In Figure 2.1.8, we have shown thermogravimetric analysis (TGA) of the as-synthesized Bi₂O₃ nanoparticles. As pointed out earlier, the as-synthesized nanoparticles are capped by the biomolecules that stabilized them against aggregation.

The presence of this coating, even after intense centrifugation, is proven by the observation of almost 48 % weight-loss during heating the particles up to 700°C, which is attributed to

the loss of moisture and biomolecules bound on the nanoparticle surface [33]. A further increase in the temperature shows loss of weight that can be accounted for the decomposition of Bi₂O₃ nanoparticles.

The powder XRD at temperatures above 700°C will reveal further structural information at high temperatures.

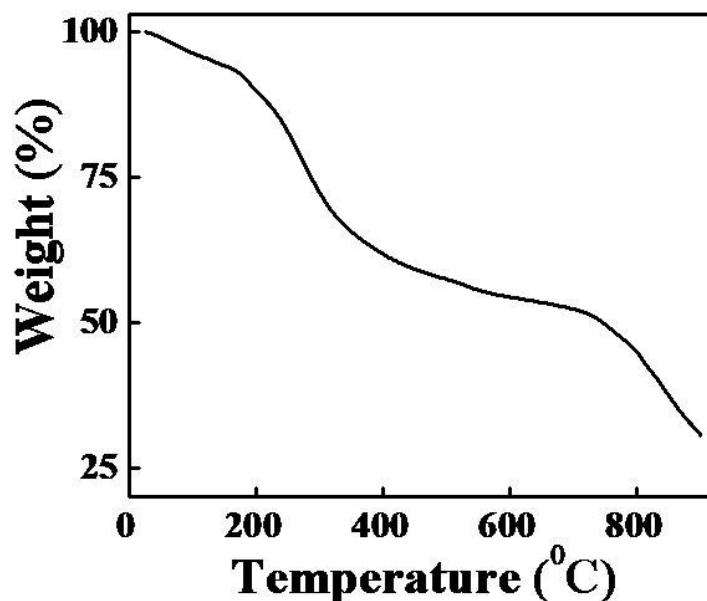


Figure 2.1.8: TGA of as-synthesized sample of Bi₂O₃ nanoparticles, showing the % weight loss with respect to a steady increase in temperature.

2.1.5 Conclusions

From the above analysis and results, at this stage, we hereby confirm and prove the formation of bismuth oxide (Bi₂O₃) nanoparticles by using the mesophilic fungus *Fusarium oxysporum*. We have successfully achieved particles whose size ranges from 5-8 nm at room temperature, which is extremely difficult to obtain by other synthesis routes. It is also clear that the proteins secreted by the microorganism play a crucial role in defining the morphology and stability of the nanoparticles formed. In conclusion, we have synthesized for the first time the monoclinic phase of Bi₂O₃ with a robust layer of proteins. The Bi₂O₃ so formed is characterized by TEM, HR-TEM, XRD, EDAX, FTIR, XPS and TGA. As-synthesized as well as calcined nanoparticles showed excellent crystallinity. TGA data indicates presence of a structural transition at higher temperatures. We are currently exploring a vast variety of fungi to understand their influence on the crystalline phase and morphology of Bi₂O₃

nanoparticles. Thus, we conclude that microorganisms such as fungi have proven themselves as possible eco-friendly inorganic nanofactories. It is this wonderful capacity of these organisms which can be exposed for the synthesis of excellent nanomaterials in a very straightforward and hygienic manner.

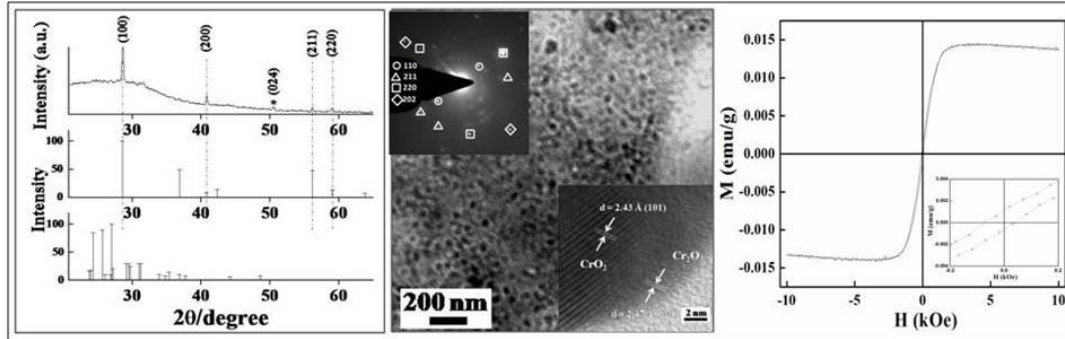
References

- [1] Fan, H. T., Teng, X. M., Pan, S. S., Ye, C., Li, G. H., Zhang, L. D., *Appl. Phys. Lett.*, **2005**, 87, 231916.
- [2] Rao, C. N. R., Rao, S. G. V., Ramdas, S., *J. Phys. Chem.*, **1969**, 73, 672.
- [3] Dong, W., Zhu, C., **2003**, *J. Phys. Chem. Solids.*, 64, 265.
- [4] Adamian, Z. N., Abovian, H. V., Aroutiounian, V. M., *Sens. Actuators B.*, **1996**, 35/36, 241-243.
- [5] Schuisky, M., Harsta, A., *Chem. Vap. Depos.*, **1996**, 2, 9, 23.
- [6] Kang, S. W., Rhee, S. W., *Thin Solid Films.*, **2004**, 468, 79.
- [7] Higaki, K., Kudo, S., Ohnishi, H., *Electrochem. Solid-State. Lett.*, **1998**, 1, 107.
- [8] Schumb, W. C., Rittner, E. S., *J. Am. Chem. Soc.*, **1943**, 65, 1055.
- [9] Cornei, N., Tancret, N., Abraham, F., Mentre, O., *Inorg. Chem.*, **2006**, 45, 4886.
- [10] Leontie, L., Caraman, M., Delibas, M., Rusu, G.I., *Mater. Res. Bull.*, **2001**, 36, 1629-1637.
- [11] Leontie, L., Caraman, M., Visinoiu, A., Rusu, G. I., *Thin Solid Films.*, **2005**, 473, 230.
- [12] Levin, E. M., Roth, R. S., *J. Res. Natl. Bur. Stand.*, **1964**, 68A, 2, 189-195.
- [13] Levin, E. M., Roth, R. S., *J. Res. Natl. Bur. Stand.*, **1964**, 68A, 2, 197-206.
- [14] Skorodumova, N. V., Jonsson, A. A., Herranen, M., Stromme, M., Niklasson, G. A., Johansson, B., Simak, S. I., *Appl. Phys. Lett.*, **2005**, 62, 41910.
- [15] Adamian, Z. N., Abovian, H. V., Aroutiounian, V. M., *Sens. Actuators B.*, **1996**, 35-36, 241.
- [16] Kunej, S., Guha, J. P., Suvorov, D., *Acta. Chim. Slov.*, **2004**, 51, 551.
- [17] Keuger, J., Winkler, P., Luderitz, E., Luck, M., Wolf, H. U., Bismuth, Bismuth Alloys, and Bismuth Compounds, Ullmann's Encyclopedia of Industrial Chemistry, Wiley-VCH Verlag GmbH, Weinheim, Germany, **2000**.
- [18] Madler, L., Pratsinis, S. E., *J. Am. Ceram. Soc.*, **2002**, 85, 1713.
- [19] Patil, M. M., Deshpande, V. V., Dhage, S. R., Ravi, V., *Mater. Lett.*, **2005**, 59, 2523.
- [20] (a) Anilkumar, M., Pasricha, R., Ravi, V., *Ceram. Int.*, **2005**, 889, 31889, (b) George, J., Pradeep, B., Joseph, K.S., *Thin. Solid. Films.*, **1987**, 148, 181.

-
- [21] (a) Mukherji, P., Senapati, S., Mandal, D., Ahmad, A., Khan, M. I., Kumar, R., Sastry, M., *Chem. Bio. Chem.*, **2002**, 3, 461. (b) Bansal, V., Rautaray, D., Bharde, A., Ahire, K., Sanyal, A., Ahmed, A., Shastry, M., *J. Mater. Chem.*, **2005**, 15, 2583; (c) Bansal, V., Poddar, P., Ahmad, A., Sastry, M. *J. Am. Chem. Soc.*, **2006**, 128, 11959.
- [22] The XRD patterns were indexed with reference to the crystal structures from the PCPDFWIN: Bi₂O₃ (# 41-1449).
- [23] (a) Irmawati, R., Noorfarizan Nasriah, M. N., Taufiq-Yap, Y. H., Hamid, S. B., *Cat. Today.*, **2004**, 93, 701. (b) Car-razan, S. R. G., Martin, C., Rives, V., Vidal, R., *Spectrochim. Acta Part A.*, **1996**, 52, 1107.
- [24] Fruth, V., Popa, M., Berger, D., Ionica, C.M., Jitianu, M., *J. Eur. Ceram. Soc.*, **2004**, 24, 1295.
- [25] Kong, J., Yu. S., *Acta. Biochimica et Biophysica Sinica.*, **2007**, 39, 8, 549-559.
- [26] Shankar, S. S., Rai, A., Ahmad, A., Sastry, M., *Chem. Mater.*, **2005**, 17, 566.
- [27] (a) Miyama T., Yonezawa, Y., *Langmuir.*, **2004**, 20, 5918. (b) Kumar, A., Mandal, S., Selvakannan, P. R., Pasricha, R., Mandale, A. B., Sastry, M., *Langmuir.*, **2003**, 19, 6277.
- [28] Moulder, J. F., Stickle, W. F., Sobol, P. E., Bomben, D., *Handbook of X-ray Photoelectron Spectroscopy*; Physics Electronics Int.: Eden Prairie, MN, **1995**.
- [29] (a) Wagner, C. D., Riggs, W. M., Davis, L. E., Moulder J. F., Muilenberg, G. E., *Handbook of X-ray photoelectron spectroscopy*, Perkin Elmer Corp. Publishers, Eden Prairie, MN, **1979**, p. 40. (b) Schiffrin, A. A., Riemann, W., Auwarter, Y., Pennec, A., Weber-Bargioni, D., Cvetko, A., Cossaro, A., Morgante, J. V. Barth., *Proc. Natl. Acad. Sci. U.S.A.* 104, 5279. (c) Gonella, G., Terreni, S., Cvetko, D., Cossaro, A., Mattera, L., Cavalleri, O., Rolandi, R., Morgante, A., Floreano, L., Canepa, M., *J. Phys. Chem. B.*, **2005**, 109, 18003.
- [30] (a) Morgan, W. E., Stec, W. J., Van Wazer, J. R., *Inorg. Chem.* **1973.**, 12, 953. (b) Zhang, L., Chen, D., Jiao, X., *J. Phys. Chem. B.*, **2006**, 110, 2668.
- [31] Agasiev, A. A., Zeinally, A. K., Alekperov, S. J., Guseino, Ya. Yu., *Mat. Res. Bull.*, **1986**, 21, 765.
- [32] Shimizugawa, Y., Sugimoto, N., Hirao, K., *J. Non-Cryst.*, **1997**, Solids 221, 208.
-

-
- [33] Bansal, V., Rautaray, D., Ahmad, A., Sastry, M., *J. Mater. Chem.*, **2004**, 14, 3303-3305.

Chapter 2B



Fungus mediated synthesis of protein capped CrO_2 nanoparticles.

*This chapter describes the synthesis of protein capped CrO_2 nanoparticles by using the fungus *Trichothecium* sp. in ambient conditions. Among the transition metal oxides, the synthesis and study of the physical properties of chromium (IV) oxide has remained a point of strong interest due to its rich electronic properties as well as its applications as storage media in magnetic tapes and as an ideal material for spin-polarized electron injectors in magnetic tunnel junction devices. CrO_2 is a thermodynamically metastable oxide which is a ferromagnetic metal at room temperature with almost 100% spin polarization at Fermi energy. Due to its metastability, the chemical synthesis of colloidal nanoparticles of CrO_2 is not well reported.*

2.2.1 Introduction

Transition metal oxides have been of interest due to their rich electronic and catalytic properties and form the large family of materials which find utilities in areas of catalysis, superconductors, magnetoresistance, etc. These properties over the years have been successfully tapped in various forms such as epitaxial thin films, polycrystalline films, bulk single crystals and nanoparticles [1]. Among transition metal ions of the 3d series, chromium has a particular and finite position because of its variability in oxidation state, co-ordination numbers and molecular structure [2]. Among various chromium oxides, the chromium (IV) oxide has been researched over the years in various forms after it was found that it is a ferromagnetic metal at room temperature with half-metallicity [3]. Chromium has multiple oxidation states; the most common oxidation states are +2, +3 and +6; out of which +3 is most stable and other oxidation states are rare like +1, +4 and +5. Chromium forms different oxides like $\text{Cr(III)}_2\text{O}_3$, $\text{Cr(V)}_2\text{O}_5$, $\text{Cr(VI)}\text{O}_3$, etc. and only CrO_2 shows ferromagnetic behavior. It is known that among the predicted half-metallic ferromagnets, CrO_2 is one of the simplest half metallic ferromagnet transition binary metal oxide, which means that it is metallic for one spin direction and at the same time insulating for the opposite spin direction. CrO_2 has chromium ions in the Cr^{4+} ($3d^2$) state with a magnetic moment $2\mu_B$ per formula unit. In this, two 3d electrons occupy spin-split t_{2g} sub-band, out of which one is localized and the other is in a half-filled band and both are strongly coupled with on-site exchange interactions or in other words, we can say that in CrO_2 , majority of the (spin-up) electrons are delocalized which have fermi surface and show metallic behavior, while the minority (spin-down) electrons are localized and show insulating properties [4-10]. In 1971, Goodenough [11] proposed the qualitative model of CrO_2 and further in 1986, Schwarz [12] gave its band structure. The concept of ‘‘half-metallic ferromagnet’’ was introduced in 1983 by de Groot *et al.*, and means that for a particular electron-spin orientation, the material acts as a metal [13, 14]. It routinely exhibits the highest polarization at fermi level but among the lowest tunnel magnetoresistance [15]. CrO_2 is conducting at room temperature with Curie temperature (T_C) of 395 K [16] and has been widely utilized due to its application as a powder magnetic recording medium like magnetic tapes [17]. Due to its unique band structure and half metallic ferromagnetic feature, chromium dioxide (CrO_2) showed magnetotransport property and is a favorite

material for magnetoelectronic devices which require high spin polarization like magnetic tunnel junctions (MTJ) and spin valves [18]. Chromium dioxide (CrO_2) as a component finds use in wide applications in optoelectronic devices, magnetic sensors, spintronics, etc. [19].

Detailed structure of CrO_2 is well studied, which has tetragonal rutile structure with space group $P4_2/mnm$. The Cr atoms form a body-centered tetragonal lattice and are surrounded by distorted oxygen octahedral. In band structure, Cr 3d orbitals in CrO_2 are further split into a t_{2g} triplet and an e_g doublet orbital, and t_{2g} orbital form non bonding d_{xy} orbital and d_{yz} , d_{zx} doublet which forms antibonding interaction with oxygen p orbital [5-8, 20].

Surface of CrO_2 generally has a native oxygen rich layer of thermodynamically stable Cr_2O_3 which is generally 1-3 nm thick. Cr_2O_3 is antiferromagnetic with a Neel temperature of 307 K. The characterization of native oxide Cr_2O_3 surface layer on CrO_2 films by Cheng *et al.* revealed that CrO_2 might polarize the Cr_2O_3 layer. The native Cr_2O_3 surface layer acts as a tunnel barrier and is useful for applications with desirable magneto-transport properties. At temperature higher than 288°C , CrO_2 starts oxidizing into the Cr_2O_3 phase [21]. There are different methods reported for synthesizing CrO_2 nanocrystals, like hydrothermal decomposition [22] which is a very well known and common method but requires very high temperature and pressure. Chamberland *et al.* observed crystal growth of CrO_2 but it again requires very high pressure [23]. Alternatively, Chemical vapour deposition (CVD) technique was also used to produce the CrO_2 film [24]. Several of these conventional wet-chemical methods are known to often use harsh experimental conditions like high temperatures, pressure and multi-step techniques and therefore are considered to be energy intensive. Therefore it is necessary to develop alternative economical processes which can synthesize CrO_2 nanoparticles at ambient conditions. In contrast to chemical synthesis methods, biological synthesis of chromium dioxide (CrO_2) is characterized by ambient experimental conditions of temperature, pH and pressure. Previously, interaction of chromium ions with different microorganism and reduction of its toxic form into less toxic form was well studied. There are some microorganisms like *Desulfomicrobium norvegicum* [25], *Pseudomonas fluorescens* LB300 [26], *Enterobacter cloacae* HO1 [27], *Chlorella miniata* [28], *Bacillus* sp [29], etc. which can reduce the toxic chromate (Cr^{VI}) form into less toxic form. Besides this, chromate resistance gene was also observed in *Pseudomonas aeruginosa* and *Alcaligenes*

eutrophus [30]. Here in this chapter, fungus mediated extracellular biosynthesis of chromium (IV) oxide nanoparticles using *Trichothecium* sp. at ambient conditions is discussed where extracellular protein is acting both as a capping as well as a reducing agent. The structure of these particles was characterized by powder XRD, selected area electron diffraction (SAED) and high resolution transmission electron microscopy (HR-TEM). Magnetic measurements performed on the CrO₂ nanoparticles synthesized by this method described here show ferromagnetic behavior. The particle size analysis was done using TEM. Further material characterization was done using techniques such as UV-visible spectroscopy, XPS, FTIR, EDAX and TGA.

2.2.2 Experimental Details

Potassium dichromate (K₂Cr₂O₇) was obtained from S. D. fine chemical. Malt extract powder, yeast extract powder, glucose and peptone were obtained from Himedia and used as-received.

The fungus *Trichothecium* sp. was maintained on potato dextrose agar slants at 25°C. Stock cultures were maintained by sub-culturing at monthly intervals. The fungus was grown at pH 7.0 and 25°C for 96 hours; the slants were preserved at 15°C. From an actively growing stock culture, sub-cultures were made on fresh slants and after 96 hours of incubation at pH 7.0 and 25°C, were used as the starting material for synthesis of nanomaterials. For the extracellular synthesis of CrO₂ nanoparticles, the fungus was grown in 500 ml Erlenmeyer flasks each containing MGYM medium (100 ml), composed of malt extract (0.3%), glucose (1.0%), yeast extract (0.3%) and peptone (0.5%) at 25-27°C under shaking at 200 rpm for 96 hours. After 96 hours of fermentation, mycelia were separated from the culture broth by centrifugation (5000 rpm) at 10°C for 20 minutes and then the mycelia were washed thrice with sterile distilled water under sterile conditions. The harvested mycelial mass (20 gram of wet mycelia) was then resuspended in 100 ml of aqueous solution of 1mM (potassium dichromate) K₂Cr₂O₇ salt solution in 500 ml Erlenmeyer flasks and the same was put into a shaker at 25-27°C (200 rpm). The reaction was carried out for a period of 96 hours and fungal biomass was separated by filter paper to collect biomass and filtrate in sterile conditions. The filtrate was then used to check for the formation of nanoparticles by Transmission electron microscopy (TEM), Selected area electron diffraction (SAED) analysis, X-ray diffraction (XRD) analysis, Fourier transform

infrared (FTIR) spectroscopy, thermogravimetric analysis (TGA), Electron dispersive X-rays (EDAX) analysis and X-ray photoemission spectroscopy (XPS).

To remove the unbound protein and unreacted precursor, we centrifuged the filtrate three times at 15,000 rpm for 30 minutes and each time the precipitate was resuspended in de-ionized water. These particles were used in the characterization as discussed below. For magnetization vs. magnetic field measurements, we used a Magnetic Property Measurement System (MPMS) from Quantum Design Inc., USA equipped with the superconducting quantum interference device (SQUID) magnetometer and superconducting magnet. For this purpose, we took the sample in Teflon tape and packed it inside the gelatin capsules.

2.2.3 Morphological features of *Trichothecium* sp.

The fungus *Trichothecium* sp. was isolated from plant and grown on PDA medium produced slow growing colonies. Colonies on PDA pale rose in front, circular, compact, hyphae branched, septate and hyaline. Conidiophores long, slender, simple, septate bearing conidia apically, singly or held together in groups. Conidia hyaline and two celled.

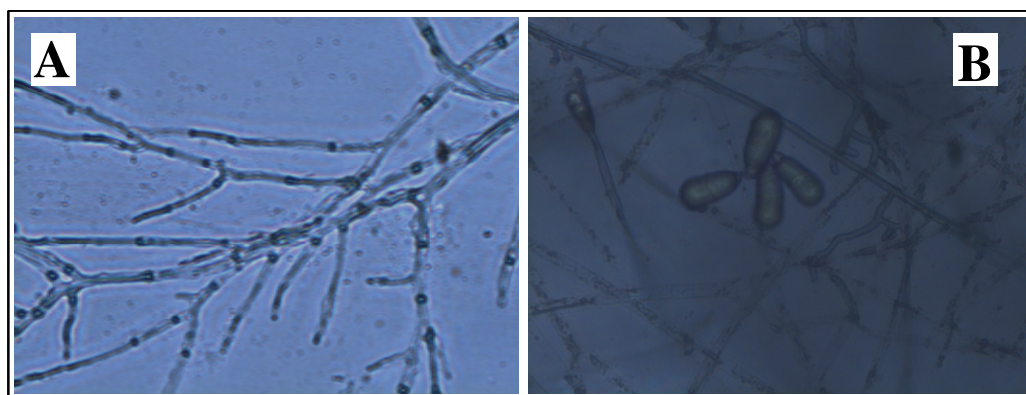


Figure: 2.2.1: Morphological features of *Trichothecium* sp. (A) mycelium (B) conidia.

2.2.4 Results and Discussions

2.2.4.1 TEM and SAED analysis

TEM analysis was performed in order to determine the size and shape of biosynthesized nanoparticles. In Figure 2.2.2 (A, C) we have shown the representative TEM image of protein capped as-synthesized CrO_2 nanoparticles obtained after reacting the fungal biomass *Trichothecium* sp. with precursor $\text{K}_2\text{Cr}_2\text{O}_7$, which shows that the CrO_2 nanoparticles formed are irregular in shape with an overall quasi-

spherical morphology. The particle size histogram of the CrO₂ particles (Fig 2.2.2D) shows that the particles range in size from 21 to 25 nm.

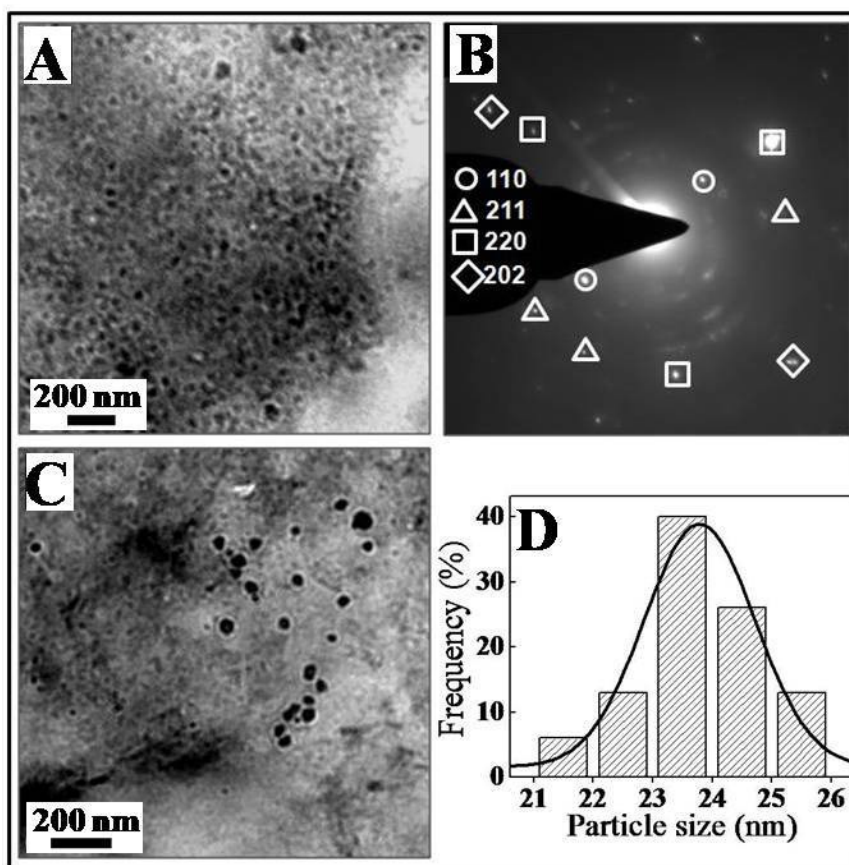


Figure 2.2.2 (A and C) Transmission electron micrograph of CrO₂ nanoparticles synthesized using *Trichothecium* sp. biomass at different magnification (B) SAED pattern recorded from extracellular CrO₂ nanoparticles shown in TEM micrograph and (D) particle size distribution of CrO₂ nanoparticles determined from TEM micrograph. The solid line is a Gaussian fit to the histogram.

These nanoparticles appear to be well separated from each other since they are stabilized by the proteins present on the surface. To better investigate the crystallinity of CrO₂ nanoparticles, we have shown the SAED pattern obtained from CrO₂ nanoparticles shown in TEM. The Scherrer ring pattern characteristic of CrO₂ is clearly observed, showing that the structures seen in TEM are nanocrystalline in nature. The extent of crystallinity observed here in biologically synthesized particles (which occurs in ambient conditions) is quite remarkable. In figure 2.2.2B we have shown the SAED pattern, which shows a spot pattern confirming crystallinity of the as-synthesized protein coated nanoparticles. We indexed the SAED spots {110}, {211}, {220} and {202} for tetragonal phase [32].

2.2.4.2 HR-TEM analysis

To better investigate crystallinity at the single particle level, we used the high resolution transmission electron microscopy (HR-TEM).

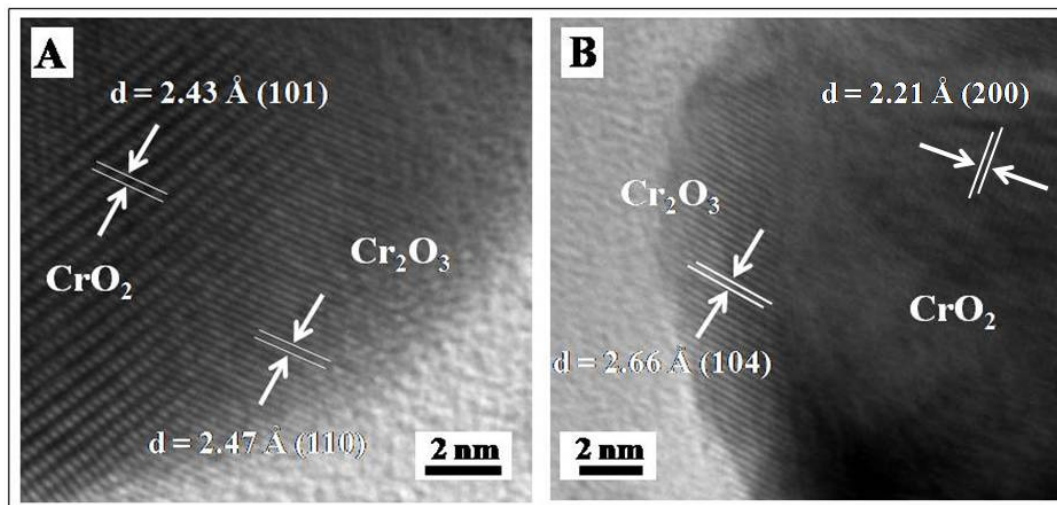


Figure 2.2.3: HR-TEM images of CrO_2 nanoparticles synthesized using *Trichothecium* sp. showing inter planar distance and presence of Cr_2O_3 layer over the CrO_2 nanoparticles.

In figures 2.2.3A and 2.2.3B, we have shown the HR-TEM images of as-synthesized CrO_2 nanoparticles after 96 hours of the reaction. As we know very well from the reported literature, CrO_2 is difficult to stabilize in oxygen rich environment while on the other hand Cr_2O_3 is a thermodynamically more stable phase. So there is chance to form thin layer (1-3 nm) of Cr_2O_3 over the surface of CrO_2 nanoparticles [31, 32]. In HR-TEM analysis, we observed Cr_2O_3 layer over the CrO_2 nanoparticle. Figure 2.2.3A and 2.2.3B show Cr_2O_3 layer which exhibits spacing of $\sim 2.47\text{\AA}$ and $\sim 2.66\text{\AA}$ for the lattice planes $\{110\}$ and $\{104\}$ respectively and CrO_2 phase having d-spacing $\sim 2.43\text{\AA}$ (figure 2.2.3A) for the lattice plane $\{101\}$ and $\sim 2.21\text{\AA}$ (figure 2.2.3B) for the lattice plane $\{200\}$ present in the core. Here we are not getting very good contrast because the nanoparticles are capped with protein. Presence of Cr_2O_3 layer over the surface of CrO_2 was further confirmed by XRD, XPS analysis and magnetic measurements.

2.2.4.3 X-ray diffraction analysis

In order to confirm the crystalline phase of as-synthesized material in detail, we prepared sample for powder X-ray diffraction. In Figure 2.2.4, we have presented the

room temperature XRD pattern obtained from as-synthesized CrO_2 nanoparticles (Fig 2.2.4A), showing intense peaks corresponding to plane {110}, {200}, {211} and {220}.

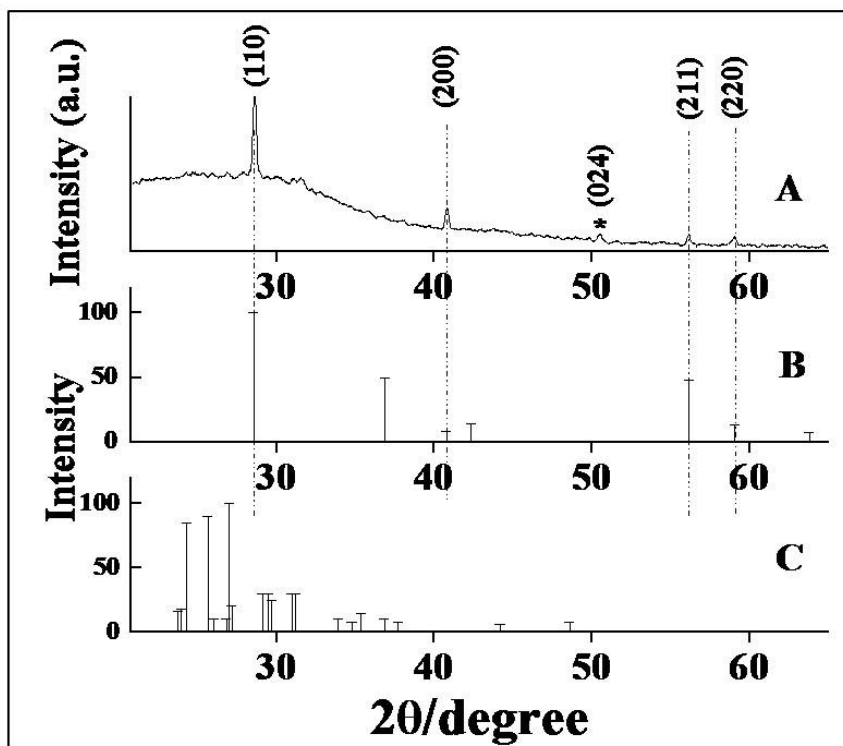


Figure 2.2.4: Powder XRD-pattern of drop-cast films of chromium Oxide (CrO_2) nanoparticles on glass after reaction with the fungus *Trichothecium* sp. for 96 hours (A), reference CrO_2 from PCPDF # 431-1040 (B) reference $\text{K}_2\text{Cr}_2\text{O}_7$ from PCPDF # 27-380 (C).

The peak position and 2θ values agree with those reported for CrO_2 nanoparticles tetragonal phase having cell parameters $a=b=4.419$, $c=2.915$, $\alpha=\beta=\gamma=90^\circ$ with space group $\text{P4}_2\text{mm}(136)$ which are close to the reported literature [32]. The broadening of these diffraction peaks indicate that the particles are having small size. However, one of the peak presenting the {024} lattice plane from the XRD pattern indicates the presence of Cr_2O_3 phase which could be because of the CrO_2 nanoparticles tending to develop a layer of more stable Cr_2O_3 layer above them [21, 31].

2.2.4.4 X-ray photoemission spectroscopy (XPS) analysis

The presence of CrO_2 nanoparticles was also confirmed by analyzing the sample by XPS as shown in figure 2.2.5. The results showed the presence of C, N, O and Cr as the prominent elements. The chemical analysis of CrO_2 nanoparticles was carried out

by X-ray photoemission spectroscopy (XPS) from the as-synthesized CrO_2 nanoparticles after 96 hours of the reaction between fungus *Trichothecium* sp. and potassium dichromate ($\text{K}_2\text{Cr}_2\text{O}_7$). The sample was prepared on silicon wafer. The background of the core level spectra was corrected using the Shirley algorithm and the chemically distinct species were resolved using a nonlinear least squares curve fitting procedure. The C 1s, N 1s, O 1s and Cr 2p core level spectra were recorded with an overall resolution of ~ 1 eV. The core level binding energies (BEs) were aligned with respect to the C 1s binding energy (BE) of 285 eV. In Figure 2.2.5, we have presented the background corrected X-Ray Photoemission Spectroscopy (XPS) of the biogenic CrO_2 nanoparticles. Figure 2.2.5A shows the C 1s core level spectrum that could be decomposed into three chemically distinct components centered at 282.40 eV, 285.0 eV and 287.70 eV respectively. The deconvoluted low binding energy peak at 282.40 eV is attributed to the presence of aromatic carbon present in amino acids from proteins bound to the surface of CrO_2 nanoparticles. The C 1s component centered at 285.0 eV is due to the electron emission from adventitious carbon or due to the core levels originating from the hydrocarbon chains present in the sample. The high binding energy peak at 287.70 eV can be attributed collectively to -COOH groups and α -carbon bound to -COOH and $-\text{NH}_2$ groups of the proteins bound to the nanoparticles surface [33]. Further, the figure 2.2.5B shows the N 1s core level spectra that could be fitted into three chemically distinct components with binding energies 397.48 eV, 400.09 eV and 402.86 eV. The lower binding energy component at 397.48 eV could be attributed to nitrogen in iminic ($\text{C}=\text{N}$) groups while binding energy component at 400.09 eV corresponds to the $-\text{NH}$ amide linkage or amidic (peptidic) nitrogen. The higher binding energy component at 402.86 eV can be attributed to the presence of protonated amines. This higher binding energy component can also be attributed to the N atoms present in amide bonds present in the capping protein [34]. Figure 2.2.5C shows Cr 2p spectrum which could be resolved into two peaks i.e. Cr $2p_{3/2}$ and Cr $2p_{1/2}$ due to the spin orbital splitting with binding energies 576.30 eV and 586.14.5 eV respectively, corresponding to CrO_2 which matches with its reported literature value [35]. Through XPS analysis, we can clearly identify the presence of Cr(IV) species in the as-synthesized samples. Since CrO_2 is difficult to stabilize in air/water where oxygen is present in abundance, there is always a possibility of formation of few atomic layers of Cr_2O_3 at the surface which is also thermodynamically more stable at room temperature [21, 31].

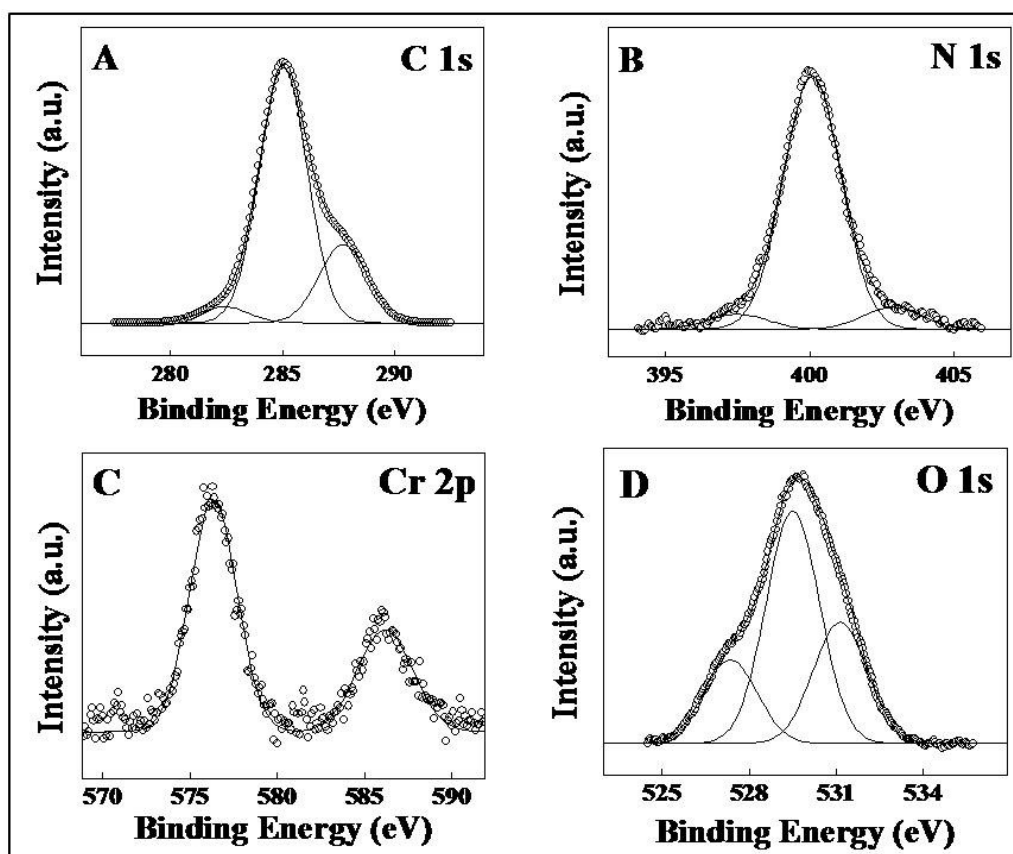


Figure 2.2.5: XPS spectra of biosynthesized CrO_2 nanoparticles synthesized by reaction between *Trichothecium* sp. and potassium dichromate ($\text{K}_2\text{Cr}_2\text{O}_7$) for 96 hours. The core level spectra were recorded from C 1s (A), N 1s (B), Cr 2p (C) and O 1s (D). The raw data is shown in the form of symbols while the chemically resolved components are shown as solid lines and are discussed in the text.

Unfortunately, it is very difficult to distinguish Cr_2O_3 from CrO_2 on the basis of XPS only because both of them give peaks at approximately the same binding energy [36]. Further, to check the presence of Cr_2O_3 in the as-synthesized CrO_2 nanoparticles, core level oxygen spectra of O1s was also analyzed which much more clearly explains the presence of both CrO_2 and Cr_2O_3 oxide phases. The peak in figure 2.2.5D corresponds to the chemically distinct O 1s core level. The O 1s spectrum could be resolved into three chemically distinct components with binding energies 527.88 eV, 529.51 eV and 531.13 eV. The O 1s component present at binding energy 529.51 eV can be assigned to the lattice oxygen of the as-synthesized CrO_2 nanoparticles. In addition to this, spectrum shows the peak at 531.13 eV which corresponds to the accepted binding energy of lattice oxygen for Cr_2O_3 oxide [37]. Since the presence of both type of oxygen species suggests the presence of both CrO_2 and Cr_2O_3 oxide phases; this could

be possible because the surface of CrO_2 has a thermodynamically stable Cr_2O_3 layer. The lower binding energy component at 529.51 eV could be assigned to the signals coming from surface proteins.

2.2.4.5 FTIR analysis

Furthermore, to investigate the presence of stretching/vibration bands present in the biosynthesized chromium dioxide (CrO_2) nanoparticles capped with protein, Fourier transform infrared (FTIR) spectra measurements were recorded. For this purpose, samples were taken in KBr pellets and measurements were taken in diffuse reflectance mode. In figures 2.2.6A & 2.2.6B, we have compared Fourier transform infrared (FTIR) spectra in two different regions for the precursor potassium dichromate ($\text{K}_2\text{Cr}_2\text{O}_7$) used and the as-synthesized CrO_2 nanoparticles. Occurrence of resonance around 900-1000 cm^{-1} region in figure 2.2.6A (curve 2) indicates the presence of O-Cr-O stretching vibration in the sample. It should be noted here that this is absent in the precursor $\text{K}_2\text{Cr}_2\text{O}_7$ (curve 1). Also, there are two types of stretchings observed here; one band at lower frequency region of around 915 cm^{-1} is attributed to excitation of the symmetric O-Cr-O stretching mode of vibration, while the other band at higher frequency region in the range of 940-1000 cm^{-1} arises due to the antisymmetric O-Cr-O stretching mode of vibration [38].

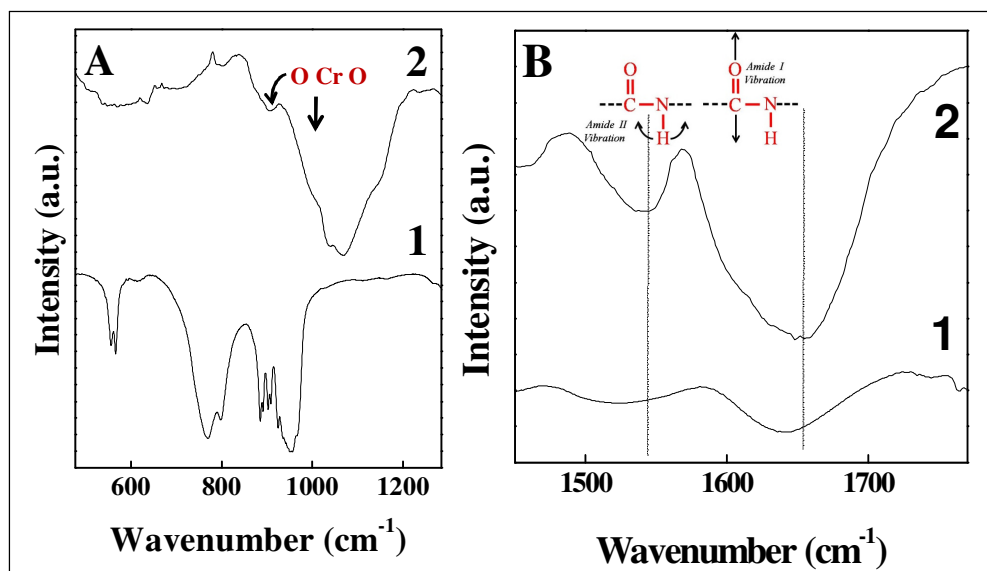


Figure 2.2.6: (A) FTIR spectra recorded from powder of $\text{K}_2\text{Cr}_2\text{O}_7$ (curve 1); and CrO_2 nanoparticles synthesized using *Trichothecium* sp. (curve 2). (B) Expanded view of the FTIR spectra shown in the region of protein amide bands.

FTIR study of the extracellularly synthesized CrO₂ nanoparticles suggests the role of some extracellular fungal enzymes/proteins which are responsible for the synthesis of CrO₂ nanoparticles. In order to confirm this, FTIR analysis of biologically synthesized CrO₂ nanoparticles was performed in the amide region speculation. In figure 2.2.6B; two absorption bands around 1655 cm⁻¹ and 1540 cm⁻¹ are present in as-synthesized CrO₂ sample which are due to the amide I and II bands which arise due to the carbonyl stretch and –N–H stretch vibrations respectively in the amide linkages of the proteins [39]. Presence of amide signatures in as-prepared CrO₂ (curve 2, Figure 2.2.6B) and their clear absence in the precursor K₂Cr₂O₇ (curve 1, figure 2.2.6B) confirms the presence of proteins in CrO₂.

2.2.4.6 UV-visible spectroscopic analysis

In figure 2.2.7, we have tried to capture the formation of CrO₂ nanoparticles by comparing the UV-visible spectra of the precursor used for the biosynthesis i.e. potassium dichromate (K₂Cr₂O₇) (curve 1) and biosynthesized CrO₂ nanoparticles

after 96 hours (curve 2) of reaction. We observed that the precursor, after reacting with the fungal mass for 96 hours, shows two significant absorption curves. The first one “b” appearing at around 270 nm and the other one “a” around 370 nm. The first absorption peak at

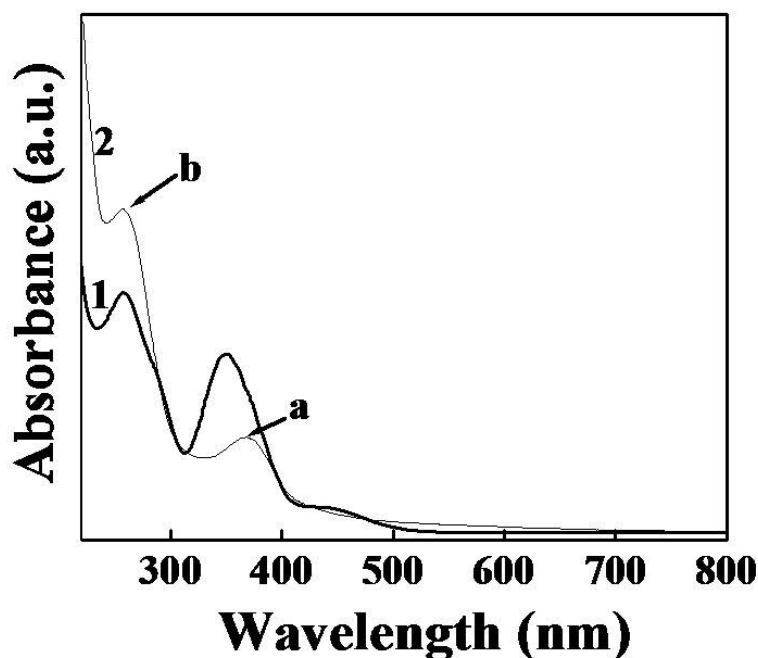


Figure 2.2.7: UV-visible spectra (1) precursor Potassium dichromate (K₂Cr₂O₇) (2) as-synthesized CrO₂ nanoparticles after 96 hours reaction with *Trichothecium* sp.

around 270 nm can be attributed to the aromatic amino acids of the proteins present at the surface of the particles as well as in the solution. It is well known that the absorption band at around 270 nm arises due to electronic excitations in tryptophan

and tyrosine residues in the proteins [40]. These biomolecules are secreted by the fungal cells collectively due to the osmotic shock after their suspension in the deionized water as well their exposure to the chromium salt. We believe that some of these biomolecules are finally responsible for converting the Cr^{+6} ions into stable CrO_2 [41]. Figure 2.2.7 (curve 2) shows the UV-visible spectroscopic profile of the protein capped CrO_2 nanoparticles. UV-visible spectroscopic analysis reveals the appearance of absorption bands at ~ 370 nm which is absent in case of precursor $\text{K}_2\text{Cr}_2\text{O}_7$ as shown in the figure 2.2.7 (curve 1).

2.2.4.7 TGA analysis

TGA was performed on as-synthesized CrO_2 nanoparticles to calculate the amount of bio-organic molecules present over the nanoparticles and decomposition of CrO_2 into Cr_2O_3 at a particular temperature range. Thermogravimetric analysis (TGA) of as-synthesized CrO_2

nanoparticles is shown in figure 2.2.8.

As pointed out earlier, the surface of nanoparticles is bound with protein/biomolecules which act as capping agents and stabilize them against aggregation which restrict their growth to nanometer regime. The presence of this coating even after

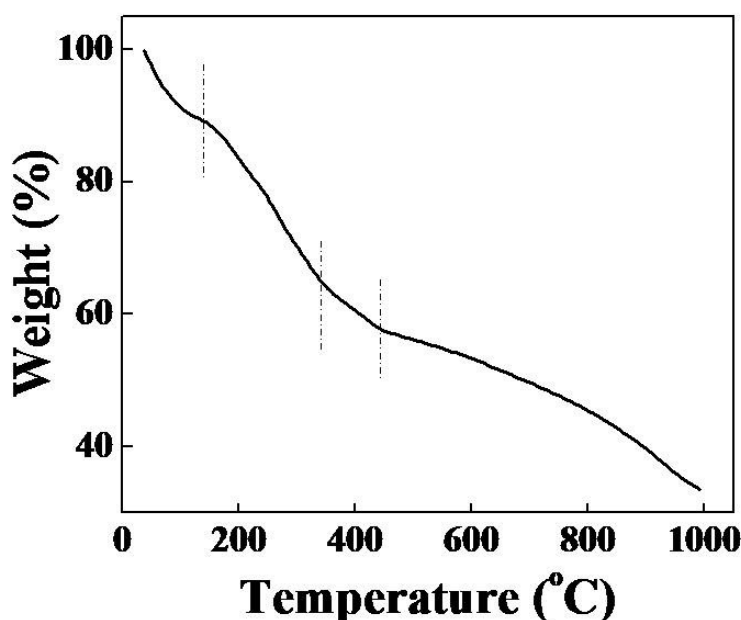


Figure 2.2.8: TGA of as-synthesized sample of CrO_2 nanoparticles, showing % weight loss with respect to a steady increase in temperature

intense centrifugation is proven by the observation of almost 52% weight-loss during heating the particles up to 670°C , which is attributed to the loss of moisture and biomolecules bound on the nanoparticle surface and decomposition of CrO_2 into Cr_2O_3 . Weight loss shown in figure 2.2.8 is a multi-step process. First loss starts at beginning due to complete loss of moisture which further continues up to 340°C and

is attributed to the partial removal of biomolecules and protein from the surface of CrO_2 nanoparticles. Second major weight loss starts at around 340°C where a steep fall occurs and continues up to 440°C corresponding to the tetragonal phase conversion of CrO_2 to corundum phase Cr_2O_3 ; decrease of mass may be due to the release of oxygen during this conversion. A further increase in the temperature shows loss of weight that can be accounted for the complete decomposition of CrO_2 to Cr_2O_3 [42].

2.2.4.8 Energy dispersive analysis of X-rays (EDAX) measurements

The elemental analysis of nanoparticles can be very informative for the study of the structural or elemental composition. The EDAX spectrum recorded from the CrO_2 nanoparticles synthesized using the fungus *Trichothecium* sp. is shown in Figure 2.2.9, which shows the presence of strong signals from chromium atoms together with weaker signals from C, O, and N atoms that arise from the proteins bound to the CrO_2 nanoparticles.

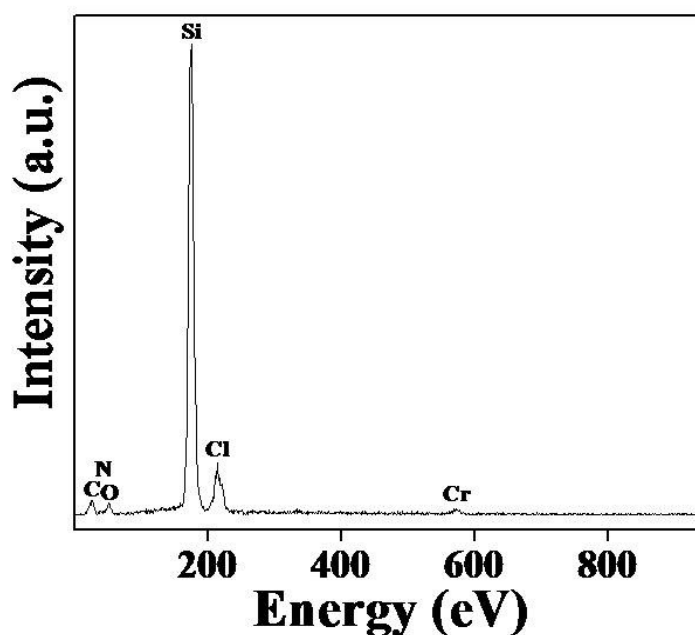


Figure 2.2.9: EDAX spectrum recorded from the CrO_2 nanoparticles formed in the filtrate after 96 hours of reaction.

2.2.4.9 Magnetic measurements

Magnetic measurements were carried out on dried, as-synthesized CrO_2 nanoparticles. Magnetization as a function of the field at room temperature was recorded by applied magnetic field) field. Temperature dependent magnetization of CrO_2 nanoparticles is studied by ZFC (Zero-field-cooled) and FC (field-cooled) modes for as-synthesized nanoparticles.

In figure 2.2.10A, we have shown the M-H (Magnetization-Applied magnetic field) behavior of as-synthesized powdered CrO_2 nanoparticles, which shows that CrO_2 is a ferromagnetic material with a small hysteric value which saturates at 2K Oe magnetic field. Since Cr_2O_3 is thermodynamically more stable at room temperature than CrO_2 , in the presence of an oxygen rich environment here is always a possibility for the formation of a few atomic layers of Cr_2O_3 at the surface of CrO_2 [21, 31]. This layer was observed in HR-TEM and XPS measurements. To further prove the presence of Cr_2O_3 layer over CrO_2 , in figure 2.2.10B, we have shown a magnified view of the M-H curve and have observed that the hysteresis loop is shifted towards the ‘-H’ direction. This behaviour is called as an exchange bias [43]. Exchange bias arises due to the coupling between the AFM and FM spins at the interface and exerts an additional torque on the FM spins, which the external field has to overcome. Exchange bias will only be observed when there is a coupling of ferromagnetic and antiferromagnetic layers. Now, we

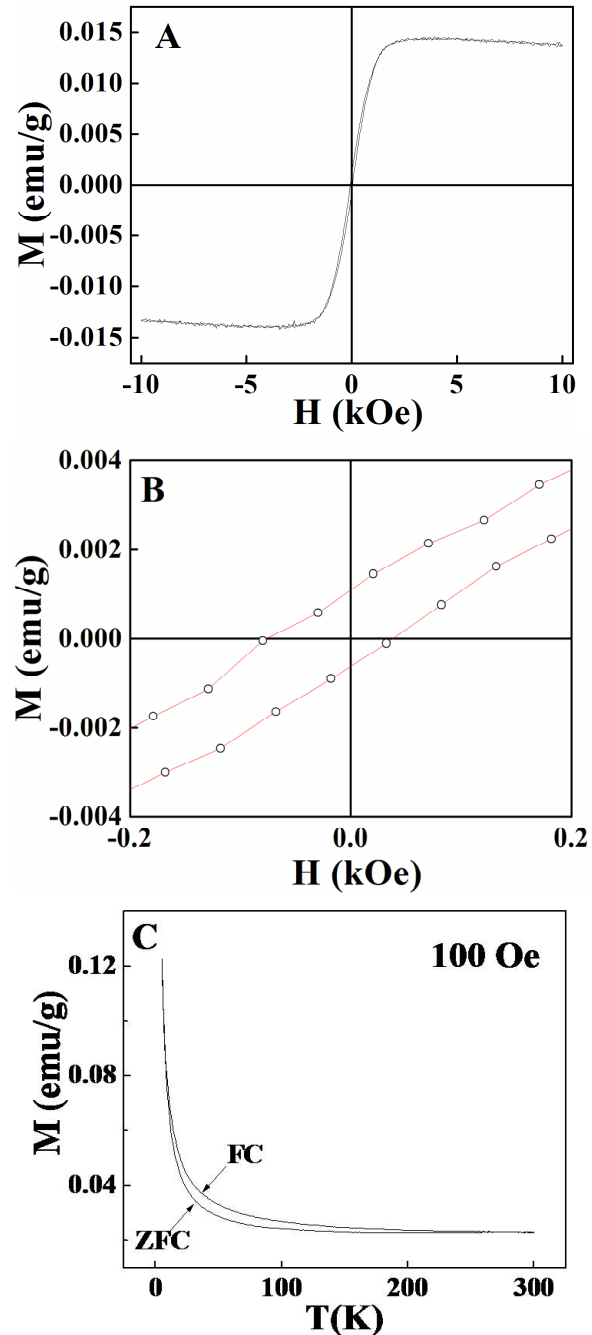


Figure 2.2.10: (A) Field dependent magnetization plots of CrO_2 nanoparticles synthesized using *Trichthecium* sp., (B), Enlarged view of field dependent magnetization plots of CrO_2 nanoparticles showing the exchange bias (C) ZFC-FC curves at 100 Oe for as-synthesized CrO_2 nanomaterials.

know that CrO_2 is ferromagnetic and in the presence of oxygen, chromium ions on the surface of CrO_2 form a Cr_2O_3 layer which is antiferromagnetic in nature. Therefore, coupling of the core CrO_2 which is ferromagnetic and the shell Cr_2O_3 which is antiferromagnetic results in an exchange bias in the CrO_2 nanoparticles. This layer works as a tunnel barrier and plays an important role in intergranular tunneling effect which makes it a perfect material for the magnetic tunneling devices [44]. We also performed the M-T (Magnetization-Temperature) measurements at an applied magnetic field of 100 Oe in a temperature range of 3 to 300 K. At first, the desired field was applied at 300 K and the sample was cooled down to 3 K (in field) and data was collected again while heating from 3 to 300 K (in field); these curves will be presented as field-cooled (FC) here. Next, we removed the magnetic field at 300 K and cooled the sample down to 3 K at the maximum cooling rate. After cooling the sample in zero field, the desired field was applied at 3 K and data was collected while heating up to 300 K. This data set will be presented as zero-field-cooled (ZFC) here. In figure 2.2.10C, we check the magnetization vs. temperature behaviour of CrO_2 nanoparticles and have shown the zero-field-cooled and field-cooled (ZFC-FC) measurements, performed at an applied external field of 100 Oe. We observed that as the temperature decreases, the magnetic moment value is going to increase. This is because as the thermal energy decreases, it favors the alignment of spin towards the direction of magnetic field. It is clearly observed in the M-T behaviour, that below 300K, FC and ZFC curve is going to bifurcate which is a typical signature of reduced particle size; probably due to enhanced interactions between the small nanoparticles.

2.2.5 Conclusions

In conclusion, nanocrystalline chromium dioxide (CrO_2) nanoparticles were synthesized by bottom-up approach in ambient conditions using fungus *Trichothecium* sp. and potassium dichromate ($\text{K}_2\text{Cr}_2\text{O}_7$) as precursor salt. It is thus concluded that the fungus-*Trichothecium* sp. secretes extracellular proteins during the reaction. These extracellular proteins in the solution might be responsible for the reduction of the metal ions present in the solution. The TEM analysis of CrO_2 nanoparticles indicates that the overall particles are irregular in shape with quasi-spherical morphology with an average particle size of 22-23 nm in diameter. Being metastable, it is very difficult to stabilize pure CrO_2 in water. HR-TEM images and XPS confirm the presence of Cr_2O_3 layer over the CrO_2 nanoparticles. XRD and

SAED analysis shows that the particles are well crystalline having tetragonal symmetry. These nanoparticles are passivated by a layer of protein as indicated by FTIR analysis, UV-visible spectroscopy and thermo-gravimetric studies (TGA) which stabilize the CrO₂ nanoparticles against aggregation. Here extracellular protein acts as both a capping as well as a reducing agent. TGA studies showed that at temperatures higher than 340°C, CrO₂ starts decomposing into Cr₂O₃. Furthermore, magnetic behaviour studies show that CrO₂ is a ferromagnetic material. The presence of Cr₂O₃ layer over the CrO₂ nanoparticles as explained by the magnetic measurement in M-H curve suggests that the CrO₂ nanoparticles synthesized by *Trichothecium* sp. show ferromagnetic and anti-ferromagnetic exchange bias between core CrO₂ and Cr₂O₃ layer.

References

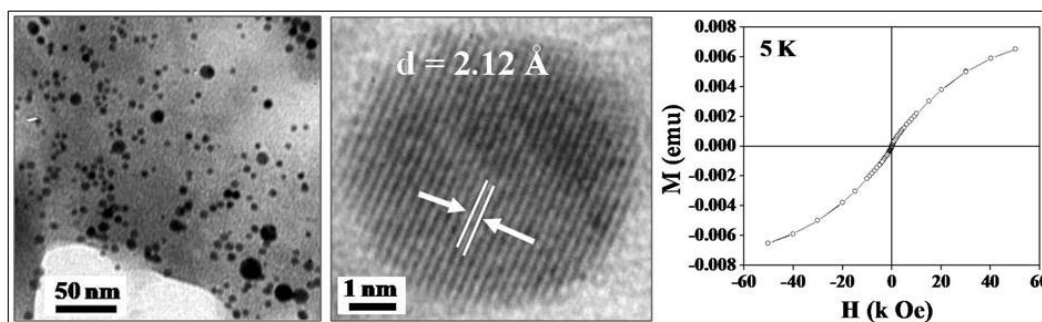
- [1] Cox, P. A., *Transition Metal Oxides: An Introduction to Their Electronic Structure and Properties.*, Oxford University Press, **2010**.
- [2] Weckhuysen, B. M., Wachs, I. E., Schoonheydt, R. A., *Chem. Rev.*, **1996**, 96, 8, 3327.
- [3] Kamper, K. P., Schmitt, W., Guntherodt, G., *Phys. Rev. Lett.*, **1987**, 59, 64, 2788.
- [4] Singley, E. J., Weber, C. P., Basov, D. N., Barry, A. Coey, J. M. D., *Phys. Rev. B.*, **1999**, 60, 6, 4126.
- [5] Lewis, S. P., Allen, P. B., Sasaki, T., *Phys. Rev. B.*, **1999**, 55, 16, 10253.
- [6] Vanleuken, H., Degroot, R. A., *Phys. Rev. B.*, **1995**, 51, 11, 7176.
- [7] Huang, D. J., Tjeng, L. H., Chen, J., Chang, C. F., Wu, W. P., Chung, S. C., Tanaka, A., Guo, G. Y., Lin, H. J., Shyu, S. G., Wu, C. C., Chen, C. T., *Phys. Rev. B.*, **2003**, 67, 21, 214419.
- [8] Coey J. M. D., Venkatesan, M., *J. Appl. Phys.*, **2002**, 91, 10, 8345.
- [9] Korotin, M. A., Anisimov, V. I., Khomskii, D. I., Sawatzky, G. A., *Phys. Rev. Lett.*, **1998**, 80, 19, 4305.
- [10] Keizer, R. S., Goennenwein, S. T. B., Klapwijk, T. M., Miao, G., Xiao, G., A. Gupta, A., *Nat. Lett.*, **2006**, 439, 825.
- [11] Goodenough, J. D., *Progress in Solid State Chemistry.*, pergamon Oxford., **1971**, 5, p.145.
- [12] Schwarz, K., *J. Phys. F.*, **1986**, 16, L211.
- [13] Degroot, R. A., Mueller F. M., Engen, P. G., Buschow, K. H. J., *Phys. Rev. Lett.*, **1983**, 50, 2024.
- [14] Allmaier, H., L. Chioncel, L., Arrigoni, E., Burzo, E., Beiușeanu, F., Katsnelson, M. I., Lichtenstein, A. I., *J. Optoelectron. Adv. Mater.*, **2008**, 10, 4, 737.
- [15] (a) Rudiger, U., Rabe, M., Samm, K., Ozyilmaz, B., Pommer, J., Fraune, M., Guntherodt, G., Senz, S., Hesse, D., *J. Appl Phys.*, **2001**, 89, 11, 7699. (b) Suzukia, K., Tedrow, P.M., *Appl. Phys. Lett.*, 74, 3, 428. (c) Li, X. W., Xiao, G., *J. Appl. Phys.*, **1999**, 85, 8, 5585. (d) Coey, J. M. D., Berkowitz, A. E., Balcells, L., Putris, F. F., *Phys. Rev. Lett.*, **1998**, 80, 17, 3815. (d) Sokolov,

-
- A., Yang, C. S., Yuan, L., Liou, S. H., Cheng, R., Xu, B., Borca, C. N., Dowben, P. A., Doudin, B., *J. Appl. Phys.*, **2002**, 81, 10, 8801.
- [16] Hwang, H. Y., Cheong, S. W., *Science.*, **1997**, 278, 28, 1607.
- [17] (a) Luis, F., Bartolome, J., Tejada, J., Martinez, E., *J. Magn. Magn. Mater.*, **1996**, 157, 158, 266. (b) Maestro, P., Andriamandroso, D., Demazeau, G., Pouchard, M., Hagenmuller, P., **1982**, *IEEE. Trans. Magn.*, 18, 5, 1000.
- [18] (a) Anguelouch, A., Gupta, A., Xiao, G., *IEEE Trans. Magn.*, **2001**, 37, 4, 2135. (b) Wang, K. Y., Spinu, L., He, J., Zhou, W., Wang, W., Tang, J., *J. Appl. Phys.*, **2002**, 91, 10, 8201. (c) Gupta, A., Li, X. W., Xiao, G., *J. Appl. Phys.*, **2000**, 87, 9, 6073.
- [19] (a) Brandle, H., Weller, D., Parkin, S. S. P., Scott, J. C., Fumagalli, P., Reim, W., Gambino, R. J., Ruf, R., Guntherodt, G., *Phys. Rev. B.*, **1992**, 46, 21,13889. (b) Costescu, R. M., Cahill, D. G., Fabreguette, F. H., Sechrist, Z. A., George, S. M., *Science.*, **2004**, 303, 989. (c) Rabe, M., Dreben, J., Dahmen, D., Pommer, J., Stahl, H., Rudiger, U., Guntherodt, G., Senz, S., Hesse, D., *J. Magn. Magn. Mat.*, **2000**, 211, 314.
- [20] Schlottmann, P., *Phys. Rev. B.*, **2003**, 67, 17, 174419.
- [21] Cheng, R., Komesu, T., Jeong, H. K., Yuan, L., Liou, S. H., Doudin. B., Dowben, P. A., Losovj, Y. B., *Phys. Lett. A.*, **2002**, 302, 211.
- [22] (a) Chamberland, B. L., *CRC Crit. Rev. Solid. State. Mater. Sci.*, **1977**, 7, 1. (b) Swoboda, T. J., Arthur, P., Cox, N. L., Ingraham, J. N., Opegard, A. L., Sadler, M.S., *J. Appl. Phys.* 1961, 32, 3745.
- [23] Chamberland, B. L., *Mater. Res. Bull.*, **1967**, 2, 827.
- [24] (a) Desisto, W. J., Broussard, P. R., Ambrose, T. F., Nadgorny, B. E., Osofsky, M. S., *Appl. Phys. Lett.*, **2000**, 76, 25, 3789. (b) Ivanov, P. G., Watts, S. M., Lind, D. M., *J. Appl. Phys.*, **2001**, 89, 2, 1035.
- [25] Brunet, F. B., Foucher, S., Morin, D., Ignatiadis, I., *Water, Air, Soil Pollution.*, **2004**, Focus 4, 127.
- [26] Bopp, L. H., Ehrlich, H. L., *Arch. Microbiol.*, **1988**, 155, 4426 .
- [27] Wang, P., Mori, T., Komori, K., Sasatsu, M., Toda, K., Ohtake, H., *Appl. Environ. Microbiol.*, **1989**, 55, 1665.
- [28] Han, X., Wong, Y. S., Wong, M. H., Tam, N. F. Y., *J. Hazard. Mater.*, **2007**, 146, 65.
- [29] Wang, Y., Xiao, C., *Water. Res.*, **1995**, 24, 2467.
-

-
- [30] Alvarez, A. H., Sanchez, R. M., Cervantes, C., *J. Biotech.*, **1999**, 181, 23, 7398.
- [31] (a) Dai, J., Tang, J., *Appl. Phys. Lett.*, **2000**, 77, 18, 2840-2843. (b) Zheng, R. K., Liu, H., Wang, Y., Zhang, X. X., *Appl. Phys. Lett.*, **2004**, 84, 5, 702.
- [32] The XRD patterns were indexed with reference to the crystal structures from the PCPDFWIN: CrO₂ (# 431-1040), Cr₂O₃ (# 38-1479), K₂Cr₂O₇ (# 27-380)
- [33] (a) Seo, K. I., McIntyre, P. C., Kim, H., Saraswat, K. C., *Appl. Phys. Lett.*, **2005**, 86, 082904. (b) Uddin, I., Adyanthaya, S., Syed, S., Selvaraj, K., Ahmad, A., Poddar, P., *J. Nanosci. Nanotechnol.*, **2008**, 8, 3909. (c) Wagner, C. D., Riggs, W. M., Davis, L. E., Moulder J. F., Muilenberg, G. E., *Handbook of X-ray Photoelectron Spectroscopy*, Perkin Elmer Corp. Publishers, Eden Prairie, MN **1979**.
- [34] Bureau, C., Valin, F., Lecayon, G., Charlier, J., Detalle, V., *J. Vac. Sci. Technol. A* **1997**, 2, 353. (b) Wagner, M. S., McArthur, S. L., Shen, M. C., Horbett, T. A., Castner, D. G., *J. Biomater. Sci. Polym. Ed.* **2002**, 13, 407.
- [35] (a) Ikemoto, I., Ishii, K., Kinoshita, S., Kuruda, H., Franco, M. A. A., Thomas, J.M., *J. Solid. State. Chem.*, **1976**, 17, 425-430. (b) Bullen, H. A., Garrett, S. J., *Chem. Mater.* **2002**, 14, 243.
- [36] Cheng, R., Borca, C. N., Pilet, N., Xu, B., Yuan, L., Doudin, B., Liou, S. H., Dowben, P. A., *Appl. Phys. Lett.*, **2002**, 81, 11, 2109.
- [37] Cheng, R., Xu, B., Borca, C. N., Sokolov, A., Yang, C. S., Yuan, L., Liou, S. H., Doudin, B., Dowben, P. A., *Appl. Phys. Lett.*, **2001**, 79, 19, 3122.
- [38] (a) Li, G. L., Xu, W. G., Li, Q. S., *J. Mol. Struct.*, **2000**, 498, 61. (b) Zhou, M., Zhang, L., Shao, L., Wang, W., Fan, K., Qin, Q., *J. Phys. Chem. A.*, **2001**, 105, 47, 10747. (c) Trpkovska, M., Soptrajanov, B., Pejov, L., *J. Mol. Struct.*, **2003**, 654, 21. (d) Almond, M. J., Hahne, M., *J. Chem. Soc. Dalton. Trans.*, **1988**, 2255.
- [39] Grdadolnik, J., *Bull. Chem. Technol. Macedonia*, **2002**, 21, 1, 23.
- [40] Antoine, R., Dugourd, P., *Phys. Chem. Chem. Phys.*, **2011**, DOI: 10.1039/c1cp21531k
- [41] Dor, B. L., Shimony, Y., *J. Cryst. Growth*, 1974, 24/25, 175.
- [42] (a) D. Rodbell, D., Devries, R. *Mat. Res. Bull.*, **1967**, 2, 4, 491. (b) Chen, Y. J., Zhang, X. Y., Li, Z. Y., *Chem. Phys. Lett.*, **2003**, 375, 213.
-

-
- [43] (a) Kiwi, M., *J. Magn. Magn Mater.*, 2001, 234, 584. (b) Srinath, S., Frey, N. A., Srikanth, H., Miao, G. X., Gupta, A., *Adv. Sci. Technol.*, **2006**, 45, 2528-2533. (c) Nogues, J., Sort, J., Langlais, V., Skumryev, V., Surinach, S., Munoz, J. S., Baro, M.D., *Phys. Rep.*, **2005**, 422, 65. (d) Frey, N. A., Srinath, S., Srikanth, H., *Phys. Rev. B.*, **2006**, 74, 024420.
- [44] (a) Hwang, H. Y., Cheong, S. W., *Science.*, **1997**, 278, 1607. (b) Barry, A., Coey, J. M. D., Viret, M., *J. Phys.: Condens. Matter.*, **2000**, 12, L173.

Chapter 2C



Fungus based synthesis of Mn_5O_8 nanoparticles.

*This chapter describes the synthesis of Manganese oxide (Mn_5O_8) nanoparticles using fungus *Fusarium oxysporum*. The compound Mn_5O_8 exists in mixed valencies of Mn^{2+} and Mn^{4+} and has a monoclinic structure. Mn_5O_8 nanoparticles have also drawn attention due to their antiferromagnetic nature. Here we report extracellular synthesis of Mn_5O_8 nanoparticles in the size range of 10-11 nm at room temperature by challenging the fungus *Fusarium oxysporum* with manganese acetate as precursor. These nanoparticles are now characterized by different techniques like UV-visible spectroscopy, FTIR and microscopy techniques. The phase is confirmed by techniques like XRD and XPS. Thus these Mn_5O_8 nanoparticles can be applicable in various fields.*

2.3.1 Introduction

The development of nanoparticles is aggressively considered not only for their fundamental scientific interests but also for many technological applications. Transition metal oxides have been studied due to their richness of interesting electrical, magnetic and optical properties which is mainly due to multivalent nature of transition metal ions, narrow *d*-band, etc. Magnetism in these oxides is especially interesting in comparison to simple metals because the electronic states in these oxides are more atom-like. The electrons in these oxides can be described by the same quantum numbers that apply to isolated atoms [1]. The ordering of different sublattices due to the super exchange interaction is reflected in paramagnetic to antiferromagnetic type of transitions.

Manganese, the second most abundant transition element and the tenth most abundant element in the earth's crust, exists in a number of oxidation states, among which the Mn(II), Mn(III) and Mn(IV) are of greatest environmental importance [2]. Manganese oxides have a relevant importance in modern solid state technology, owing to their peculiar properties. They are widely used in optoelectronic devices [3], as an attractive material for their good electrolytic properties and exhibit high oxide ion conductivity and are widely used in various applications such as micro-electronics [4], sensor technology [5], catalysts [6], ion-exchange [7], super capacitors [8], magnetic recording media [9] etc. Among various transition metal oxides, Mn-oxides have been of special interest due to their rich structural and compositional variants such as MnO, Mn₂O₃, Mn₃O₄, Mn₅O₈ and MnO₂. Moreover, multiple oxidation states (Mn²⁺, Mn³⁺, Mn⁴⁺ etc.) makes this family of compounds quite attractive [10]. Mn as a bulk metal is a paramagnet at room temperature and undergoes antiferromagnetic ordering below 100 K while MnO crystallizes in cubic structure and shows antiferromagnetic behavior in bulk form with T_N = 125 K. Mn₃O₄ is known to have a tetragonally distorted spinel structure below 1443 K with ionic structure Mn²⁺ [Mn₂³⁺] O₄. Among all the Mn-oxide phases, Mn₃O₄ is the only phase that orders ferromagnetically below 42K in bulk form [11]. On the other hand, MnO₂ is known to be antiferromagnetic below 84 K.

W. Feitknecht reported Mn₅O₈ for the first time [12] and it was further confirmed by R. Giabanori *et. al.* [13]. Mn₅O₈ has mixed valencies of Mn²⁺ and Mn⁴⁺. Mn₅O₈ has a monoclinic crystal structure with space group $C_{2h}^3 - C2/m$ and oxygen in *bc* plane

[15]. In this, between two alternative oxygen planes, two dimensional octahedral sheets of $[\text{Mn}_3^{4+}\text{O}_8]^{4-}$ consisting of Mn^{4+} ions are present. The Mn^{2+} are present above and below the Mn^{4+} valencies and hold negatively charged $\text{Mn}_3\text{O}_8^{4-}$ layers and form the undulating Mn^{2+} layer between $\text{Mn}_3\text{O}_8^{4-}$ layers. The six oxygen ions co-ordinate with Mn^{2+} and form a trigonal prism [14, 15]. Mn_5O_8 nanoparticles have also drawn attention due to their antiferromagnetic behaviour. We know that in Mn_5O_8 two types of Mn valencies Mn^{2+} and Mn^{4+} are present, and both have different types of magnetic moments. In Mn_5O_8 complex there are two sub-lattices for Mn^{2+} ion and two sub-lattices for Mn^{4+} ions present, so these magnetic moments cancel each other for antiferromagnetic behavior. Mixed valence nature of Mn_5O_8 nanoparticles make it a promising material for catalytic applications and due to its potential ionic conductivity, Mn_5O_8 nanoparticles can be used for batteries or fuel cells.

An alternative synthesis approach based on using the microbes is proposed. It has been successfully used to synthesize several materials which are quite difficult to achieve using traditional wet-chemical methods at (or around) room temperature. It is interesting to know that these microbes have the potential to perform certain reactions in ambient conditions and are able to stabilize these phases in a high crystalline form which normally requires high pressure and/or temperature [16].

In this study, we were curious to investigate the possible phase of manganese oxide nanoparticles after reacting the mesophilic fungus *Fusarium oxysporum* with manganese (II) acetate tetrahydrate $[(\text{CH}_3\text{CO}_2)_2\text{Mn}\cdot 4\text{H}_2\text{O}]$. However, in this chapter we have demonstrated the synthesis of nanoparticles of Mn_5O_8 . The choice of the mesophilic fungus *Fusarium oxysporum* for this purpose was not random, but directed towards the fact that these fungi produce a vast array of extracellular hydrolases and various reductases, to degrade their host plants in their natural habitats. Moreover, this fungus is easy to culture and maintain at ambient temperatures. Also, it can hydrolyze oxide precursors to form respective oxide nanoparticles extracellularly in an aqueous environment at room temperature and since these eukaryotic fungi when exposed to extremes of environmental conditions are forced to resort to specific defense mechanism to nullify such a stress, including the toxicity of foreign metal ions or metals; this fungus is exposed to such a stress during its life cycle in order to combat such a stress by producing certain extracellular enzymes which reduce the toxicity of metal ions or eliminate it by changing the oxidation state of the metal ions. Moreover, this fungus is a eukaryotic organism which adds up to its value [17].

2.3.2 Experimental Details

Manganese (II) acetate tetrahydrate $[(\text{CH}_3\text{CO}_2)_2\text{Mn}\cdot 4\text{H}_2\text{O}]$ (99+% purity, Catalogue Number 22,100-7) was purchased from Aldrich. Malt extract powder, yeast extract powder, glucose and peptone were obtained from Himedia, India. All the chemicals were used as-received.

The fungus *Fusarium oxysporum* was maintained on potato dextrose agar slants at 25°C. Stock cultures were maintained by sub-culturing at monthly intervals. The fungus was grown at pH 7.0 and 25°C for 120 hours; the slants were preserved at 15°C. From an actively growing stock culture, sub-cultures were made on fresh slants and after 120 hours of incubation at pH 7.0 and 25°C, were used as the starting material for synthesis of nanomaterials. For the extracellular synthesis of Mn_5O_8 nanoparticles, the fungus was grown in 500 ml Erlenmeyer flasks each containing MGY medium (100 ml), composed of malt extract (0.3%), glucose (1.0%), yeast extract (0.3%) and peptone (0.5%) at 25-27°C under shaking at 200 rpm for 96 hours. After 96 hours of fermentation, mycelia were separated from the culture broth by centrifugation (5000 rpm) at 10°C for 20 minutes and then the mycelia were washed thrice with sterile distilled water under sterile conditions. The harvested mycelial mass (20 gram of wet mycelia) was then resuspended in 100 ml of aqueous solution of 1mM Manganese (II) acetate tetrahydrate $[(\text{CH}_3\text{CO}_2)_2\text{Mn}\cdot 4\text{H}_2\text{O}]$ salt solution in 500 ml Erlenmeyer flasks and the same was put into a shaker at 25-27°C (200 rpm). The reaction was carried out for a period of 96 hours and fungal biomass was separated by filter paper to collect biomass and filtrate in sterile conditions.

The filtrate was then used to check the formation of nanoparticles by Transmission electron microscopy (TEM), Selected area electron diffraction (SAED) analysis, X-ray diffraction (XRD) analysis, Fourier transform infrared (FTIR) spectroscopy, Thermogravimetric analysis (TGA), Electron dispersive X-rays (EDAX) analysis and X-ray photoelectron spectroscopy (XPS).

To remove the unbound protein and unreacted precursor, we centrifuged the filtrate three times at 15,000 rpm for 30 minutes and each time the precipitate was resuspended in deionized water. These particles were used in the characterization as discussed below. To further remove the remaining surface layer of proteins, we calcined the as-synthesized particles at 400°C for three hours. For magnetization vs. magnetic field measurements, we used a magnetic property measurement system

(MPMS) from Quantum Design Inc., USA equipped with the superconducting quantum interference device (SQUID) magnetometer and superconducting magnet. For this purpose, we took the sample in teflon tape and packed it inside the gelatin capsules. The fungus *Fusarium oxysporum* was used for nanoparticle synthesis. Fungal strain analysis is already explained in chapter 2A.

2.3.3 Results and Discussions

2.3.3.1 TEM analysis

To further probe the morphology of these oxide nanoparticles, we performed a detailed electron microscopy study on the centrifuged particles. In Figure 2.3.1(A, B) we have shown the representative TEM images of protein functionalized as-synthesized Mn_5O_8 nanoparticles obtained after reacting the fungal biomass with precursor $(CH_3CO_2)_2Mn \cdot 4H_2O$, which shows that the Mn_5O_8 nanoparticles formed are irregular in shape with an overall quasi-spherical morphology.

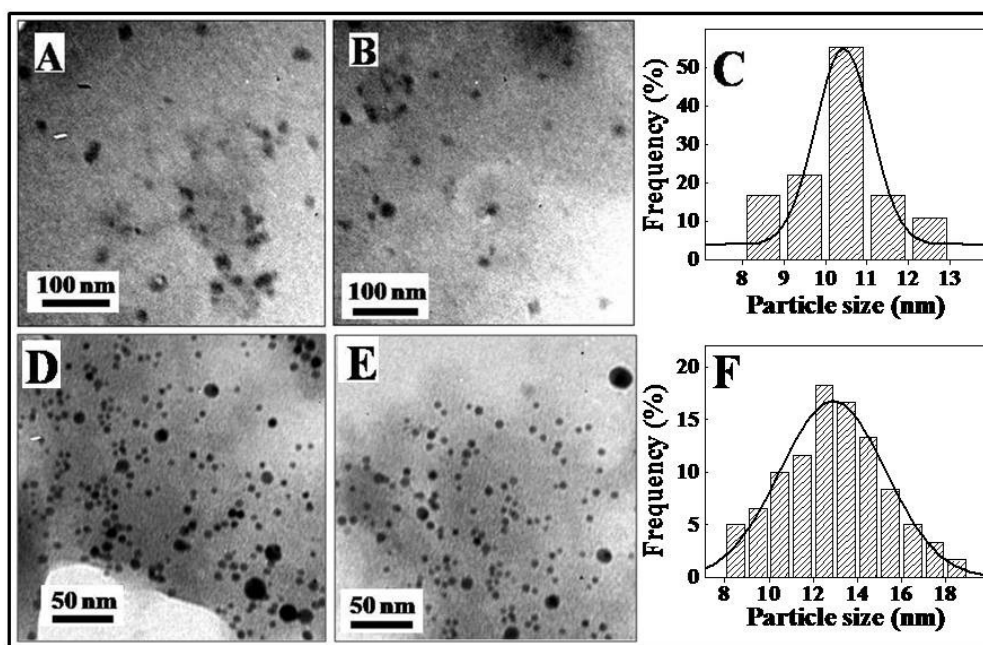


Figure 2.3.1: Transmission electron micrograph of Mn_5O_8 nanoparticles synthesized using *Fusarium oxysporum* biomass before (A, B) and after calcination at 400°C for 3 hours (D, E). Particle size distribution of Mn_5O_8 nanoparticles determined from TEM micrographs before (C) and after calcinations (F). The solid line is a Gaussian fit to the histogram.

The particle size histogram of the as-synthesized Mn_5O_8 nanoparticles shows that the average particle size is around 10-11 nm (figure 2.3.1C). These nanoparticles appear

to be well separated from each other since they are stabilized by the proteins present on the surface. One of the important observation found in bottom-up biosynthetic approach for synthesizing metal oxide nanoparticles is that the particle size obtained here is always relatively smaller in comparison to other wet-chemical techniques. This can be explained on the basis that extracellular protein responsible for synthesis as well as capping of metal oxide nanoparticles bind to the surface of these nanoparticles during their growth and hence restrict any further growth of nanoparticles. Presence of protein is further explained by FTIR, UV-visible spectroscopy and TGA analysis. To further investigate the effect of the calcination on the particle morphology as well as crystallinity, we calcined these particles at 400°C for 3 hours in air, which resulted into degradation of protein layer. In Figure 2.3.1(D, E), we have shown the TEM images of calcined nanoparticles which shows a slight increase in the average particle size. Particle size distribution curve of calcined nanoparticles (figure 2.3.1F) shows an increase in particle size up to 13 nm. This change in the size of as-synthesized nanoparticles could be attributed to partial loss of surface capped proteins.

2.3.3.2 HR-TEM and SAED analysis

To better investigate, crystallinity at the single particle level, we used the high resolution transmission electron microscopy. In figures 2.3.2 A & 2.3.2 B, we have respectively shown the HR-TEM and SAED image of as-synthesized Mn_5O_8 nanoparticles after approximately 96 hours of reaction. The figures 2.3.2C & 2.3.2D show the HR-TEM images of the calcined samples (at 400°C for 3 hours). The extent of single-crystallinity observed here in biologically synthesized particles (which happen in ambient conditions) is quite remarkable. The level of crystallinity increases remarkably after calcinations as observed from the figure 2.3.2 C & 2.3.2D. The lattice planes exhibit a spacing of $\sim 2.32\text{\AA}$ for the as-synthesized sample (figure 2.3.2A) and $\sim 2.12\text{\AA}$ and $\sim 2.41\text{\AA}$ for the sample calcined at 400°C (figure 3C, D) having the lattice planes $\{\bar{2}21\}$, $\{\bar{3}12\}$ and $\{021\}$ respectively. In figure 2.3.2B, we have shown the SAED pattern, which shows a diffuse ring pattern confirming crystallinity of the as-synthesized protein coated nanoparticles. The diffraction spots could be indexed on the basis of Mn_5O_8 crystal structure where the value of 'd spacing' obtained is well matched with standard literature values [18].

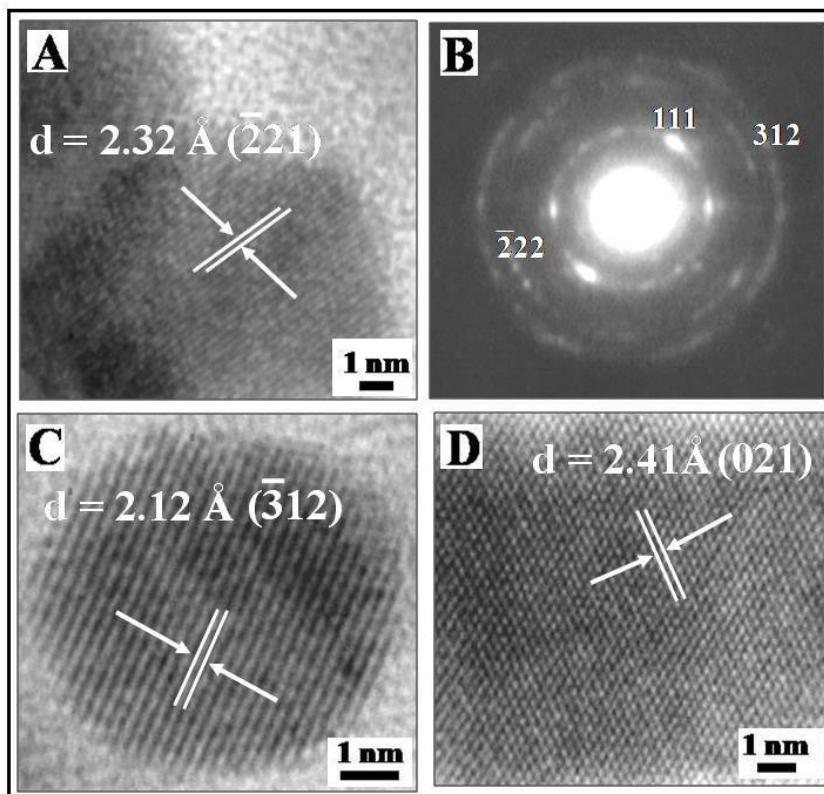


Figure 2.3.2: HR-TEM images of Mn_5O_8 nanoparticles synthesized using *Fusarium oxysporum* before (A) and after calcination at $400^\circ C$ for 3 hours (C, D) showing interplanar distance and SAED pattern for as-synthesized nanoparticles recorded from extracellular Mn_5O_8 nanoparticles shown in TEM micrograph (B).

2.3.3.3 X-ray diffraction analysis

To further verify the crystallinity of Mn_5O_8 nanoparticles formed by reaction of precursor $[(CH_3CO_2)_2Mn \cdot 4H_2O]$ with the fungus *Fusarium oxysporum*, we analyzed the X-ray diffraction patterns of as-synthesized Mn_5O_8 nanoparticles. Figure 2.3.3B shows the XRD patterns recorded from drop cast films of Mn_5O_8 nanoparticles. As-prepared Mn_5O_8 nanoparticles show well-defined Bragg's reflections indicating that the particles are crystalline in nature. In Figure 2.3.3, we compared the room temperature XRD patterns obtained from as-synthesized particles (fig 2.3.3B) and standard XRD profile (figure 2.3.34A) obtained from JCPDS data base of Mn_5O_8 nanoparticles, which show monoclinic Mn_5O_8 phase and with cell parameters $a=10.39\text{\AA}$, $b=5.730\text{\AA}$, $c=4.866\text{\AA}$, $\alpha=\gamma$, $\beta=109.62^\circ$ with the space group $C2/m(12)$ and true formula of Mn_5O_8 nanoparticle being " $Mn_2^{2+}Mn_3^{4+}O_8$ " [18 - 20]. There was absence of any other phase of manganese oxide. The ' 2θ ' values obtained in XRD pattern of particles match well with the standard ' 2θ ' values [$21.63^\circ \{ \bar{2}01 \}$, 24.09

\AA $\{\bar{1}11\}$, 28.71 \AA $\{111\}$, 31.53 \AA $\{\bar{3}10\}$, 36.31 \AA $\{\bar{2}20\}$, 38.28 \AA $\{\bar{2}21\}$, 40.47 \AA $\{\bar{1}12\}$, 46.38 \AA $\{112\}$, 48.90 \AA $\{\bar{4}20\}$, 51.43 \AA $\{\bar{1}31\}$, 54.02 \AA $\{131\}$ and 55.73 \AA $\{\bar{3}30\}$] of the monoclinic phase of Mn_5O_8 nanoparticles. The standard and observed experimental 2θ values are in good agreement. However many of the lines are broadened because of the small crystalline size [21]. In the course of this study, we for the first time have synthesized Mn_5O_8 nanoparticles in ambient conditions.

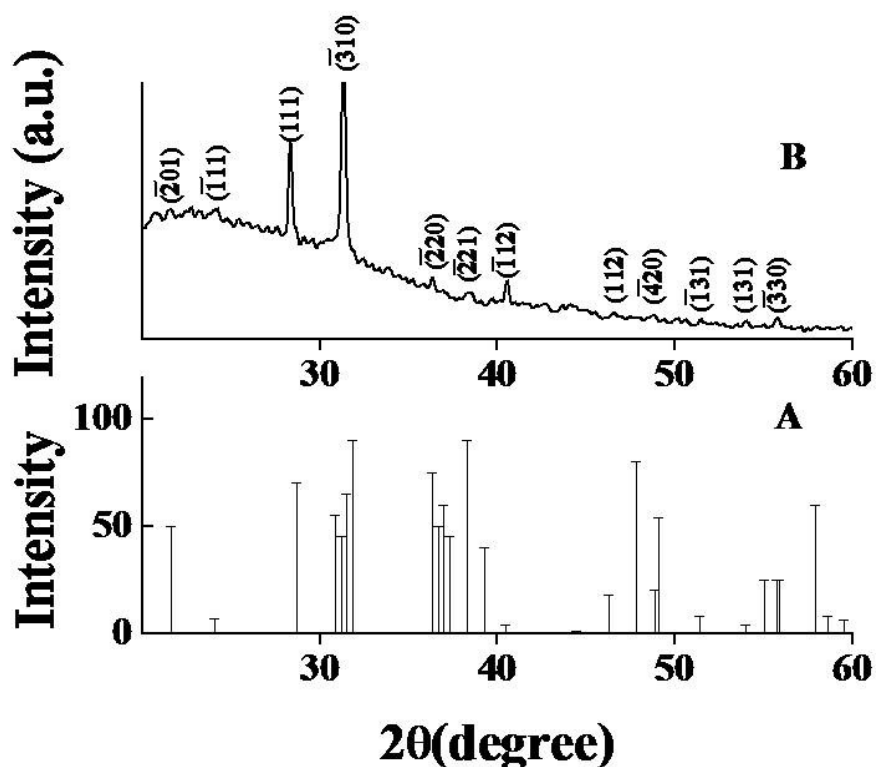


Figure 2.3.3: Powder XRD-pattern of drop-cast films of manganese oxide (Mn_5O_8) nanoparticles on glass after reaction with the fungus *Fusarium oxysporum* for 96 hours (B) and reference Mn_5O_8 from PCPDF # 39-1218 (A).

2.3.3.4 FTIR analysis

In figure 2.3.4A & 2.3.4B, we have compared Fourier transform infrared (FTIR) spectra in two different regions for the precursor manganese (II) acetate tetrahydrate $[(\text{CH}_3\text{CO}_2)_2\text{Mn} \cdot 4\text{H}_2\text{O}]$, uncalcined (as-synthesized) and calcined Mn_5O_8 nanoparticles taken in KBr pellets. It can be noticed that the after calcination, the absorption peaks are more prominent. In figure 2.3.4A, both uncalcined (curve 2) and calcined (curve 3) nanoparticles showed the presence of a prominent absorption

around 528 and 619 cm^{-1} due to Mn-O stretching in the Mn_5O_8 nanoparticles [22, 23], and in figure 2.3.4A (curve 1) there are a number of bands that are characteristic of the acetate anion, which appear at around 613 cm^{-1} [$\pi(\text{COO}^-)$] and 667 ($\delta[\text{OCO}]$) cm^{-1} stretching in the

manganese acetate used as the precursor salt [24]. In figure 2.3.4B, two absorption bands around 1655 and 1540 cm^{-1} are present in

uncalcined Mn_5O_8 sample, these are due to the amide I and II bands which arise due to the carbonyl stretch and –N–H stretch

vibrations respectively in the amide linkages of the proteins. Calcination of Mn_5O_8 particles at 400°C for three hours results in the denaturation of proteins as is evident from the disappearance of bands around 1655 and 1540 cm^{-1} for the calcined Mn_5O_8 sample [25]. This shows the removal of protein from the surface of manganese oxide (Mn_5O_8) nanoparticles after calcinations, this again gives evidence that nanoparticles are capped with protein and restricts its growth during its synthesis. This is why nanoparticles synthesized by biosynthetic methods are much smaller in size.

2.3.3.5 UV-visible spectroscopic analysis

In figure 2.3.5, we have tried to capture the formation of Mn_5O_8 nanoparticles by comparing between the UV-visible spectra of the precursor used for the biosynthesis-manganese (II) acetate tetrahydrate [$(\text{CH}_3\text{CO}_2)_2\text{Mn}_4\text{H}_2\text{O}$] (curve 1), biosynthesized Mn_5O_8 nanoparticles after 72 hours (curve 2) and 96 hours (curve 2) of reaction.

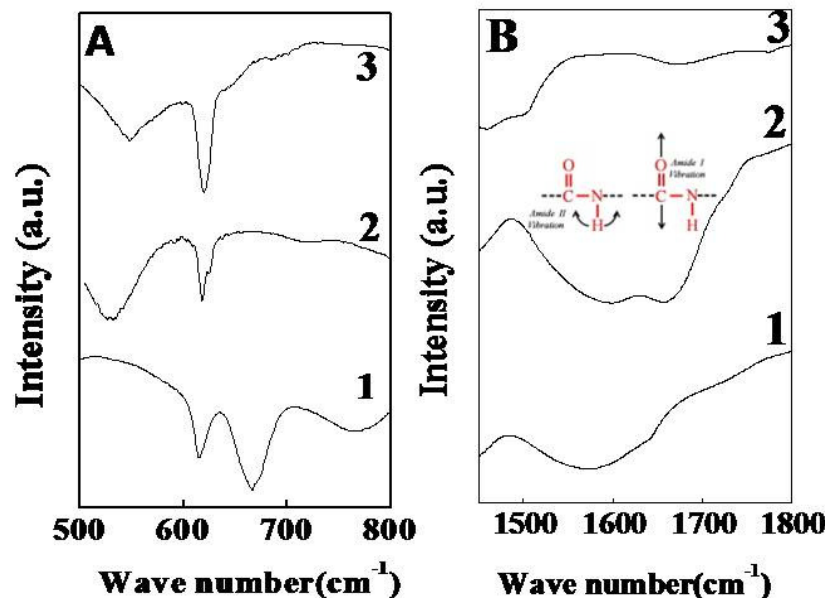


Figure 2.3.4: (A) FTIR spectra recorded from powder of $(\text{CH}_3\text{CO}_2)_2\text{Mn}_4\text{H}_2\text{O}$ (curve 1); Mn_5O_8 nanoparticles synthesized using *Fusarium oxysporum* before (curve 2) and after calcination at 400°C for 3 hours (curve 3). (B) Expanded view of the FTIR spectra shown in the region of the protein amide bands.

We observed that the precursor does not show any significant absorption in the entire range of measurement. However, after reacting with the fungal mass for 72 and 96 hours, we find a

significant absorption in curves 2 and 3 with two broad shoulders appearing, first one below 300 nm and the other one in a range from 315 nm to 350 nm. The first absorption peak below 300 nm (more precisely- at around 270 nm) can be attributed to the aromatic amino acids

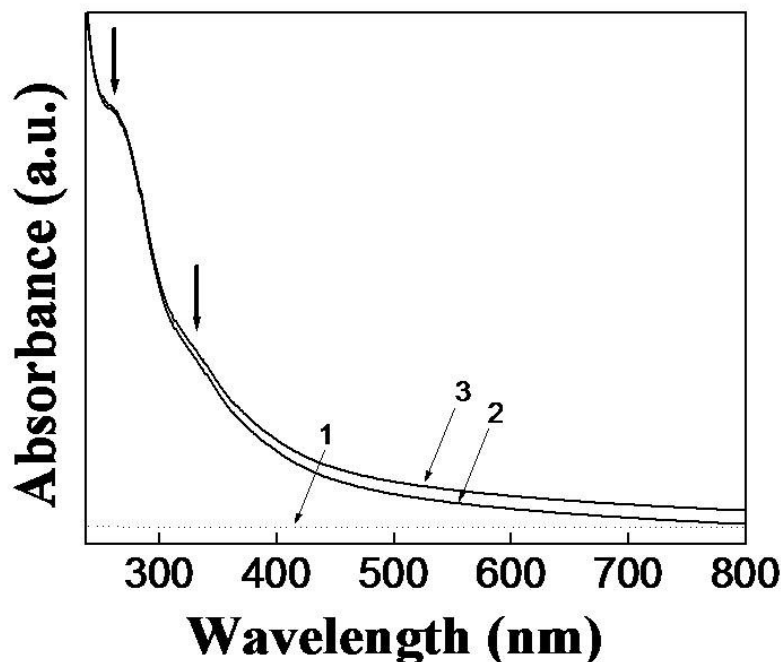


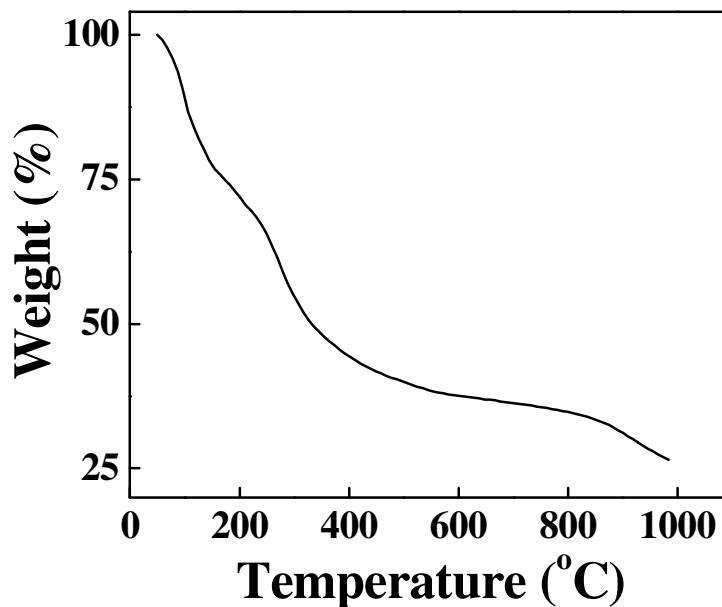
Figure 2.3.5 : UV-visible spectra (1) Precursor Manganese acetate tetrahydrate $[(CH_3CO_2)_2Mn \cdot 4H_2O]$ (2) as-synthesized Mn_5O_8 nanoparticle after 72 hours (3) 96 hours of reaction.

of the proteins present at the surface of the particles as well as in the solution. It is well known that the absorption band around 270 nm arises due to electronic excitations in tryptophan and tyrosine residues in the proteins [26]. These biomolecules are secreted by the fungal cells collectively due to the osmotic shock after their suspension in the deionized water as well its exposure to the Mn-salt. We believe that some of these biomolecules are finally responsible for converting the Mn^{2+} ions into stable Mn_5O_8 . Again in contrast to the absorption spectra of the precursor alone (curve 1), the broad shoulder above 300 nm might be due to the allowed $O^{2-} \rightarrow Mn^{2+}$ charge transfer transitions in Mn_5O_8 nanoparticles with no considerable change in the absorption intensity after 72 hours of the reaction [27-29]. This observation provides first hand evidence of the oxidization of the Mn^{2+} ions in the solution phase after incubating with fungus.

2.3.3.6 TGA analysis

Thermogravimetric analysis (TGA) was performed on as-synthesized Mn_5O_8 nanoparticles to calculate the amount of bio-organic molecules present over the nanoparticles. In

Figure 2.3.6, we have shown the thermogravimetric analysis (TGA) of as-synthesized Mn_5O_8 nanoparticles. As pointed out earlier, the as-synthesized nanoparticles are capped with biomolecules that stabilize them against



aggregation. The presence of this coating, even after

Figure 2.3.6: TGA of as-synthesized sample of Mn_5O_8 nanoparticles, showing % weight loss with respect to a steady increase in temperature.

intense centrifugation, is proven by the observation of almost 64% weight-loss during heating the particles up to 700°C, which is attributed to the loss of moisture present in the sample and decomposition of protein/ biomolecules bound on the surfaces of nanoparticles. A further increase in the temperature shows loss of weight that can be accounted for the decomposition of Mn_5O_8 nanoparticles [30].

2.3.3.7 Energy dispersive analysis of X-rays (EDAX) measurements

The elemental analysis of nanoparticles can be very informative for the study of the structural or elemental composition. The EDAX spectrum recorded from the Mn_5O_8 nanoparticles synthesized using the fungus *Fusarium oxysporum* is shown in Figure 2.3.7, which shows the presence of strong signals from manganese atoms together with weaker signals from C, O, N, and S atoms that arise from proteins bound to the Mn_5O_8 nanoparticles. This is again proof that capping of biomolecules/protein on the surface of nanoparticles gives stability to the oxide nanoparticles. The peak

corresponding to silicon arises from the substrate on which the sample is prepared for the EDAX analysis [31].

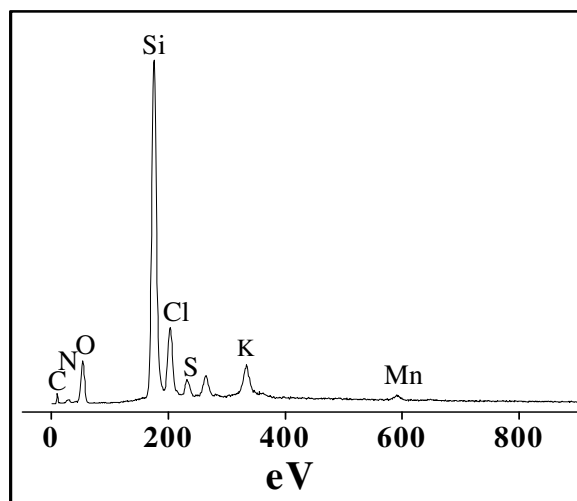


Figure 2.3.7: EDAX spectrum recorded from the Mn_5O_8 nanoparticles formed in the filtrate after 96 hours of reaction.

2.3.3.8 X-ray photoemission spectroscopy (XPS) analysis

The presence of Mn_5O_8 nanoparticles was also confirmed by analyzing the sample by XPS as shown in figure 2.3.8. The results showed the presence of C, N, O and Mn as the prominent elements. The chemical analysis of Mn_5O_8 nanoparticles was carried out by X-ray photoelectron spectroscopy (XPS) from the as-synthesized Mn_5O_8 nanoparticles after 96 hours of the reaction between fungus *Fusarium oxysporum* and manganese (II) acetate tetrahydrate $[(CH_3CO_2)_2Mn_4H_2O]$. The sample was prepared on silicon wafer. The core level spectra were background-corrected using the Shirley algorithm and the chemically distinct species were resolved using a nonlinear least squares curve fitting procedure. The C 1s, N 1s, O 1s and Mn 2p core level spectra were recorded with an overall resolution of ~ 1 eV. The core level binding energies (BEs) were aligned with respect to the C 1s binding energy (BE) of 285 eV. In Figure 2.3.8, we have presented the background-corrected X-Ray Photoemission Spectroscopy (XPS) of the biogenic Mn_5O_8 nanoparticles. As we know very well, XPS is a highly surface sensitive technique and the protein present on the surface of nanoparticles can easily be identified using XPS. So to further proof that the Mn_5O_8 nanoparticles are capped with protein; C1s, N1s, and O1s XPS analysis was done from biogenic Mn_5O_8 nanoparticle sample. Figure 2.3.8A shows the C 1s core level spectrum that could be decomposed into three chemically distinct components centered at 283.12 eV, 284.91.0 eV and 285.81 eV respectively.

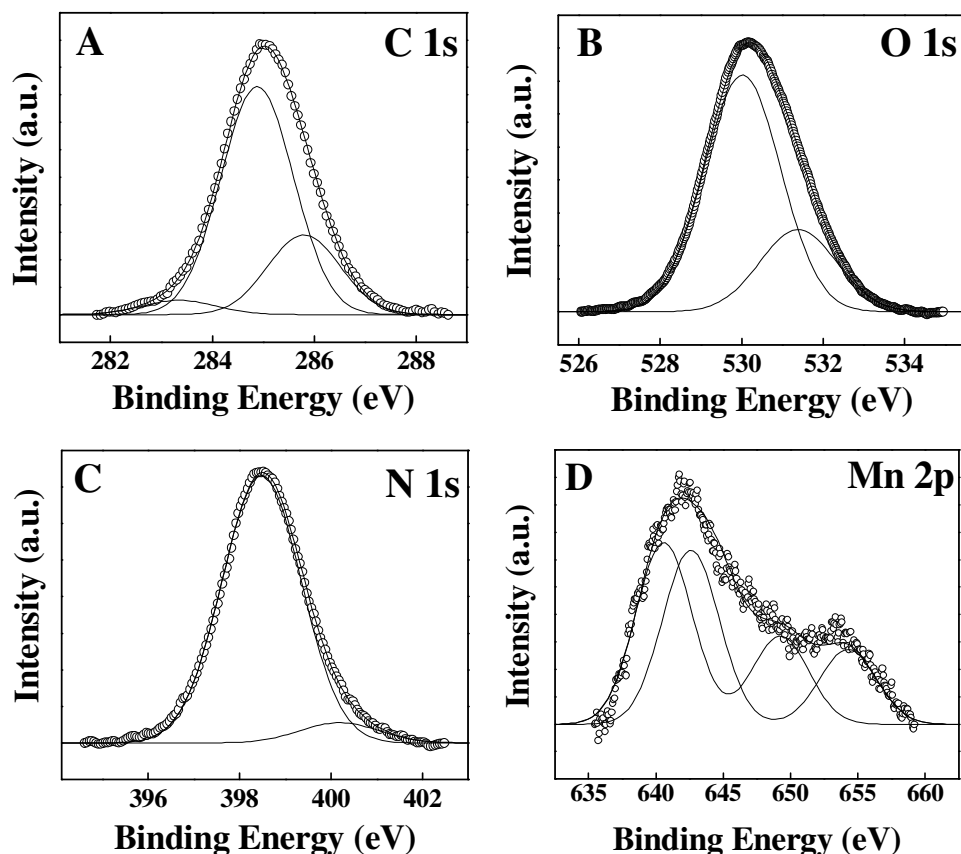


Figure 2.3.8 : XPS spectra of biosynthesized Mn_5O_8 nanoparticles synthesized by reaction between *Fusarium oxysporum* and manganese (II) acetate tetrahydrate $[(CH_3CO_2)_2Mn_4H_2]$ for 96 hours. The core level spectra is recorded from C 1s (A), O 1s (B), N 1s (C) and Mn 2p (D). The raw data is shown in the form of symbols, while the chemically resolved components are shown as solid lines and are discussed in the text.

The deconvoluted low binding energy peak at 283.12 eV is attributed to the presence of aromatic carbon present in amino acids from proteins bound to the surface of Mn_5O_8 nanoparticles [32]. The high binding energy peak at 285.81 eV is attributed to electron emission from carbons in carbonyl groups (aldehydic or ketonic carbon) present in proteins bound to the nanoparticles surface [33-34]. The C 1s component centered at 284.91 eV is due to electron emission from adventitious carbon present in the sample. The peak in figure 2.3.8B corresponds to the chemically distinct O 1s core level. The O 1s spectrum (Figure 2.3.8B) could be resolved into two chemically distinct components with binding energies 530.08 eV and 531.38 eV. The O 1s component present at lower binding energy at 530.08 eV can be assigned to the lattice oxygen of the as-prepared Mn_5O_8 nanoparticles. Beside this, the peak in figure 2.3.8B

corresponds to the chemically distinct O 1s core level with binding energy of about 531.38 eV. This may be attributed to the mixed contributions from surface hydroxide (OH groups) and C=O group present in capping proteins present on the surface of as-synthesized Mn₅O₈ nanoparticles [35-37]. Furthermore, figure 2.3.8C shows the N 1s core level spectra that could be fitted into two chemically distinct components centering at 398.48 eV and 400.18 eV. The lower binding energy component could be assigned free N₂ while higher binding energy component can be attributed nicely with values reported for –NH amide linkage in the capping proteins [38-39]. So, from the above observation in XPS data we can easily conclude that nanoparticles are capped with protein, and the growth of oxide nanoparticle is restricted at nanometer scale due to surface bound protein which acts as a capping agent and further stabilizes the oxide nanoparticle in nanometer regime. Presence of mixed valence state in manganese oxide are well studied [40]. As we know that Mn₅O₈ have two possible types of Mn valencies Mn²⁺ and Mn⁴⁺ respectively and XPS analysis of Mn₅O₈ nanoparticles further proves the presence of both oxidation state of Mn (Mn²⁺ and Mn⁴⁺) in Mn₅O₈. Figure 2.3.8D shows the Mn 2p spectrum of as-synthesized Mn₅O₈ nanoparticles decompose into Mn²⁺ and Mn⁴⁺ components. Further Mn²⁺ component could be resolved into two peaks with binding energies of 640.5 and 649.3 eV, which attribute to Mn 2p_{3/2} and Mn 2p_{1/2} respective peaks in divalent manganese ion which is further explained by previous studies that Mn²⁺ have comparable lower binding energy values than Mn³⁺ and Mn⁴⁺ ions. Similarly in figure 2.3.8D, Mn⁴⁺ component could be resolved into two peaks with binding energies of 642.5 and 654.2 eV which correspond for Mn 2p_{3/2} and Mn 2p_{1/2} respective peaks in tetravalent manganese ion, which matches well with previous literature [41-43]. XPS analysis of Mn₅O₈ nanoparticle clearly identifies the presence of two mixed valencies (Mn²⁺ and Mn⁴⁺) of manganese ion and forms the chemical formula like “ Mn₂²⁺Mn₃O₈⁴⁺ ” [44].

2.3.3.9 Magnetic measurements

Magnetic measurements were carried out on dried, as-synthesized Mn₅O₈ nanoparticles. Temperature dependent magnetization of Mn₅O₈ nanoparticles is studied by ZFC (Zero-field-cooled) and FC (field-cooled) modes for as-synthesized nanoparticles. Magnetization as a function of the field at temperature 300K and 5K was recorded by applied magnetic field. As we know very well, in antiferromagnetic material in different sub-lattices, electronic spin moments are exactly equal and

opposite which make net magnetic moment to zero. In Mn_5O_8 , manganese ions have two mixed valencies (Mn^{2+} and Mn^{4+}), which have interlayer exchange coupling with different magnetic moments. These two Mn ions interact antiferromagnetically and hence their magnetic moments cancel each other [45]. In figure 2.3.9A, we check the magnetization vs. temperature behavior of Mn_5O_8 and have shown the zero-field-cooled and field-cooled (ZFC-FC) measurements performed at an applied external field of 100 Oe. We observed that below 300K, sample show clear separation in ZFC and FC curves. This characteristic behavior is because of reduction in particle size and probably due to the enhanced interaction between the small nanoparticles. As the temperature goes down further at around 126K there is a sudden change in the

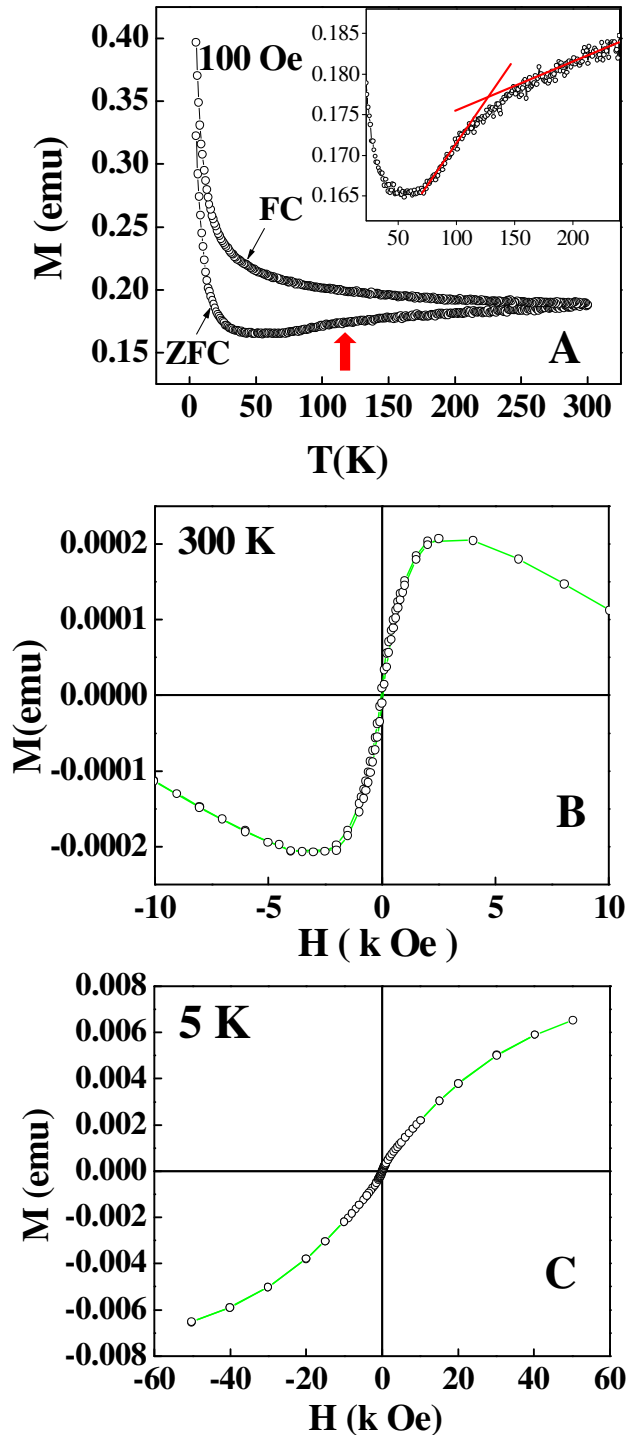


Figure 2.3.9: ZFC-FC curves at 100 Oe for as-synthesized Mn_5O_8 nanomaterials (A). Field dependent magnetization plots of Mn_5O_8 nanoparticles synthesized using *Fusarium oxysporum* at 300 K (B) and 5K (C).

slope of ZFC curve (inset figure 2.3.9A). This change in the ZFC curve corresponds to the Neel temperature transition in Mn_5O_8 nanoparticles, as compared to earlier reported around 136K [14, 45-47]. It might be because of the reduced particle size which again reduces the antiferromagnetic coupling, resulting in lowering of the Neel temperature [48, 49]. Since the Mn_5O_8 nanoparticles were synthesized by biological approach and were capped by protein layer which was observed in FTIR, XPS and TGA analysis, we did not get sharp Neel temperature transition in ZFC curve in magnetization vs. temperature measurement. Furthermore, at temperatures below 20K, magnetic moment in both FC and ZFC curve increases, which could be because of spin thermal vibration reduction. Figure 2.3.9B and C shows the magnetization curves (M-H curves) obtained from as-synthesized powdered Mn_5O_8 nanoparticle at 300 K and 5 K respectively. Since Mn_5O_8 nanoparticles having antiferromagnetic property below its Neel temperature ($\sim 126 T_N$ in this case) above this temperature, the system is paramagnetic in nature. But in figure 2.3.9B, M-H curve at 300K shows very little hysteresis with coercivity value of about 40 Oe. This small opening of loop or small coercivity value is because of nanosize effect or due to the very small size of the particles which increase surface anisotropy and the amount of uncompensated/canted surface spins due to the increased surface-to-volume ratio in Mn_5O_8 nanoparticles. Further, in M-H curve at 300K, we observed that at applied magnetic (H) field around 4k Oe all surface frustrated spins become saturated. With further increase, the applied magnetic field moment value goes down. This decrease in moment value is explained by diamagnetic contribution coming from protein present on the surface of nanoparticles. Figure 2.3.9C showed M-H curve at 5K (below the Neel temperature), in which again small hysteresis loop was again observed with coercivity value about 70 Oe. This increase in coercivity (H_C) in comparison to coercivity obtained at 300K in M-H curve is due to reduction in thermal energy.

2.3.4 Conclusions

In conclusion from the above analysis and results, we hereby confirm and prove the formation of Mn_5O_8 nanoparticles of average particle size around 10-11 nm by the fungus *Fusarium oxysporum*. The Mn_5O_8 so formed is characterized by TEM, XRD, FTIR, XPS, and TGA. As-synthesized as well as calcined particles showed excellent crystallinity. FTIR, TGA and XPS analysis explained the presence of proteins on the

surface of nanoparticles. It is confirmed by XPS data that Mn_5O_8 have two mixed manganese ion valencies (Mn^{2+} and Mn^{4+}) and antiferromagnetic transitions were further proved by magnetic measurements.

References

- [1] Robert C O Handley (1999), *Modern magnetic materials: principles and applications*, 123.
- [2] Gao, T., Norby, P., Krumeich, F., Okamoto, H., Nesper, R., Fjellvag, H., *Int. J. Inorg. Mater.*, **2001**, 3, 2001, 889.
- [3] Lu, X., Zheng, D., Zhai, T., Liu, Z., Huang, Y., Xie, S., Tong, Y., *Energy Environ. Sci.*, **2011**, Advance Article DOI: 10.1039/c1ee01338f
- [4] Ramesham, R., Daud, T., Moopenn, A., Thakoor, A. P., Khanna, S. K., *J. Vac. Sci. Technol. B*, **1989**, 3, 7, 450.
- [5] (a) Miyazaki, K., Hieda, M., Kato, T., *Ind. Eng. Chem. Res.* **1997**, 36, 88. (b) Edwin, A. M., Raj, S., Mallika, C., Sreedharan, O. M., Nagaraja, K. S., *Mater. Lett.*, **2002**, 53, 316. (c) Lima, A. S., Bocchi, N., Gomes, H. M., Teixeira, M. F. S., *Sensors*, **2009**, 9, 6613. (d) Beyene, N. W., Petr, K., Schachl, K., Alemu, H., Turkusic, E., Copra, A., Moderegger, H., Svancara, I., Vytras, K., Kalcher, K., *Talanta*, **2004**, 64, 1151.
- [6] (a) Katz, K., *Adv. Catal.*, **1953**, 5177. (b) Kim, S. H., Kim, S. J., Oh, S. M., *Chem. Mater.* **1999**, 11, 557. (c) Nayak, S. K., Jena, P., *J. Am. Chem. Soc.* **1999**, 121, 644. (d) Baldi, M., Finocchio, E., Milella, F., Busca, G., *Appl. Catal. B.*, **1998**, 16, 43. (e) Espinal, L., Suib, S. L., Rusling, J. F., *J. Am. Chem. Soc.*, **2004**, 126, 7676.
- [7] Wang, Y., Cao, G. Z., *Adv. Mater.*, **2008**, 20, 2251.
- [8] Athouel, L., Moser, F., Dugas, R., Crosnier, O., Belanger, D., Brousse, T., *J. Phys. Chem. C*, **2008**, 112, 7270.
- [9] (a) Park, j., Kang, E., Bae, C. J., Park, J. G., Noh, H. J., Kim, J. Y., Park, J. H., Park, H. M., Hyeon, T., *J. Phys. Chem. B.*, **2004**, 108, 13594. (b) Seo, W. S., Jo, H. H., Lee, K., Kim, B., Oh, S. J., Park, J. T., *Angew. Chem. Int. Ed.*, **2004**, 43, 1115.
- [10] (a) Nohman, A. K. H., Zaki, M. I., Mansour, S. A. A., Fahim R. B., Kappenstein, C., *Thermochim. Acta.*, **1992**, 210, 103. (b) Wells, A. F., In: 4th ed, *Structural inorganic chemistry.*, Oxford, Clarendon Press, 1975, pp. 458. (c) Post, J. E., *Proc. Natl. Acad. Sci. U.S.A.*, **1999**, 96, 3447.

-
- [11] Ip, K., Frazier, R. M., Heo, Y. W., Norton, D. P., Abernathy, C. R., Peartona, S. J., Kelly, J., Rairigh, R., Hebard, A. F., Wilson, V R. G., *J. Vac. Sci. Technol. B.*, **2003**, 4, 21.
- [12] Feitknecht, F., *Pure. Appl. Chem.*, **1964**, 9, 423.
- [13] Giabanori, R., Leuenberg, U., *Helv. Chim. Acta.*, **1969**, 52, 2333.
- [14] Gao, T., Norby, P., Krumeich, F., Okamoto, H., Nesper, R., Fjellvag, H., *J. Phys. Chem. C.*, **2010**, 114, 2, 922.
- [15] White, T. R., Glaunsinger, W. S., *J. Solid State. Chem.*, **1979**, 29, 205.
- [16] (a) Bansal, V., Poddar, P., Ahmad, A., Sastry, M., *J. Am. Chem. Soc.*, **2006**, 128, 11958. (b) Uddin, I., Adyanthaya, S., Syed, A., Selvaraj, K., Ahmad, A., Poddar, P., *J. Nanosci. Nanotechnol.*, **2008**, 8, 3909. (c) Bharde, A., Wani, A., Shouche, Y., Joy, P, A., Prasad, B. L. V., Rautaray, D., Sanyal, A., Sastry, M., *J. Am. Chem. Soc.*, **2005**, 127, 9326. (d) Rautaray, D., Ahmad, A., Sastry, M., *J. Am. Chem. Soc.*, **2003**, 125, 14656. (e) Bansal, V., Rautaray, D., Bharde, A., Ahire, K., Sanyal, A., Ahmad, A., Sastry, M., *J. Mater. Chem.* **2005**, 15, 2583. (f) A. Bharde, A., Rautray, D., Sarkar, I., Seikh, M. Sanyal, A., Ahmad, A., Sastry, M., *Small*, **2006**, 2, 135. (g) Ahmad, A., Jagadale, T., Dhas, V., Khan, S., Patil, S., Pasricha, R., Ravi, V., Ogale, S., *Adv. Mater.*, **2007**, 19, 3295.
- [17] (a) Kumar, S. A., Kazemian, M., Gosavi, S. W., Kulkarni, S., Parischa, R., Ahmad, A., Khan, M. I., *Biotechnol. Lett*, **2007**, 29, 439. (b) Kumar, S. A., Kazemian, M., Gosavi, S. W., Kulkarni, S., Ahmad, A., Khan, M. I., *Biotechnol. Appl. Biochem.*, **2007**, 47, 191. (c) Bansal, V., Rautaray, D., Ahmad, A., Sastry, M., *J. Mater. Chem.*, **2004**, 14, 3303.
- [18] The XRD patterns were indexed with reference to the crystal structures from the PCPDFWIN: Mn₅O₈ (# 39-1218).
- [19] Oswald, H. R., Feitknecht, W., Wampetich. M. J., *Nature.*, **1965**, 207, 72.
- [20] Oswald H. R., Wampetich, M. J. *Helv. Chim. Acta.*, **1967**, 50, 2023.
- [21] Rask, J. H., Buseck, P. R., *Am. Mineral.*, **1986**, 71, 805.
- [22] Gillot, B., Guendouzi, M .E., Laarj, M., *Mater. Chem. Phys.*, **2001**, 70, 54.
- [23] Zaki, M. I., Hasan, M. H., Pasupulety, L., Kumari, K., *New J. Chem.*, **1998**, 875.
- [24] Mohamed, M. A., Halawy, S. A., *Thermoch. Acta.*, **1994**, 242, 173.
-

-
- [25] Ganim, Z. H., Chung, S., Smith, A.W., Deflores, L. P., Jones, K. C., Tokmakoff, A., *Acc. Chem. Res.*, **2008**, 41, 3432.
- [26] Kumar, S. A., Ansary, A. A., Ahmad, A., Khan, M. I., *J. Biomed. Nanotechnol.*, **2007**, 3, 2, 190.
- [27] Palmer, S., Reddy, B. J., Frost, L. R., *Polyhydron.*, **2007**, 26, 524.
- [28] Macstre, J. B., Lopez, E. F., Amores, J. M., Casero, R. R., Escribano, V. S., Bernal, E. P., *Int. J. Mater.*, **2001**, 3, 889.
- [29] Baldi, M., Milella, F., Amores, J. M. G., Busca, G., *J. Mater. Chem.*, **1998**, 8, 11, 2525.
- [30] Rautaray, D., Sanyal, A., Adyanthaya, S. D., Ahmad, A., Sastry, M., *Langmuir*, **2004**, 20, 6827.
- [31] Rautaray, D., Sanyal, A., Bharde, A., Ahmad, A., Sastry, M., *Cryst. Growth Des.*, **2005**, 5, 2, 399.
- [32] Kumar, A., Mandal, S., Selvakannan, P. R., Pasricha, R., Mandale, A. B., Sastry, M., *Langmuir*, **2003**, 19, 6277.
- [33] Seo, K. I., McIntyre, P. C., Kim, H., Saraswat, K. C., *Appl. Phys. Lett.*, **2005**, 86, 082904.
- [34] Wagner, C. D., *J. Vac. Sci. Technol.* **1978**, 15, 518.
- [35] Margalit, R., Vasquez, R. P., *J. Protein. Chem.*, **1990**, 9, 1, 105.
- [36] Moulder, J. F., Stickle, W. F., Sobol, P. E., Bomben, D., *Handbook of X-ray Photoelectron Spectroscopy*; Physics Electronics Int.: Eden Prairie, MN, **1995**.
- [37] Sally, L. M., Griesser, H. J., Wagner, M. S., Castner, D. G., McLean, K. M., Kingshott, P., *Biopolymers at Interfaces, Second Edition*, CRC Press, **2003**, ch. 24.
- [38] Nguyen, T. D., Mrabet, D., Vu, T. T. D., Dinh, C. T., Do, T., *Cryst. Eng. Comm.*, **2011**, 13, 1450.
- [39] Bureau, C., Valin, F., Lecayon, G., Charlier, J., Detalle, V., *J. Vac. Sci. Technol. A.*, **1997**, 2, 353.
- [40] (a) Allen, G. C., Harris, S. J., Jutson, J. A., Dyke, J. M., *Appl. Surf. Sci.*, **1989**, 37, 111. (b) Bagus, P. S., S. Ilton, E. S., *Phys. Rev. B.*, **2006**, 73, 155110. (c) Audi, A. A., Sherwood, P. M. P., *Surf. Interface. Anal.*, **2002**, 33, 274. (d) Devries, A. H., L. Hozoi, L., Broer, R., *Phys. Rev. B.*, **2002**, 66, 035108.
- [41] Gao, T., Norby, P., Krumeich, F., Okamoto, H., Nesper, R., Fjellvag, H., *J. Phys. Chem. C.*, **2010**, 114, 922.
-

-
- [42] (a) Stranick, M. A., *Surf. Sci. Spectra.*, **1999**, 6, 31-38. (b) Lopez de Mishima, B. A., Ohtsuka, T., Konno, H., Sato, N., *Electrochim. Acta.*, **1991**, 36, 9, 1485. (b) Han, Y. F., Chen, F., Zhong, Z., Ramesh, K., Chen, L., Widjaja, E., *J. Phys. Chem. B.*, **2006**, 110, 24450-24456. (d) Rosso, J. J., Hochella, M. F., *Surf. Sci. Spectra.*, **1996**, 4, 253.
- [43] Wanger, C. D., Riggs, W. M., Davis, L. E., Moulder, J. F., *Hand book of X-ray photoelectroscopy.*, Perkin-Elmer Co-orporation.
- [44] Klingsberg, C., Roy, R., *J. Am. Ceram. Soc.* **1960**, 43, 620.
- [45] Punnoose. A., Magnone. H., Seehra. M., *IEEE Trans. Magn.*, **2001**, 37, 4, 2150.
- [46] Yamamoto, N., Kiyama, M., Takada, T., *Jpn. J. Appl. Phys.*, **1973**, 12, 11, 1827-1828.
- [47] Thota, S., Prasad, B., Kumar, J., *Mater. Sci. Eng B.*, **2010**, 167, 3, 153.
- [48] Zheng, X. G., Xu. C. N., Nishikubo. K., Nishiyama, K., Higemoto, W., Moon, W. J., Tanaka E., Otabe, E. S., *Phys. Rev B.*, **2005**, 72, 014464.
- [49] He, L., Chen, C., Wang, N., Zhou, W., Guo, L., *J. Appl. Phys.*, **2007**, 102, 103911.

Chapter 3



Bottom-up biosynthetic approach to synthesize sulphide nanoparticles.

*In this chapter we describe the synthesis of highly fluorescent, water dispersible Bi_2S_3 nanoparticles by reacting the fungus *Fusarium oxysporum* with bismuth nitrate pentahydrate [$\text{Bi}(\text{NO}_3)_3 \cdot 5\text{H}_2\text{O}$] alongwith Na_2SO_3 as precursors at room temperature. Transmission electron micrograph (TEM) showed that the biosynthesized Bi_2S_3 nanoparticles are quasi-spherical in shape with an average particle size of 15 nm. Selected area electron diffraction (SAED) and powder XRD show that particles are perfectly crystalline with an orthorhombic structure. The protein capped Bi_2S_3 nanoparticles maintain long term stability and show a band gap of 3.04 eV. Further characterization of Bi_2S_3 nanoparticles was done using techniques such as UV, PL, XPS, FTIR and TGA. These Bi_2S_3 nanoparticles were used in SPECT-CT probe for small animal imaging. This was injected into rats and biodistribution image and clearance time from blood was calculated.*

3.1 Introduction

The advent of reliable production of nanometer scale semiconductor particles has opened a frontier in material science. Semiconductor with nanometer sized crystals have unique photochemical and photophysical properties which are not found in either individual molecules or bulk solids [1, 2]. Semiconductor nanocrystals are unique for studying because their size dependent optical properties are convenient probes for the processes occurring in the nanometer regime. The quantum size effect is most pronounced for semiconductor nanoparticles where the band gap increases with decreasing size resulting in the interband transition shifting to higher frequencies. These quantum confined nanoparticles are brighter, more stable against photobleaching than organic dyes and can be excited for multicolour emission with a single light source. These semiconductor nanoparticles can be conjugated with biomolecules such as peptides, antibodies, small molecule ligands and therapeutic drugs for use in bioimaging [4]. Therefore, developing reliable protocols for the synthesis of nanometer scale semiconductor particles is a problem of great importance. Among various nanomaterials, metal sulphides are significant due to their optical, electronic and magnetic properties and have attracted extensive attention for promising applications in many fields [5-8]. These physical and chemical properties of metal sulphides are relative to their morphology, size, phase, etc. which in turn depends on their method of synthesis. Although great progress has been achieved on the synthesis considering the excitement of understanding new sciences, numerous protocols have been designed for the synthesis of metal sulphide nanocrystallites over a range of composition, sizes and shapes [9, 10]. Steigerwald *et al.* demonstrated the synthesis of sulphide nanoparticles by reacting an alkaline solution of the metal salt with H₂S in the presence of a stabilizing agent [11]. Several groups reported the synthesis of sulphide nanoparticles by thermolysis of single source precursors [12-14]. However, most of the methods employ high temperature and involve the use of expensive and toxic organic agents and a series of complicated procedures, non-polar organic solvents or caustic chemicals, suffer from agglomeration and are non-uniform in size distribution.

Among the numerous metallic sulphides, bismuth sulphide (Bi₂S₃) is one of the most important V-VI semiconductor with direct band gap of 1.3 eV [15]. It belongs to the family of main group metal chalcogenides $A_2^V B_3^{VI}$ (A= As, Sb and Bi, B= S, Se and

Te) class of semiconductors and has attracted great attention for its numerous significant applications including photovoltaic materials, photodiode arrays, sensor and thermoelectric cooling devices based on the Peltier effect [16, 17]. It shows excellent electrochemical hydrogen storage property [18, 19]. Recently, Bi_2S_3 nanoparticles have found new applications as imaging agents in X-ray computed tomography in biomedical sciences. There are many methods that have been exploited to synthesize nanostructured Bi_2S_3 with different morphologies such as ultrasonic method [20], microwave-assisted route [21], photochemical synthesis method [22] and thermal decomposition [23]. There are also many solution based synthetic procedures available like solvothermal/hydrothermal processes [24, 25] and template growth [26]. However, most of the techniques mentioned above need rigorous conditions such as relatively higher temperature and pressure, reactions in organic solvents and the preparation procedures are complex. Therefore, it remains a challenge to develop an alternative for the development of eco-friendly processes for the synthesis of Bi_2S_3 nanocrystals at ambient conditions. Recognizing that production of nanomaterials by biological methods would address the shortcomings of the chemical method and lead to potentially large cost reduction; biomaterials and biological structures of higher complexity can act as active units for the synthesis of nanoparticles. Several biomimetic synthesis approaches, wherein biomolecules or microbes participate either in the reduction, oxidation or hydrolysis of the precursors or act as templates, are gaining popularity as these novel synthesis methods do not require high temperature, pressure or extreme pH conditions. These reactions are often environment friendly and efficiency of these natural synthesis processes is often very high. Biological synthesis of metal sulphide nanoparticles is gaining importance since it occurs in aqueous medium under ambient experimental conditions. Biosynthetic approach comprises the use of microorganisms, small biomolecules, biological templates and small peptides for the synthesis of various metal sulphide nanoparticles. These biomolecules have been used for capping the sulphide nanoparticles. Ahmad *et al.* have developed methods for the synthesis of gold and silver nanoparticles [27], metal sulphides and nano-oxides [28] in aqueous solutions. Besides this, there are some reports where prokaryotes as well as eukaryotes produce semiconductor nanoparticles within the cell wall of the microorganisms. The intracellular synthesis of CdS semiconductor nanoparticles using the bacteria *Klebsiella aerogenes* [29] alongwith two different yeast species *Schizosaccharomyces*

pombe and *Candida glabrata* was reported [30]. On the other hand, Kowshik *et al.* used another yeast species, *Turolopsis* sp. [31] for the synthesis of intracellular PbS nanoparticles. In previous report from the National Chemical Laboratory (NCL, Pune, India), Ahmad *et al.* reported the extracellular synthesis of CdS nanoparticles using fungus *Fusarium oxysporum* [32]. There are some reports where biological approaches to synthesize semiconductor nanocrystals have been extended to intact biological particles; like viral scaffolds have been used as template for the nucleation and assembly of CdS and PbS crystalline nanowires [33]. Biomolecule-assisted synthesis of various nanomaterials have been a new and promising method. Yi Xie *et al.* reported biomolecule-assisted synthesis of single crystalline Bi₂S₃ nanostructures. In this report, an amino acid cysteine acts as a sulphur source as well as a capping agent in the synthesis of Bi₂S₃ nanocrystals [34]. In another report, Komarneni *et al.* used a large polypeptide (GSH) to synthesize the highly ordered snowflake structure of bismuth sulphide nanorods under microwave irradiation. Glutathione molecule was used as an assembling molecule as well as the sulphur source [35].

Already, a lot off work has been done to understand the biosynthetic approach to synthesize the metal sulphide nanoparticles. A potential implication of biological synthesis that we have envisaged is making use of the hydrolytic enzymes secreted by the fungi for the synthesis of sulphide nanoparticles. Here, we report the orthorhombic Bi₂S₃ quantum dots preparation by reacting the mesophilic fungus *Fusarium oxysporum* with bismuth nitrate pentahydrate [Bi(NO₃)₃·5H₂O] and sodium sulphite (Na₂SO₃) as precursors salt. Transmission electron micrograph (TEM) showed that the as-synthesized Bi₂S₃ nanoparticles are quasi-spherical in shape with an average particle size of 15 nm. Selected area electron diffraction (SAED) and powder XRD show that particles are perfectly crystalline with an orthorhombic structure. The particle surfaces are passivated by a robust layer of protein which provides stability in aqueous medium. The particle size analysis was perfomed using TEM. The protein capped Bi₂S₃ quantum dots maintain a long-term stability and shows a blue shift with a band gap of 3.04 eV. Further material characterization was done using techniques such as UV, PL, XPS, FTIR and TGA. Fungal strain analysis is already explained in chapter 2A

3.2 Experimental Details

Bismuth (III) nitrate pentahydrate [$\text{Bi}(\text{NO}_3)_3 \cdot 5\text{H}_2\text{O}$] and sodium sulphite (Na_2SO_3) guaranteed reagent (GR) grade were purchased from Aldrich. Malt extract powder, yeast extract powder, glucose, and peptone were obtained from Himedia, India. All the chemicals were used as-received. The fungus *Fusarium oxysporum* was maintained on potato dextrose agar slants at 25°C. Stock cultures were maintained by sub-culturing at monthly intervals. The fungus was grown at pH 7.0 and 25°C for 120 hours; the slants were preserved at 15°C. From an actively growing stock culture, sub-cultures were made on fresh slants and after five days of incubation at pH 7.0 and 25°C, were used as the starting material for synthesis of nanomaterials. For the extracellular synthesis of Bi_2S_3 nanoparticles, the fungus was grown in 500 ml Erlenmeyer flasks each containing MGYP medium (100 ml), composed of malt extract (0.3%), glucose (1.0%), yeast extract (0.3%) and peptone (0.5%) at 25-27°C under shaking at 200 rpm for 96 hours. After 96 hours of fermentation, mycelia were separated from the culture broth by centrifugation (5000 rpm) at 10°C for 20 minutes and then the mycelia were washed thrice with sterile distilled water under sterile conditions. The harvested mycelial mass (20 gram of wet mycelia) was then resuspended in 100 ml of aqueous solution of 1mM $\text{Bi}(\text{NO}_3)_3 \cdot 5\text{H}_2\text{O}$ and 5mM Na_2SO_3 salt solution in 500 ml Erlenmeyer flasks and the same was put into a shaker at 25-27°C (200 rpm). The reaction was carried out for a period of 96 hours and fungal biomass was separated by filter paper to collect biomass and filtrate in sterile conditions. The biotransformation was routinely monitored at different time intervals. To remove the unbound protein and unreacted precursor, we centrifuged the filtrate three times at 15,000 rpm for 30 minutes and each time the precipitate was resuspended in the de-ionized water. Further characterization of extracellular nanoparticles was carried out by Transmission electron microscopy (TEM), Selected area electron diffraction (SAED) analysis, X-ray diffraction (XRD) analysis, Fourier transform infrared (FTIR) spectroscopy, Thermogravimetric analysis (TGA), Electron dispersive X-rays (EDAX) analysis and X-ray photoemission spectroscopy (XPS).

3.2.1 CT Contrast study

Confirmation of Bi_2S_3 nanoparticles to act as CT contrast agents was done by performing phantom studies at various concentrations in saline namely 50 mg/ml,

100mg/ml, 200mg/ml and 500mg/ml at CT tube current of 2.5mA and tube voltage of 140 KVp.

3.2.2 Radiolabelling of Bismuth sulphide Bi_2S_3 nanoparticles with Tc-99m:

$^{99\text{m}}\text{Tc-Bi}_2\text{S}_3$ nanoparticles were prepared by dissolving 10 mg of Bi_2S_3 nanoparticles in 1ml of distilled water followed by the addition of 100 μg of $\text{SnCl}_2 \cdot 2\text{H}_2\text{O}$ and the pH was adjusted to 6.5. The content was filtered through a 0.22 μm membrane filter into a sterile vial. Approximately 2 mci Tc-99m was added to the content, mixed and incubated for 10-15min. The percent radiolabel was determined by using instant thin layer chromatography (ITLC) method.

3.2.3 Radiochemical purity (RCP):

The radiochemical purity of Tc-99m with Bi_2S_3 nanoparticles was estimated by instant thin layer chromatography (ITLC) using silica gel coated fiber sheets. ITLC was performed using 100% acetone and 0.9% saline as the mobile phase. A measured amount of 2-3 μl of the radiolabeled complex was applied at a point 1 cm from one end of an ITLC-SG strip and allowed to run for approximately 10 cm. Amount of reduced/hydrolyzed Tc-99m was determined using pyridine: acetic acid: water (3:5:1.5 v/v) as mobile phase and ITLC as the stationary phase and the radioactivity distribution over the strip was determined with a radioactivity well counter (ECIL). Radiochemical purity (RCP) was calculated as the fraction of radioactivity that remained at the origin and was designated as % RCP.

3.2.4 Biodistribution of radiolabelled nanoparticles:

Male Sprague Dawley rat weighing (180-220 gram) was selected for evaluating the localization of the labelled complex. $^{99\text{m}}\text{Tc-Bi}_2\text{S}_3$ nanoparticles 14.8 MBq were administered through the penile vein of rat. The biodistribution studies of labelled Bi_2S_3 nanoparticles were evaluated after 45 min post injection.

3.3 Results and Discussions

3.3.1 UV-visible spectroscopic analysis

In figure 3.1(A), we have tried to capture the formation of Bi_2S_3 nanoparticles by comparing the UV-visible spectra of the precursors used for the biosynthesis i.e $\text{Bi}(\text{NO}_3)_3 \cdot 5\text{H}_2\text{O}$ and Na_2SO_3 (curve 1), with biosynthesized Bi_2S_3 nanoparticles after 72 hours (curve 2) and 96 hours (curve 3) of reaction. We observed that the precursor

does not show any significant absorption in the entire range of measurement. However, after the reaction with the fungal mass for 72 and 96 hours, we find a significant absorption in curves 2 & 3 with two broad shoulders appearing, first at ca 270 nm and the other one in a range of 310 to 350 nm.

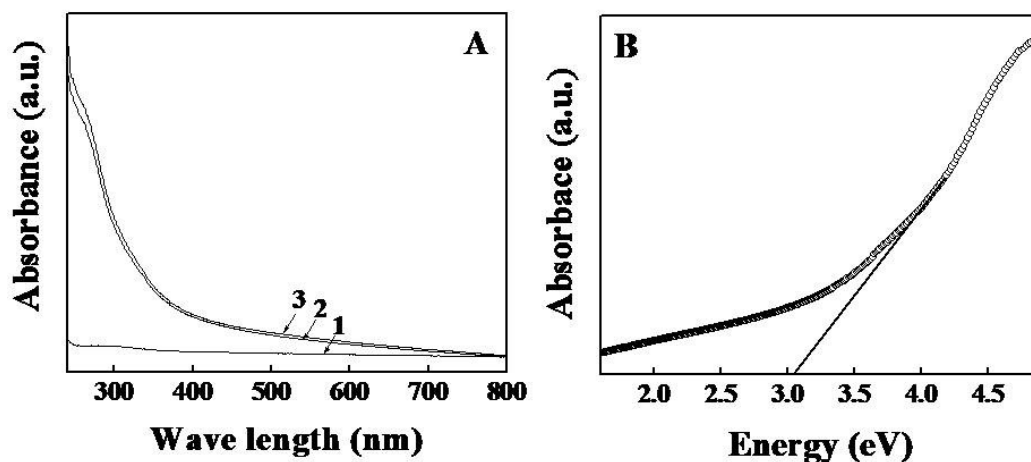


Figure 3.1: (A) UV-vis spectra of (1) Precursor salt and (2) as-synthesized extracellular Bi_2S_3 nanoparticles after 72 and (3) after 96 hours of reaction. (B) Band gap energy curve of Bi_2S_3 nanoparticles obtained by UV-vis spectroscopic analysis performed on Bi_2S_3 nanoparticles after 96 hours of reaction. Tangent drawn to the absorption edge corresponds to the band gap energy of Bi_2S_3 nanoparticles.

The appearance of absorption edge at ca 270 nm can be assigned to the aromatic amino acids such as tryptophan, tyrosine and phenyl aniline present in the protein, which is secreted in the solution by the fungus *Fusarium oxysporum*. We believe that some of the biomolecules are responsible for converting Bi^{3+} and S^{2-} ions into stable Bi_2S_3 nanoparticles. Figure (3.1A) shows the UV-visible spectroscopic profile of protein capped bismuth sulphide nanoparticle formation using fungus *Fusarium oxysporum*. UV-visible spectroscopic analysis reveals the presence of broad shoulder in a range from 310 to 350 nm and corresponds to excitonic transition in Bi_2S_3 nanocrystallites. There is absence of an absorption edge due to formation of particles of different sizes [36, 37]. We know that the fundamental property of semiconductors is its band gap as we know that bulk Bi_2S_3 has band gap energy of 1.3 eV. All semiconductors show size quantization effects as the size of semiconductor material is reduced. Figure (3.1B) corresponds to the band gap energy analysis after 96 hours of reaction. The band gap energy value obtained is about 3.04 eV, which is considerably

higher than the band gap energy of bulk Bi_2S_3 . The increase in band gap energy is due to the reduction in size of Bi_2S_3 and could be a consequence of size quantization effect.

3.3.2 Photoluminescence (fluorescence) measurements of Bi_2S_3 nanoparticles.

Luminescence characteristics of Bi_2S_3 nanoparticles were studied by fluorescence measurement of the Bi_2S_3 nanoparticles by exciting the reaction mixture at 310 nm.

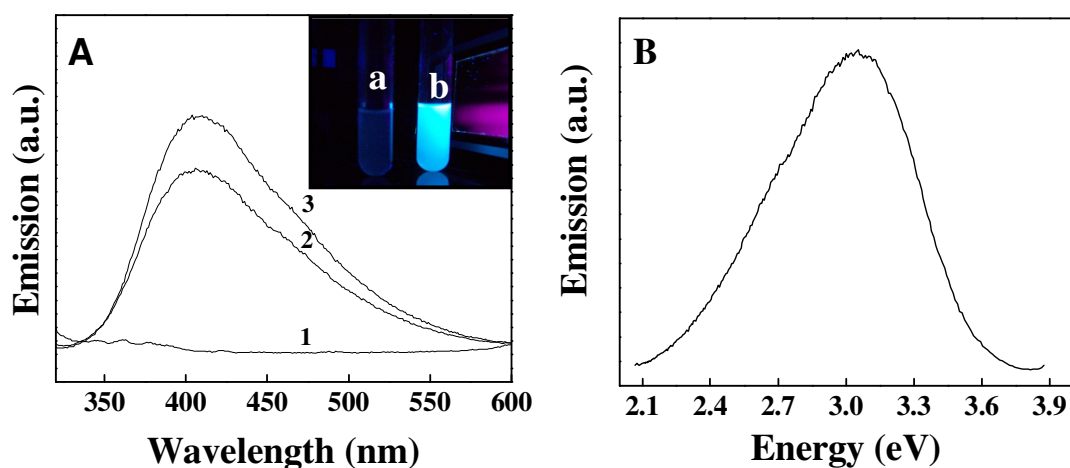


Figure 3.2: Photoluminescence/ Fluorescence emission spectra of (1) Precursor salt and (2) as-synthesized Bi_2S_3 nanoparticles after 72 and (3) 96 hours of reaction. The inset shows a glass vial containing (a) Precursor salt (b) biogenic Bi_2S_3 nanoparticle solution after irradiation with UV light of 365 nm. (B) Spectrum in terms of the energy scale corresponding to the emitted light.

An emission band centered at 410 nm (Fig 3.2A) is observed which is comparable to the emission peaks of Bi_2S_3 nanoparticles, which is attributable to the band gap or near band gap emission resulting from the recombination of the electron-hole pairs in the Bi_2S_3 nanoparticles. The band gap of as-prepared Bi_2S_3 nanoparticles is calculated to be 3.04 eV from emission spectra which is much larger than bulk Bi_2S_3 which is due to size quantum effects. When the size of particle decreases, discrete sub-bands are formed in valence and conduction bands which lead to the quantization of energy level [37-39]. The inset Figure (3.2A) shows glass vial containing precursor reaction solution at the beginning (time $t=0$, vial a) and after 96 hours of reaction (vial b). A strong blue-green emission from as-synthesized nanoparticles were observed when excited at a wavelength of 365 nm while no fluorescence was obtained from precursor

salt solution. The blue-green luminescence is significant for several applications. Figure (3.2B) shows the PL spectrum of as-synthesized Bi_2S_3 nanoparticles in terms of energy. A strong peak at 3.04 eV is observed from as-synthesized Bi_2S_3 nanoparticles. The blue shift in the energy of PL spectrum could be assigned to the emission from holes and electron traps frequently located at the surface on the particles due to the large surface area of the particles at smaller size.

3.3.3 TEM, HR-TEM and SAED analysis

To further probe the morphology of these sulphide nanoparticles, we performed a detailed electron microscopy study on the as-synthesized nanoparticles.

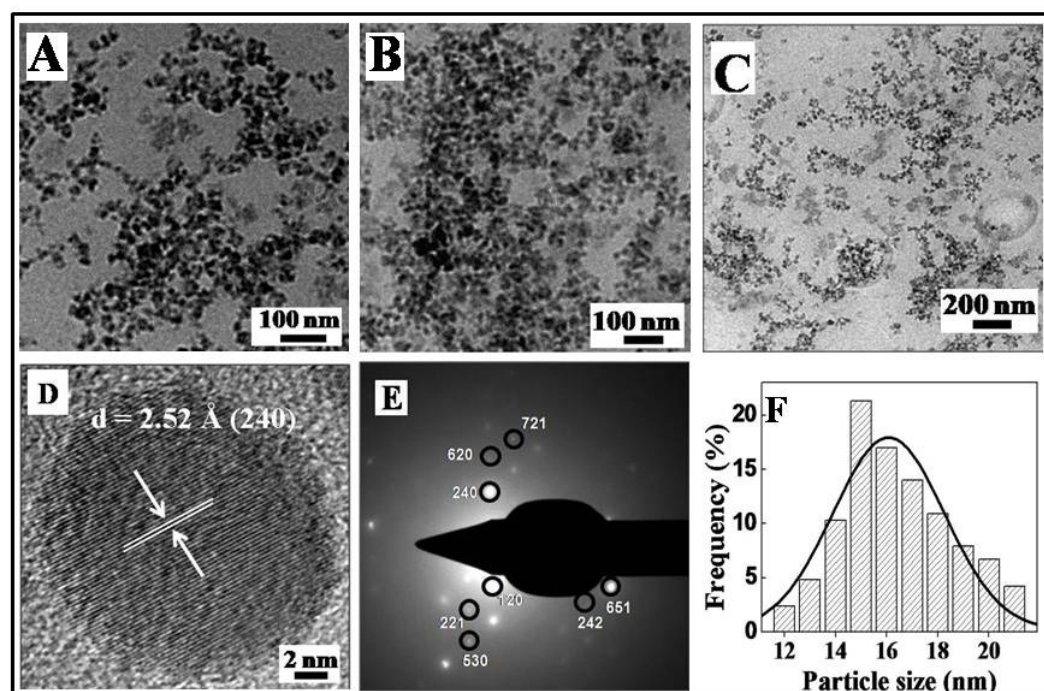


Figure 3.3: (A-C) Transmission electron micrograph (TEM) of Bi_2S_3 nanoparticles solution formed by the reaction of precursor solution with *Fusarium oxysporum* biomass for 96 hours at different magnifications (D) HR-TEM image of Bi_2S_3 nanoparticles showing inter planar distance (E) SAED pattern recorded from extracellular Bi_2S_3 nanoparticles shown in TEM micrograph and (F) particle size distribution of Bi_2S_3 nanoparticles synthesized using fungus *Fusarium oxysporum* determined from TEM micrograph.

In Figure 3.3 (A-C), we have shown the representative TEM images of protein capped as-synthesized Bi_2S_3 nanoparticles, which show that the average particle size is around 15 nm with an overall quasi-spherical morphology. To better investigate the crystallinity at single particle level, we used high resolution transmission electron

microscopy (HR-TEM). In figure 3D, we have shown the HR-TEM image of as-synthesized Bi_2S_3 nanoparticles after approximately 96 hours of reaction. The extent of single crystallinity observed here in biologically synthesized particles (which happen in ambient conditions) is quite remarkable. The lattice planes exhibit a spacing of $\sim 2.52\text{\AA}$ for the as-prepared sample having the lattice planes $\{240\}$. To better investigate the crystallinity of particle, we have shown the SAED image of as-synthesized Bi_2S_3 nanoparticles after approximately 96 hours of reaction. The Scherrer ring pattern characteristic of Bi_2S_3 is clearly observed, showing that the structures seen in TEM are nanocrystalline in nature. In figure (3.3E), we have shown the SAED pattern which shows a spot pattern confirming crystallinity of the as-synthesized protein-coated nanoparticles. These spot pattern were referred for $\{120\}$, $\{240\}$, $\{242\}$, $\{651\}$, $\{620\}$, $\{221\}$, $\{630\}$ and $\{721\}$ crystal planes, which matches well with the reported values [40]. Figure (3.3F) shows the particle size distribution of Bi_2S_3 nanoparticles which reveals that the average particle size of Bi_2S_3 nanoparticles is about 15 nm.

3.3.4 X-ray diffraction analysis

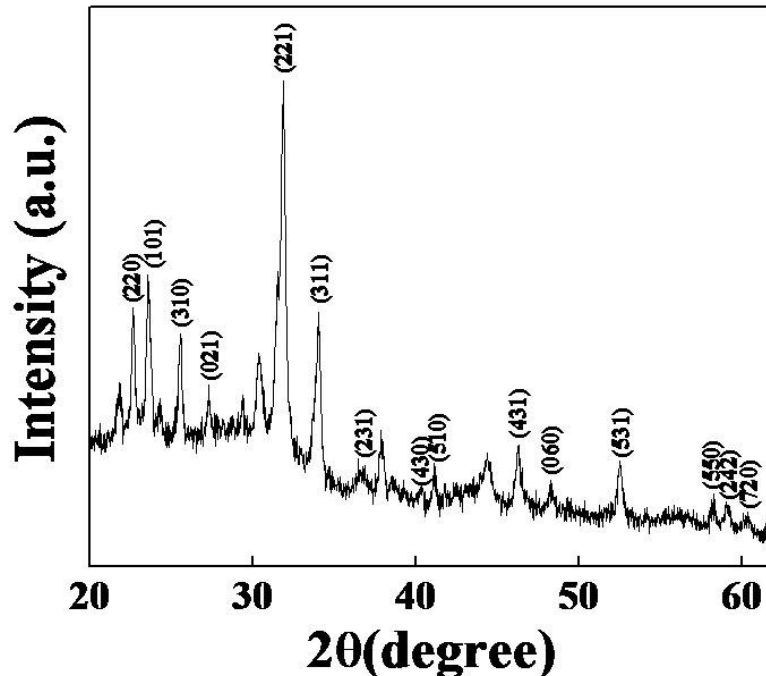


Figure 3.4: Powder XRD-pattern of drop-cast films of Bismuth sulphide (Bi_2S_3) nanoparticles on glass after reaction with the fungus *Fusarium oxysporum*. The Bragg reflections arising from the film are indexed with the respective crystal planes.

To verify the crystallinity of Bi_2S_3 nanoparticles using X-ray diffraction analysis technique, we analyzed the X-ray diffraction patterns recorded from drop cast films of as-synthesized Bi_2S_3 nanoparticles on glass substrate showing intense peaks corresponding to plane {220}, {101}, {310}, {021}, {221}, {311}, {231}, {430}, {510}, {431}, {060}, {531}, {550}, {242} and {720}. The peak position and 2θ values agree with those reported for Bi_2S_3 nanoparticles (figure 3.4). Almost all peaks in the pattern could be indexed to orthorhombic Bi_2S_3 with cell parameters of $a=11.14$, $b=11.30$, $c=3.981$ and $\alpha=\beta=\gamma=90^\circ$ and space group Pbnm(62) which are close to the reported literature [40]. The broadening of these diffraction peaks indicates that the nanoparticles are having a small size.

3.3.5 TGA analysis

In Figure 3.5, we have shown the thermogravimetric analysis (TGA) of as-synthesized Bi_2S_3 nanoparticles. As pointed out earlier, the as-synthesized nanoparticles are capped with biomolecules that stabilize them against aggregation. The presence of this coating, even after intense centrifugation is proven by the

observation of almost 53% weight-loss during heating of particles up to 650°C , which is attributed to the loss of moisture and biomolecules bound on the nanoparticle surfaces. A further increase in the temperature shows loss of weight that can be accounted for the melting of Bi_2S_3 nanoparticles [41, 42].

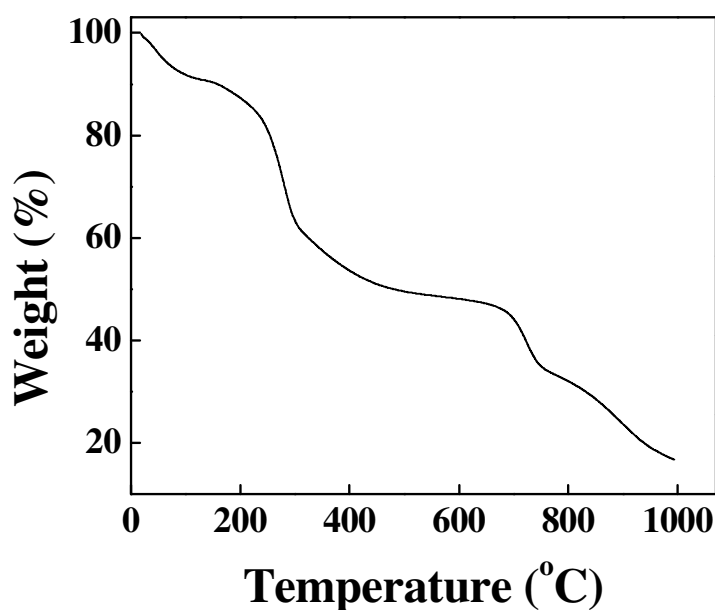


Figure 3.5: TGA of as-synthesized sample of Bi_2S_3 nanoparticles showing the % weight loss with respect to a steady increase in temperature.

3.3.6 FTIR analysis

In Figure 3.6, we have compared Fourier transform infrared (FTIR) spectra for the precursors $[\text{Bi}(\text{NO}_3)_3 \cdot 5\text{H}_2\text{O}]$, Na_2SO_3 , and uncalcined (as-synthesized) and calcined Bi_2S_3 nanoparticles taken in KBr pellets. In figure 3.6 (curve 3), two absorption bands around 1655 and 1540 cm^{-1} are present in uncalcined Bi_2S_3 sample and are due to the amide I and II bands which arise due to the carbonyl stretch and $-\text{N}-\text{H}$ stretch vibrations respectively in the amide linkages of the proteins [43]. Calcination of Bi_2S_3 particles at 400°C for three hours results in the denaturation of proteins as is evident from the disappearance of bands around 1650 and 1540 cm^{-1} for the calcined Bi_2S_3 sample (curve 4). This shows the removal of protein from the surface of Bi_2S_3 nanoparticles after calcination.

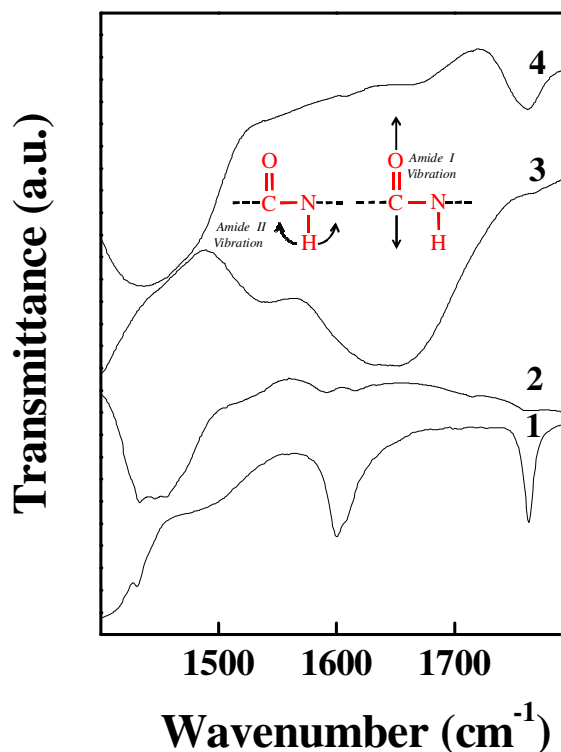


Figure 3.6: FTIR spectra recorded from powder of $\text{Bi}(\text{NO}_3)_3 \cdot 5\text{H}_2\text{O}$ (curve 1), Na_2SO_3 (curve 2), Bi_2S_3 nanoparticles synthesized using *Fusarium oxysporum* showing protein amide band region before (curve 3) and after calcination at 400°C for 3 hours (curve 4).

3.3.7 X-ray Photoelectron spectroscopy (XPS)

XPS is also used to determine the composition and purity of the Bi_2S_3 nanoparticles. The sample was prepared on silicon wafer. The results showed the presence of C, N, O, Bi and S as prominent elements. The core level spectra were background-corrected using the Shirley algorithm and the chemically distinct species were resolved using a nonlinear least squares curve fitting procedure. The binding energy of the $\text{C}1s$ transition is used as a reference to standardize the binding energy of other elements. Detailed spectra of the $\text{Bi}4f$ and $\text{S}2s$ core levels are shown in the figure 3.7A and 3.7B respectively; we have presented the background corrected XPS results of the as-

synthesized Bi_2S_3 nanoparticles. Figure 3.7A shows Bi4f spectrum which could be resolved into two peaks ($4f_{5/2}$ and $4f_{7/2}$) due to the spin-orbit coupling with binding energies 158.2 and 164.5 eV respectively and the peak at 225 attributed to the S 2s transition [44 - 46].

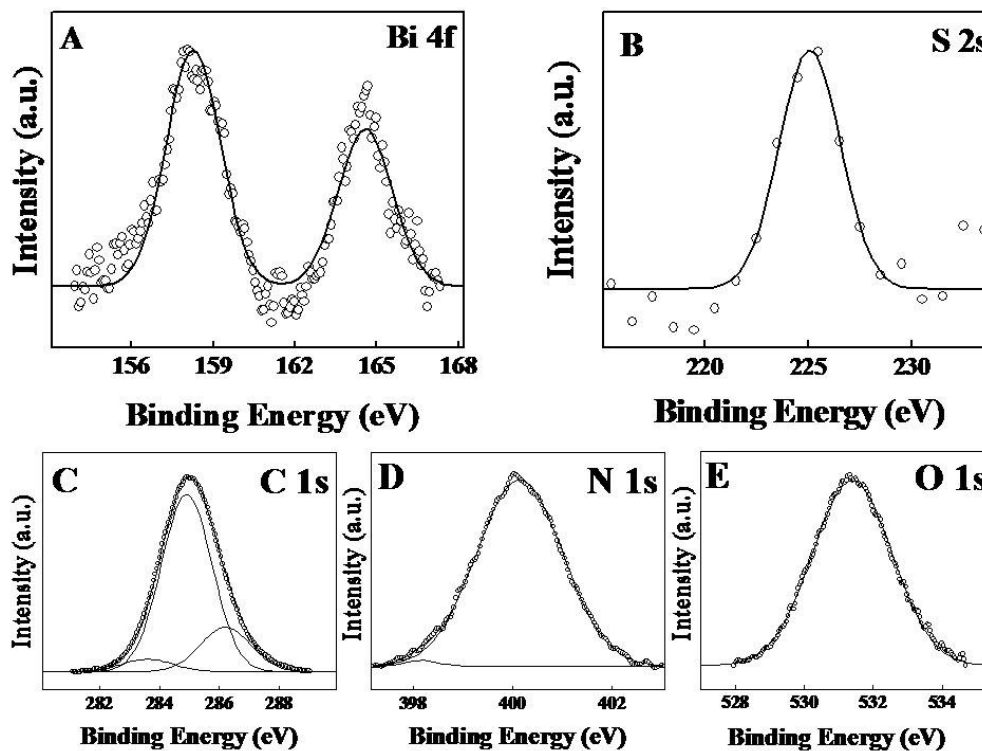


Figure 3.7: XPS spectra of biosynthesized Bi_2S_3 nanoparticles synthesized by reaction between *Fusarium oxysporum*, $\text{Bi}(\text{NO}_3)_3 \cdot 5\text{H}_2\text{O}$ and Na_2SO_3 for 96 hours. The core level spectra recorded Bi 4f (A) and S2s (B). The raw data is shown in the form of symbols, while the chemically resolved components are shown as solid lines and are discussed in the text.

To further proof that the Bi_2S_3 nanoparticles are capped with protein; C1s, N1s, and O1s XPS analysis was done from as-synthesized nanoparticle sample. Figure 2.7C shows the C 1s core level spectrum that could be decomposed into three chemically distinct components centered at 283.58 eV, 284.90 eV and 286.12 eV respectively. The deconvoluted low binding energy peak at 283.58 eV is attributed to the presence of aromatic carbon present in amino acids from proteins bound to the surface of Bi_2S_3 nanoparticles [47]. The C 1s component centered at 284.90 eV is due to electron emission from adventitious carbon present in the sample. The high binding energy peak at 286.12 eV is attributed to electron emission from carbons in carbonyl groups

(aldehydic or ketonic carbon) present in proteins bound to the nanoparticles surface [48]. The peak in figure 2.7D shows the N 1s core level spectra that could be fitted into two chemically distinct components centering at 398.17 eV and 400.15 eV. The lower binding energy component could be assigned free N₂ while higher binding energy component can be attributed nicely with values reported for –NH amide linkage in the capping proteins [49-50]. Furthermore, figure 3.7E corresponds to the chemically distinct O 1s core level with binding energy of about 531.36 eV. This may be attributed to the mixed contributions from surface hydroxide (OH groups) and C=O group present in capping proteins present on the surface of as-synthesized Bi₂S₃ nanoparticles [51].

3.3.8 Energy Dispersive Analysis of X-rays (EDAX) analysis

The elemental analysis of nanoparticles can be very informative for the study of the structural or elemental composition. Figure 3.8 corresponds to the EDAX analysis performed on a Bi₂S₃

nanoparticle which shows the presence of strong signals from bismuth and sulphur atoms together with weaker signals from C, O, N, and S atoms that arise from proteins bound to the Bi₂S₃ nanoparticles [52].

The peak corresponding to silicon arises from the substrate on which the sample is prepared for the EDAX analysis.

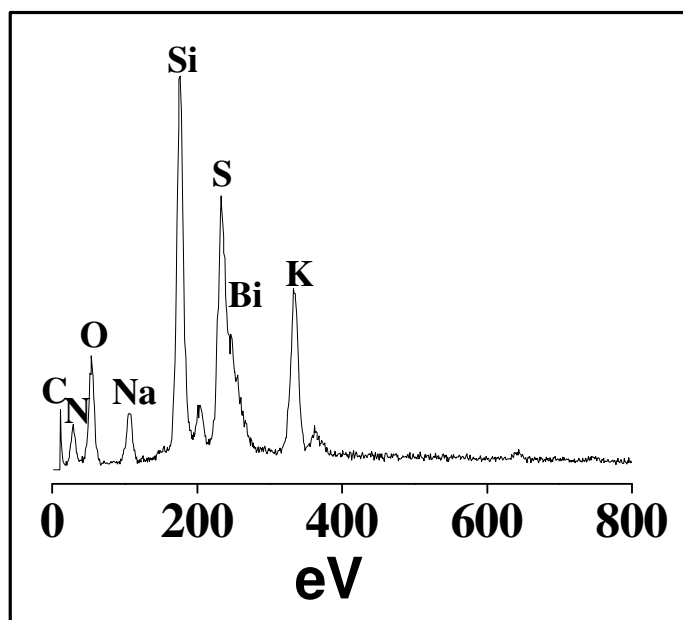


Figure 3.8: EDAX spectrum recorded from the Bi₂S₃ nanoparticles formed in the filtrate after 96 hours of reaction.

3.3.9 CT Contrast analysis

The use of nanomaterials for one of the most common imaging technique is gaining popularity. Confirmation of Bi_2S_3 nanoparticles to act as CT contrast agents was done by performing phantom studies at various concentrations in saline, at CT tube current of 2.5mA and tube voltage of 140 KVp.

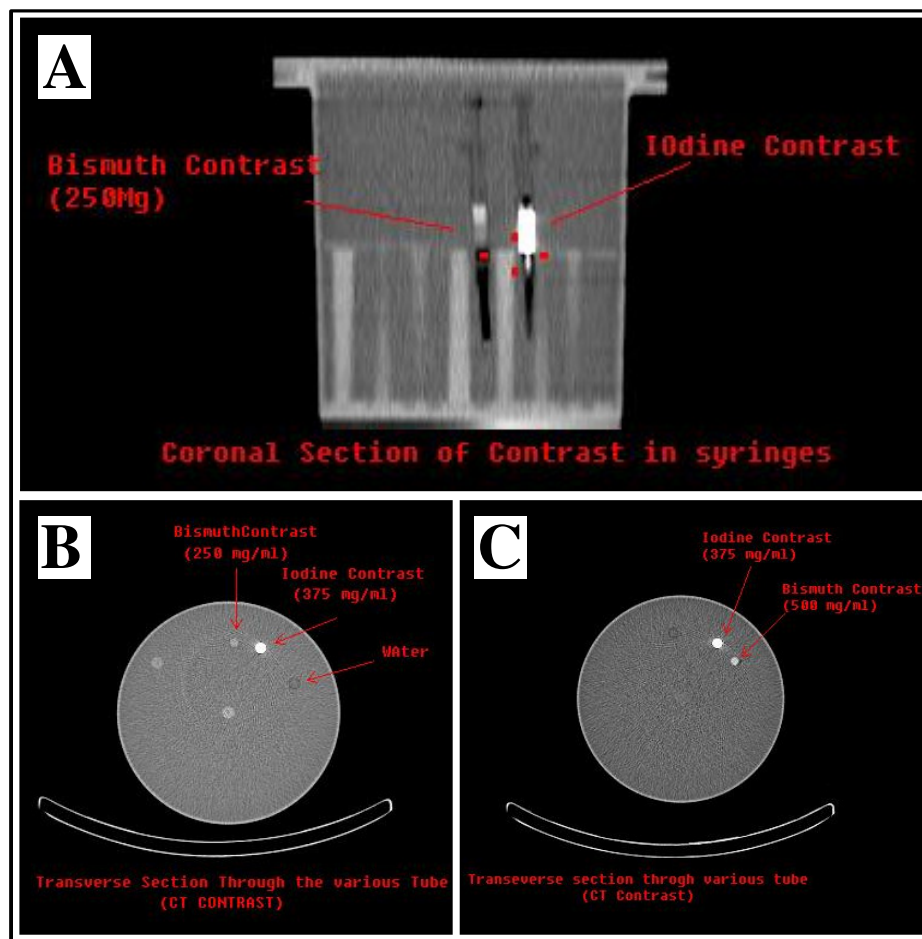


Figure 3.9: CT Contrast photograph for Bi_2S_3 nanoparticle (A) Coronal section and (B, C) transverse section for different concentrations.

To find out the molar concentration of Bi_2S_3 to determine the CT Contrast level, different tubes at various molar concentrations of Bi_2S_3 nanoparticles with saline and commercial iodine contrast as standards were exposed to X-rays and current voltage settings available on dedicated animal SPECT-CT scanner (50 KVp, 0.5m A) was used. Contrast from figure 3.9A shows coronal section of contrast in syringes; left side syringe having 250 mg Bi_2S_3 nanoparticles and right side syringe having iodine

contrast agent. In transverse section (figure 3.9B, C) through various tubes, figure 3.9B showing Bi_2S_3 nanoparticles (250 mg/ml), iodine contrast agent (375mg/ml) and distilled water in various tube. Bi_2S_3 nanoparticles showing good contrast. When we increase the Bi_2S_3 nanoparticles concentration (500 mg/ml) showing very good contrast comparable to iodine (figure 3.9C), water contrast image also showing in one used as blank. From above study we can say that Bi_2S_3 nanoparticles are very good CT contrast agents and have better stability than iodated compounds which unlike Bi_2S_3 have no specific distribution and show rapid pharmacokinetics.

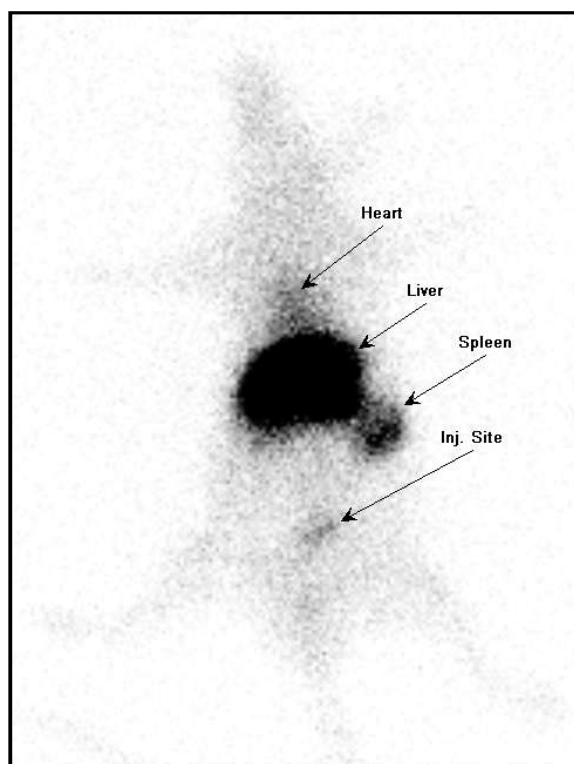
3.3.10 Radiolabelling and Biodistribution studies

3.3.10.1 Complex formation study:

On the basis of chromatographic analysis, the radiolabeling efficiency was found to be more than 90% consistently.

3.3.10.2 Biodistribution & Gamma Scintigraphic imaging of $^{99\text{m}}\text{Tc-Bi}_2\text{S}_3$ nanoparticles in normal rat:

Localization and biodistribution study of $^{99\text{m}}\text{Tc-Bi}_2\text{S}_3$ nanoparticles in normal healthy rats over time was determined by gamma camera imaging, is shown in figure 3.10. The study clearly indicates the biodistribution of the complex ($^{99\text{m}}\text{Tc-Bi}_2\text{S}_3$ nanoparticle), these Bi_2S_3 nanoparticles were taken up in the liver, heart, kidneys and cleared through urine within 45 minutes.



Biodistribution of $^{99\text{m}}\text{Tc-Bi}_2\text{S}_3$ nanoparticles in rat.

Further to prove the biodistribution of Bi_2S_3 nanoparticles in rat, in figure 3.11 the first column from top to bottom depicts 3D data of Planar micro CT (without any contrast), Bi_2S_3 nanoparticle micro CT, Bi_2S_3 99mTc-SPECT and co-registered Bi_2S_3 nanoparticle SPECT-CT respectively.

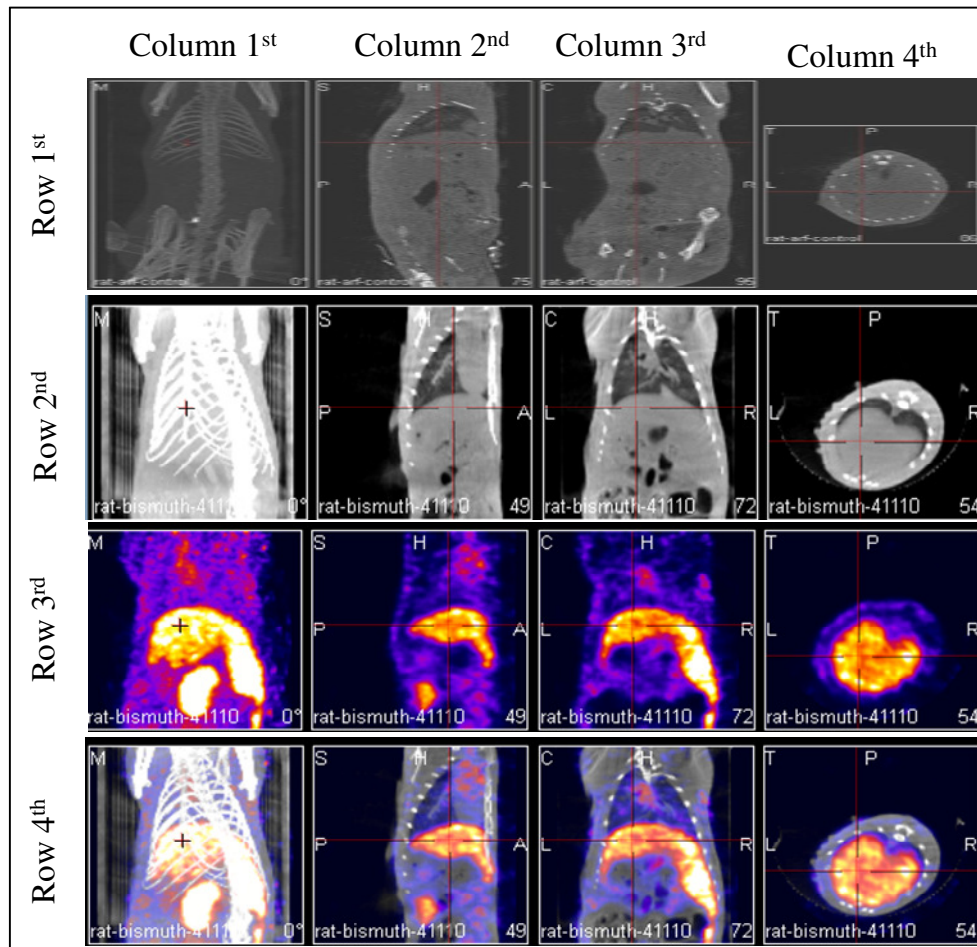


Figure 3.11: Serial in vivo image of biodistribution of Bi_2S_3 nanoparticles in rat: (Row 1st) Control μ -CT, (Row 2nd) μ -CT Bi_2S_3 , (Row 3rd) μ -SPECT Bi_2S_3 and (Row 4th) μ -SPECT-CT- Bi_2S_3 nanoparticles.

The 2nd, 3rd and 4th column depict saggital, coronal and transverse image section of Plane CT, Bi_2S_3 nanoparticles CT, Bi_2S_3 nanoparticle 99mTc-SPECT and co-registered Bi_2S_3 nanoparticle SPECT-CT. The images in 2nd row show enhanced CT contrast in liver with Bismuth nanoparticles as compared to non-injected planar CT in 1st row due to innate characteristics of Bismuth sulphide. 3rd row shows contours of liver in various sections based on distribution of same 99mTc- Bi_2S_3 nanoparticles which are forming contrast in 2nd row CT image. 4th row shows coregistered SPECT-CT image with colors depicting 99mTc-signal from radio-labelled nanoparticles and

shades of grey showing CT contrast distribution in liver due to innate character of Bi_2S_3 nanoparticles to stop X-rays and thus produce CT contrast. Thus Bi_2S_3 nanoparticles radiolabelled with $^{99\text{m}}\text{Tc}$ act as dual probe due to $^{99\text{m}}\text{Tc}$ able to show location of attached nanoparticle and nanoparticle innately acting as CT contrast.

3.4 Conclusion

In conclusion, the present studies shows that the fungus *Fusarium oxysporum* can be used for the biosynthesis of Bi_2S_3 nanoparticles. We have synthesized orthorhombic Bi_2S_3 nanoparticles capped by proteins. XRD and SAED patterns indicated that the product was pure orthorhombic with as-synthesized nanoparticles showing excellent crystallinity. TEM images showed that the particles are quasi spherical in shape with an average particle size of 15 nm. Using fungus for the room temperature synthesis of these nanoparticles is an exciting route and leads to an eco-friendly and economically viable method for the synthesis of sulphide nanomaterials of technological interest. The results prove that the fungus mediated biosynthesis method is a simple, eco-friendly and efficient method which can be used to synthesize highly crystalline semiconductor particles. These Bi_2S_3 nanoparticles were also used in SPECT-CT probe for small-animal imaging. These were injected into rats and biodistribution image and clearance time from the blood was calculated.

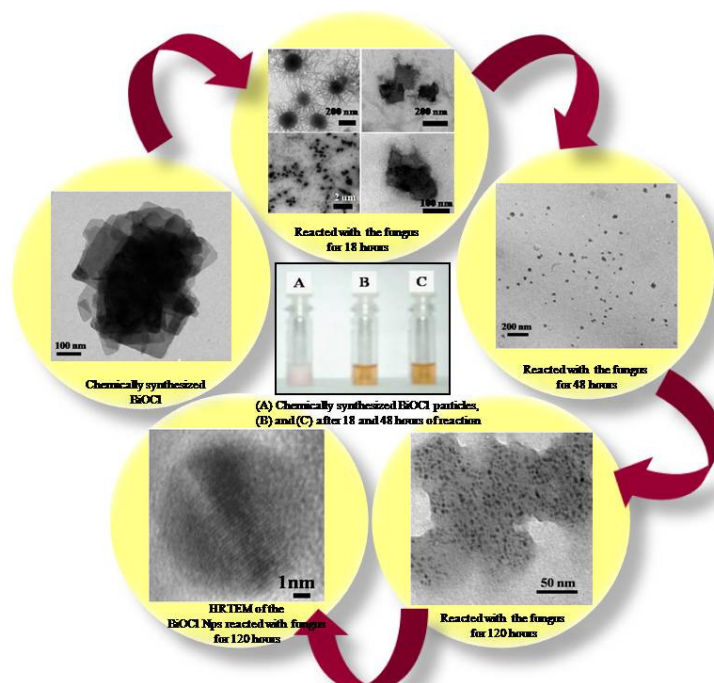
References

- [1] Alivisatos, A. P., *Science.*, **1996**, 271, 5251, 933.
- [2] Efros, A. L., Rosen, M., *Annu. Rev. Mater. Sci.*, **2000**, 30, 475.
- [3] Nozik, A. J., Memming, R., *J. Phys. Chem.*, **1996**, 100, 13061.
- [4] Michalet, X., Pinaud, F. F., Bentolila, L. A., Tsay, J. M., Doose, S., Li, J. J., Sundaresan, G., Wu, A. M., Gambhir, S. S., Weiss. S., *Science.*, **2005.**, 307, 538.
- [5] Kitova, S., Eneva, J., Panov, A., Haefke, H., *J. Imaging Sci. Technol.*, **1994**, 38, 484.
- [6] Chon, J. W. M., Zijlstra, P., Gu, M., van Embden, J., Mulvaney, P., *Appl. Phys. Lett.*, **2004**, 85, 5514.
- [7] Rao, C. N. R., Deepak, F. L., Gundiah, G., Govindaraj, A., *Prog. Solid State Chem.*, **2003**, 31, 5.
- [8] Hu, Y. J., Chen, F., Chen, W. M., Li, X. L., *Adv. Funct. Mater.*, **2004**, 14, 383.
- [9] El-Sayed, M. A., *Acc. Chem. Res.*, **2004**, 37, 326.
- [10] Kumar, S., Thomas, N., *Small.*, **2006**, 2, 316.
- [11] Steigerwald, M. L., Alivisatos, A. P., Gibson, J. M., Harris, T. D., Kortan, R., Muller, A.J., Thayer, A. M., Duncan, T. M., Douglass, D. C., Brus, L. E., *J. Am. Chem. Soc.*, **1988**, 110, 3046.
- [12] Lee, S. M., Jun, Y. W., Cho, S. N., Cheon, J., *J. Am. Chem. Soc.*, **2002**, 124, 11244.
- [13] Jun, Y. W., Jung, Y. Y., Cheon, J. *J. Am. Chem. Soc.*, **2002**, 124, 615.
- [14] Pradhan, N., Efrima, S., *J. Am. Chem. Soc.*, **2003**, 125, 2050.
- [15] Grigas, J., Talik, E., Lazauskas, V., *Phys. Status Solidi B.*, **2002**, 232, 220.
- [16] Miller, B., Heller, A., *Nature.*, **1976**, 262, 680.
- [17] Rabin, O., Perez, J. M., Grimm, J., Wojtkiewicz, G., Weissleder, R., *Nat. Mater.* **2006**, 5, 118, 122.
- [18] Zhang, B., Ye, X. C., Hou, W. Y., Zhao, Y., Xie, Y., *J. Phys. Chem B.*, **2006**, 110, 8978.
- [19] Li, L. S., Sun, N. J., Huang, Y. Y., Qin, Y., Zhao, N. N., Gao, J. N., Li, M. X., Zhou, H. H., Qi, L. M., *Adv. Funct. Mater.*, **2008**, 18, 1194.

-
- [20] Wang, H., Zhu, J.J., Zhu, J.M., Chen, H.Y., *J. Phys. Chem B.*, **2002**, 106, 3848.
- [21] He, R., Qian, X., Yin, J., Z.K. Zhu, *J. Cryst. Growth.*, **2003**, 252, 505.
- [22] Zhao, W. B., Zhu, J.J., Xu, J.Z., Chen, H.Y., *Inorg. Chem. Commun.*, **2004**, 7, 847.
- [23] Shen, X. P., Yin, G., Zhang, W. L., Xu, Z., *Solid State Comm.*, **2006**, 140, 116.
- [24] Chai, D. L., Yuan, X. S., Yang, B. J., Qian, Y. T., *Solid. State. Commun.*, **2008** 148444.
- [25] Zhao, Y., Zhu, X., Huang, Y.Y., Wang, S.X., Yang, J.L., Xie, Y.J., *J. Phys., Chem. C.*, **2007**, 111, 12145.
- [26] Jiang, J., Yu, S.H., Yao, W.T., Ge, H., Zhang, G.Z., *Chem. Mater.*, **2005**, 17 6094.
- [27] Sastry, M., Ahmad, A., Khan, M. I., Kumar, R., *Curr. Sci.*, 85, 2, 162.
- [28] Uddin, I., Adhynthaya, S., Syed, A., Selvaraj, K., Ahmad, A., Poddar, P., *J. Nanosci. Nanotechnol.*, **2008**, 8,3909.
- [29] Holmes, J. D., Smith, P. R., Evans-Gowing, R., Richardson, D. J., Russell, D. A., Sodeau, J. R., *Arch. Microbiol.*, **1995**, 163, 143.
- [30] Dameron, C. T., Reese, R. N., Mehra, R. K., Kortan, A. R., Carroll, P. J., Steigerwald, M. L., Brus, L. E., Winge, D. R., *Nature.*, **1989**, 338, 596.
- [31] Kowshik, M., Vogel, W., Urban, J., Kulkarni, S. K., Paknikar, K. M., *Adv. Mater.* **2002**, 14, 815.
- [32] Ahmad. A., Mukherjee, P., Mandal, D., Senapati, S., Khan, M, I., Kumar, R., Sastry, M., *J. Am. Chem. Soc.*, **2002**, 124, 12108.
- [33] Shenton, W., Douglas, T., Young, M., Stubbs, G., Mann, S. *Adv. Mater.*, **1999**, 11, 253.
- [34] Zhang, B., Ye, X., Hou, W., Zhao, Y., Xie, Yi., *J. Phys. Chem. B.*, **2006**, 110, 8978.
- [35] Lu, Q., Gao, F., Komarneni, S., *J. Am. Chem. Soc.*, **2004**, 126, 54.
- [36] Peter, L. M., Wijayantha, K. G. U., Jason Riley, D., Waggett, J. P., *J. Phys. Chem. B.*, **2003**, 107, 8378.
- [37] Dolatyari, A. A., *Radiat. Eff. Defects. Solids*, **2008**, 163, 2, 123.
- [38] Zhao, W. B., Zhu, J. J., Zhao, Y., Chen, H. Y., *Mater. Sci. Eng B.*, **2004**, 11, 307.

-
- [39] Wang S. F., Gu, F., Yang, Z. S., Lu, M. K., Zhou, G. J., Zou, G. W., *J. Cryst. Growth.*, **2005**, 282, 79.
- [40] The XRD patterns were indexed with reference to the crystal structures from the PCPDFWIN: Bi₂S₃ (# 17-0320).
- [41] Zhang H. X., Ge, J. P., Li, Y. D., *Chem. Vap. Deposition*, **2005**, 11, 3, 147.
- [42] Glatz A. C., Meikleham, V. F., *J. Electrochem. Soc.*, **1963**, 110, 12, 1231.
- [43] Grdadolnik, J., *Bull. Chem. Technol. Macedonia*, **2002**, 21, 1, 23.
- [44] Chen, R., So, M. H., Che, C. M., Sun, H., *J. Mater. Chem.*, **2005**, 15, 4540.
- [45] Lu, J., Han, Q., Yang, X., Lu, L., Wang, X., *Mater. Lett.*, **2007**, 61 2883.
- [46] Chastain, J., (1992) Handbook of X-ray Photoelectron Spectroscopy, Perkin Elmer, Norwalk.
- [47] Kumar, A., Mandal, S., Selvakannan, P. R., Pasricha, R., Mandale, A. B., Sastry, M., *Langmuir*, **2003**, 19, 6277.
- [48] Seo, K. I., McIntyre, P. C., Kim, H., Saraswat, K. C., *Appl. Phys. Lett.*, **2005**, 86, 082904.
- [49] Nguyen, T. D., Mrabet, D., Vu, T. T. D., Dinh, C. T., Do, T., *Cryst. Eng. Comm.*, **2011**, 13, 1450.
- [50] Bureau, C., Valin, F., Lecayon, G., Charlier, J., Detalle, V., *J. Vac. Sci. Technol. A.*, **1997**, 2, 353.
- [51] Margalit, R., Vasquez, R. P., *J. Protein. Chem.*, **1990**, 9, 1, 105.
- [52] Shen, X. P., Yin, G., Zhang, W., Xu, Z., *Solid State. Commun.*, **2005**, 134, 239.

Chapter 4



Top-down bio-milling technique for the size reduction of chemically synthesized BiOCl nanoplates.

*This chapter describes the bio-milling of chemically synthesized BiOCl nanoplates using the alkalo-thermotolerant fungus *Humicola* sp. In top-down approach, we show that the fungal biomass can be used to break-down the chemically synthesized larger particles (200-250 nm) into particles as small as 5-6 nm while maintaining their crystallinity and phase at the nanolevel. We have named this technique as “bio-milling”. We believe that this technique can be used to synthesize several nanoparticles of oxides whose synthesis in the size less than 10 nm by conventional wet-chemical methods is difficult.*

The work described in this chapter has been published by Baishakhi Mazumder, **Imran Uddin**, Shadab Khan, Venkat Ravi, Kaliaperumal Selvraj, Pankaj Poddar*, Absar Ahmad*, *J. Mater. Chem.*, 2007, 17, 3910 – 3914.

4.1 Introduction

Top-down approach involves starting with a block of material and etching or milling it down to the desired shape and size. In this method, we start with bulk material and then break it up into smaller pieces until the nanoparticles of desired size are achieved. The best known example of top-down approach is the photolithography technique used in semiconductor industry to create integrated circuits by etching patterns of silicon wafers [1]. The metal is chiseled out selectively using high energy beam to obtain desired patterns onto silicon substrate. The top-down approach can be considered as the one with which the human race first learned to fabricate materials and in due course of time, perfected this art by being able to engineer structures at sub-micron levels. The top-down approach for nanofabrication is the one first suggested by Richard Feynman in his famous American Physical Society lecture in 1959 entitled “There’s plenty of room at the bottom”. Top-down approach is one of the oldest routes for the synthesis of nanoparticles. But its popularity has reduced with time, as its efficiency to produce decontaminated, monodispersed materials and also very small particles of few nanometers are questionable due to the unavailability of suitable tools. The main challenge for top-down manufacture is the creation of increasingly small structure with sufficient accuracy that is the imperfection of surface structure. It can cause significant crystallographic damage to processed pattern and additional defects may be introduced during etching steps. For example, nanowires made by lithography are not smooth and may contain a lot of impurities and structural defects on surface. Below certain size range, synthesis of nanoparticles by the top-down approach becomes costly and laborious. This approach can also produce surface defects, internal stresses and contaminations due to harsh conditions at the time of synthesis of nanoparticles. Such imperfections would have a significant impact on the physical properties and surface chemistry of nanostructures and nanomaterials, since the surface over volume ratio in nanostructures and nanomaterials is very large. The surface imperfection would result in a reduced conductivity due to inelastic surface scattering, which in turn would lead to the generation of excessive heat and thus impose extra challenges to the device design and fabrication. Regardless of the surface imperfections and other defects, top-down method continues to play an important role in the synthesis and fabrication of nanostructures and nanomaterials [2]. For the past few years, the biological methods

such as microbial (fungi, yeast and bacteria), plant extract and biomimetic synthesis routes have been gaining popularity over the traditional wet-chemical methods due to various advantages over these methods (especially in the case of oxide nanoparticle synthesis) as the biological synthesis methods avoid the use of harsh chemicals and take place in ambient conditions without the need of further treatment. In this technique, the as-synthesized particles are extremely stable due to the inherent coating at the surface by proteins, which enables them to be suspended in the aqueous medium. In this “bottom-up synthesis” approach, the metal salts are fed to the biomass which in turn secretes enzymes to form the nanoparticles. So far, the microbial techniques have been used to synthesize a range of metal [3] and binary oxides (TiO_2 , SiO_2 , ZrO_2 , Fe_3O_4 and Bi_2O_3 etc.) [4-7]. However, further research needs to be done to fine-tune the synthesis parameters to meet the challenges related to the scale-up of synthesis, better control over the particle size and shape and the synthesis of various other complex ternary oxide phases. Moreover, the synthesis mechanism and the involvement of various biomolecules needs to be understood completely over time.

Herein, for the first time the process has been applied in a research lab. In our opinion, this process carries huge technical importance as it provides a very simple route to form small particles over traditional top-down methods (such as lithography, pulsed laser deposition, etc.), which are quite expensive. We have developed a novel “top-down” biosynthesis approach, while learning from nature, where the degradation of rocks [8] (such as granite, sandstone, bricks, etc.) in the form of fine particles is carried out over a long period of time by microorganisms such as bacteria, fungi, yeast and algae [9]. In some cases, these microorganisms are found to actually bore paths into various materials [10, 11]. However, in nature, due to the lack of nutrients, this process is quite slow and uncontrolled. After learning from this “top-down” approach used by nature, we have accelerated this process in the laboratory environment by selectively using certain fungal species in the presence of nutrient media. We, for the first time have named this process as “bio-milling”, which is equivalent to the “ball-milling” process commonly used by material scientists and engineers to break down large particles into smaller sizes. Synthesizing the nanocrystals of less than 10 nm size is a very challenging task for chemical methods, while it can be easily achieved by applying the biological methods like bio-milling, where the nanoparticles synthesized are in the range of less than 10 nm.

Hence Bio-milling is a “Green Top-Down Approach” used to synthesize complex oxide nanoparticles with particle sizes less than 10 nm with the proper crystalline phase by synergistically utilizing both chemical and biological synthesis techniques [12]. So, here we follow the novel green route of “Bio-milling”. Biomilling is considered very much similar to bioleaching [13], where extraction of specific metals from their ores through the use of microorganisms takes place but the exact mechanism of bio-milling is not known as yet. We need bio-milling technique to get small sized, complex oxides nanoparticles which are very difficult to synthesize by bottom-up approach but can be easily synthesized by the top-down approach method (Bio-milling). In case of nanoparticles synthesized by biomilling, the crystal structure remains the same while only the number of unit cells present in a particle decrease which is important through an industrial point of view. Bio-milling is less costly than physical and chemical methods. There is no need of extreme conditions of temperature and pH in case of bio-milling. There are no pollution problems in case of bio-milling as no toxic chemical is released during this process. In this effort, we have chosen BiOCl as a model system.

Bismuth oxychloride is an important class of ternary compound which belongs to the family of main group multicomponent metal oxyhalides (V–VI–VII) having tetragonal crystal system [14-15]. The structure of BiOCl is known to have a layered structure, in which [Cl-Bi-O-Bi-Cl] sheets are stacked together through the Cl atoms along the *c*-axis by the non-bonding interactions. In each [Cl-Bi-O-Bi-Cl] layer, a bismuth center is surrounded by four oxygen and four chlorine atoms in an asymmetric decahedral geometry [16]. The weak inter-layer van der Waals interactions and strong intra-layer bondings give rise to a highly anisotropic structure, and give unique electrical, optical, and mechanical properties [17, 18] which have made BiOCl attractive in applications such as pharmaceuticals [19], cosmetics [20] and photocatalysis [21]. Bismuth oxychloride was the first ever synthetic, non-toxic, nacreous compound. It exhibits many intriguing properties such as photoluminescence, photoconductivity, thermally stimulated conductivity and good catalytic activities [22, 23]. We report here for the first time the use of fungal biomass, at 50°C temperature, to break down chemically synthesized BiOCl nanoplates (sizes ~200-250 nm) into very small particles (<10 nm) while maintaining their crystalline structure and phase purity. We have named this novel technique as “bio-milling”. In this way, the environment friendly bio-milling, which is carried out

at ambient conditions, mitigates the shortcomings of chemical processes which are applied for the synthesis of nanoparticles.

4.2 Experimental details

For bio-milling purposes; we isolated an alkalotolerant and thermophilic fungus *Humicola* sp. (HAA-SHC-2) from self-heating compost. We maintained this fungus on MGYP (malt extract, glucose, yeast extract, and peptone) agar slants. The stock cultures were maintained by sub-culturing at monthly intervals. After growing the fungus at pH 9 and 50°C for 96 hours, the slants were preserved at 15°C. From an actively growing stock culture, sub-cultures were made on fresh slant and after 96 hours of incubation at pH 9 and 50°C, were used as the starting material for further experiments. In order to break down the chemically synthesized BiOCl nanoplates (edge lengths 200-250 nm) to small sizes, the fungus was grown in 250 ml Erlenmeyer flasks containing 50 ml of the MGYP medium at pH 9 with shaking for 96 hours. The fungal mycelia (20 gram) was separated from the culture broth by centrifugation and was resuspended in 100 ml of an aqueous suspension of the BiOCl particles in 250 ml Erlenmeyer flasks at pH 9 and kept on the shaker at 50°C (200 rpm) and maintained in the dark. The reduction in the size of the BiOCl particles in the solution was monitored by periodic sampling (over 120 hours) of aliquots of the aqueous component for further characterization.

4.3 Results and Discussions

4.3.1 Visible analysis

To monitor the effects of the fungus on the particles, we picked up the samples from the flask containing the fungal biomass after 18, 48 and 120 hours. We observed that the particles dispersed in the flask which initially formed a cloudy and unstable suspension in the aqueous medium (Fig. 4.1A) but were slowly (over a period of 18-120 hours) taken into the solution by the biomass, with no precipitate left at the bottom of the reaction flask after almost 18 hours. In Fig. 4.1B and 4.1C, we show images of the suspensions of the particles after 18 and 48 hours of reaction with the fungus where a clear suspension of particles can be observed. It should be noted that this particle suspension was quite stable over a period of several months.

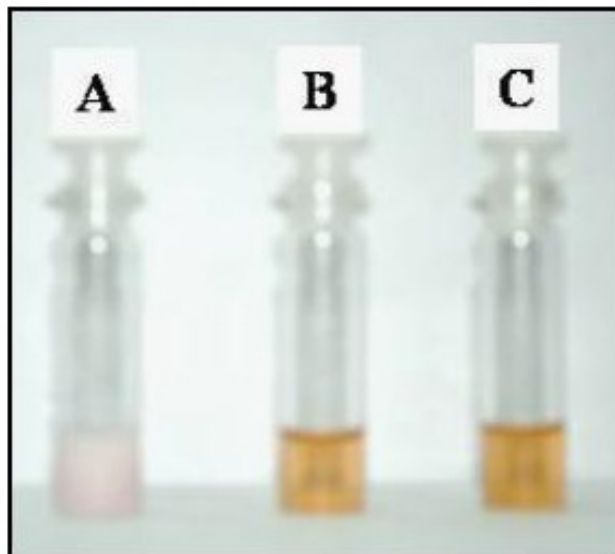


Figure 4.1: Photograph of the BiOCl particles suspended in water: (A) chemically synthesized BiOCl , (B) and (C) after 18 and 48 hours of reaction with the fungal biomass respectively.

4.3.2 TEM and SAED analysis

In Fig. 4.2 (A and B), we show transmission electron micrographs (TEM) of the chemically synthesized BiOCl nanoparticles at different length scales. For this purpose, the as-synthesized particles were suspended in amylacetate and were drop-cast on the TEM grid. We noted that the dispersion of the particles in the solvent was quite poor due to the large size of the particles as well as the absence of any capping agents. The TEM images show that these particles are quite flat and almost square in shape. The agglomeration of the particles is due to the absence of any capping agent at the surface of each particle. Fig. 4.2(C) shows the particle size distribution histogram which shows that the edge length of these particles is quite long (in the range 200-250 nm), while in Fig. 4.2(D), we show the selected area electron diffraction (SAED) pattern which exhibits a diffused ring pattern which confirms the crystallinity of chemically synthesized BiOCl nanoplates. As mentioned above, these chemically synthesized particles were now fed to the alkalotolerant and thermophilic fungus, *Humicola* sp.

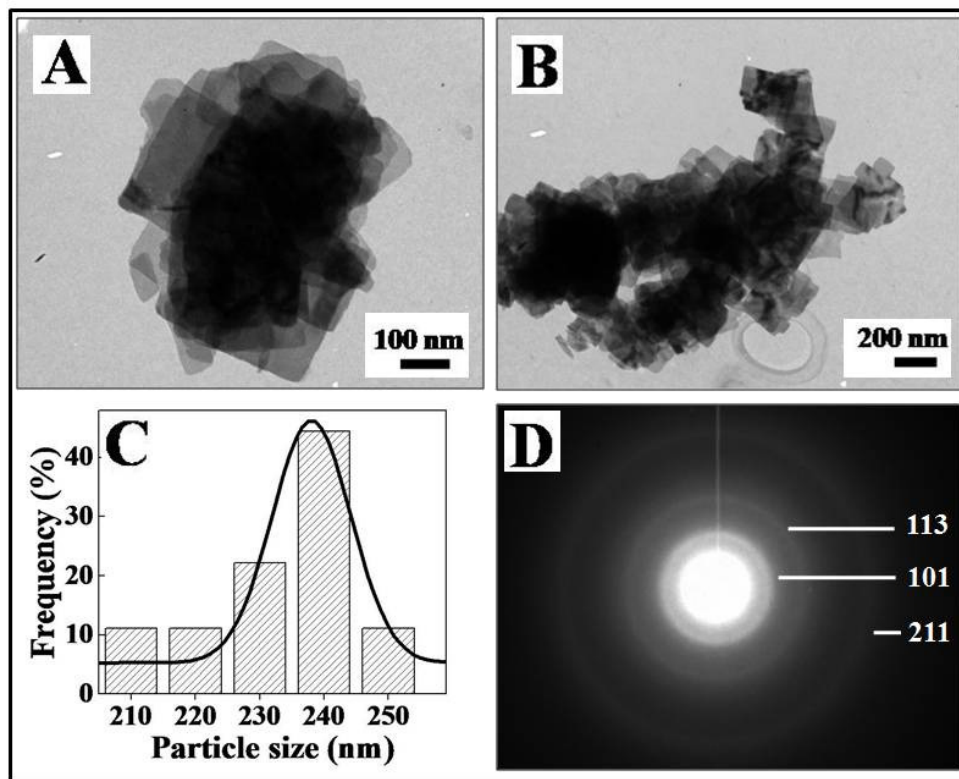


Figure 4.2: Transmission Electron Micrograph (TEM) of chemically synthesized BiOCl (A and B), Particle size distribution histogram. The solid line is a Gaussian fit to the histogram (C) and Selected area electron diffraction (D).

To further investigate the effect of the fungus on the surface morphology of these particles, we also imaged the particles taken from the reaction flask after 18, 48 and 120 hours. In Fig. 4.3(A-E), we present various TEM micrographs of the supernatant solution after 18 hours. As can be seen from these images, the nanoplates start fragmenting and form spherical particles of smaller sizes due to the reaction with the biomass. The tendril like structures as seen in some of these images (especially 4.3A and 4.3C) are possibly formed by the fungal mycelia.

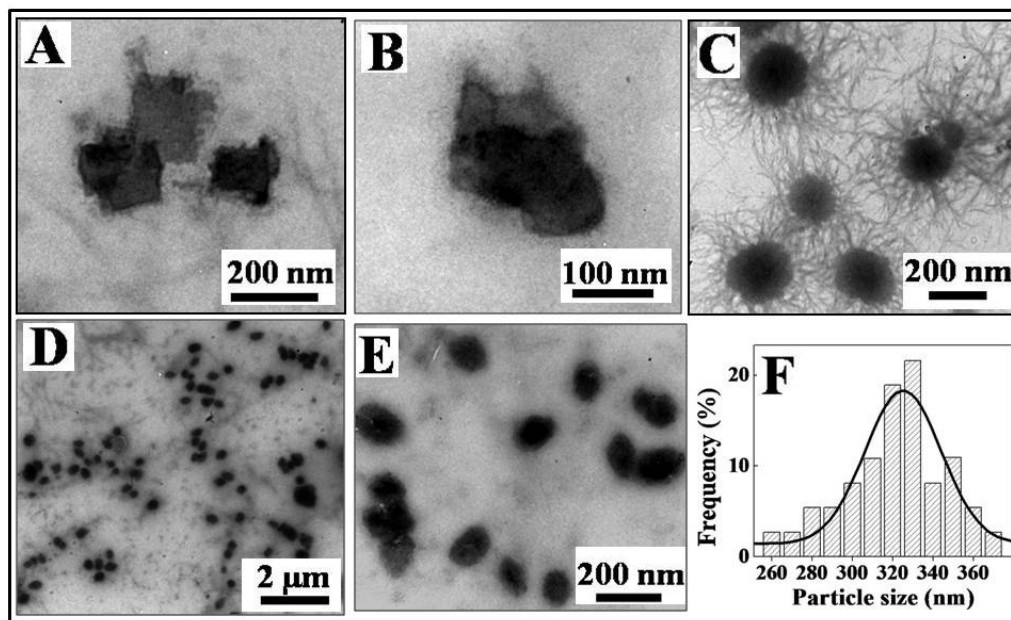


Figure 4.3: (A–E) Transmission electron micrographs (TEM) of the chemically synthesized BiOCl particles reacted with the *Humicola* sp. biomass at different magnification for 18 hours. (F) Particle size distribution histogram determined from TEM micrograph.

In Fig. 4.4 (A, B), we show TEM images of the particles taken from the flask after 48 hours of the reaction. The particle size histogram presented in Fig. 4.4 (C) shows that the particle size decreases significantly from hundreds of nanometers to around 50 nm.

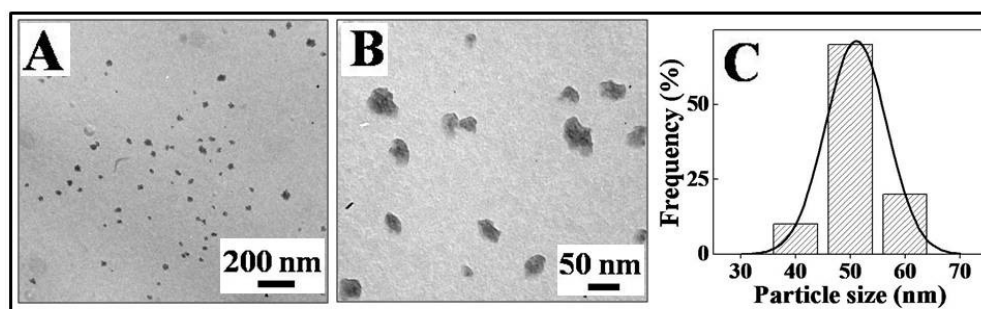


Figure 4.4: (A, B) Transmission electron micrographs (TEM) of the chemically synthesized BiOCl particles reacted with the *Humicola* sp. biomass at different magnification for 48 hours. (C) Particle size distribution histogram determined from TEM micrograph.

Further, in Fig. 4.5 (A-E), we show the TEM images of the particles after nearly 120 hours of reaction. It should be noted that the particles, which were initially much

larger in size, have broken down to particles with sizes between 4-8 nm with a quasi-spherical geometry as shown in the histograms [Fig. 4.5(F)], with the average particle size at around 6 nm, which is quite remarkable.

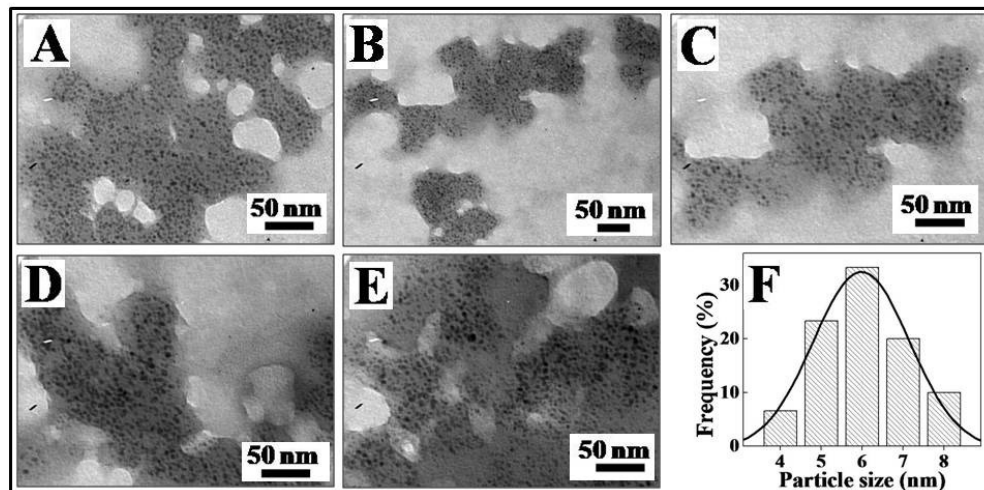


Figure 4.5: (A, E) Transmission electron micrographs (TEM) of the chemically synthesized BiOCl particles reacted with the *Humicola* sp. biomass for 120 hours. (F) Particle size distribution histogram determined from TEM micrograph.

As we mentioned earlier, in nature, various kinds of microorganisms including fungus are known to degrade rocks to form smaller particles over a very long period of time. However, to the best of our knowledge, this is the first time that this process has been applied in a research lab. In our opinion, this process carries huge technical advantages over traditional top-down methods (such as lithography, pulsed laser deposition, etc.) which are quite expensive. Moreover, the bio-milling process provides a very simple and economical route to form smaller particles while maintaining proper crystallinity. We believe that the scaling-up of this synthesis process could be easily demonstrated by optimizing the parameters such as the type of microorganism, medium, pH and temperature as well as by using large fermenters for the reaction.

4.3.3 HR-TEM analysis

In Fig 4.6 (A, B), we show the HR-TEM images of the BiOCl nanoparticles after nearly 120 hours of reaction where the lattice planes exhibit spacings of $\sim 1.57 \text{ \AA}$ and $\sim 1.83 \text{ \AA}$ corresponding to the lattice planes $\{212\}$ and $\{113\}$ respectively [24].

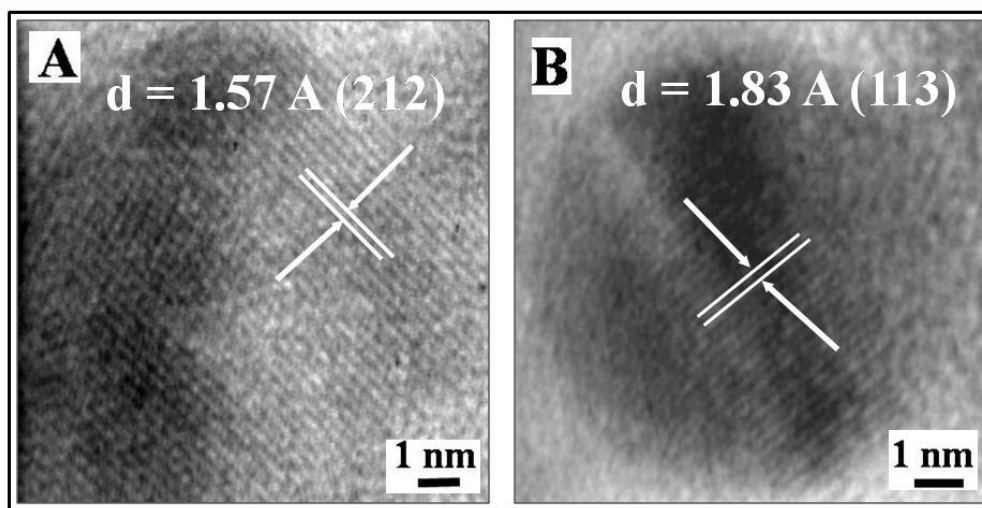


Figure 4.6: HR-TEM micrographs of the BiOCl nanoparticles reacted with the fungus *Humicola* sp. for 120 hours.

4.3.4 X-ray diffraction analysis

To further check the effect of the exposure of the fungus on the crystallinity of the chemically synthesized BiOCl particles at various time scales, we performed powder XRD on the samples after 18, 48 and 120 hours of reaction time. The results are shown in Fig. 4.7. The XRD profile of the chemically synthesized BiOCl nanoplates matches very well with that reported in the literature [24, 25]. It is known that BiOCl has a tetragonal structure with reported unit cell parameters $a=b=3.89$, $c=7.37$, $\alpha=\beta=\gamma=90^\circ$ with space group $P4/nmm(129)$. The XRD pattern in Fig. (4.7B) corresponding to the sample treated for 18 hours shows an elevated background due to the presence of the fungal biomass. This is the same for the case of the pattern corresponding to the sample treated for 48 hours (Fig 4.7C). However, the changes in the relative intensities of the $\{002\}$ and $\{101\}$ reflections are due to the possible isotropic size reduction of the crystallites during the course of fungal treatment. However, the XRD pattern of the final sample after 120 hours (fig 4.7D) of treatment matches that of the chemically synthesized initial powder in terms of the 2θ positions as well the peak intensities. Further, the low background and sharper peaks suggest that the particles retain their crystallinity even after the bio-milling process. As indicated earlier, the change in the preferred orientation with digestion time (seen as the change in the relative peak intensities) is not surprising in the present work because the chemically synthesized particles show a plate-like structure and after

reacting the particles with the fungus, the particle morphology changes from flat to sphere-like structures thereby exposing various other crystalline planes for the incident X-rays which results in the change in the line intensities.

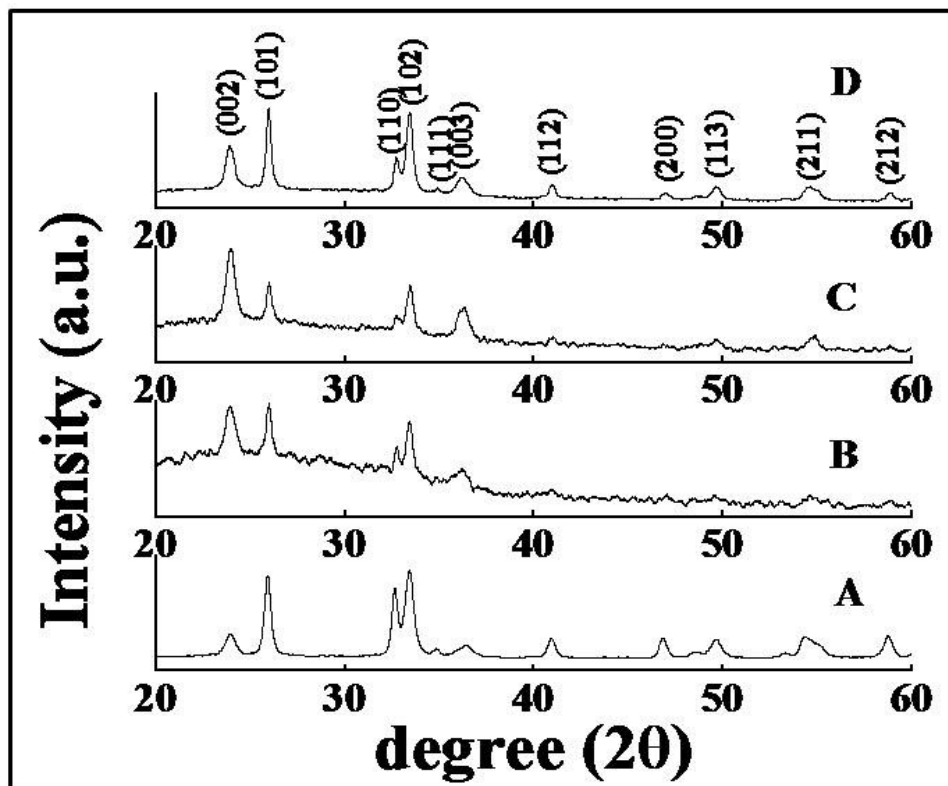


Figure 4.7: Powder X-ray diffraction patterns of BiOCl: (A) as-synthesized by chemical methods and reacted with the fungus for (B) 18, (C) 48 and (D) 120 hours.

Additionally, it has been seen that the difference in the sample preparation for powder X-ray diffraction can significantly contribute towards the overall texture of the sample. It should be noted here that we did not attempt to calculate the particle size from Scherrer's formula as in this case the calculation of the crystallite sizes from the line broadening of the XRD peaks will be prone to errors as during the "bio-milling process" it is not certain that there is 100% fragmentation of the chemically synthesized particles. There might be a few particles remaining in the samples picked up for XRD which are still not fully fragmented, leading to particular line widths. Additionally, due to the smoothing process of the raw XRD data to get rid of the protein background, using the peak heights for further analysis might not be error-free.

4.3.5 FTIR and PAGE analysis

In Fig 4.8, the FTIR spectra in different regions for the chemically synthesized particles (lower panel) and the biomilled particles after 120 hours (upper panel) are shown. In Fig 4.8, curve A and B show the presence of the absorption band around 538 cm^{-1} due to the stretching of the Bi–O corresponding to valent symmetrical A_{2u} -type vibrations of the Bi–O bond in BiOCl nanoplates [15, 26]. In Fig 4.8 (C) two absorption bands centered around 1658 and 1535 cm^{-1} are attributed to the amide I and II bands respectively which arise due to the carbonyl stretch and – N–H stretch vibrations respectively in the amide linkages of the proteins. The amide bands that arise from the vibration of the peptide groups provide information on the secondary structure of polypeptides and proteins. The amide I band arises principally from the C=O stretching vibration of the peptide group. The amide II band is primarily N–H bending with a contribution from C–N stretching vibrations [27, 28], whereas figure 4.8 (D) shows the absence of amide bands in the chemically synthesized BiOCl nanoplates.

To identify the number of proteins secreted by the fungus and their molecular weights, the fungus biomass [20 gram of wet mycelia] was resuspended in 100 ml of sterile distilled water for a period of 72 hours. The mycelia were then removed by centrifugation and the aqueous supernatant thus obtained was concentrated by ultra-filtration using a YM3 (molecular weight cut-off 3000) membrane and then dialyzed thoroughly against distilled water using a 3000 cut-off dialysis bag. This concentrated aqueous extract containing protein was analyzed by PAGE (polyacrylamide gel electrophoresis) carried out at pH 8.8 [29]. In Fig. 4.8 (E), the preliminary gel electrophoresis measurement indicates that the fungus secretes four distinct proteins ranging in weight from 97 to 20 kDa. One or more of these proteins might be the enzymes that reduce the size of BiOCl and capped BiOCl nanoparticles formed by the reduction process. It is possible that more than one protein might take part in the capping and stabilization of the BiOCl nanoparticles. The exact mechanism leading to the reduction of nanosized BiOCl is yet to be elucidated for this fungus. We are currently separating and concentrating the different proteins released by the fungus *Humicola* sp. to test and identify the ones active in the above processes.

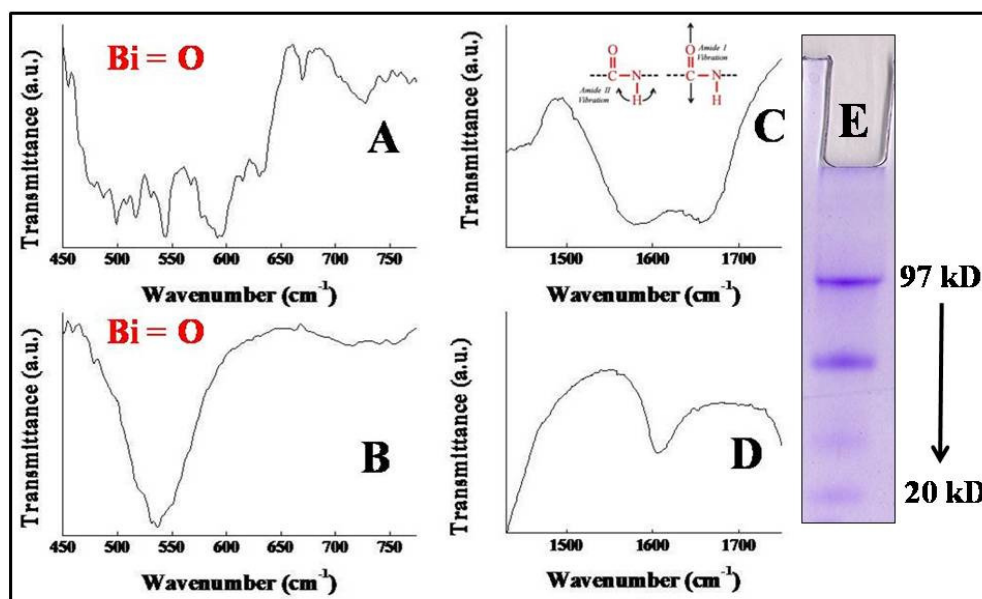


Figure 4.8: FTIR spectra of BiOCl: (A) reacted with the fungus, (B) as-synthesized by the chemical method. (C) Expanded view of the FTIR spectra shown in the region of the protein amide bands for biomilled BiOCl, (D) chemically synthesized BiOCl. Fig 4.8(E) Preliminary gel electrophoresis (SDS PAGE, pH 8.8) for *Humicola* sp. (HAA-SHC-2) showing four distinct protein bands.

4.4 Conclusion and future perspectives

Living organisms have a huge potential for the production of nanoparticles/nanodevices of wide applications. By using the organisms from simple bacteria to highly complex eukaryotes in the reaction mixture, the production of nanoparticles/nanodevices with desired shape and size can be obtained. Bio-milling is less costly than physical and chemical methods. Bio-milling is carried out at room temperature and there is no need of extreme conditions of temperature and pH. Bio-milling is a “Green Top-Down Approach” used to synthesize complex oxide nanoparticles with particle sizes less than 10 nanometer with proper crystalline phase by synergically utilizing both chemical and biological synthesis techniques and proves to be eco-friendly. Although nano-biotechnology is at its infancy, there are various examples explained in this thesis through which this technology would attract the attention of researchers owing to its innumerable and novel applications. Among these, a few studies have shown that different kinds of reductases of these organisms might be involved in the mechanisms of production of nanoparticles and attribute them various shapes and sizes. However, the elucidation of exact mechanism of nanoparticles production using living organisms needs much more experimentation.

The effects of nanotechnology on human health based applications are still unknown. Nano-biotechnology could dramatically improve public health, but there is concern over possible unforeseen adverse effects. Therefore, studies and monitoring methods are needed to determine what environmental and health risks are associated with nanomaterials and nano applications. In future, we could imagine a world where medical nanodevices would be routinely implanted or even injected into the bloodstream to monitor health and to automatically participate in the repair of systems that deviate from the normal pattern. The continued advancement in the field of biomedical nanotechnology is the establishment and collaboration of research groups in complementary fields. However, nanotechnology in medicine faces enormous technical hurdles in which long delays and numerous failures are inevitable. Likewise, it should not be taken for granted the dangers and negative consequences of nanobiotechnology when applied in warfare, in the hands of terrorists and disasters associated with its application in energy generation when and wherever it strikes, or the risks associated with nanoparticles in blood circulation. It should be appreciated that nanotechnology is not in itself a single emerging scientific discipline but rather a meeting point of traditional sciences like chemistry, physics, biology and materials science to bring together the required collective knowledge and expertise required for the development of these novel technologies. Due to the present challenges in the conventional wet-chemical methods for the preparation of nanomaterials, especially in the synthesis of complex oxide materials in extremely small size (<10 nm), there is a strong need to investigate the methods which are cost effective, eco-friendly and industrially feasible from several aspects.

In this work, we report the synthesis of nanoparticles by top-down approach (bio-milling) using the biological system i.e. *Humicola* sp. We present this novel technique developed at NCL, Pune (India) by which it was possible to reduce the size of chemically synthesized micron sized BiOCl nanocrystals using *Humicola* sp. at 50°C temperature into the nanosized particles while maintaining the excellent crystallinity of the material. This “green technique” which has a potential for commercial application into a large scale synthesis of nanomaterials with a simple route is named as “bio-milling”. Bio-milling is a new concept for top-down synthesis of nanoparticles but very less is known about the exact mechanism. So, until now it is at a research level at N.C.L. In our opinion, this process carries huge technical importance as it provides a very simple route to form small particles over traditional top-down

methods (such as lithography, pulsed laser deposition, etc.), which are quite expensive. Future investigations are in progress to understand the amino acid sequence of this protein and the nature of the interaction of this protein with BiOCl nanoparticles. Since we can also sort out the gene of interest and analyze its sequence, the proteins of interest can be separated and purified from the bulk so that these proteins can be tested for bio-milling. We believe that the scaling-up of this synthesis process could be easily demonstrated by optimizing parameters such as the type of microorganism, medium, pH and temperature as well as by using large fermenters for the reaction.

References

- [1] Gates, B. D., Xu, Q., Stewart, M., Ryan, D., Willson, C. G., Whitesides, G. M., *Chem. Rev.* **2005**, 105, 4, 1171.
- [2] Cao, G., *Nanostructures and Nanomaterials: Synthesis, Properties & Applications.*, **2003**, Imperial College press.
- [3] Sastry, M., Ahmad, A., Khan, M. I., Kumar, R., *Curr. Sci.*, **2003**, 85, 2.
- [4] Bansal, V., Rautaray, D., Bharde, A., Ahire, K., Sanyal, A., Ahmad, A., Sastry, M., *J. Mater. Chem.*, **2005**, 15, 2583.
- [5] Bansal, V., Rautaray, D., Ahmad, A., Sastry, M., *J. Mater. Chem.*, **2004**, 14, 3303.
- [6] Bharde, A., Wani, A., Shouche, Y., Joy, P. A., Sastry, M., *J. Am. Chem. Soc.*, **2005**, 127, 9326.
- [7] Uddin, I., Adyanthaya, S., Syed, S., Selvaraj, K., Ahmad, A., Poddar, P., *J. Nanosci. Nanotechnol.*, **2008**, 8, 3909.
- [8] Ehrlich, H. L., *Chem. Geol.*, **1996**, 132, 5.
- [9] Hirsch, F. E., Eckhardt, W., Palmer., J.R., *J. Microbiol. Methods*, **1995**, 23, 143.
- [10] Bansal, V., Sanyal, A., Rautaray, D., Ahmad, A., Sastry, M., *Adv. Mater.*, **2005**, 17, 889.
- [11] Mulligan, C. N., Kamali, M., *J. Chem. Technol. Biotechnol.*, **2003**, 78, 497.
- [12] Mazumder, B., Uddin, I., Khan, S., Ravi, V., Selvraj, K., Poddar, P., Ahmad A., *J. Mater. Chem.*, **2007**, 17, 3910.
- [13] Rohwerder, T., Gehrke, T., Kinzler, K., Sand, W., *Appl. Microbiol. Biotechnol.*, **2003** 63, 239.
- [14] Deng, Z., Chen, D., Peng, B., Tang, F., *Cryst. Growth. Des.*, **2008**, 8, 8, 2995.
- [15] Deng, Z., Tang, F., Muscat, A, J., *Nanotechnology.*, **2008**, 19, 295705.
- [16] Cao, S., Guo, C., Lv, Y., Guo, Y., Qian Liu, Q., *Nanotechnology.*, **2009**, 20, 275702.
- [17] Berlincourt, D. *J. Acoust. Soc. Am.*, **1992**, 91, 3034.
- [18] Whatmore, R. W. *Rep. Prog. Phys.*, **1986**, 49, 1335.
- [19] Geng, J., Hou, W. H., Lv, Y. N., Zhu, J. J., Chen, H. Y., *Inorg. Chem.*, **2005**, 44, 8503.
- [20] Zhu, L. Y., Xie, Y., Zheng, X. W., Yin, X., Tian, X. B., *Inorg. Chem.*, **2002**, 41, 4560.

-
- [21] Zhang, K. L., Liu, C. M., Huang, F. Q., Zheng, C., Wang, W. D., *Appl. Catal. B: Environ.*, **2006**, 68 125.
- [22] Ma, J., Liu, X., Lian, J., Duan, X., Zheng, W., *Cryst. Growth. Des.*, **2010**, 10, 6, 2522.
- [23] Huang, W. L., *J. Comput. Chem.*, **2009**, 30, 1882.
- [24] The XRD patterns were indexed with reference to the crystal structures from the PCPDFWIN: BiOCl (# 85-0861).
- [25] Bannister, F. A., Hey, M. H., *Nature.*, **1934**, 134, 855.
- [26] Davies, J. E.D., *J. Inorg. Nucl. Chem.*, **1973**, 35, 1531.
- [27] Rautaray, D., Sanyal, A., Adyanthaya, S. D., Ahmad, A., Sastry, M., **2004**, *Langmuir.*, 20, 6827.
- [28] Haris, P. I., Severcan, F., *J. Mol. Catal B: Enzym.*, **1999**, 7, 207.
- [29] Laemmli, U. K., *Nature.*, **1970**, 227, 680.

Chapter 5



General discussion and conclusions

This chapter contains the concluding remarks on the salient features of the work, described in this thesis and discusses the possible avenues for future work.

5.1 Summary of the work

The work carried out in this thesis mainly concentrates on bioinspired inorganic nanomaterials synthesis and their applications.

We have synthesized a range of water soluble and protein capped metal oxides and fluorescent nanomaterials using the mesophilic fungus *Fusarium oxysporum*, alkalotolerant mesophilic fungus *Trichothecium* sp. and thermophilic fungus *Humicola* sp. The reasons why each of the above mentioned microorganisms were used for the synthesis of above specific inorganic nanomaterials are as follows.

1. We have screened a number of mesophilic, alkalotolerant, alkalophilic, endophytic and thermophilic microorganisms in order to synthesize very important water dispersible, protein capped half metallic ferromagnetic CrO₂ nanoparticles extracellularly. Out of several microorganisms screened, only an alkalotolerant mesophilic fungus *Trichothecium* sp. produces protein capped; water dispersible, extracellular CrO₂ nanoparticles in range of 21-25 nm size at room temperature.
2. Our group has already synthesized a range of metal nanoparticles, binary and ternary oxide nanoparticles, alongwith sulphide and quantum dot nanomaterials of different sizes and shapes using the mesophilic fungus *Fusarium oxysporum*. This led us into thinking toward the possibility of the synthesis of protein capped water dispersible Bi₂O₃, antiferromagnetic Mn₅O₈ and highly fluorescent Bi₂S₃ nanoparticles extracellularly.
3. Our group at N.C.L has already reported the extracellular synthesis of silicate nanoparticles using thermophilic fungus *Humicola* sp. This has prompted us to use this fungus for the size reduction of technologically important water soluble protein capped BiOCl nanoparticles extracellularly.

Several biomimetic synthesis approaches, where biomolecules or microbes participate either in the reduction, oxidation or hydrolysis of the precursors or act as templates are gaining popularity as these novel synthesis methods do not require high temperature, pressure or extreme pH conditions. These reactions are often environment friendly and efficiency of these natural synthesis processes is often very high. Thus, we conclude that microorganisms such as fungi have proved themselves as possible eco-friendly inorganic nanofactories. It is the wonder capacity of these

organisms which can be exposed for the synthesis of excellent nanomaterials through a very straight forward and hygienic route.

In the present thesis, we have explored a fungi mediated biological approach toward the synthesis of inorganic nanomaterial and an attempt has been made to design biological methods for the synthesis of complex transition metal oxide and metal sulphide nanoparticles. There are basically two different biosynthetic approaches for the synthesis of chemically difficult to synthesize nanoparticles: the “bottom-up” and the “top-down” approach.

In the first approach (bottom-up), we demonstrate that the fungal biomass is capable of synthesizing some difficult phase of transition metal oxide and metal sulphide nanoparticles at room temperature by reacting the metal ion salts such as acetate, nitrate and chromate with the fungus *Fusarium oxysporum* and *Trichothecium* sp. We observed that the mesophilic fungus *Fusarium oxysporum*, on exposure to chemical precursors like bismuth nitrate is capable of synthesizing Bi_2O_3 nanoparticles having particle size 5-10 nm, under ambient conditions which is extremely difficult to obtain by any other synthetic routes. Similarly, after reacting *Fusarium oxysporum* with manganese(II)acetate tetrahydrate, Mn_5O_8 nanoparticles of an average particle size of around 10-11 nm were obtained. Mn_5O_8 nanoparticles have complex electronic structure with presence of two mixed valencies (Mn^{2+} and Mn^{4+}) of manganese ion and form the chemical formula like “ $\text{Mn}_2^{2+}\text{Mn}_3^{4+}\text{O}_8$ ”, which was confirmed by XPS analysis. Magnetic measurements show that these nanoparticles exhibit antiferromagnetic behavior. Furthermore, nanocrystalline chromium dioxide (CrO_2) was synthesized by using the fungus *Trichothecium* sp. and potassium dichromate ($\text{K}_2\text{Cr}_2\text{O}_7$) was used as precursor salt. These nanoparticles have an average particle size of around 22 to 24 nm and show ferromagnetic behaviour. Being metastable in an oxygen rich environment, CrO_2 nanoparticles show presence of Cr_2O_3 layer over themselves which was further confirmed by the HR-TEM images, XPS analysis and magnetic measurements. Furthermore, ferromagnetic and antiferromagnetic coupling of CrO_2 and Cr_2O_3 layers results in exchange bias in the CrO_2 nanoparticles and is confirmed by the M-H curves in magnetic measurement. CrO_2 is half metallic ferromagnetic, having highest spin polarization; but amongst the lowest tunnel magnetoresistant ones and is a favorite material for magnetoelectronic devices and as storage media in magnetic tapes. These oxide nanoparticles are capped by a protein which restricts its growth during its synthesis. Hence, nanoparticles synthesized by

biosynthetic approach are much smaller in size. This extracellular protein acts as a reducing agent as well as provides long term stability in aqueous medium which binds to the surface of the nanoparticles and thus prevents aggregation.

Further, we have extended the same approach to synthesize bismuth sulphide (Bi_2S_3) nanoparticles in aqueous phase which shows semiconductor behaviour. Orthorhombic Bi_2S_3 nanoparticles were prepared by reacting the mesophilic fungus *Fusarium oxysporum* with bismuth nitrate ($\text{Bi}(\text{NO}_3)_3 \cdot 5\text{H}_2\text{O}$) and Na_2SO_3 as a precursor. Biogenic bismuth sulfide nanoparticles were highly stable and exhibited excellent optical properties. Transmission electron micrograph (TEM) images showed that nanoparticles are quasi-spherical in shape with an average particle size of 15 nm and shows a blue shift with a band gap of 3.04 eV. These Bi_2S_3 nanoparticles were used in SPECT-CT probe for small-animal imaging. This was injected into rats and biodistribution image and clearance time from blood was calculated.

In the second approach (top-down), we show that the fungal biomass can be used to breakdown the chemically synthesized larger BiOCl particles (150-200 nm) into particles as small as 5-6 nm while maintaining the crystallinity and phase at the nano level. We have named this technique as “bio-milling”. We believe that this technique can be used to synthesize several oxide nanoparticles whose synthesis in the size less than 10 nm by conventional wet-chemical methods is difficult. In nature, the microorganisms including fungus are known to degrade rocks to form smaller particles over a very long period of time. However, to the very best of our knowledge, this is for the first time that the process has been applied in a research lab. In our opinion, this process carries huge technical importance as it provides a very simple route to form small particles over traditional top-down methods (such as lithography, pulsed laser deposition, etc.) which are quite expensive. We believe that the scaling-up of this synthesis process could be easily demonstrated by optimizing parameters such as the type of microorganism, medium, pH and temperature as well as by using large fermentors for the reaction.

So, these studies suggest that both the biosynthesis approaches (bottom-up and top-down) can lead toward the solution to fulfill the demands of development of reliable and eco-friendly processes for the synthesis of complex metal oxide and metal sulphide nanomaterials. Thus, the production of nanomaterials by biological methods provides an edge over other synthesis routes in terms of low energy intake and leads to a potentially large cost reduction.

5.2 Scope for future work

The prospective applications and potential of the bio-inspired inorganic nanomaterial synthesis which is described in this thesis are limited only by the hypothesis and opinion of the researcher. Biological methods for the synthesis of inorganic nanoparticles described here are in the preliminary stage and need to be optimized before they can be compared with the existing chemical methodologies. Furthermore, the fungus mediated synthesis approach that we have used for synthesizing inorganic nanoparticles can be extended for synthesizing other complex ternary metal oxides, multiferroics, core shells etc. which are difficult to achieve using conventional synthesis routes and have different properties and applications. In addition, there is a need for the in-depth characterization of nanomaterials which we have synthesized by both the approaches. It would also be useful to study in detail the electronic structure and magnetic properties like ferromagnetic resonance of biosynthesized CrO_2 nanoparticles which make it a favorite material for various potential applications. Similarly, it would be interesting as well to investigate the detailed optical properties of Bi_2S_3 quantum dots synthesized using *Fusarium oxysporum*. Investigation of temperature dependent photoluminescent properties alongwith its stability and toxicity studies would be important for finding out its biomedical applications.

Effect of various experimental parameters such as incubation temperature, aerobic or anaerobic conditions, use of alternate precursor salt, detailed analysis of interaction of metal ions, interaction of bulk particles with fungal biomass in case of top-down approach (biomilling) and extracellular protein/biomolecules secreted from the fungus, etc. would give valuable information with which properties of nanoparticles e.g. shape, size, monodispersity, etc. could be controlled. Besides these, other aspects like identification of microorganism which could synthesize nanomaterials of interest and in-depth study of the nature of the interaction of fungal biomass and precursor salt (bulk particles in case of bio-milling) need to be studied. One of the most challenging aspect of both the biosynthetic approaches (bottom-up and top-down) of nanomaterials synthesis is to perform a detailed investigation of their biochemical mechanism and identify the type and number of proteins/enzymes and their subsequent DNA fragments involved in the bio-milling and biosynthesis process. This would lead to the synthesis of respective nanomaterials in bulk quantities and thus the biosynthesis approach would be able to meet the industrial needs.

Our group at N.C.L, Pune, has already made significant progress towards the synthesis of inorganic nanomaterials of different chemical compositions such as metal, metal oxides, metal sulphides, quantum dots, alloys and synthesis of nanoparticle-drug conjugates. Biosynthesis of technologically challenging materials as the ones synthesized above may find applications in imaging, diagnostics and therapeutics, etc. The nanomaterials which we have synthesized using fungal routes are water dispersible, protein capped and may bind to various receptors such as EGFR(Epidermal growth factor receptor), EpCAM (Epithelial cell adhesive molecule), folic acid and other cancer biomarkers without targeting agents. Since the nanomaterials which we have synthesized through the microbial routes can act as antiangiogenic or angiogenic molecule, these protein capped inorganic nanomaterials can also be taken into consideration to be used directly as a drug in future without any side effects.

Appendix I: Instrumental details

Transmission electron microscope:

TEM measurements were performed on a JEOL Model 1200EX instrument operated at an accelerating voltage of 80 kV. HR-TEM measurements were carried out using a JEOL–JEM-2010 UHR instrument operated at an acceleration voltage of 200 kV with a lattice image resolution of 0.14 nm. In addition to this, for HR-TEM measurements, a TECHNAI G2 F30 S-TWIN instrument (Operated at an acceleration voltage of 300 kV with a lattice resolution of 0.14 nm and a point image resolution of 0.20 nm) was also employed. The same set of instruments was used for selected area electron diffraction analyses. For this purpose, we prepared the samples by drop-coating the particles suspended in aqueous medium on carbon coated copper grids and allowing the solvent to evaporate. Selected area electron diffraction (SAED) analysis was also carried out on the same grids.

X-ray diffraction

Powder XRD patterns were recorded using a Philips X'PERT PRO instrument equipped X'celerator, a fast solid-state detector on drop-coated sample on glass substrate. The sample was scanned using X'celerator with a total number of active channels of 121. Iron-filtered Cu K α radiation ($\lambda=1.5406 \text{ \AA}$) was used. XRPD patterns were recorded in the 2θ range of 20° - 80° with a step size of 0.02° and a time of 5 seconds per step.

X-ray photoelectron spectroscopy

Measurements were carried out on a VG MicroTech ESCA 3000 instrument at a pressure better than 10^{-9} Torr. The spectra were recorded with un-monochromatized MgK α radiation (photon energy = 1253.6 eV) at a pass energy of 50 eV, electron takeoff angle (angle between electron emission direction and surface plane) of 60° and a resolution of 0.1 eV. The core level spectra were background corrected using the Shirley algorithm and the chemically distinct species were resolved using a nonlinear least squares curve fitting procedure. The core level binding energies (BEs) were aligned with respect to the C 1s

binding energy (BE) of 285 eV. For this, the sample was prepared on silicon substrate by drop-coating.

UV-visible-NIR spectrophotometry:

UV-Visible spectroscopy measurements were carried out on Jasco dual-beam spectrophotometer (model V-570) operated at a resolution of 1nm.

Fluorescence spectrophotometer:

Fluorescence spectra were recorded on a CARY Eclipse instrument from Varian with a slit width of 5 nm.

FTIR spectrophotometer:

FTIR spectroscopy measurements on nanocrystal's powder taken in KBr pellet were carried out using a Perkin-Elmer Spectrum One instrument. To obtain good signal to noise ratio, 128 scans of the film were taken in the range of 450 – 4000 cm^{-1} at a resolution of 4 cm^{-1} .

Thermo gravimetric analyzer

Thermogravimetric analysis (TGA) experiments was carried out using a Q5000 V2.4 Build 223 instrument by applying a scan rate of 10°C min^{-1} in N_2 environment. For this purpose, we first dried the sample under incandescent lamp to form powder.

Energy dispersive analysis of X-rays (EDAX)

Energy dispersive analysis of X-rays (EDAX) measurements were performed on a Leica Stereoscan-440 scanning electron microscope (SEM) instrument equipped with Phoenix. For this, the sample was prepared on silicon substrate by drop-coating.

Magnetic measurement

For magnetization vs. magnetic field measurements, we used a Magnetic Property Measurement System (MPMS) from Quantum Design Inc., USA equipped with SQUID magnetometer and superconducting magnet. For this purpose, we took the sample in Teflon tape and packed it inside the gelatin capsules.

Appendix II: List of Publications

- [1] “Structure and Microbial Synthesis of Sub-10 nm Bi_2O_3 Nanocrystals” **Imran Uddin**, Suguna Adyanthaya, Asad Syed, K. Selvaraj, Absar Ahmad*, Pankaj Poddar* *J. Nanosci. Nanotechnol.*, 2008. 8, 3909 – 3913.
- [2] “Bio-milling technique for size reduction of chemically-synthesized BiMnO_3 nanoplates” Baishakhi Mazumder, **Imran Uddin**, Shadab Khan, Venkat Ravi, Kaliaperumal Selvraj, Pankaj Poddar*, Absar Ahmad*, *J. Mater. Chem.*, 2007, 17, 3910 – 3914.
- [3] “Nano-colloid as dual-function probe for SPECT and CT in small animal imaging” Sanjay Gambhir, Absar Ahmad, **Imran Uddin**, Veeresh Dube, Subhash Kheruka, Utham Kumar, *J. Nucl. Med.*, 2011, 52 (Supplement 1), 1613
- [4] *Synthesis and study of physical properties of protein functionalized CrO_2 nanoparticles synthesized by microbial method*” **Imran Uddin**, Pankaj Poddar, Absar Ahmad* (Communicated)
- [5] “Synthesis of monoclinic Mn_5O_8 nanoparticles using microbial method and study of mechanism ” **Imran Uddin**, Pankaj Poddar, Absar Ahmad* (Communicated)
- [6] “Fungus mediated synthesis of Bi_2S_3 quantum dot” **Imran Uddin**, Absar Ahmad* (Communicated)

Appendix III: List of abbreviations

λ	Wavelength
μL	Micro liter
μg	Micro gram
AFM	Atomic Force Microscopy
\AA	Angstrom
a.u.	Arbitrary units
$^{\circ}\text{C}$	Degree Celsius
CT	Computed tomography
DRS	Diffuse reflectance mode
etc.	Etcetera
eV	Electron volts
Fig.	Figure
FC	Field Cooled
FTIR	Fourier Transform Infrared spectrophotometer
H	Applied magnetic field
HRTEM	High Resolution Transmission Electron Microscopy
kDa	Kilo Dalton
M	Magnetization
MGYP	Malt extract, glucose, yeast extract and peptone
MRI	Magnetic Resonance Imaging
MEMS	Micro Electro Mechanical Systems
nm	Nanometer
NIR	Near infra-red
PDA	Potato dextrose agar
QDs	Quantum dots
rpm	Rotations per minute
SPECT	Single photon emission computed tomography
SAED	Selected Area Electron Diffraction
SPR	Surface Plasmon resonance
SEM	Scanning Electron Microscopy
TGA	Thermogravimetric Analysis
TEM	Transmission Electron Microscopy
UV-vis	Ultraviolet-Visible
XRD	X-Ray Diffraction
XPS	X-Ray Photoelectron Spectroscopy
ZFC	Zero Field Cooled